Université catholique de Louvain
Institut de recherche en
mathématique et physique

Combinatorial and analytical aspects of the two-periodic dimer model

Nicolas Robert

Thesis submitted in partial fulfilment of the requirements for
the degree of Docteur en Sciences

Thesis committee:

Prof. Philippe Ruelle *(Supervisor)*	UCLouvain
Prof. Christophe Charlier *(Secretary)*	UCLouvain
Prof. Pierre-Emmanuel Caprace *(President)*	UCLouvain
Prof. Christian Walmsley Hagendorf	UCLouvain
Prof. Tom Claeys	UCLouvain
Prof. Andrea Sportiello	Université Paris Nord
Prof. Jean-Marie Stéphan	École Normale Supérieure de Lyon

January 2026

Combinatorial and analytical aspects of the two-periodic dimer model

by Nicolas Robert

This work was partially supported by the F.R.S.-FNRS under the FRIA grant FC50105, and by the F.R.S.-FNRS and the FWO through the Belgian EOS Project No. 30889451 'PRIMA–Partners in Research on Integrable Models and Applications'.

Remerciements

Une thèse, c'est l'accomplissement de quatre années de travail, de recherche et parfois – avec un peu de chance – de découvertes scientifiques. Mais pas seulement. C'est aussi une période durant laquelle on fait de nouvelles rencontres, où l'on partage notre travail avec des collègues ou des amis, où l'on s'accomplit. Ces quelques lignes sont dédiées à ces personnes, qui de près ou de loin, ont contribué à rendre ces quatre années si belles.

En tout premier, et à juste titre, j'aimerais remercier mon promoteur de thèse, Philippe Ruelle. Tu m'as fait découvrir la beauté de la physique mathématique et as su me faire apprécier sa rigueur. Je dois également te remercier pour ta disponibilité, ton expertise et tes conseils avisés qui m'auront guidé tout au long de cette thèse. Par la même occasion, je tiens à remercier les membres de mon jury, les professeurs Christian Walmsley Hagendorf, Tom Claeys, Christophe Charlier, Pierre-Emmanuel Caprace, Andrea Sportiello et Jean-Marie Stéphan, pour le temps qu'ils ont consacré à la lecture de ce manuscrit et d'autant plus pour l'intérêt qu'ils lui ont manifesté lors de nos interactions.

Je me dois également de dire merci à mes nombreux collègues qui ont rendu ce temps à l'institut aussi vivant, et admettre que l'atmosphère conviviale de la tour B et du cyclotron me manquera. Parmi mes collègues en physique-mathématique : merci Sandrine de m'avoir guidé dans les méandres du métier de jeune chercheur alors que l'espèce des physiciens-mathématiciens était proche de l'extinction. Merci Bryan pour nos brefs échanges durant mes premières semaines qui m'ont été d'une aide inestimable. Merci Alexandre pour ton expertise scientifique sur les nombreuses facettes des modèles intégrables. Merci Nathan

pour ta bonne humeur et ton enthousiasme, ce fut un plaisir de pouvoir discuter des fonctions thêta avec toi. Je remercie de manière plus générale l'ensemble des doctorants et postdocs de la tour B que j'ai pu côtoyer. Maxime (pour m'avoir fait découvrir les tiramisus aux spéculoos), Robynn, Nadia, Leon (pour les afterworks) et tous les autres. Je remercie également les secrétaires de l'institut : Cathy, Martine, Elodie et Carine, pour l'organisation des nombreux événements festifs et l'aide apportée au quotidien.

Il m'est impossible de ne pas mentionner mes compagnons et amis avec qui j'ai traversé mes années d'études en physique, et pour certains d'entre eux, le doctorat par la suite. Yannis, Justin, Arnaud B., Mathilde et Benoît, sans vous le chemin n'aurait pas été le même, pour sûr. Merci pour les moments de camaraderie entre les cours ainsi que pour les discussions passionnées autour de la physique. Vous m'avez tiré vers le haut et invité à me dépasser tout au long de ce parcours.

Je voudrais également remercier mes amis de plus longue date, que je connais d'avant l'université, et qui sont restés au long des années à m'écouter m'enthousiasmer – et parfois me plaindre – de sciences et d'autres. Il serait dur de résumer tous les bons moments passés ensemble, tant ils sont nombreux. Merci Arnaud L., Aymeric, Loïc, Anthony, Leiv, Constantin, Cassandra.

Pour finir, je remercie ma famille pour son soutien et son amour ; une force sur laquelle j'ai toujours pu me reposer. Merci à Camille d'être dans ma vie.

List of publications

This thesis is based on the following research papers, each of them corresponding to a chapter:

[1] J.-F. de Kemmeter, N. Robert and P. Ruelle, *On λ-determinants and tiling problems*, J. Phys. A: Math. Theor. **57 1** (2023) 015209.

[2] N. Robert, H. Rosengren, P. Ruelle and C. Walmsley Hagendorf, *Arctic curve in the elliptic SOS model at the free-fermion point*, in preparation.

[3] N. Robert and P. Ruelle, *GUE-corners in two-periodic Aztec diamonds*, arXiv preprint `arXiv:2509.14071 [math-ph]` (2025).

[4] N. Robert and P. Ruelle, *Two-periodic dimer models on the plane*, in preparation.

Contents

Introduction **1**

1 On λ-determinants and tiling problems **11**

1.1 General octahedron recurrence 16

1.2 Face weights 19

1.2.1 Restricted weights: λ-determinants 20

1.2.2 Applications to periodic and biased Aztec diamonds 22

1.2.3 Applications to subgraphs of Aztec diamonds . . . 29

1.2.4 General weights: the generalized Robbins-Rumsey formula 34

1.2.5 General weights: shuffling algorithm and condensation 43

1.3 Inhomogeneous λ-determinants 46

1.A On elliptic curves related to Aztec diamonds 52

1.B Generalized Somos-4 sequences 58

2 Arctic curves in the elliptic SOS model at the free-fermion point **63**

2.1 Generalities on the six-vertex model 63

2.2 The elliptic SOS model 67

2.3 From the two-periodic 6V model to Aztec diamonds . . . 72
2.3.1 Correspondence between partition functions 72
2.3.2 Condensation algorithm and Aztec diamond partition function 79
2.3.3 Elliptic parametrization and explicit check on the partition functions 82
2.4 One-refined tangent method 84
2.4.1 One-refined partition function 85
2.4.2 Path generating function 91
2.4.3 One-refined parametrization of the arctic curve . . 96
2.5 Two-refined tangent method 99
2.5.1 Two-refined partition function 101
2.5.2 Two-refined parametrization of the arctic curve . . 107
2.6 Algebraic curve and limit cases 108
2.7 Numerical simulations 115
2.8 Conclusion and outlook 116
2.A Some identities on theta functions 117
2.B Details of the saddle point analysis 120
2.B.1 Non-elliptic case 121
2.B.2 Elliptic case 127

3 GUE-corners process in two-periodic Aztec diamonds 135

3.1 Biased Aztec diamonds 137
3.1.1 Interlaced particles and adjacency 137
3.1.2 Probability density function 140
3.1.3 Distribution on first levels 144

3.1.4 Convergence to the GUE-corners process 148
3.2 Two-periodic Aztec diamonds 150
3.2.1 Probability density function 153
3.2.2 Distribution on first levels 160
3.2.3 Generating functions, asymptotics and convergence to the GUE-corners process 167
3.3 Connections with the octahedron recurrence 172
3.4 Discussion 176
3.A Alternating sum of powers 179

4 Two-periodic dimer models on the plane 181
4.1 Kasteleyn matrix and partition function 182
4.2 From discrete to Majorana fermions 188
4.3 One-periodic weights 194
4.3.1 Dimer correlations 195
4.3.2 Plaquette correlations 197
4.4 Two-periodic weights 200
4.5 Ghost systems 202
4.6 Symplectic fermions 205
4.7 Outlook 207
4.A Inverse discrete Laplacian 207
4.A.1 Massless Green matrix 208
4.A.2 Massive Green matrix 209

Conclusion 211

Bibliography 215

Introduction

The study of *phase transitions*, namely sudden changes in the physical properties of matter when external parameters are varied, is along some of the most interesting problems of physics. Why does the water freeze at some temperature? What is the melting point of iron? Why do some materials keep a residual magnetization at sufficiently low temperature? Such questions are naturally addressed in the framework of *statistical mechanics*. This branch of physics more generally aims to study the macroscopic properties of systems with many components (e.g. a gas composed of billions of molecules) starting from the laws that describe the interactions between microscopic individuals [5]. As one can imagine, describing the explicit behaviour of every component would be both troublesome and not very enlightening. The strategy therefore relies on a statistical description of the system, retaining only the meaningful average quantities (e.g. density, pressure, temperature, etc.). Statistical mechanics is particularly effective on systems with very simple interaction laws between their constituents. For this reason, physicists frequently rely on the study of *models* which are idealized versions of the reality. A model does not have to give a perfect account of nature, but rather to retain only the essential features needed to reproduce the physical phenomenon under study. For instance, in the famous *Ising model*[1], introduced to describe ferromagnetism, the range of interaction between the discrete spin variables is limited to the nearest neighbours.

[1]The model was proposed by W. Lenz and solved by E. Ising, his PhD student, in one dimension in 1924 [6]. However, the model did not exhibit the expected spontaneous magnetization at the time. In 1944, L. Onsager found a solution for the two-dimensional version of the model at zero external magnetic field reproducing this time the ferromagnetic transition [7]. The model and its generalizations have kept the name Ising.

We know that the real situation is more complicated, nevertheless, this approximation still captures the ferromagnetic phase transition occurring at some *critical* temperature and allows us to compute the critical exponents.

Another common simplification consists in regarding the components of the system as living on a two-dimensional lattice (or a one-dimensional lattice with time evolution) with a finite number of sites/vertices. By letting the number of sites grow to infinity while simultaneously reducing the lattice spacing, one can then approximate a continuous medium while retaining the microscopic lattice structure. This particular limit is usually called the *scaling limit*. In two dimensions, this approach presents many advantages, one of the greatest being that some of these models are *exactly solvable* [8]. Roughly speaking, this property of a model refers to the ability of expressing statistical quantities (e.g. probability density, correlation functions, etc.) in terms of simple mathematical expressions by using analytical methods. What do we mean by simple mathematical expressions? This is in fact mainly conventional. For instance, the solutions may sometimes be given in terms of rational expressions or finite sums, but in other cases, they may involve elliptic functions or determinants of orthogonal polynomials. Yet, the basis of accepted functions to be exactly solvable is not rigid and may depend from one situation to another. For this reason the concept of exact solvability (in this sense) is not always perfectly clear. To get a better grasp of its meaning and origin, it is useful to consider the closely related notion of *integrability*. Classically, a system is called integrable if there are sufficiently many symmetries (or conserved quantities) to completely characterize the motion. It extends to the notion of *quantum integrability* (see [9] for a pedagogical introduction), usually referring to the fact that the system can be shown to satisfy the *Yang-Baxter equation* [10,11]. This underlying mathematical structure somewhat justifies the exact solvability of some models. For the past century, mathematical-physicists extensively studied these *integrable systems*. A certain number of them is inspired by physics and attempts to model the properties of some materials (for instance the Ising model mentioned above and generalizations thereof). But there are also some other models, primarily interesting for their theoretical aspects and their connections with different areas of mathematics.

The phase transitions mentioned earlier are a common feature that brought a lot of attention to some of these models. They are pertinent both from a physical perspective and for the hidden and rich mathematics underlying their description. A prime example of such transitions is certainly that concerning the states of matter (solid, liquid, gas) which are examples of *first order transitions*.

Yet, some transitions are more subtle. Take for instance the liquid-gas transition line in the temperature-pressure diagram. One can follow this line while the temperature increases until it suddenly ends at some *critical* values of temperature and pressure. At this point, the distinction between liquid and gas vanishes. This phenomenon, called critical opalescence, is characterized by a divergence of the correlation length resulting in a scale invariance (scale-free) of the system and algebraic (in inverse power law) decay of correlation functions. The same critical behaviour occurs in the two-dimensional Ising model and many other models. It is generally the signature of a *second order phase transition*. This terminology refers to the fact that there is no direct discontinuity in the matter density, in contrast with the liquid-gas transition, and can be seen as more subtle. Some famous examples are superconductivity and superfluidity which are the properties of some materials at low temperature to have respectively zero electrical resistance or zero viscosity. Other concrete examples in nature of such critical behaviour exist, sometimes in unexpected places. To mention an instance outside physics, it was observed that the movement synchronization in large schools of fish, or flocks of flying birds presented the same kind of scale-free property and could be modelized as a system at criticality [12]. Such systems are in fact ubiquitous in statistical physics and particularly interesting for their mathematical structure. In particular, it is well known that they can be described by *conformal field theories* (CFTs), due to the scale invariance. The model at the center of this thesis belongs to this class.

The *monomer-dimer model* was originally introduced by Fowler and Rushbrooke [13] in an attempt to describe molecular arrangements and statistical properties in liquids made of both mono-atomic and di-atomic molecules. The complete description being combinatorially too hard, they restricted to the case of purely di-atomic species on planar lattice, leading to the so-called ***dimer model***. Besides its physical interpre-

tation, the model exhibits a strong combinatorial structure and was investigated by mathematicians ever since (see [14] for a detailed introduction). The model can be defined as follows. Let us consider a planar graph G with vertices and edges. A perfect matching of G is a subset M of edges such that every vertex of G belongs to one and only one edge of M. Equivalently, it can be seen as a covering of the edges by dimers, namely a bond between two vertices, such that all the vertices are covered by one single dimer. An example of perfect matching on a rectangular graph is given in Figure 1-left. In this thesis, we will mainly consider graphs that are connected subgraphs of $\mathbb{Z}^2$. In this case, in order to admit a perfect matching, the graph is necessarily bipartite and we are allowed to distinguish two different parity classes for the vertices, as depicted in black and white in the figure. The dimer model studies the statistical properties of the set of perfect matchings. To do so, one has to define a probability measure on this set which is generally done by primarily assigning a weight $w(e)$ to the edges e of the graph. We then give a perfect matching M a weight $w(M)$ corresponding to the product of all edges covered in M. The probability of occurrence of M is simply

$$\mathbb{P}(M) = \frac{w(M)}{Z_G}, \qquad Z_G = \sum_M w(M) = \sum_M \prod_{e \in M} w(e),$$

where Z_G is the *partition function*; the weighted sum over all configurations (perfect matchings). In case $w(e) = 1$ for all edges, every matching is equally weighted, and Z_G corresponds to the number of perfect matchings on G. We refer to this situation as the *uniform* probability measure. Other typical measures studied in this thesis are the *biased* and/or *two-periodic* weightings. They are properly defined in the next chapters.

The model can equivalently be seen as a purely combinatorial problem consisting of the tiling of a certain planar domain by dominos (see Figure 1-middle). In this picture, the vertices are replaced by non-overlapping unit squares forming the cells of a rectangular grid, and dimers are replaced by 1×2 dominos. The bipartite character of the lattice leads us to distinguish four different kinds of dominos according to the parity of their locations, these are depicted in Figure 1-right. The chosen colours here have no link with the probability distribution.

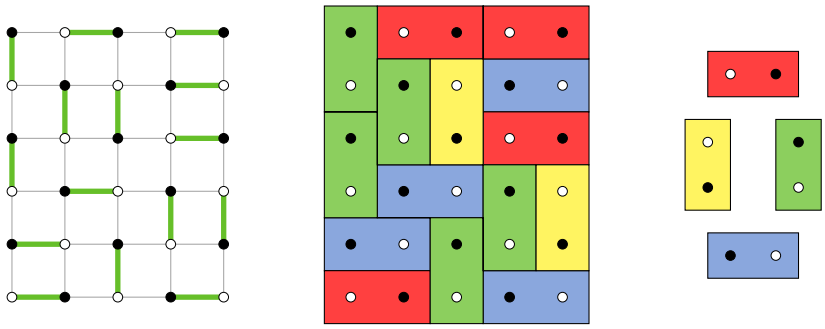

Figure 1: *Left*: example of perfect matching on a 5×6 rectangular graph. *Center*: same configuration represented in terms of dominos. *Right*: colouring convention according to the parity of lattice sites.

One major breakthrough in the field of perfect matchings /domino tilings was accomplished by Temperley, Fisher [15, 16], and Kasteleyn [17] in 1961. In these works, the partition function on a $L \times M$ rectangular domain was computed, leading to the remarkable formula

$$Z_{L\times M} = \prod_{\ell=1}^{\lceil L/2\rceil} \prod_{m=1}^{\lceil M/2\rceil} \left[4\cos^2\left(\frac{\ell\pi}{L+1}\right) + 4\cos^2\left(\frac{m\pi}{M+1}\right)\right].$$

For instance, one can easily deduce from it the number of tilings on a chessboard-like domain: $Z_{8\times 8} = 12\,988\,816$.

The method developed by Kasteleyn [18] is actually much more general and applies to any planar graph with arbitrary edge weights. In particular, it gives a determinantal or Pfaffian formula for the partition function in terms of a certain oriented adjacency matrix of the graph, usually called a Kasteleyn matrix. However, the question of whether this determinant can be evaluated in closed form and/or analysed asymptotically remains difficult in general and strongly dependent on the domain and the probability measure. It also provides determinantal formulas for n-point correlation functions between dimers. On subgraphs of $\mathbb{Z}^2$, these are known to decrease algebraically at long range[2]. This properties indicate that the dimer model is critical in the scaling limit and can be described by a CFT, as mentioned above. More details about the Kasteleyn theory are given in Chapter 4.

[2]This result may depend on the lattice one considers, for triangular lattice for instance the decay is exponential.

More recently, in 1992, N. Elkies et al. [19,20] considered domino tilings on slightly different domains, with staircase-shaped boundaries. They called such domains *Aztec diamonds*, referring to the shape that resembles to the profile of an Aztec temple. An illustration is provided in Figure 2. Since then, this model received a lot a attention from the community due to the rich mathematical structure it exhibits. One prominent aspect being the *spatial phase transition* (i.e. a genuinely different behaviour in the domino organization according to their absolute position on the domain), occurring at large size. Let us define an Aztec diamond of order n as the collection of unit squares whose centers of coordinates $(x, y) \in (\mathbb{Z} + \frac{1}{2})^2$ are living in $|x| + |y| \leqslant n$. Using the uniform probability measure, the *arctic circle theorem* [21] states the following: with a probability that goes to 1 as n increases, the dominos in the four corners are fully-ordered (in the form of a brick-wall pattern), whereas all the randomness and disorder accumulate inside a circular region in the center (see Figure 2). The ordered regions are often called *frozen* referring to the statistics of the dominos that converges to deterministic values. By opposition, the disordered central region is called *liquid*, *temperate* or *rough*. The interface that separates the different regions is by extension called the *arctic curve*. In the limit where n goes to infinity the curve converges to a perfect circle, for the uniform measure. The appearance of this arctic phenomenon can be seen as a consequence of the domain boundaries, with staircase shapes, which strongly constrain the organization of the dominos near the edges. It then propagates deeply enough inside the domain to lead to a macroscopic effect on average configurations.

After the introduction of Aztec diamonds, the study of arctic phenomena gained a lot of interest and was pursued in many other models such as *Alternating Sign Matrices* (ASMs) [22,23], *the six-vertex model* [24–26], *tilings of hexagons* [27–29], etc. The Aztec diamond nevertheless remains among the simplest instances where this phenomenon occurs, and mathematicians continue to study its generalizations. One direction aims to modify the domain as in double Aztec diamonds [30,31], holey Aztec diamonds, or Aztec rectangles [32] for instance. Another direction consists in modifying the probability measure; some well-known measures studied in this thesis are the *biased* and/or *two-periodic* weightings. Higher periodicities also exist (see for instance [33–35]) but they will not be

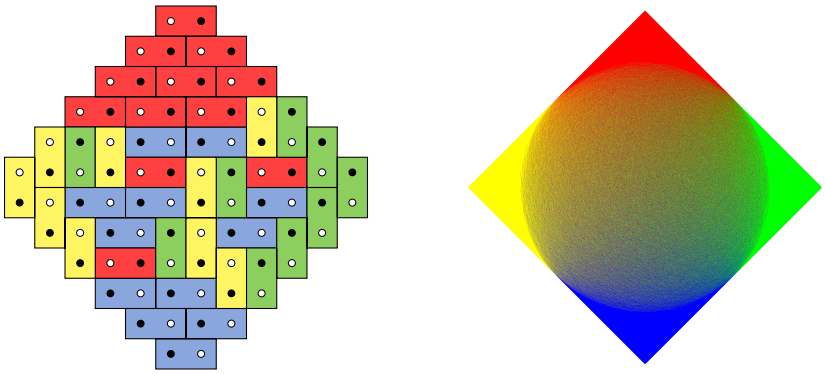

Figure 2: *Left*: tiling of an Aztec diamond of order $n = 6$. *Right*: tiling of an Aztec diamond of order $n = 3000$. Both pictures were randomly generated with uniform measure using the shuffling algorithm. The code was kindly provided by Bryan Debin.

considered in this manuscript. A peculiar phenomenon occurring with periodic weights is a non-trivial deformation of the arctic curve, and the appearance of a new region in the very center of the diamond sometimes called *gaseous* or *smooth* (see Figure 3). Similarly to the liquid one, this region is also disordered, however, the behaviour of the dimers inside is genuinely different; they are more likely to group themselves in 2×2 plaquettes made of two parallel dimers. Besides, the correlations between dominos also behave differently, and decrease exponentially in this phase. In particular, it means that the model is off-critical in this region and that, if a field theoretic description exist, the theory would have to be massive. The two-periodic weights therefore appear as relevant parameters of this off-critical extension. This aspect makes the two-periodic weighting particularly interesting to study, both from the perspective of spatial phase transitions and from the field theoretic approach.

Another remarkable aspect in Aztec diamonds is its numerous connections with determinantal point processes and distributions issued from random matrix theory. For instance, it was shown that the fluctuation of the arctic curve follow the Tracy-Widom distribution [36] which also describes the normalized largest eigenvalue in matrices from the *Gaussian Unitary Ensemble* (GUE) [37] and other random matrix ensembles.

Outline

This thesis is the compilation of four different research projects I investigated during my PhD. Each project corresponds to a chapter; the ordering aims to be pedagogical.

In Chapter 1, we review the connections between the partition functions of Aztec diamonds for general weightings and the *octahedron recurrence* [33]. This recurrence is a generalization of the Desnanot-Jacobi formula for determinants. We make use of the Dodgson condensation algorithm to compute the partition function of the model for different measures and subdomains. Many examples (old and new) are given. From this point of view, the tilings provide a combinatorial interpretation of λ-determinants and the general Robbins-Rumsey formula [38]. The link between Aztec diamonds and ASMs is also reviewed.

In Chapter 2, we use the technology introduce in the first chapter to obtain a closed formula for the partition function of the biased two-periodic Aztec diamonds in terms of elliptic functions [39]. We introduce and make the link with the *elliptic solid-on-solid* (8VSOS) model at the free-fermion point [40–42]. It allows us to use the inhomogeneous extension of the model to compute refined partition functions and consequently obtain the arctic curve of the model via the tangent method [43]. The main results are a parametric form and an algebraic equation for the curve. These parametrizations remain to be properly studied and the project is still ongoing. Let us mention that the main input to this project was made by Prof. Hjalmar Rosengren, who first pointed out to us a possible relation between biased two-periodic Aztec diamonds and the 8VSOS model, and later applied the two-refined tangent method to obtain the current conjecture on the arctic curve. I subsequently confirmed this result using the one-refined tangent method and, with the help of Prof. Philippe Ruelle, clarified the link between the two models. Prof. Christian Walmsley Hagendorf derived the general solution for the (r_k) sequence in terms of elliptic functions mentioned in Section 2.3.3 and deduced from it the partition function.

Links between uniform Aztec diamonds and random matrices are numerous in the literature. In particular [44, 45] established that, under correct rescaling, the probability density function of a certain subclass

of dominos converges to the GUE-corners (GUE minor) process in the large size limit. In Chapter 3, we are interested to see whether this result holds when we modify the probability measure on the space of configurations. In the first part, we look at the case of biased Aztec diamonds, where different weights are associated to vertical and horizontal dominos. In the second part, we examine the case of two-periodic weightings. In both situations, we observe the convergence to GUE-corners with a rescaling that depends on the weighting.

In Chapter 4, we study the dimer model on the infinite plane, and more specifically, investigate the field-theoretic structure for one- and two-periodic weightings. From one side, using the Kasteleyn's Pfaffian formula, we find a description based on Majorana fermions (more precisely, we obtain a ghost system from which the Majorana fermions are recovered as a special case). From another side, using the relations between the dimer model, spanning trees, and the sandpile model, we find a description in terms of symplectic fermions. The two-periodic measure being an off-critical extension of the uniform dimer model, the theories in this case are massive generalization of the corresponding CFTs.

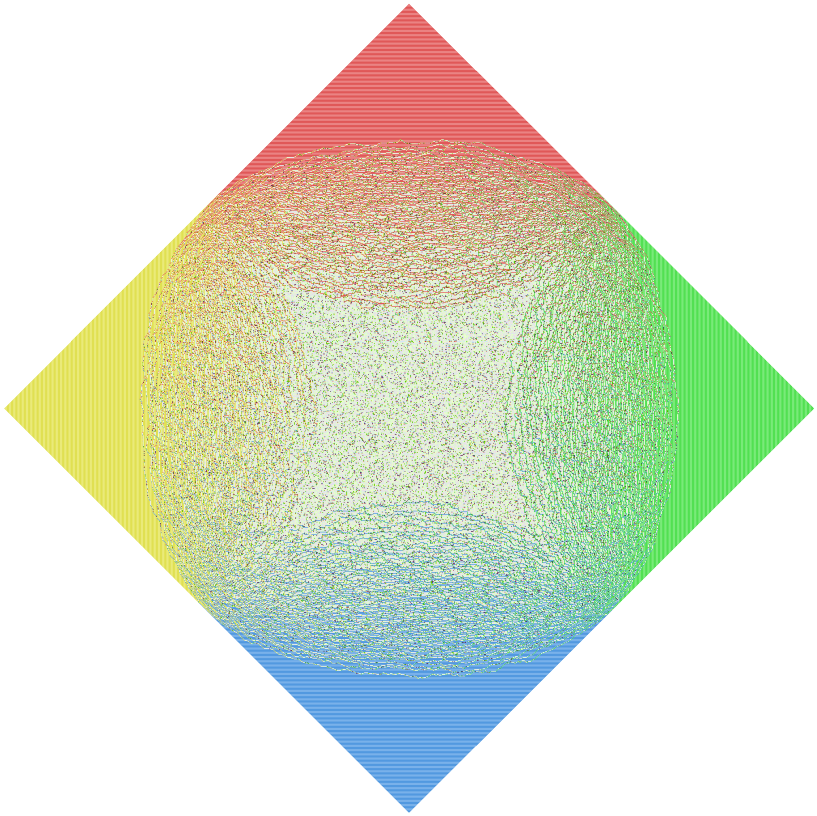

Figure 3: Aztec diamond tiling of order $n = 1000$ with two-periodic measure, $a/b = 2$. Eight colours are used to highlight the gaseous region. See Figure 3.5 for an accurate definition. We are grateful to Christophe Charlier for providing the code that generated this picture.

Chapter 1

On λ-determinants and tiling problems

This chapter uses material from [1] written with Philippe Ruelle and Jean-François de Kemmeter.

In this chapter, we review the connections between the octahedron recurrence, λ-determinants and tiling problems. This provides in particular a direct combinatorial interpretation of the λ-determinant (and generalizations thereof) of an arbitrary matrix in terms of domino tilings of Aztec diamonds. We also reinterpret the general Robbins-Rumsey formula for the rational function of consecutive minors, given by a summation over pairs of compatible alternating sign matrices, as the partition function for tilings of Aztec diamonds equipped with a general measure.

The λ-determinants have been introduced by Robbins and Rumsey [38] by generalizing the Desnanot-Jacobi formula for ordinary determinants. Let A be a square $n \times n$ matrix and denote by $A_{\mathrm{UL}}, A_{\mathrm{LL}}, A_{\mathrm{UR}}$, and A_{LR} the $(n-1)\times(n-1)$ restrictions of A to the upper-left, lower-left, upper-right and lower-right corners of A, and denote by A_{C} the $(n-2)\times(n-2)$ central restriction of A. The Desnanot-Jacobi identity reads

$$\det A \cdot \det A_{\mathrm{C}} = \det A_{\mathrm{UL}} \cdot \det A_{\mathrm{LR}} - \det A_{\mathrm{LL}} \cdot \det A_{\mathrm{UR}}. \tag{1.1}$$

Setting the determinant of an order zero matrix to 1 and that of an order 1 matrix equal to the matrix entry itself, this identity allows one to compute recursively the determinant of a matrix of any order (provided the required minors are non-zero). For $n = 2$, one easily recovers from (1.1) the usual form for the determinant of a 2×2 matrix on [46] has used the identity (1.1) to propose the condensation method, an efficient algorithm that reduces the computation of a determinant to the evaluation of connected 2×2 minors.

Robbins and Rumsey defined the λ-determinants, denoted by $\det_\lambda$, by deforming the above identity by the introduction of a complex parameter λ,

$$\det_\lambda A \cdot \det_\lambda A_{\mathrm{C}} = \det_\lambda A_{\mathrm{UL}} \cdot \det_\lambda A_{\mathrm{LR}} + \lambda \det_\lambda A_{\mathrm{LL}} \cdot \det_\lambda A_{\mathrm{UR}}. \quad (1.2)$$

The parameter λ does not affect the determinants of matrices of order 0 and 1, so that 2×2 λ-minors are simply given by

$$\det_\lambda \begin{pmatrix} a & b \\ c & d \end{pmatrix} = ad + \lambda\, bc, \quad (1.3)$$

from which λ-determinants of higher order can be evaluated recursively. Dodgson's condensation method applies equally well to the computation of λ-determinants provided λ-minors are used instead of usual minors. Let us briefly recall how this goes [46].

As mentioned above, the method computes the λ-determinant of a matrix A in a recursive manner, by defining a finite sequence of matrices of decreasing order. If A is $n \times n$, the sequence is initiated by setting $A_0 = (1)_{1 \leqslant i,j \leqslant n+1}$, the all-ones matrix of size $n + 1$, and $A_1 = A$. Then for $2 \leqslant k \leqslant n$, the matrix A_k, of size $n + 1 - k$, is obtained by computing all connected 2×2 λ-minors of A_{k-1} and dividing entrywise by the central submatrix of A_{k-2}. Explicitly the entries of A_k are given by

$$(A_k)_{i,j} = \frac{(A_{k-1})_{i,j}\,(A_{k-1})_{i+1,j+1} + \lambda\,(A_{k-1})_{i+1,j}\,(A_{k-1})_{i,j+1}}{(A_{k-2})_{i+1,j+1}}. \quad (1.4)$$

Then A_k is the matrix of all connected λ-minors of A of size k, so that the last term in the sequence yields the result, $A_n = \det_\lambda A$. The method proves to be very efficient but can be problematic since the entries by which we divide may vanish. When $\det_\lambda A$ is known to exist (like for

$\lambda = -1$), the problems can be cured by row or column permutations on A (meaningful only for $\lambda = -1$) or by regularization, see [47] for a short discussion in this direction. As a simple application, the λ-determinant of a general matrix of order 3 is found to be

$$\det_\lambda \begin{pmatrix} a_{11} & a_{12} & a_{13} \\ a_{21} & a_{22} & a_{23} \\ a_{31} & a_{32} & a_{33} \end{pmatrix} = a_{11}\, a_{22}\, a_{33} + \lambda\, a_{12}\, a_{21}\, a_{33} + \lambda\, a_{11}\, a_{23}\, a_{32}$$
$$+ \lambda^2 a_{12}\, a_{23}\, a_{31} + \lambda^2 a_{13}\, a_{21}\, a_{32} + \lambda^3 a_{13}\, a_{22}\, a_{31} + \lambda(1+\lambda)\frac{a_{12}\, a_{21}\, a_{23}\, a_{32}}{a_{22}}. \tag{1.5}$$

It is a textbook result that the ordinary determinant of an $n \times n$ matrix A can be written explicitly (and non-recursively) in terms of its entries a_{ij} as a sum over the symmetric group S_n, $\det A = \sum_{\sigma \in S_n} \varepsilon_\sigma\, A^{B(\sigma)}$; here ε_σ is the parity of the permutation σ, $B(\sigma)$ is the $n \times n$ permutation matrix associated with σ and A^B denotes the product $\prod_{1 \leqslant i,j \leqslant n} a_{ij}^{b_{ij}}$.

A natural question is thus whether there exists an analogous formula for λ-determinants. The result obtained by Robbins and Rumsey is not only that such a formula exists but also that the set of matrices playing the role of the permutation matrices in the case of ordinary determinants is universal, independent of $\lambda \neq -1$. It was in this context that alternating sign matrices made their appearance for the first time [22, 23]. An alternating sign matrix B is a square matrix with entries $-1, 0, 1$ such that all row and column sums are equal to 1, and such that the non-zero entries ± 1 alternate both in rows and columns. The set of alternating sign matrices of order n will be denoted by ASM_n (it contains in particular all permutation matrices $B(\sigma)$ of size n).

The remarkable formula proved in [38] reads,

$$\det_\lambda A = \sum_{B \in \mathrm{ASM}_n} \lambda^{P(B)}\, (1+\lambda)^{N_-(B)}\, A^B, \tag{1.6}$$

where $N_-(B)$ is the number of entries of B equal to -1 (later on, we will also use $N_+(B)$, the number of entries equal to $+1$), and $P(B) = \mathrm{Inv}(B) - N_-(B) \geqslant 0$ with the inversion number given by $\mathrm{Inv}(B) = \sum_{i<k} \sum_{j>\ell} b_{i,j} b_{k,\ell}$ (for a permutation σ, $\mathrm{Inv}(B(\sigma))$ is the minimal number of transpositions of adjacent elements by which σ can be obtained

from the identity). The number $P(B)$ has been given a more direct interpretation in [48], as the number of zeros in B which have non-zero entries to the right and below, and such that the first non-zero entry in both directions is a 1.

Comparing (1.6) with (1.5), one recognizes the first six terms as given by the six permutation matrices of size 3, while the last term involves the only alternating sign matrix of order 3 with a unique entry -1. For $\lambda = -1$, the summation reduces to alternating sign matrices with $N_-(B) = 0$, that is, to permutation matrices, so one recovers the usual formula quoted above. One also sees from the expression (1.6) that, except in the case $\lambda = -1$, the λ-determinant of a matrix involves positive and negative powers of its entries, and therefore may be undefined if some entries are zero. When λ is taken as an indeterminate, the λ-determinant of a generic matrix of size n is a polynomial in λ of degree $\frac{n(n-1)}{2}$.

The first indication of a relation between λ-determinants and tiling problems stems from the discovery by Kuo that the number T_n of domino tilings of an Aztec diamond of order n satisfies the following recurrence relation [49],

$$T_n\, T_{n-2} = 2T_{n-1}^2, \tag{1.7}$$

It is indeed reminiscent of the general form of the λ-Desnanot-Jacobi identity for a 1-determinant ($\lambda = 1$) if T_n can be written as $T_n = \det_1 A$ for a suitable matrix A (such that the two terms in the r.h.s. of (1.2) are equal). The boundary values $T_0 = 1$ and $T_1 = 2$ confirm that A can be taken to be the all-ones constant matrix of order $n+1$, leading to $T_n = 2^{n(n+1)/2}$. Even though the matrix A is very simple in this case, with all entries equal to 1, the summation in (1.6) is not trivial to evaluate since the alternating sign matrices get weighted according to the number of -1 they contain. The Dodgson condensation algorithm however furnishes the result in a straightforward way, as does the recurrence (1.7) itself.

If we want to assign different weights (or relative probabilities) to the domino tilings, the formulation in terms of perfect matchings of the dual Aztec graph is more convenient. Kuo showed in [49] that a quadratic recurrence relation similar to the Desnanot-Jacobi identity holds for a general weighting of the edges of the Aztec graph, and applied it in a few examples, among which a particular two-periodic weighting of the Aztec diamond and some other holey domains. Speyer [50] slightly generalized

Kuo's recurrence by adding face weights, and, placing it in a wider context, called it the octahedron recurrence (the term has been used earlier, though it is hard to trace its origin). As far as Aztec diamonds are concerned, both Kuo's and Speyer's articles write the quadratic recurrence relation for the most general weighting; the relation they found is a generalized form of the λ-Desnanot-Jacobi identity and leads to inhomogeneous λ-determinants [48], see Section 1.3.

Let us consider weighted perfect matchings of Aztec graphs, for which the weighting is defined in terms of face weights. In this case, the weight of a dimer in a given perfect matching is proportional to the inverse product of the weights of the faces it is adjacent to (see Section 1.1 for more details), and the weight of a perfect matching is the product of the weights of all dimers. In addition to these face weights, we assign each vertical dimer a bias in the form of an extra factor $\sqrt{\lambda}$. Let us symbolically denote by W the collection of all face weights, and by $T_n(W|\lambda)$ the partition function, that is, the sum of the weights of all perfect matchings of the order n Aztec graph. Then $T_n(W|\lambda)$ satisfies the octahedron recurrence [49, 50]

$$T_n(W|\lambda)\cdot T_{n-2}(W_{\mathrm{C}}|\lambda) = T_{n-1}(W_{\mathrm{UL}}|\lambda)\cdot T_{n-1}(W_{\mathrm{LR}}|\lambda) + \lambda\, T_{n-1}(W_{\mathrm{LL}}|\lambda)\cdot T_{n-1}(W_{\mathrm{UR}}|\lambda), \quad (1.8)$$

where the weight systems $W_{\mathrm{UL}}, W_{\mathrm{LR}}, W_{\mathrm{LL}}, W_{\mathrm{UR}}$ and W_{C} are the restrictions of W to the Aztec subgraphs in the four corners[1] and in the center, of order $n-1$ and $n-2$ respectively. When all weights are equal to 1, namely the distribution on perfect matchings is uniform, $T_n(W=1|\lambda=1)$ is just the number of domino tilings, and the previous recurrence reduces to (1.7).

The similarity of the octahedron recurrence and the Desnanot-Jacobi identity for λ-determinants is striking, and has been noticed by many authors. One should not expect that the solutions of the former can always be cast as λ-determinants (we will indeed see that this is not the case), but one can hope that λ-determinants can be given a combinatorial interpretation as partition functions of weighted perfect matchings. The

[1] If the central face of the order n graph is centered at the coordinates $(0,0)$, those of the four restrictions $\mathrm{UL}, \mathrm{LR}, \mathrm{LL}, \mathrm{UR}$ are centered at $(-1,0), (1,0), (0,-1), (0,1)$ respectively.

simplest example has been mentioned above, namely the 1-determinant of the all-ones matrix, $\det_1(a_{i,j}=1)_{1\leqslant i,j\leqslant n+1}$, is the number of perfect matchings of the order n Aztec graph. One can readily generalize it to any λ and get $\det_\lambda(a_{i,j}=1)_{1\leqslant i,j\leqslant n+1}=(1+\lambda)^{n(n+1)/2}$, the partition function for perfect matchings with bias $\sqrt{\lambda}$ for each vertical dimer. The latter has been noted by Propp in [47], who went further on to propose another example: if a number of 1's are replaced by 0's in the four corners of the all-ones matrix, the 1-determinant of the resulting matrix yields the number of domino tilings of a square of side n. This last example is a strong hint of a more general structure. To the best of our knowledge, no systematic combinatorial interpretation has been given to general λ-determinants in the context of domino tilings.

The main goal of this chapter is precisely to fill this gap, by giving several combinatorial interpretations of general λ-determinants in relation to perfect matchings of Aztec graphs. This will give us the opportunity to review basic and well-known material about alternating sign matrices in the context of tiling problems. Formulating the counting of perfect matchings in terms of λ-determinants, and more generally the partition functions when non-trivial weightings are used, does not always make their explicit evaluation easy. However this formulation offers an important conceptual understanding and at the same time provides an extremely versatile method, applicable to many cases that would otherwise be hard to tackle by standard methods. Finally, it gives a straight, computationally efficient and quick mean to obtain numerical results. Many illustrative examples will be given.

As a last remark, and because asymptotic values are in general more useful than exact values at finite size, the use of λ-determinants also prompts the intriguing question of whether Szegö limit theorems could be formulated for them, when applied to Toeplitz matrices.

1.1 General octahedron recurrence

The Aztec diamond of order n is a planar domain formed of unit cells with staircase boundaries; the left panel of Figure 1.1 depicts an order 6 Aztec diamond. The number of unit cells on the rows varies from 2

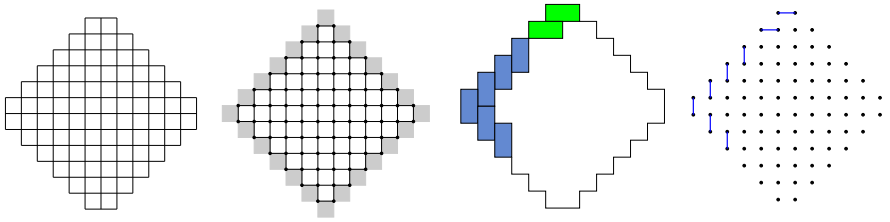

Figure 1.1: The two figures on the left show the Aztec diamond of order 6, and next to it, its extended dual graph $\widehat{\mathcal{A}}_n$ with the boundary faces (shaded). The two right figures show a partial domino tiling and the corresponding partial perfect matching of $\mathcal{A}_n$.

to $2n$. Domino tilings of Aztec diamonds can equally be described as perfect matchings of the dual graph $\mathcal{A}_n$: a perfect matching M of $\mathcal{A}_n$ is a subset of edges such that every vertex of the graph is the endpoint of one and only one edge in M. The edges of a perfect matching are also called dimers, see Figure 1.1 where a partial tiling and its dimer content are shown. Finally the graph $\mathcal{A}_n$ may be extended to $\widehat{\mathcal{A}}_n$ by including all faces around the boundary of $\mathcal{A}_n$, shown in shaded gray in Figure 1.1. The faces of $\widehat{\mathcal{A}}_n$ contained in $\mathcal{A}_n$ are called inner faces; the others are called boundary faces. Note that the extension $\widehat{\mathcal{A}}_n$ does not contain more edges or more vertices than $\mathcal{A}_n$.

Perfect matchings of Aztec graphs (or any graph) can be given different weights, which depend on their dimer content. We will consider here two types of weightings, $w_F(M)$ and $w_E(M)$, defined in terms of weights attached to the faces of the graph or attached to its edges. In what follows, we choose a coordinate system such that the faces of $\widehat{\mathcal{A}}_n$ are centered at integer coordinates (k, ℓ) with $|k| + |\ell| \leqslant n$; the central face is centered at $(0, 0)$.

In the first weighting, we assign each face (including the boundary faces) a weight $x_{k,\ell}$, see Figure 1.2. For each face (k, ℓ), we count the number $N_{k,\ell}$ of dimers which are adjacent to that face and let it contribute a factor $x_{k,\ell}^{1-N_{k,\ell}}$ to the weight of a perfect matching. The total weight of M is the product of these factors, $w_F(M) = \prod_{(k,\ell)\in\widehat{\mathcal{A}}_n} x_{k,\ell}^{1-N_{k,\ell}}$. We note that $1 - N_{k,\ell}$ is equal to $0, +1$ or -1 for an inner face and equal to 0 or $+1$ for a boundary face.

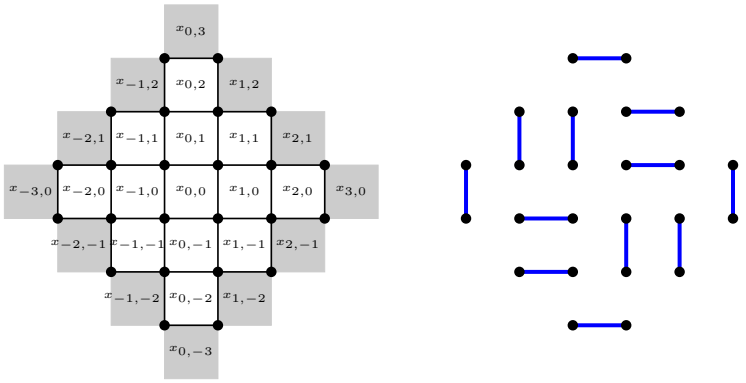

Figure 1.2: *Left*: the extended graph $\hat{\mathcal{A}}_3$ of order 3 with the face variables. *Right*: example of perfect matching with a face weight $w_F(M) = x_{1,-2}\, x_{-2,-1}\, x_{-1,-1}^{-1}\, x_{1,-1}^{-1}\, x_{0,0}\, x_{-1,1}^{-1}\, x_{1,1}^{-1}\, x_{2,1}\, x_{-1,2}$.

For the second weighting, all edges e of the graph are assigned a weight $w(e)$. The weight of a perfect matching is then the product of the weights of the edges contained in the matching, $w_E(M) = \prod_{e\in M} w(e)$. In practice, and because every edge is adjacent to an even face ($k+\ell$ even), it is enough to assign weights $\alpha_{k,\ell}, \beta_{k,\ell}, \gamma_{k,\ell}$ and $\delta_{k,\ell}$ to the east, north, west and south edges of the even faces. It will be convenient to assign edge weights to odd faces too. Since the east edge of an odd face is the west edge of the right neighbouring even face, we set $\alpha_{k,\ell} = \gamma_{k+1,\ell}$ for $k+\ell$ odd; similarly we set $\beta_{k,\ell} = \delta_{k,\ell+1}$, $\gamma_{k,\ell} = \alpha_{k-1,\ell}$ and $\delta_{k,\ell} = \beta_{k,\ell-1}$ for $k+\ell$ odd.

Both weightings $w_F(M)$ and $w_E(M)$ are complete in the sense that either weight uniquely determines M, and so are mutually redundant. We nevertheless keep them both since, depending on the specialization of weights we are interested in, one may be more convenient than the other. Let

$$T_{n;(0,0)} = \sum_{M \text{of} \mathcal{A}_n} w_F(M)\, w_E(M) = \sum_{M \text{of} \mathcal{A}_n} \prod_{(k,\ell)\in\widehat{\mathcal{A}}_n} x_{k,\ell}^{1-N_{k,\ell}} \times \prod_{e\in M} w(e) \tag{1.9}$$

be the partition function for perfect matchings of the Aztec graph of order n, with face and edge weights as defined above. The subscript $(0,0)$ indicates that the central face of the Aztec graph has weight $x_{0,0}$. Then the partition functions satisfy the following quadratic recurrence

relation [49, 50]

$$T_{n;(0,0)}\,T_{n-2;(0,0)} = \beta_{0,n-1}\,\delta_{0,1-n}\,T_{n-1;(-1,0)}\,T_{n-1;(1,0)} + \alpha_{n-1,0}\,\gamma_{1-n,0}\,T_{n-1;(0,-1)}\,T_{n-1;(0,1)}, \quad (1.10)$$

where $T_{k;(i,j)}$ is the partition function for the perfect matchings of the subgraph $\mathcal{A}_k \subset \mathcal{A}_n$ of order k whose central face has weight $x_{(i,j)}$, and computed with respect to the face and edge weights inherited from $\widehat{\mathcal{A}}_n$, so that $T_{k;(i,j)}$ depends on a subset of the weights used for $T_{n;(0,0)}$. As noted before, the order $n-1$ subgraphs centered at $(-1,0)$, $(1,0)$, $(0,-1)$ and $(0,1)$ correspond, after the rotation of the order n Aztec graph by 45 degrees clockwise so that the graph roughly looks like a square, to the UL, LR, LL and UR restrictions alluded to above in (1.8).

Together with the initial conditions for $n = 0$ and $n = 1$, namely,

$$T_{0;(i,j)} = x_{i,j}, \quad T_{1;(i,j)} = x_{i,j}^{-1}\,(\alpha_{i,j}\,\gamma_{i,j}\,x_{i,j-1}\,x_{i,j+1} + \beta_{i,j}\,\delta_{i,j}\,x_{i-1,j}\,x_{i+1,j}), \quad (1.11)$$

the partition functions for all higher values of n are uniquely determined. As n increases, the full expressions of $T_{n;(0,0)}$ become rapidly large and awkward.

At this level of generality, there does not seem to be any relation with λ-determinants because the coefficients of the two terms in the r.h.s. of the recurrence (1.10) both depend on n. In order to establish a relation, an easy start is to set the horizontal edge weights $\beta_{i,j}, \delta_{i,j}$ equal to 1 and the vertical edge weights $\alpha_{i,j}, \gamma_{i,j}$ equal to $\sqrt{\lambda}$. Although it considerably simplifies the expressions of the partition functions, it alone does not guarantee that the latter can be written as λ-determinants (of what matrix?). In general, they cannot as we will see in the next section, although algorithmically, the general case remains very close to a λ-determinant.

1.2 Face weights

In this section, we keep general face weights, for both inner and boundary faces, and restrict the edge variables to a constant weight $\sqrt{\lambda}$ on vertical dimers, which we call a vertical bias. A good starting point is to write

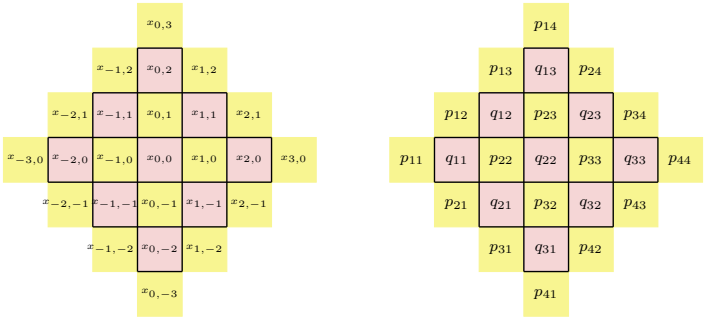

Figure 1.3: Relabelling of the general weights $x_{k,\ell}$ into $p_{i,j}$ and $q_{i,j}$ forming two matrices of order $n+1$ and n, respectively ($n = 3$ in the figures).

out the corresponding partition function for $n = 2$. Before doing that, it turns out to be more convenient to change coordinates and use different labels for even and odd faces. The new labelling is depicted in Figure 1.3.

The resulting labelling makes two matrices appear: a larger one, P, of order $n + 1$, whose entries are located on the yellow faces (of the same parity as n), and a smaller one, Q, of order n, whose entries occupy the red faces (of parity opposite to that of n).

We will refer to this as the (P, Q) weighting, and will denote the partition functions by $T_n(P, Q|\lambda)$, in which P and Q have respectively order $n+1$ and n. If we want to set all weights p_{ij} or q_{ij} to 1, we will write $P = 1$ or $Q = 1$ (not to be confused with the identity matrix $\mathbb{I}$); similarly we write P^{-1} or Q^{-1} for the matrices whose entries are p_{ij}^{-1} or q_{ij}^{-1}.

1.2.1 Restricted weights: λ-determinants

In terms of the (P, Q) weighting and the choice of edge weights $\alpha_{i,j} = \gamma_{i,j} = \sqrt{\lambda}$ and $\beta_{i,j} = \delta_{i,j} = 1$, the octahedron recurrence (1.10) reads

$$T_n(P,Q|\lambda)\,T_{n-2}(P_{\rm C},Q_{\rm C}|\lambda) = T_{n-1}(P_{\rm UL},Q_{\rm UL}|\lambda)\,T_{n-1}(P_{\rm LR},Q_{\rm LR}|\lambda) + \lambda\,T_{n-1}(P_{\rm LL},Q_{\rm LL}|\lambda)\,T_{n-1}(P_{\rm UR},Q_{\rm UR}|\lambda), \quad (1.12)$$

with initial conditions (for $n = 0$, the matrix Q has size zero and is represented by $-$)

$$T_0(p_{11}, -|\lambda) = p_{11}, \qquad T_1\left(\begin{pmatrix} p_{11} & p_{12} \\ p_{21} & p_{22} \end{pmatrix}, q_{11}\big|\,\lambda\right) = \frac{p_{11}\,p_{22} + \lambda\,p_{12}\,p_{21}}{q_{11}}. \tag{1.13}$$

Coming back to $n = 2$, the eight perfect matchings and their weights are listed below; the partition function $T_2(P, Q|\lambda)$ is the sum of the eight contributions.

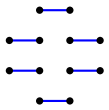
$= \dfrac{p_{11}\,p_{22}\,p_{33}}{q_{11}\,q_{22}}$

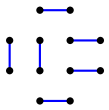
$= \lambda\,\dfrac{p_{12}\,p_{21}\,p_{33}}{q_{11}\,q_{22}}$

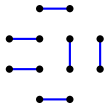
$= \lambda\,\dfrac{p_{11}\,p_{23}\,p_{32}}{q_{11}\,q_{22}}$

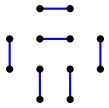
$= \lambda^2\,\dfrac{p_{12}\,p_{23}\,p_{31}}{q_{12}\,q_{21}}$

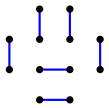
$= \lambda^2\,\dfrac{p_{13}\,p_{21}\,p_{32}}{q_{12}\,q_{21}}$

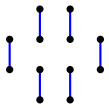
$= \lambda^3\,\dfrac{p_{13}\,p_{22}\,p_{31}}{q_{12}\,q_{21}}$

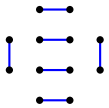
$= \lambda\,\dfrac{p_{12}\,p_{21}\,p_{23}\,p_{32}}{p_{22}\,q_{12}\,q_{21}}$

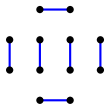
$= \lambda^2\,\dfrac{p_{12}\,p_{21}\,p_{23}\,p_{32}}{p_{22}\,q_{11}\,q_{22}}$

In agreement with the recurrence (1.12), one may indeed check that it is equal to

$$\begin{aligned} T_2(P, Q|\lambda) \;&=\; T_2\left(\begin{pmatrix} p_{11} & p_{12} & p_{13} \\ p_{21} & p_{22} & p_{23} \\ p_{31} & p_{32} & p_{33} \end{pmatrix}, \begin{pmatrix} q_{11} & q_{12} \\ q_{21} & q_{22} \end{pmatrix}\Big|\,\lambda\right) \\ &= \frac{T_1\left(\begin{pmatrix} p_{11} & p_{12} \\ p_{21} & p_{22} \end{pmatrix}, q_{11}\big|\,\lambda\right) \cdot T_1\left(\begin{pmatrix} p_{22} & p_{23} \\ p_{32} & p_{33} \end{pmatrix}, q_{22}\big|\,\lambda\right)}{T_0(p_{22}, -|\lambda)} \\ &\quad + \lambda\,\frac{T_1\left(\begin{pmatrix} p_{21} & p_{22} \\ p_{31} & p_{32} \end{pmatrix}, q_{21}\big|\,\lambda\right) \cdot T_1\left(\begin{pmatrix} p_{12} & p_{13} \\ p_{22} & p_{23} \end{pmatrix}, q_{12}\big|\,\lambda\right)}{T_0(p_{22}, -|\lambda)} \\ &= \frac{1}{p_{22}}\Big[\frac{p_{11}\,p_{22} + \lambda\,p_{12}\,p_{21}}{q_{11}} \cdot \frac{p_{22}\,p_{33} + \lambda\,p_{23}\,p_{32}}{q_{22}} \\ &\quad + \lambda\,\frac{p_{21}\,p_{32} + \lambda\,p_{22}\,p_{31}}{q_{21}} \cdot \frac{p_{12}\,p_{23} + \lambda\,p_{13}\,p_{22}}{q_{12}}\Big]. \end{aligned} \tag{1.14}$$

Comparing with the general expression (1.5) of the λ-determinant of a general matrix of order 3, one immediately observes that $T_2(P,1|\lambda) = \det_\lambda P$. Likewise for $P=1$, the partition function reads

$$T_2(1,Q|\lambda) = (1+\lambda)^2\Big[\frac{1}{q_{11}q_{22}} + \frac{\lambda}{q_{12}q_{21}}\Big] = (1+\lambda)^2 \det_\lambda(Q^{-1}). \quad (1.15)$$

This gives us a first general result.

Theorem 1.2.1. *The partition functions for perfect matchings of the order n Aztec graph with respect to the general (P,Q) weighting and vertical bias $\sqrt{\lambda}$ satisfy the following identities,*

$$T_n(P,1|\lambda) = \det_\lambda P, \qquad T_n(1,Q|\lambda) = (1+\lambda)^n \det_\lambda(Q^{-1}). \quad (1.16)$$

Proof. From (1.13), the two identities hold for $n = 0, 1$. (Note that for $n = 0$ and $n = 1$, P has size 1 and 2, whereas Q has size 0 and 1.) Therefore they hold for any n since in each case, both sides satisfy the same recurrence relations, given by (1.12) and (1.2) for the l.h.s. and for the r.h.s. respectively. □

In the rest of this section, we consider some applications of these two formulae.

1.2.2 Applications to periodic and biased Aztec diamonds

At a basic level, the partition function for all faces equal to 1 easily follows from Theorem 1.2.1.

Corollary 1.2.2. *[19, 47] The partition function $T_n(\lambda)$ for perfect matchings of the Aztec graph of order n with vertical bias $\sqrt{\lambda}$ is given by*

$$T_n(\lambda) = (1+\lambda)^{n(n+1)/2}. \quad (1.17)$$

Proof. Straightforward from the condensation algorithm since $T_n(\lambda) = T_n(1,1|\lambda)$ is the λ-determinant of the all-ones matrix of order $n+1$. The recurrence $T_n(\lambda) = (1+\lambda)^n T_{n-1}(\lambda)$ also follows by combining the two identities in (1.16). □

One may refine the previous result by restricting to those perfect matchings having a fixed number of vertical dimers along the NW boundary.

Corollary 1.2.3. *The refined partition function $T_{n,\ell}(\lambda)$ for the perfect matchings of the Aztec graph of order n which have exactly ℓ vertical dimers along the NW boundary is given by*

$$T_{n,\ell}(\lambda) = \binom{n}{\ell} \lambda^\ell \, (1+\lambda)^{n(n-1)/2}, \qquad 0 \leqslant \ell \leqslant n. \tag{1.18}$$

Proof. For any perfect matching, among the $n+1$ outer faces along the NW boundary, n are adjacent to one dimer and one is adjacent to none: the face with weight $p_{1,\ell+1}$ is adjacent to no dimer if the matching has exactly ℓ vertical dimers along the NW boundary, see Figure 1.1. Taking $P = 1$ except the first row set to $(p_{11}, p_{12}, \ldots, p_{1,n+1})$ and $Q = 1$, we obtain

$$T_n(P, 1|\lambda) = \sum_{\ell=0}^{n} p_{1,\ell+1} \, T_{n,\ell}(\lambda). \tag{1.19}$$

It follows that $T_{n,\ell}(\lambda) = \det_\lambda P_\ell$ where P_ℓ is the all-ones matrix except for the first row, equal to $(0, \ldots, 0, 1, 0, \ldots, 0)$ with the unique 1 in position $\ell + 1$. The condensation method is easily worked out to compute $\det_\lambda P_\ell$ and yields the result. □

According to the Robbins-Rumsey formula (1.6), the value $T_{n,\ell}(\lambda = 1)$ yields the 2-enumeration[2] of the alternating sign matrices of size $n+1$ which have the unique 1 in the first row at position $\ell + 1$ [51], while $T_n(\lambda = 1)$ yields the 2-enumeration of all alternating sign matrices of order $n+1$.

Corollary 1.2.4. *[33, 52] The partition function $T_n(a, b)$ for perfect matchings of the two-periodic Aztec graph of order n with parameters a, b and no vertical bias ($\lambda = 1$) is given by*

$$T_n(a,b) = \Big(\frac{2}{ab}\Big)^{\lfloor \frac{(n+1)^2}{4} \rfloor} (a^2+b^2)^{\lfloor \frac{n^2}{4} \rfloor} \times \begin{cases} 1 & \text{if } n = 0 \bmod 2, \\ b & \text{if } n = 1 \bmod 4, \\ a & \text{if } n = 3 \bmod 4. \end{cases} \tag{1.20}$$

[2] The 2-enumeration of a set S of alternating sign matrices is the weighted enumeration of S, where each matrix B of S contributes a factor $2^{N-(B)}$.

Proof. The two-periodic weighting of the Aztec graph of order n corresponds to $P = 1$ and Q the matrix with $q_{11} = a$ and the two parameters a, b alternating on rows and columns. As there is no bias, from Theorem 1.2.1, we can write $T_n(a, b)$ as the 1-determinant of Q^{-1}, namely,

$$T_n(a,b) = 2^n \det{}_1 Q^{-1} = 2^n \det{}_1 \begin{pmatrix} a^{-1} & b^{-1} & a^{-1} & \cdots \\ b^{-1} & a^{-1} & b^{-1} & \cdots \\ a^{-1} & b^{-1} & a^{-1} & \cdots \\ \vdots & \vdots & \vdots & \ddots \end{pmatrix}_{n\times n} . \quad (1.21)$$

Let us examine the condensation algorithm in order to compute this 1-determinant. The matrix Q^{-1} is a symmetric Toeplitz matrix, with two alternating quantities on the first row, which completely determine the whole matrix. The algorithm produces a sequence of matrices A_k of decreasing order, starting with $A_0 = 1$ and $A_1 = Q^{-1}$, all of which are symmetric Toeplitz matrices with two alternating quantities on the first row. Let us denote them by a_k and b_k, with $a_0 = b_0 = 1$ and $a_1 = a^{-1}$, $b_1 = b^{-1}$. The condensation algorithm implies that a_k and b_k satisfy the following coupled recurrence relations,

$$a_k = \frac{a_{k-1}^2 + b_{k-1}^2}{a_{k-2}}, \qquad b_k = \frac{b_{k-1}^2 + a_{k-1}^2}{b_{k-2}}, \quad (1.22)$$

and finishes with $a_n = \det_1 Q^{-1}$.

Defining $r_k \equiv b_k/a_k$, the first recurrence relation yields

$$\frac{a_k}{a_{k-1}} = \frac{a_{k-1}}{a_{k-2}}(1+r_{k-1}^2) = a^{-1}\,(1+r_1^2)\ldots(1+r_{k-2}^2)\,(1+r_{k-1}^2), \qquad k \geqslant 1. \quad (1.23)$$

Forming the telescopic product, we obtain, with $r_0 = 1$,

$$T_n(a,b) = 2^n\, a_n = a^{-n}\,(1+r_0^2)^n\,(1+r_1^2)^{n-1}\,(1+r_2^2)^{n-2}\ldots(1+r_{n-1}^2). \quad (1.24)$$

Taking the ratio of the two relations in (1.22), we see that r_k satisfies $r_k = r_{k-2}^{-1} = r_{k-4}$ and is therefore 4-periodic. From $r_0 = 1$ and $r_1 = \frac{a}{b}$, we obtain the explicit values $r_k = 1, \frac{a}{b}, 1, \frac{b}{a}$ for $k = 0, 1, 2, 3 \bmod 4$, from which the product in the previous equation is straightforward to evaluate and yields the result. □

Problem 1.2.5. *A natural and seemingly innocuous generalization of the previous result would be to add vertical bias and compute $T_n(a,b|\lambda)$. One would similarly find $T_n(a,b|\lambda) = (1+\lambda)^n \det_\lambda Q^{-1}$, and that likewise, the A_k matrices are symmetric Toeplitz with two alternating quantities in the first row. The bias variable λ enters the recurrence relations, which are now given by (the initial conditions remain unchanged and the definition of $r_k = b_k/a_k$ is the same)*

$$a_k = \frac{a_{k-1}^2 + \lambda\, b_{k-1}^2}{a_{k-2}}, \qquad b_k = \frac{b_{k-1}^2 + \lambda\, a_{k-1}^2}{b_{k-2}}, \qquad r_k = \frac{\lambda + r_{k-1}^2}{1+\lambda\, r_{k-1}^2}\,\frac{1}{r_{k-2}}. \tag{1.25}$$

Solve these to compute $a_n = \det_\lambda Q^{-1}$, and/or find the asymptotic value of a_n for large n.

Following the proof of Corollary 1.2.4, we readily obtain, for $k \geqslant 1$,

$$\frac{a_k}{a_{k-1}} = \frac{a_{k-1}}{a_{k-2}}(1+\lambda\, r_{k-1}^2) = a^{-1}\,(1+\lambda\, r_1^2)\ldots(1+\lambda\, r_{k-2}^2)\,(1+\lambda\, r_{k-1}^2), \tag{1.26}$$

from which the partition function for general values of a, b, λ follows,

$$T_n(a,b|\lambda) = (1+\lambda)^n\, a_n = a^{-n} \prod_{k=0}^{n-1} (1+\lambda\, r_k^2)^{n-k}. \tag{1.27}$$

We note that under the exchange of a and b, the two sequences (a_k) and (b_k) are interchanged, so that

$$T_n(b,a|\lambda) = (1+\lambda)^n\, b_n = r_n\, T_n(a,b|\lambda). \tag{1.28}$$

The determination of the partition functions for periodic Aztec graphs of order n with vertical bias $\sqrt{\lambda}$ only requires the knowledge of the n first terms in the sequence (r_k). However these are rational functions of λ and $t \equiv r_1 = \frac{a}{b}$ and become rapidly untractable, for instance r_4 is equal to

$$\frac{t^8\lambda^3 + t^6\,(2\lambda^3+3\lambda^2-2\lambda+1) + 3t^4\lambda\,(\lambda^2+1) + t^2\lambda\,(\lambda^3-2\lambda^2+3\lambda+2) + \lambda}{t^8\lambda + t^6\lambda\,(\lambda^3-2\lambda^2+3\lambda+2) + 3t^4\lambda\,(\lambda^2+1) + t^2\,(2\lambda^3+3\lambda^2-2\lambda+1) + \lambda^3}. \tag{1.29}$$

A partial solution to Problem 1.2.5 can be given as follows. Going back to the case $\lambda = 1$, one checks that the above expression for

r_4 collapses to 1, and that r_5 equals t, implying that the sequence $(r_k)_{k\geqslant 0}$ is 4-periodic, as noted above, and has a simple expression, $r_k = 1, t, 1, t^{-1}, 1, t, 1, t^{-1}, \ldots$ for $k \geqslant 0$. This suggests to see whether other values of λ make the sequence periodic. The conditions for the sequence to be p-periodic, $r_{k+p} = r_k$ for all $k \geqslant 0$, read $r_p = 1$ and $r_{p+1} = t$, or equivalently $r_{p-1} = t^{-1}$ and $r_p = 1$.

For $p = 2$, the two conditions yield $t = 1$ and a constant sequence $r_k = 1$; this corresponds to the usual, one-periodic measure with a vertical bias (one recovers the result of Corollary 1.2.2 up to a power of a). For higher values of p, the two conditions imply a polynomial relation between λ and t, the analysis of which can however be simplified. Indeed, we note that, when extended towards the negative values of k, the sequence (r_k) satisfies $r_{-k} = r_k^{-1}$, for all $k \geqslant 0$; this implies that a sequence which is p-periodic on $\mathbb{Z}_+$ is also p-periodic on $\mathbb{Z}$, $r_{k+p} = r_k$ for all $k \in \mathbb{Z}$. For even p, we have $r_{-p/2} = r_{p/2} = r_{p/2}^{-1}$ and therefore $r_{p/2}^2 = 1$; for odd p, we have similarly $r_{-(p+1)/2} = r_{(p-1)/2} = r_{(p+1)/2}^{-1}$. Restricting to positive sequences (t and λ are both positive), we see that in both cases, the p-periodicity implies a single condition,

$$r_{\frac{p-1}{2}} r_{\frac{p+1}{2}} = 1 \quad \text{for } p \text{ odd}, \qquad r_{\frac{p}{2}} = 1 \quad \text{for } p \text{ even}. \tag{1.30}$$

Conversely these relations alone imply a mirror-inversion property, $r_{p-k} = r_k^{-1}$, which itself implies $r_{p-1} = t^{-1}$, $r_p = 1$ and therefore the p-periodicity.

The resulting polynomial conditions are straightforward to compute. For p up to 12, by imposing (1.30), we find the following periodicity conditions, where $\tau_k \equiv t^k + t^{-k}$,

$$p = 3: \quad \lambda - (1+\tau_1) = 0, \tag{1.31a}$$

$$p = 4: \quad \lambda - 1 = 0, \tag{1.31b}$$

$$p = 5: \quad \lambda^3 - (3+2\tau_1+\tau_3)\,\lambda^2 + (1-2\tau_1-\tau_2)\,\lambda + (1+\tau_1+\tau_2) = 0, \tag{1.31c}$$

$$p = 6: \quad (1+\tau_1)\,\lambda - 1 = 0, \tag{1.31d}$$

$$\begin{aligned} p = 7: \quad & \lambda^6 - (6+3\tau_1+2\tau_3+\tau_5)\,\lambda^5 + (7-7\tau_1-5\tau_2-4\tau_3-\tau_4+\tau_5)\,\lambda^4 \\ & + (12\tau_2+5\tau_3+2\tau_4-\tau_5)\,\lambda^3 + (17+12\tau_1+5\tau_2-\tau_3+5\tau_4+\tau_5+\tau_6)\,\lambda^2 \\ & + (2-\tau_1+4\tau_2+3\tau_3)\,\lambda - (1+\tau_1+\tau_2+\tau_3) = 0, \end{aligned} \tag{1.31e}$$

$$p = 8: \quad \lambda^2 - (4+\tau_2)\,\lambda + 1 = 0, \tag{1.31f}$$

$$p = 9: \quad \lambda^9 - (9+3\tau_1+3\tau_3+2\tau_5+\tau_7)\,\lambda^8$$

$$
\begin{aligned}
&+(10-28\tau_1-20\tau_2-16\tau_3-10\tau_4-6\tau_5-4\tau_6+2\tau_7-\tau_8)\,\lambda^7\\
&-(74+50\tau_1+4\tau_2+35\tau_3+14\tau_4+5\tau_5+4\tau_6+9\tau_7-\tau_8+\tau_9)\,\lambda^6\\
&+(16-40\tau_1-56\tau_2-16\tau_3+8\tau_4-38\tau_5+8\tau_6-2\tau_7-\tau_8)\,\lambda^5\\
&-(16+5\tau_1-56\tau_2+44\tau_3+8\tau_4-18\tau_5+8\tau_6-\tau_7-\tau_8)\,\lambda^4\\
&+(74-22\tau_1+4\tau_2+42\tau_3+14\tau_4-4\tau_5+4\tau_6-\tau_8)\,\lambda^3\\
&-(10-28\tau_1-20\tau_2+17\tau_3-10\tau_4-\tau_5-4\tau_6-\tau_8)\,\lambda^2\\
&+(9-6\tau_1+6\tau_3)\,\lambda-(1+\tau_3)=0, \qquad (1.31g)
\end{aligned}
$$

$$
p=10: \quad (1+\tau_1+\tau_2)\,\lambda^3+(1-2\tau_1-\tau_2)\,\lambda^2-(3+2\tau_1+\tau_3)\,\lambda+1=0, \qquad (1.31h)
$$

$$
\begin{aligned}
p=11: \quad &\lambda^{15}-(15+5\tau+4\tau_3+3\tau_5+2\tau_7+\tau_9)\,\lambda^{14}+\ \ldots\ +\\
&-(1+\tau_1+\tau_2+\tau_3+\tau_4+\tau_5)=0, \qquad (1.31i)
\end{aligned}
$$

$$
p=12: \quad \lambda^4-(6+2\tau_2+\tau_4)\lambda^3-(8+8\tau_2+\tau_4)\lambda^2-(6+2\tau_2+\tau_4)\lambda+1=0. \qquad (1.31j)
$$

Remark 1. The conditions for $p=3$ and $p=6$ are related by $\lambda \leftrightarrow \lambda^{-1}$, and the same is true for $p=5$ and $p=10$. This relation between the conditions for p and $2p$ is general for p odd, and is a simple consequence of the fact that the inversion of λ keeps the odd terms of the sequence (r_k) invariant but inverts the even terms, $r_{2k+1}(\lambda^{-1},t)=r_{2k+1}(\lambda,t)$ and $r_{2k}(\lambda^{-1},t)=r_{2k}^{-1}(\lambda,t)$. Consequently, when one inverts the even terms in a p-periodic sequence, p odd, the new sequence $\tilde{r}_k$ ceases to be p-periodic because it satisfies $\tilde{r}_{\frac{p+1}{2}}=\tilde{r}_{\frac{p-1}{2}}$, and becomes $2p$-periodic since $\tilde{r}_p=1$. For p a multiple of 4, a p-periodic sequence remains p-periodic under $\lambda \leftrightarrow \lambda^{-1}$; the corresponding polynomial equation must therefore be invariant under the inversion of λ.

Remark 2. The mirror-inversion symmetry of a periodic sequence implies that for any p, the polynomials are invariant under $t \leftrightarrow t^{-1}$ since inverting t is equivalent to run the recurrence backwards, starting from $r_p=1$, $r_{p-1}=t^{-1}$ down to $r_1=t$, $r_0=1$. The middle conditions (1.30) are thus also invariant.

When the sequence (r_k) is periodic, the explicit calculation of the partition functions simplifies. We will denote the partition function by $T_n^{(p)}(a,b|\lambda)$ in case r_k is p-periodic. Let us note that for fixed p, this

leaves a finite number of possible values for λ in terms of $t = \frac{a}{b}$, namely the solutions of the polynomial equation for periodicity p. These partition functions satisfy the same relation under the exchange of a and b,

$$T_n^{(p)}(b, a|\lambda) = (1+\lambda)^n\, b_n = r_n\, T_n^{(p)}(a, b|\lambda). \tag{1.32}$$

Indeed the exchange of a and b inverts the value of t but preserves the polynomial equations, from Remark 2 above, and therefore the value of λ. The next result provides the explicit expression of $T_n^{(p)}(a, b|\lambda)$ for the three simplest cases, $p = 3$, 6 and 8, namely those for which t leaves one or two possible values for λ. In the other cases, the partition functions can be computed but their expressions remain complicated.

Corollary 1.2.6. *The partition functions $T_n^{(p)}(a, b|\lambda)$ with periodicity $p = 3$, 6 and 8 are given by,*

$$p=3 : T_n^{(3)}(a,b|\lambda) = \Big(\frac{a+b}{ab}\Big)^{\lfloor\frac{(2n+1)(n+1)}{3}\rfloor} (a^2+b^2)^{\lfloor\frac{n^2}{3}\rfloor} \times (1, b, a) \quad \textit{for} \quad n = (0,1,2) \bmod 3, \tag{1.33a}$$

$$p=6 : T_n^{(6)}(a,b|\lambda) = \Big(\frac{a+b}{ab}\Big)^{\lfloor\frac{(2n+1)(n+1)}{3}\rfloor} (a^2+b^2)^{\lfloor\frac{n^2}{3}\rfloor} \Big(\frac{ab}{a^2+ab+b^2}\Big)^{\frac{n(n+1)}{2}} \times (1, b, b, 1, a, a) \quad \textit{for} \quad n = (0,1,2,3,4,5) \bmod 6, \tag{1.33b}$$

$$p=8 : T_n^{(8)}(a,b|\lambda) = (ab)^{-\lfloor\frac{n+1}{2}\rfloor} \Big(\frac{a^2+b^2}{ab}\Big)^{\lfloor\frac{3n^2}{8}\rfloor} \lambda^{\lfloor\frac{n^2}{8}\rfloor} (1+\lambda)^{\lfloor\frac{(n+1)^2}{4}\rfloor} \times \Big(1, b, \tfrac{\lambda a^2+b^2}{a^2+b^2}, b, 1, a, \tfrac{a^2+\lambda b^2}{a^2+b^2}, a\Big) \quad \textit{for} \quad n = (0,1,2,3,4,5,6,7) \bmod 8. \tag{1.33c}$$

Proof. When $p = 3$ and $p = 6$, λ is uniquely fixed to $(1+t+t^{-1})^{\pm 1}$ and the sequences (r_k) explicitly read 1, t, $t^{-1}, \ldots$ and 1, t, t, 1, t^{-1}, $t^{-1}, \ldots$ respectively. For $p = 8$, it is given by

$$1,\ t,\ \frac{\lambda + t^2}{1 + \lambda\, t^2},\ t,\ 1,\ t^{-1},\ \frac{1 + \lambda\, t^2}{\lambda + t^2},\ t^{-1},\ \ldots \tag{1.34}$$

with λ one of the two roots of (1.31f). In each case the product in (1.27) is then easily computed. □

Remarkably, the polynomial expressions in (1.31) exactly reproduce[3] certain polynomial relations in [39], which the authors obtain when characterizing the finite periodicity of a flow defined in terms of translations in an elliptic curve depending on λ and t. This is rather surprising because, being related to the iteration of a Wiener-Hopf factorization, the periodicity considered in [39] has a totally different origin from ours. It would be interesting to understand and connect the two points of view. We collect in Appendix 1.A some of the facts about the sequence (r_k) which partially clarify the connection; at this stage however, we do not claim a full understanding.

In fact, it turns out that the two sequences (a_k) and (b_k) exhibit a rather natural relation with the curve studied in [39]. As pointed out to us by Michael Somos, (a_k) and (b_k) are Somos-4 sequences, which themselves can be quite generally related to translational flows on elliptic curves [53]. For the specific sequences (a_k) and (b_k) defined in (1.25), the relevant elliptic curve is precisely the curve discussed in [39]; we refer to the Appendix 1.A for more details. In Appendix 1.B, we give a combinatorial proof that (a_k) and (b_k) are Somos-4 sequences

Comment. At the time we concluded this work on λ-determinants, our understanding of the situation was the one described above. Since then, we continued the study of the (r_k) sequence and C. Walmsley Hagendorf helped us to find an explicit solution in terms of *theta functions* leading to a closed formula for the partition function valid for any λ and t. The pursue of this work was fruitful and led to another collaboration which constitutes the second chapter of this thesis. In particular, the general solution of the (r_k) sequence is given in Section 2.3.3.

1.2.3 Applications to subgraphs of Aztec diamonds

Theorem 1.2.1 can be used to compute the number of perfect matchings of subgraphs of Aztec graphs, as noticed by Propp and mentioned in the Introduction.

Corollary 1.2.7. *[47] The partition function for perfect matchings of a square grid of size $2n$ with vertical bias $\sqrt{\lambda}$ is equal to $\lambda^{-n(n-1)/2}\ \det_\lambda P_{\mathrm{sq}}$,*

[3] There are some differences, due to the assumption $0 < \lambda < 1$ made in [39].

where $P_{\rm sq}$ is the all-ones matrix of order $2n$ in the corners of which 1's are replaced by 0's.

Proof. Let us consider a square grid of size $2n$-by-$2n$ (the size refers to the number of vertices in each row and each column; it coincides with the size of the square domain tiled by dominos, and materialized in Figure 1.4 by the shaded square). As one can see in Figure 1.4 for $n = 3$, it can be embedded in an Aztec graph of order $2n - 1$ or $2n$. We discuss the first option as the second one is a bit less economical. To reduce the Aztec graph to the square subgraph, the trick is to choose the face weights in such a way that the region which is exterior to the square is totally frozen. A simple way to achieve this is to set to zero the variables of all the faces shown in yellow, because this freezes the dimer arrangement in the four corners, leaving the central square free, as shown in Figure 1.4. To see this, one notes that the yellow boundary faces must be adjacent to a single dimer (they cannot be adjacent to two dimers, and if one was adjacent to no dimer, its zero face weight would bring a vanishing contribution). This fixes the dimers along the boundaries of the four corners, and in turn forces a similar arrangement in the corners. Thus each yellow face is adjacent to a single dimer and contributes a face factor equal to 1. In terms of the (P, Q) weighting, this choice of face weights corresponds to take $Q = 1$ and $P = P_{\rm sq}$ obtained from the all-ones matrix of size $2n$ by inserting in the four corners triangular arrays full of 0's. The number of 0's in each corner is $\frac{n(n-1)}{2}$.

Finally the λ-determinant of $P_{\rm sq}$ includes the vertical bias $\sqrt{\lambda}$ for each of the $n(n-1)$ vertical dimers in the W and E corners. Dividing by $\lambda^{n(n-1)/2}$ yields the required partition function.

We note that because $P_{\rm sq}$ contains many zeros, the condensation algorithm will output undeterminate ratios at intermediate steps. It may be regularized by replacing all zeros in $P_{\rm sq}$ by a formal variable t. The above argument (no yellow face can be adjacent to two dimers) ensures that the λ-determinant of the new $P_{\rm sq}$ is a polynomial in t. Its limit for t going to zero yields the correct result. □

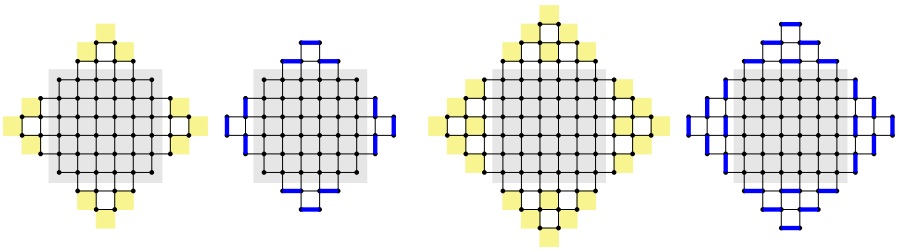

Figure 1.4: *Left:* the figure shows an Aztec diamond of order 5 with, in gray, the square subgraph of size 6. *Right:* the same square subgraph is embedded in a diamond of order 6. In both cases, the yellow faces are those for which the face variable is set to zero, forcing the arrangement of blue dimers.

More examples of this kind may be given, including rectangular subgraphs. For instance, taking $Q = 1$ and for P the tridiagonal matrix of size $n+1$ with ones on the three main diagonals, we obtain the Fibonacci polynomials[4], $\det_\lambda P = F_{2n+1}(\sqrt{\lambda})$, namely the partition function for biased perfect matchings of a $2 \times 2n$ rectangular graph. The following example concerns the holey Aztec diamond.

Let us denote by $p_i(n)$, for $i = 0, 1, 2$, the fractions of perfect matchings of the Aztec graph of order n which have i dimers adjacent to the central face. In order to compute these fractions, we attach a weight 1 to all faces of the Aztec graph, except the central face which is assigned a weight t. The central face belongs to a size $n+1$ matrix P_t if n is even or to a size n matrix Q_t if n is odd, where both P_t and Q_t are all-ones matrices with t as central entry. The corresponding partition function $T_n[t]$ takes the form (recall that $T_n = 2^{n(n+1)/2}$ is the partition function for $t = 1$)

$$T_n[t] = \Big(p_0(n)\, t + p_1(n) + \frac{p_2(n)}{t}\Big)\, T_n, \tag{1.35}$$

and, from Theorem 1.2.1, can be computed as $T_n[t] = \det_1 P_t$ if n is even, or $T_n[t] = 2^n \det_1 Q_t^{-1} = 2^n \det_1 Q_{t^{-1}}$ if n is odd.

In addition to the fact that the three numbers $p_i(n)$ sum up to 1, they satisfy an additional non-trivial identity, derived by Propp [54] and gen-

[4]The Fibonacci polynomials satisfy $F_{n+1}(x) = xF_n(x) + F_{n-1}(x)$ with $F_1(x) = 1$ and $F_2 = x$.

eralized by Kuo [49]. For any face of a planar graph bordered by four edges, it relates the fraction of perfect matchings for which the face is adjacent to two dimers and the fractions of those for which a dimer is on one of the four edges. In the present case, the identity reads

$$4p_2(n) = \big[p_1(n) + 2p_2(n)\big]^2. \tag{1.36}$$

Expressing $p_0 = (1-\sqrt{p_2})^2$ and $p_1 = 2\sqrt{p_2}(1-\sqrt{p_2})$ in terms of p_2, we obtain

$$L_n(t) \equiv \frac{T_n[t]}{T_n} = \frac{1}{t}\left[\sqrt{p_2(n)} + \left(1-\sqrt{p_2(n)}\right)t\right]^2. \tag{1.37}$$

Let us now fix n to be even. Since the matrix P_t used for n even is identical to the matrix Q_t used for $n+1$, we obtain, using $T_{n+1} = 2^{n+1}\,T_n$,

$$L_n(t) = \frac{\det_1 P_t}{T_n} = \frac{\det_1 Q_t}{T_n} = 2^{-(n+1)}\,\frac{T_{n+1}[t^{-1}]}{T_n} = \frac{T_{n+1}[t^{-1}]}{T_{n+1}} = L_{n+1}(t^{-1}). \tag{1.38}$$

This provides a very simple proof that[5]

$$p_i(n+1) = p_{2-i}(n), \qquad \text{for all } n \text{ even}. \tag{1.39}$$

It is therefore sufficient to focus on n even. Let us write

$$L_n(t) = \frac{1}{4t}\Big[(1-\alpha_n) + (1+\alpha_n)t\Big]^2, \qquad 1-\alpha_n = 2\sqrt{p_2(n)}. \tag{1.40}$$

Explicit numerical calculations of 1-determinants led us to formulate a conjecture for the numbers α_n, which we subsequently proved.

Corollary 1.2.8. *The numbers α_n in the sequence given in (1.40) are given by $2^{-n}\binom{n/2}{n/4}^2$ for $n = 0 \bmod 4$, and by 0 for $n = 2 \bmod 4$; for n odd, they are equal to $\alpha_n = -\alpha_{n-1}$.*
It follows that the three fractions $p_i(n)$, for n even, are given by

$$(p_0, p_1, p_2) = \begin{cases} \dfrac{1}{4}\left[1 + 2^{-n}\left(\dfrac{\frac{n}{2}}{\frac{n}{4}}\right)^2\right]^2, \dfrac{1}{2}\left[1 - 2^{-2n}\left(\dfrac{\frac{n}{2}}{\frac{n}{4}}\right)^4\right], \dfrac{1}{4}\left[1 - 2^{-n}\left(\dfrac{\frac{n}{2}}{\frac{n}{4}}\right)^2\right]^2, \\ \dfrac{1}{4}, \dfrac{1}{2}, \dfrac{1}{4}, \end{cases} \tag{1.41}$$

[5] This relation also directly follows by using the shuffling algorithm to go from order n to order $n+1$.

for $n = 0 \bmod 4$ and $n = 2 \bmod 4$ respectively. For n odd, the fractions are related to the previous ones by $p_i(n) = p_{2-i}(n-1)$.
From the Robbins-Rumsey formula (1.6), the numbers $2^{n(n+1)/2} p_i(n)$ for n even are the 2-enumeration of the alternating sign matrices of size $n+1$ having their central entry equal to $1-i$, and similarly, $2^{n(n-1)/2} p_i(n)$ for n odd yields the 2-enumeration of the alternating sign matrices of size n having their central entry equal to $i-1$.

Proof. Ciucu has provided a proof that $p_2(n) = \frac{1}{4}$ when $n = 2, 3 \bmod 4$ [55], and also mentions a proof by Propp for all values of n, which, as far as we know, has remained unpublished. Here we present a unified proof based on the trivariate generating function for one minus the average number of dimers adjacent to the face (i, j) in the Aztec graph of order n, that is, for the numbers $p_0(i, j; n) - p_2(i, j; n)$.

By using the octahedral recurrence, they satisfy a Laplacian-like linear recurrence which allows one to determine the generating function. This function has been computed in [33] to which we refer for the details. In our notations, it reads

$$\begin{aligned} G(x, y, z) &= \sum_{n=0}^{\infty} \sum_{i,j=-n}^{n} [p_0(i, j; n) - p_2(i, j; n)] x^i \, y^j \, z^n \\ &= \frac{1 - z}{1 + z^2 - \frac{z}{2}(x + x^{-1} + y + y^{-1})}. \end{aligned} \tag{1.42}$$

For $i = j = 0$, the coefficients reduce to $p_0(n) - p_2(n)$. With the identity (1.36) and the relation $p_0 + p_1 + p_2 = 1$, a proof that $p_0 - p_2 = 0$ or $\pm 2^{-n} \binom{n/2}{n/4}^2$ is enough to prove (1.41).

Let us first omit the term $-z$ in the numerator of G. The nth z-derivative at $z = 0$ yields (using e.g. Faà di Bruno's formula for the multiple derivative of the composition of two functions),

$$\begin{aligned} p_0(n) - p_2(n) &= \frac{1}{1 + z^2 - \frac{z}{2}(\dots)} \Big|_{x^0, y^0, z^n} \\ &= 2^{-n} \sum_{r=0}^{\lfloor \frac{n}{2} \rfloor} (-4)^r \binom{n-r}{r} (x + x^{-1} + y + y^{-1})^{n-2r} \Big|_{x^0, y^0} \\ &= 2^{-n} \sum_{r=0}^{\frac{n}{2}} (-4)^r \binom{n-r}{r} \binom{n-2r}{\frac{n}{2} - r}^2 \delta_{n,\text{even}} \end{aligned}$$

$$= (-1)^{\frac{n}{2}} \sum_{k=0}^{\frac{n}{2}} (-\tfrac{1}{4})^k \binom{\frac{n}{2}+k}{2k} \binom{2k}{k}^2 \delta_{n,\text{even}}. \tag{1.43}$$

This proves that the function $\left[1+z^2-\frac{z}{2}(x+x^{-1}+y+y^{-1})\right]^{-1}$ has only even powers of z upon taking the constant terms in x, y. The term $-z$ in the numerator of $G(x,y,z)$ then produces the odd terms and readily implies $p_0(n)-p_2(n) = -\left[p_0(n-1)-p_2(n-1)\right]$ for n odd. The remaining sum in (1.43) for n even is, up to a sign, a specialization of the following family of polynomials,

$$f_m(x) = \sum_{k=0}^{m} \binom{m+k}{2k} \binom{2k}{k}^2 x^k. \tag{1.44}$$

These have been shown [56] to satisfy the identity $f_m(y(1+y)) = \left[P_m(2y+1)\right]^2$ in terms of the Legendre polynomials P_m. Substituting m for $\frac{n}{2}$ and taking $x = -\frac{1}{4}$, $y = -\frac{1}{2}$, we obtain, for n even,

$$\begin{aligned} p_0(n) - p_2(n) &= (-1)^{\frac{n}{2}}\, f_{\frac{n}{2}}(-\tfrac{1}{4}) = (-1)^{\frac{n}{2}}\, \left[P_{\frac{n}{2}}(0)\right]^2 \\ &= \begin{cases} 2^{-n} \binom{\frac{n}{2}}{\frac{n}{4}}^2 & \text{if } n = 0 \bmod 4, \\ 0 & \text{if } n = 2 \bmod 4. \end{cases} \end{aligned} \tag{1.45}$$

This concludes the proof. □

1.2.4 General weights: the generalized Robbins-Rumsey formula

Theorem 1.2.1 readily implies that to any perfect matching of the Aztec diamond of order n, one can associate two alternating sign matrices, of size n and $n+1$ [19].

In the case of a $(P,1)$ weighting, the λ-determinant formula implies that every perfect matching of an Aztec diamond of order n can be associated with an alternating sign matrix B of order $n+1$. Indeed, by comparing the weight $\prod_{i,j} p_{ij}^{1-N_{i,j}}$ of a perfect matching with the factor $P^B = \prod_{i,j} p_{ij}^{b_{ij}}$ in the Robbins-Rumsey formula, we obtain $b_{ij} = 1 - N_{i,j}$ for all p_{ij} faces (yellow faces in Figure 1.3). An example is shown in Figure 1.5

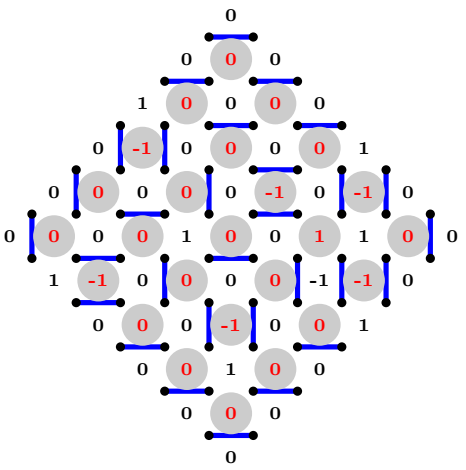

$$B = \begin{pmatrix} 0 & 0 & 0 & 1 & 0 & 0 \\ 1 & 0 & 0 & 0 & 0 & 0 \\ 0 & 0 & 1 & 0 & 0 & 0 \\ 0 & 0 & 0 & 0 & 0 & 1 \\ 0 & 1 & 0 & -1 & 1 & 0 \\ 0 & 0 & 0 & 1 & 0 & 0 \end{pmatrix}$$

$$B' = \begin{pmatrix} 0 & 0 & 1 & 0 & 0 \\ 1 & 0 & 0 & 0 & 0 \\ 0 & 0 & 0 & 1 & 0 \\ 0 & 1 & 0 & -1 & 1 \\ 0 & 0 & 0 & 1 & 0 \end{pmatrix}$$

Figure 1.5: On the left are shown a perfect matching of the Aztec diamond of order 5 and, on each face, the value of 1 minus the number of dimers adjacent to that face. The associated alternating sign matrices B and B' contain respectively the numbers in black and the opposite of those in red in shaded circles.

in which the matrix B is written in black. While it is manifest from this correspondence that the first and last rows and columns contain no -1 (and therefore a single 1), it is not so clear that the matrix so obtained is actually sign alternating; by thinking about the ways the dimers must be arranged around a face with $N_{i,j} = 0$ or 2, it is not too difficult to convince oneself that it is. The correspondence is not bijective: a matrix B is associated with $2^{N_-(B)}$ distinct matchings. Indeed an entry $b_{ij} = -1$ is attached to a face which is adjacent to two dimers; such a face can be flipped to produce a matching that is distinct but of equal weight (a flip is a rotation of two parallel dimers located around a face). With a vertical bias $\sqrt{\lambda}$, the two matchings related by a flip contribute a relative factor equal to 1 and λ, so that every entry -1 in B contributes an overall factor $1 + \lambda$; this gives a simple combinatorial explanation of the factor $(1+\lambda)^{N_-(B)}$ in the Robbins-Rumsey formula (1.6). As for the factor $\lambda^{P(B)} = \lambda^{\mathrm{Inv}(B)-N_-(B)}$ we note that $\mathrm{Inv}(B)$ is half the maximal number of vertical dimers among the $2^{N_-(B)}$ distinct matchings obtained from each other by flips at the faces where $b_{ij} = -1$.

The λ-determinant formula for the $(1, Q)$ weighting leads to a similar correspondence. However because $T_n(1, Q|\lambda)$ is proportional to the λ-determinant of Q^{-1}, identifying the weight $\prod_{i,j} q_{ij}^{1-N_{i,j}}$ of a perfect matching with the factor $Q^{-B'}$ in the Robbins-Rumsey formula, leads to an alternating sign matrix B' of order n given by $b'_{ij} = N_{i,j} - 1$ for all the q_{ij} faces, see Figure 1.5. The prefactor $(1+\lambda)^n$ and the term $(1+\lambda)^{N_-(B')}$ nicely combine to give

$$\begin{aligned} T_n(1, Q|\lambda) &= (1+\lambda)^n \sum_{B' \in \mathrm{ASM}_n} \lambda^{P(B')} (1+\lambda)^{N_-(B')} Q^{-B'} \\ &= \sum_{B' \in \mathrm{ASM}_n} \lambda^{P(B')} (1+\lambda)^{N_+(B')} Q^{(-B')}. \end{aligned} \tag{1.46}$$

This preserves the above combinatorial interpretation of the power of $1+\lambda$, since the flippable faces are now associated to the entries $+1$ of B', in number equal to $N_+(B')$.

Except if B is a permutation matrix, neither B nor B' completely determines the perfect matching it is associated with, but the pair (B, B') does; one of the proofs in [19] for the number of domino tilings of Aztec diamonds is precisely based on this bijection (from what follows, the smaller matrix B' alone never determines completely the perfect matching). Because the two matrices B and B' are defined from a single matching, they ought to be related in some way; indeed such a pair of alternating sign matrices has been called compatible in [38]. An algebraic criterion for compatibility has been given in [38], in the form of inequalities (see below), but the notion of compatibility is easier to understand in terms of perfect matchings, since it merely reduces to the fact that the pair (B, B') is unambiguously associated with a perfect matching in the way described above. The number of pairs of compatible matrices, indicated by $B \approx B'$, and their explicit construction when one of the two is given, is as follows.

As explained above, an arbitrary alternating sign matrix B of size $n+1$ fixes the arrangement of dimers around the p-faces, except at the faces p_{ij} adjacent to two dimers, where $b_{ij} = -1$. Any choice at each of these faces, two horizontal or two vertical dimers, fixes one of the $2^{N_-(B)}$ perfect matchings compatible with B, and produces that many different alternating sign matrices B' by reading off the values $N_{ij} - 1$ at the q_{ij} faces. If B is a permutation matrix, $N_-(B) = 0$, there is a unique matrix

B' compatible with B because B alone determines a unique perfect matching.

In a similar way, an alternating sign matrix B' of size n completely determines the dimer arrangement around the q-faces, except when a face q_{ij} is adjacent to two dimers, where $b'_{ij} = 1$. This time, all possible choices at those faces yield a total of $2^{N_+(B')}$ different perfect matchings and so many matrices B. In conclusion, we have

$$\#\,\text{compatible pairs } (B, B') = \begin{cases} 2^{N_-(B)} & \text{for fixed } B, \\ 2^{N_+(B')} & \text{for fixed } B'. \end{cases} \tag{1.47}$$

At this stage, the picture we have is the following. We have two (partial) face weightings for perfect matchings of the Aztec diamond of order n, defined by $(P, 1)$ and $(1, Q)$ respectively. Upon the addition of a vertical bias $\sqrt{\lambda}$, the corresponding partition functions are given by λ-determinants, which, together, give rise to a bijection between the set of perfect matchings and pairs of compatible alternating sign matrices (B, B'), of size $n+1$ and n. Can one then write the partition function for a general weighting (P, Q) in terms of pairs of compatible alternating sign matrices ?

To see this, let us come back to the expressions, for $n = 0, 1, 2$, of the partition functions for general weightings, given earlier in (1.13) and (1.14),

$$T_0(p_{11}, -|\lambda) = p_{11}, \qquad T_1\left(\begin{pmatrix} p_{11} & p_{12} \\ p_{21} & p_{22} \end{pmatrix}, q_{11}|\,\lambda\right) = \frac{p_{11}\,p_{22} + \lambda\,p_{12}\,p_{21}}{q_{11}},$$

$$T_2\left(\begin{pmatrix} p_{11} & p_{12} & p_{13} \\ p_{21} & p_{22} & p_{23} \\ p_{31} & p_{32} & p_{33} \end{pmatrix}, \begin{pmatrix} q_{11} & q_{12} \\ q_{21} & q_{22} \end{pmatrix}\Big|\,\lambda\right) = \frac{1}{p_{22}}\Big[\frac{p_{11}\,p_{22} + \lambda\,p_{12}\,p_{21}}{q_{11}} \times$$
$$\times\,\frac{p_{22}\,p_{33} + \lambda\,p_{23}\,p_{32}}{q_{22}} + \lambda\,\frac{p_{21}\,p_{32} + \lambda\,p_{22}\,p_{31}}{q_{21}} \cdot \frac{p_{12}\,p_{23} + \lambda\,p_{13}\,p_{22}}{q_{12}}\Big]. \tag{1.48}$$

One may observe that T_1 and T_2 are obtained from T_0 by successive substitutions. Indeed T_1 is obtained from T_0 by the substitution

$$p_{11} \longrightarrow \frac{p_{11}\,p_{22} + \lambda\,p_{12}\,p_{21}}{q_{11}}. \tag{1.49}$$

Then T_2 is obtained from T_1 by the further substitution, for $1 \leqslant i, j \leqslant 2$

$$q_{11} \longrightarrow p_{22} \qquad \text{and} \qquad p_{ij} \longrightarrow \frac{p_{ij}\, p_{i+1,j+1} + \lambda\, p_{i,j+1}\, p_{i+1,j}}{q_{ij}}. \tag{1.50}$$

In the next step, T_3, given by

$$T_3\left(\begin{pmatrix} p_{11} & p_{12} & p_{13} & p_{14} \\ p_{21} & p_{22} & p_{23} & p_{24} \\ p_{31} & p_{32} & p_{33} & p_{34} \\ p_{41} & p_{42} & p_{43} & p_{44} \end{pmatrix}, \begin{pmatrix} q_{11} & q_{12} & q_{13} \\ q_{21} & q_{22} & q_{23} \\ q_{31} & q_{32} & q_{33} \end{pmatrix} \Big| \lambda\right) = \frac{1}{T_1\left(\begin{pmatrix} p_{22} & p_{23} \\ p_{32} & p_{33} \end{pmatrix}, q_{22} \Big| \lambda\right)} \times$$

$$\times \left\{ T_2\left(\begin{pmatrix} p_{11} & p_{12} & p_{13} \\ p_{21} & p_{22} & p_{23} \\ p_{31} & p_{32} & p_{33} \end{pmatrix}, \begin{pmatrix} q_{11} & q_{12} \\ q_{21} & q_{22} \end{pmatrix} \Big| \lambda\right) \cdot T_2\left(\begin{pmatrix} p_{22} & p_{23} & p_{24} \\ p_{32} & p_{33} & p_{34} \\ p_{42} & p_{43} & p_{44} \end{pmatrix}, \begin{pmatrix} q_{22} & q_{23} \\ q_{32} & q_{33} \end{pmatrix} \Big| \lambda\right) \right.$$

$$\left. + \lambda\, T_2\left(\begin{pmatrix} p_{21} & p_{22} & p_{23} \\ p_{31} & p_{32} & p_{33} \\ p_{41} & p_{42} & p_{43} \end{pmatrix}, \begin{pmatrix} q_{21} & q_{22} \\ q_{31} & q_{32} \end{pmatrix} \Big| \lambda\right) \cdot T_2\left(\begin{pmatrix} p_{12} & p_{13} & p_{14} \\ p_{22} & p_{23} & p_{24} \\ p_{32} & p_{33} & p_{34} \end{pmatrix}, \begin{pmatrix} q_{12} & q_{13} \\ q_{22} & q_{23} \end{pmatrix} \Big| \lambda\right) \right\}, \tag{1.51}$$

can itself be obtained from T_2 by similar substitutions, namely

$$p_{22} \longrightarrow T_1\left(\begin{pmatrix} p_{22} & p_{23} \\ p_{32} & p_{33} \end{pmatrix}, q_{22} \Big| \lambda\right) = \frac{p_{22}\, p_{33} + \lambda\, p_{23}\, p_{32}}{q_{22}}, \tag{1.52}$$

and the replacement of each of the four ratios in (1.48) by T_2 functions, for instance,

$$\frac{p_{11}\, p_{22} + \lambda\, p_{12}\, p_{21}}{q_{11}} \longrightarrow T_2\left(\begin{pmatrix} p_{11} & p_{12} & p_{13} \\ p_{21} & p_{22} & p_{23} \\ p_{31} & p_{32} & p_{33} \end{pmatrix}, \begin{pmatrix} q_{11} & q_{12} \\ q_{21} & q_{22} \end{pmatrix} \Big| \lambda\right). \tag{1.53}$$

This replacement of a T_1 by a T_2 function is precisely obtained by the substitutions mentioned in (1.50), and the same holds for the other three ratios.

This is the general pattern: the partition function $T_n(P, Q|\lambda)$ for a general weighting (P, Q) and a vertical bias $\sqrt{\lambda}$ is the result of the repeated application to $T_0 = p_{11}$ of the substitution S given by,

$$S \ : \quad q_{ij} \longrightarrow p_{i+1,j+1} \qquad \text{and} \qquad p_{ij} \longrightarrow \frac{p_{ij}\, p_{i+1,j+1} + \lambda\, p_{i,j+1}\, p_{i+1,j}}{q_{ij}}, \tag{1.54}$$

for $i, j \geqslant 1$.

The substitution law given by S was precisely at the heart of [38], whose main purpose was to give a non-recursive expression of the n-th iterate

of S. In the present notations, their Theorem 1 yields the following combinatorial result.

We define, following [38], the corner sum matrix $\bar{A}$ of a matrix $A = (a_{ij})_{1\leqslant i,j\leqslant n}$ of size n, by

$$\bar{a}_{ij} = \sum_{k\leqslant i}\sum_{\ell\leqslant j} a_{k\ell}. \tag{1.55}$$

and note that A can be fully recovered from $\bar{A}$ by

$$a_{ij} = \bar{a}_{ij} - \bar{a}_{i,j-1} - \bar{a}_{i-1,j} + \bar{a}_{i-1,j-1}, \qquad \text{with } a_{0j} = a_{i0} = 0. \tag{1.56}$$

Theorem 1.2.9. *The partition function for perfect matchings of the order n Aztec graph with respect to the general face weighting (P, Q) and vertical bias $\sqrt{\lambda}$, is given recursively by $T_n(P, Q|\lambda) = S^n(p_{11})$ for the substitution S defined in (1.54), and non-recursively by the two alternative expressions,*

$$T_n(P,Q|\lambda) = \sum_{B\in \mathrm{ASM}_{n+1}} \sum_{\substack{B'\in \mathrm{ASM}_n \\ B'\approx B}} \lambda^{P(B)+|\bar{B}'|-|\bar{B}'|_{\min}} P^B Q^{-B'}, \tag{1.57a}$$

$$= \sum_{B'\in \mathrm{ASM}_n} \sum_{\substack{B\in \mathrm{ASM}_{n+1} \\ B\approx B'}} \lambda^{P(B')+|\bar{B}|_{\max}-|\bar{B}|} P^B Q^{-B'}. \tag{1.57b}$$

$P(B)$ has been defined earlier, right after (1.6), and for any matrix A, $|\bar{A}|$ is the sum of all elements of $\bar{A}$ defined in (1.55). Finally $|\bar{B}'|_{\min} = \min_{B'\approx B} |\bar{B}'|$ and $|\bar{B}|_{\max} = \max_{B\approx B'} |\bar{B}|$.

Proof. We refer the reader to the proof given in [38]. Their Theorem 1 is formulated differently, with, inside the summation, the exponent of λ given by $F(B) - F(B') = (n+1)^2 + |\bar{B}'| - |\bar{B}|$. Using the various relations derived in [38], their formula can however be recast in the above two forms, more suitable to recover the special cases $P = 1$ and $Q = 1$. □

As the expressions (1.57) involve not only the pair (B, B') but also their corner sum matrices, we recall here some of the results of [38].

For a given $B \in \mathrm{ASM}_{n+1}$, an alternating sign matrix B' in ASM_n is compatible with B if and only if the following conditions hold,

$$\max(\bar{b}_{ij}, \bar{b}_{i+1,j+1}-1) \leqslant \bar{b}'_{ij} \leqslant \min(\bar{b}_{i,j+1}, \bar{b}_{i+1,j}), \qquad \text{for all } 1 \leqslant i,j \leqslant n. \tag{1.58}$$

Moreover Lemma 2 of [38] states that for every i, j between 1 and n, the lower and upper bounds in the previous inequality are equal unless $b_{i+1,j+1} = -1$, in which case they differ by 1. It follows that for those i, j such that $b_{i+1,j+1} \neq -1$, the entries $\bar{b}'_{i,j} = \max(\bar{b}_{ij}, \bar{b}_{i+1,j+1} - 1)$ are completely fixed by $\bar{B}$; for those i, j such that $b_{i+1,j+1} = -1$, the entries $\bar{b}'_{ij}$ can be either $\max(\bar{b}_{ij}, \bar{b}_{i+1,j+1}-1)$ or $\max(\bar{b}_{ij}, \bar{b}_{i+1,j+1}-1)+1$. This yields, as anticipated, a total of $2^{N_-(B)}$ distinct matrices $\bar{B}'$ from which the B' themselves can be computed.

When B' ranges over the set of matrices compatible with B, the difference $\Delta(B') \equiv |\bar{B}'| - |\bar{B}'|_{\min}$ takes the integer values from 0 to $N_-(B)$. There is a unique B' with $\Delta(B') = 0$, there are $N_-(B)$ matrices B' with $\Delta(B') = 1$, and in general exactly $\binom{N_-(B)}{k}$ matrices B' with $\Delta(B') = k$. We therefore obtain

$$\sum_{\substack{B' \in \mathrm{ASM}_n \\ B' \approx B}} \lambda^{\Delta(B')} = (1+\lambda)^{N_-(B)}, \tag{1.59}$$

and recover the expression $T_n(P, 1) = \det_\lambda P$.

Similarly for a fixed $B' \in \mathrm{ASM}_n$, a matrix B in ASM_{n+1} is compatible with B' if and only if its corner sum matrix $\bar{B}$ satisfies

$$\max(\bar{b}'_{i,j-1}, \bar{b}'_{i-1,j}) \leqslant \bar{b}_{ij} \leqslant \min(\bar{b}'_{i,j}, \bar{b}'_{i-1,j-1} + 1), \quad \text{for all } 1 \leqslant i,j \leqslant n, \tag{1.60}$$

with the convention $\bar{b}'_{i,0} = \bar{b}'_{0,j} = 0$. From Lemma 4 of [38], the lower and upper bounds are equal if $b'_{i,j} \neq 1$, and differ by 1 if $b'_{ij} = 1$, so that following the same arguments as above, one finds that there are $2^{N_+(B')}$ matrices B which are compatible with B'. One also finds that $\Delta(B) \equiv |\bar{B}|_{\max} - |\bar{B}|$ ranges over the integer values form 0 to $N_+(B')$, to obtain the following identity,

$$\sum_{\substack{B \in \mathrm{ASM}_{n+1} \\ B \approx B'}} \lambda^{\Delta(B)} = (1+\lambda)^{N_+(B')} = (1+\lambda)^n (1+\lambda)^{N_-(B')}. \tag{1.61}$$

It implies the expression found earlier for $T_n(1, Q|\lambda) = (1+\lambda)^n \det_\lambda Q^{-1}$.

As a final remark to close this section, we observe that with a general weighting (P, Q), the vertical bias $\sqrt{\lambda}$ is redundant since the weighting (P, Q) is complete in itself. This implies that the dependence in λ may be absorbed into a redefinition of P and Q, yielding an identity of the form $T_n(P, Q|\lambda) \sim T_n(P_\lambda, Q_\lambda|1)$ where the entries of P_λ and Q_λ are those of P and Q multiplied by appropriate powers of λ. Interestingly, this point of view allows us to re-derive the dependence in λ in the generalized Robbins-Rumsey formula. Let us see how this works.

Because we want to absorb edge weights into face weights, it is more convenient to consider the following modified face weighting given by

$$\widetilde{w}_F(M) = \prod_{(k,\ell)\in\widehat{\mathcal{A}}_n} x_{k,\ell}^{-N_{k,\ell}}. \tag{1.62}$$

It differs from the weighting used so far by the global factor $\prod_{k,\ell} x_{k,\ell} = (\prod_{i,j} p_{ij})(\prod_{i,j} q_{ij})$, which can be reinstated at the end. With respect to $\widetilde{w}_F(M)$, the edge which is adjacent to the p_{ij} and $q_{i'j'}$ faces contributes a face weight equal to $(p_{ij}q_{i'j'})^{-1}$ times 1 if the edge is horizontal, or $\sqrt{\lambda}$ if it is vertical.

The goal is thus to transfer the edge weights $\sqrt{\lambda}$ to the face weights. We introduce the following matrices P_λ and Q_λ, containing the new face weights,

$$\begin{aligned} (P_\lambda)_{ij} &= \lambda^{\sigma_{ij}}\, p_{ij}, \qquad \sigma_{ij} = i + j - 1 - ij, \\ (Q_\lambda)_{ij} &= \lambda^{\tau_{ij}}\, q_{ij}, \qquad \tau_{ij} = \tfrac{i+j-1}{2} - ij. \end{aligned} \tag{1.63}$$

This must be accompanied by gauge transformations [34]. A gauge transformation consists in assigning an extra factor w_v to the weights of all the edges around a vertex v. Because exactly one of these edges will belong to an arbitrary matching, this will simply multiply the partition function by an overall factor w_v. As gauge transformations can be performed independently on all vertices, the weights w_v can be chosen so that, when combined with the powers of λ in P_λ and Q_λ, they yield the desired result. For that, we use the following factors for the gauge transformations on the four vertices around the face q_{ij},

$$\lambda^{-\gamma_{ij}/2}, \qquad \lambda^{-(\gamma_{ij}+i+j-1)/2}, \qquad \lambda^{-(\gamma_{ij}+j-i)/2}, \qquad \lambda^{-(\gamma_{ij}+2j-1)/2}, \tag{1.64}$$

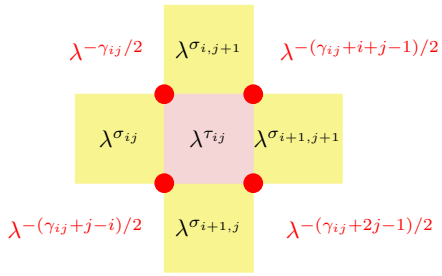

Figure 1.6: Illustration of the redefinition of the vertical bias into face weights and gauge transformations: the central red face is the face q_{ij} and the four yellow surrounding faces are the faces p_{ij} (left), $p_{i,j+1}$ (top), $p_{i+1,j}$ (bottom) and $p_{i+1,j+1}$ (right). The powers of λ marked in the faces are those appearing in the redefined matrices P_λ and Q_λ. The gauge transformations at the four vertices around the face q_{ij} have parameters written in red.

in the order top-left, top-right, bottom-left and bottom-right (see Figure 1.6), and with $\gamma_{ij} = (i-1)(2j-1)$.

One can check that the powers of λ attached to the faces together with the extra edge weights coming from the gauge transformations guarantee that all horizontal edges have weight 1 and all vertical edges have weight $\sqrt{\lambda}$ (in addition to the weight $(p_{ij}q_{i'j'})^{-1}$ coming from adjacent faces). For instance, for the left (vertical) edge of the face q_{ij}, we obtain the factor

$$\lambda^{-\sigma_{ij}} \cdot \lambda^{-\tau_{ij}} \cdot \lambda^{-\gamma_{ij}/2} \cdot \lambda^{-(\gamma_{ij}+j-i)/2} = \sqrt{\lambda}, \tag{1.65}$$

while for the upper (horizontal) edge of the same face, we have

$$\lambda^{-\sigma_{i,j+1}} \cdot \lambda^{-\tau_{ij}} \cdot \lambda^{-\gamma_{ij}/2} \cdot \lambda^{-(\gamma_{ij}+i+j-1)/2} = 1. \tag{1.66}$$

The identity relating the partition functions $T_n(P, Q|\lambda)$ and $T_n(P_\lambda, Q_\lambda|1)$ requires to include two factors. One is related to the gauge transformations and is the product of the factors at all sites; one finds that it is equal to $\lambda^{-n^3(n+1)/2}$. The other comes from the difference between the two measures $\widetilde{w}_F(M)$ and $w_F(M)$. The λ-dependence of the global factor $\prod_{k,\ell} x_{k,\ell}$ is given by $\prod_{i,j=1}^{n+1} \lambda^{\sigma_{ij}} \cdot \prod_{i,j=1}^{n} \lambda^{\tau_{ij}} = \lambda^{-n^2(n^2+n+1)/2}$; we

divide by this factor to eliminate it. Altogether we obtain

$$\begin{aligned} T_n(P,Q|\lambda) &= \lambda^{-n^3(n+1)/2}\,\lambda^{n^2(n^2+n+1)/2}\,T_n(P_\lambda,Q_\lambda|1) \\ &= \lambda^{n^2/2}\sum_{B\approx B'}\lambda^{\sum_{i,j=1}^{n+1}\sigma_{ij}b_{ij}-\sum_{i,j=1}^{n}\tau_{ij}b'_{ij}}\;P^B\,Q^{-B'} \\ &= \sum_{B\approx B'}\lambda^{(n+1)^2+|\bar{B}'|-|\bar{B}|}\;P^B\,Q^{-B'}, \end{aligned} \tag{1.67}$$

where we have used $\sum_{ij} ij\, b_{ij} = |\bar{B}|$, valid for any alternating sign matrix. The power of λ in the sum is the one given in [38].

1.2.5 General weights: shuffling algorithm and condensation

Basic and local modifications of graphs can lead to efficient recursive algorithms which allow one to compute partition functions of weighted perfect matchings. Such algorithms have been described and used by many authors [19,47,50,57,58], under different names; in the context of Aztec graphs, we will refer to the shuffling algorithm.

The two basic results underlying the shuffling algorithm are related to two local graph modifications called the vertex splitting and the urban renewal; they are illustrated in Figure 1.7. Proofs can be found in [47,50].

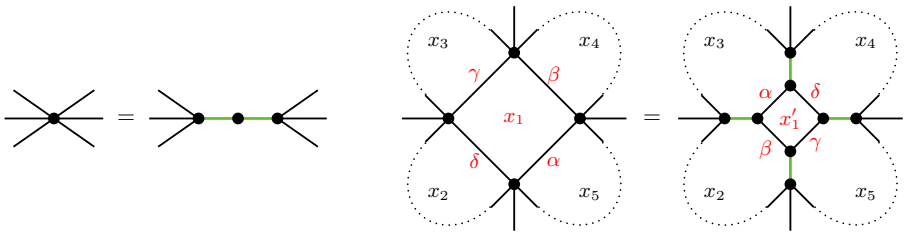

Figure 1.7: Illustration of the two local graph modifications, the vertex splitting on the left, the urban renewal on the right. The dotted lines indicate that some of the faces adjacent to the 4-cycle may be boundary (open) faces.

In the vertex splitting, any multivalent vertex can be expanded into a linear chain with three vertices, by inserting two new vertices and two

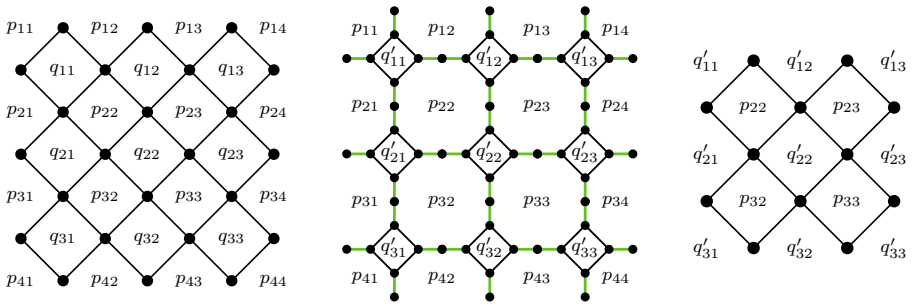

Figure 1.8: Illustration, on an order 3 Aztec graph, of the two steps involved in the shuffling algorithm.

new edges, in green. Note that the inverse transformation, the vertex merging, may also be applied. The urban renewal replaces each vertex of a 4-cycle by two vertices and one new edge, also in green. In both cases, the partition functions for the perfect matchings of the original graph G and of the modified graph G' are equal provided (1) the dimers occupying the green edges of G' have weight 1, whatever the edge and face weights in G are, and (2) the dimers occupying the black edges of G' are weighted in the same way as in G, except, in the case of the urban renewal, that the edge and face weights of the 4-cell must be modified (they are marked in red, before and after the change). The opposite edge weights are exchanged by pairs, $\alpha \leftrightarrow \gamma$ and $\beta \leftrightarrow \delta$, and the face weight of the 4-cycle is changed from x_1 to x'_1, given in terms of the weights $x_2, \ldots, x_5$ of the four adjacent faces, by,

$$x'_1 = \frac{\alpha\gamma\, x_2 x_4 + \beta\delta\, x_3 x_5}{x_1}. \tag{1.68}$$

The shuffling algorithm applied to Aztec graphs uses recursively the vertex splitting and the urban renewal, and establishes a recurrence relation between the partition functions at order n and $n-1$. Starting from an Aztec graph order n, the algorithm outputs an Aztec graph of order $n-1$, with modified face weights, such that the partition functions of both graphs are equal. Let us recall how it works [47]; the full procedure is illustrated in Figure 1.8 for an Aztec graph of order 3, which we have rotated clockwise by 45 degrees for graphical convenience.

Thus we start with an Aztec graph $\hat{\mathcal{A}}_n$ of order n, equipped with a general face weighting (P, Q) and an additional weight $\sqrt{\lambda}$ attached to each vertical edge.

The first step applies the urban renewal to all q-faces and outputs a modified graph $\hat{\mathcal{A}}_n^{\mathrm{mod}}$, as shown in the middle panel of Figure 1.8. Referring to the right panel of Figure 1.7, the edge weights around the q_{ij}-face are equal to $\alpha_{ij} = \gamma_{ij} = \sqrt{\lambda}$ and $\beta_{ij} = \delta_{ij} = 1$, so that they get simply transferred to the new q'_{ij}-face. The weights p_{ij} attached to the p-faces do not change, whereas the new weights q'_{ij}, from (1.68), are given by

$$q'_{ij} = \frac{p_{ij}\, p_{i+1,j+1} + \lambda\, p_{i,j+1}\, p_{i+1,j}}{q_{ij}}. \tag{1.69}$$

The partition function $T_n(P, Q|\lambda)$ on $\hat{\mathcal{A}}_n$ is equal to that for the perfect matchings on $\hat{\mathcal{A}}_n^{\mathrm{mod}}$ with the weights just described. Remember that the green edges have all weight 1 and are not affected by the weights of adjacent faces.

In the second step, the graph $\hat{\mathcal{A}}_n^{\mathrm{mod}}$ can be simplified. All pendant, peripheral green edges must necessarily be covered by dimers. Since all of them contribute a weight 1, these edges and their end nodes may simply be removed without changing the partition function. Then the linear chains with three vertices and two green edges, which separate the 4-cells with weights q'_{ij}, can be merged into a single vertex. After these two operations, one is left with an Aztec graph of order $n-1$, in which the p-faces have weights $(q'_{ij})_{1\leqslant i,j\leqslant n}$ and the q-faces have weights $(p_{ij})_{2\leqslant i,j\leqslant n}$; in addition the same vertical bias $\sqrt{\lambda}$ is obtained.

The shuffling algorithm as described above therefore implies the following identity on the partition functions,

$$\begin{aligned} T_n\big((p_{ij})_{1\leqslant i,j\leqslant n+1}, &(q_{ij})_{1\leqslant i,j\leqslant n}|\lambda\big) \\ &= T_{n-1}\big((q'_{ij})_{1\leqslant i,j\leqslant n}, (p_{i+1,j+1})_{1\leqslant i,j\leqslant n-1}|\lambda\big) \\ &= S\, T_{n-1}\big((p_{ij})_{1\leqslant i,j\leqslant n}, (q_{ij})_{1\leqslant i,j\leqslant n-1}|\lambda\big), \end{aligned} \tag{1.70}$$

where S is the substitution discussed in Section 1.2.4. Thus the shuffling algorithm gives the general Robbins-Rumsey formula a combinatorial content.

From the general discussion of Section 1.2.4, the partition function for a general face weighting (P, Q) and vertical bias $\sqrt{\lambda}$ does not reduce

to the computation of a λ-determinant. Let us however observe that it can be calculated by using the condensation algorithm (1.4). Instead of starting from $A_0 = (1)_{1\leqslant i,j\leqslant n+2}$ and $A_1 = P = (p_{ij})_{1\leqslant i,j\leqslant n+1}$ and running the algorithm to compute $\det_\lambda P$, one simply replaces the $n\times n$ central submatrix of A_0 by Q, and then runs the algorithm as before to produce the sequence (A_k) and eventually obtain $A_{n+1} = T_n(P, Q|\lambda)$.

Let us denote by $\mathrm{Cond}_\lambda(A_0, A_1)$ the output of the condensation algorithm applied to initial matrices A_0 and A_1. If A_0 and A_1 have size $m+1$ and m respectively, the algorithm produces a sequence of matrices (A_k), recursively computed from (1.4). We set $\mathrm{Cond}_\lambda(A_0, A_1) \equiv A_m$, so that $\mathrm{Cond}_\lambda(1, P) = \det_\lambda P$. It is not difficult to see that the above partition functions are given by

$$T_n(P, Q|\lambda) = \mathrm{Cond}_\lambda(\overline{Q}, P), \tag{1.71}$$

where $\overline{Q}$ is any $(n+2)\times(n+2)$ completion of Q whose central $n\times n$ restriction is Q.

The proof of the previous formula is straightforward. Initiating the condensation algorithm by setting $A_0 = \overline{Q}$ and $A_1 = P$, we obtain, after one step, the matrix A_2 with entries $(A_2)_{ij} = q'_{ij}$. From the way the sequence (A_k) is constructed, we have $\mathrm{Cond}_\lambda(A_{k-1}, A_k) = \mathrm{Cond}_\lambda(A_k, A_{k+1})$, and therefore we conclude

$$T_n(P, Q|\lambda) = \mathrm{Cond}_\lambda(A_0, A_1) = \mathrm{Cond}_\lambda(A_1, A_2) = T_{n-1}((q'_{ij}), (p_{i+1,j+1})|\lambda). \tag{1.72}$$

From this, one readily recovers the result quoted earlier in Theorem 1.2.1 when $P = 1$, namely

$$T_n(1, Q|\lambda) = T_{n-1}\Big((\frac{1+\lambda}{q_{ij}}), 1\Big|\lambda\Big) = \det_\lambda\Big((\frac{1+\lambda}{q_{ij}})\Big) = (1+\lambda)^n \det_\lambda(Q^{-1}). \tag{1.73}$$

1.3 Inhomogeneous λ-determinants

Apart for the vertical bias associated with the parameter λ, we have only considered face weights. Natural questions are whether there is a similar formalism for edge weights and whether face *and* edge weights

can be combined. We will see that the answers to both questions are positive. In a sense, this should not be surprising since the face and edge most general weightings are separately complete, meaning that the edge weights can be fully absorbed in face weights or vice-versa. However in the case we call inhomogeneous bias, the edge weights enter through a further generalization of λ-determinants.

In addition to the vertical bias $\sqrt{\lambda}$, one can add a horizontal bias $\sqrt{\mu}$ to all horizontal dimers. This however brings nothing really new since, up to a global factor, the partition function will depend on the ratio λ/μ. More interesting is to consider inhomogeneous bias, by which the vertical and horizontal bias depends on which row and column the dimer is located. In the notations of Section 1.1, this corresponds to take the weights $\alpha_{k,\ell}, \gamma_{k,\ell}$ resp. $\beta_{k,\ell}, \delta_{k,\ell}$ to depend on ℓ resp. k only. This system of inhomogeneous bias is precisely the situation analyzed by Di Francesco [48] (although it was not stated in these terms). Adapting his notations to the present framework, we denote by $\sqrt{\lambda_a}$ the vertical bias assigned to a vertical dimer in row a (i.e. the common value of all $\alpha_{k,a} = \gamma_{k,a}$), and similarly by $\sqrt{\mu_b}$ the horizontal bias assigned to a horizontal dimer in column b (common value of all $\beta_{b,\ell} = \delta_{b,\ell}$). For the Aztec graph of order n, the labels a and b take integer values from $-(n-1)$ to $n-1$. Let us also denote by $T_n(P, Q|\boldsymbol{\lambda}, \boldsymbol{\mu})$ the partition function for perfect matchings of the Aztec graph of order n, with a general face weighting (P, Q) and inhomogeneous bias, where $\boldsymbol{\lambda} = (\lambda_{-(n-1)}, \ldots, \lambda_{n-1})$ and $\boldsymbol{\mu} = (\mu_{-(n-1)}, \ldots, \mu_{n-1})$ are finite sequences of length $2n-1$. Because the numbers of vertical dimers in any row and of horizontal dimers in any column are even, the partition function is polynomial in the λ_a and μ_b.

In view of the general octahedron recurrence (1.10), the recurrence (1.12) generalizes to

$$\begin{aligned} T_n(P, Q|\boldsymbol{\lambda}, \boldsymbol{\mu})\, T_{n-2}(P_{\mathrm{C}}, Q_{\mathrm{C}}|\boldsymbol{\lambda}_{\mathrm{CC}}, \boldsymbol{\mu}_{\mathrm{CC}}) = \\ \mu_*\, T_{n-1}(P_{\mathrm{UL}}, Q_{\mathrm{UL}}|\boldsymbol{\lambda}_{\mathrm{C}}, \boldsymbol{\mu}_{\mathrm{L}}) T_{n-1}(P_{\mathrm{LR}}, Q_{\mathrm{LR}}|\boldsymbol{\lambda}_{\mathrm{C}}, \boldsymbol{\mu}_{\mathrm{R}}) \\ + \lambda_*\, T_{n-1}(P_{\mathrm{LL}}, Q_{\mathrm{LL}}|\boldsymbol{\lambda}_{\mathrm{C}}, \boldsymbol{\mu}_{\mathrm{C}})\, T_{n-1}(P_{\mathrm{UR}}, Q_{\mathrm{UR}}|\boldsymbol{\lambda}_{\mathrm{R}}, \boldsymbol{\mu}_{\mathrm{C}}), \end{aligned} \tag{1.74}$$

where λ_* and μ_* are the central entries of $\boldsymbol{\lambda}$ and $\boldsymbol{\mu}$ (λ_0 and μ_0 in the previous equation). Also the left, central and right truncations of $\boldsymbol{\lambda}$, and

similarly for $\boldsymbol{\mu}$, are defined by

$$\begin{aligned}\boldsymbol{\lambda}_{\mathrm{L}} &= (\lambda_{-(n-1)}, \ldots, \lambda_{n-3}),\\ \boldsymbol{\lambda}_{\mathrm{C}} &= (\lambda_{-(n-2)}, \ldots, \lambda_{n-2}),\\ \boldsymbol{\lambda}_{\mathrm{R}} &= (\lambda_{-(n-3)}, \ldots, \lambda_{n-1}),\end{aligned} \tag{1.75}$$

and $\boldsymbol{\lambda}_{\mathrm{CC}}$ and $\boldsymbol{\mu}_{\mathrm{CC}}$ refer to a double central restriction. The previous recurrence allows one to compute recursively all partition functions for $n \geqslant 2$ from the initial conditions,

$$\begin{aligned}&T_0(p_{11}, -|-, -) = p_{11},\\ &T_1\left(\left(\begin{smallmatrix} p_{11} & p_{12}\\ p_{21} & p_{22}\end{smallmatrix}\right), q_{11}|(\lambda_0), (\mu_0)\right) = \frac{\mu_0\, p_{11}\, p_{22} + \lambda_0\, p_{12}\, p_{21}}{q_{11}}.\end{aligned} \tag{1.76}$$

For $n = 2$, we obtain the following expression generalizing (1.14),

$$\begin{aligned}&T_2(P,Q|(\lambda_{-1}, \lambda_0, \lambda_1), (\mu_{-1}, \mu_0, \mu_1))\\ &\quad= \frac{1}{p_{22}}\Big[\mu_0\, \frac{\mu_{-1}\, p_{11}\, p_{22} + \lambda_0\, p_{12}\, p_{21}}{q_{11}}\, \frac{\mu_1\, p_{22}\, p_{33} + \lambda_0\, p_{23}\, p_{32}}{q_{22}}\\ &\qquad+\ \lambda_0\, \frac{\mu_0\, p_{21}\, p_{32} + \lambda_{-1}\, p_{22}\, p_{31}}{q_{21}} \cdot \frac{\mu_0\, p_{12}\, p_{23} + \lambda_1\, p_{13}\, p_{22}}{q_{12}}\Big]\\ &\quad= \mu_{-1}\mu_0\mu_1\, \frac{p_{11}\, p_{22}\, p_{33}}{q_{11}\, q_{22}} + \lambda_0\mu_0\mu_1\, \frac{p_{12}\, p_{21}\, p_{33}}{q_{11}\, q_{22}} + \lambda_0\mu_{-1}\mu_0\, \frac{p_{11}\, p_{23}\, p_{32}}{q_{11}\, q_{22}}\\ &\qquad+ \lambda_{-1}\lambda_0\mu_0\, \frac{p_{12}\, p_{23}\, p_{31}}{q_{12}\, q_{21}} +\ \lambda_0\lambda_1\mu_0\, \frac{p_{13}\, p_{21}\, p_{32}}{q_{12}\, q_{21}} + \lambda_{-1}\lambda_0\lambda_1\, \frac{p_{13}\, p_{22}\, p_{31}}{q_{12}\, q_{21}}\\ &\qquad+ \lambda_0\mu_0^2\, \frac{p_{12}\, p_{21}\, p_{23}\, p_{32}}{p_{22}\, q_{12}\, q_{21}} + \lambda_0^2\mu_0\, \frac{p_{12}\, p_{21}\, p_{23}\, p_{32}}{p_{22}\, q_{11}\, q_{22}},\end{aligned} \tag{1.77}$$

where the eight terms correspond, in the same order, to the eight dimer configurations pictured in Section 1.2.1, below (1.13). One may check that this gives the eight configurations the correct bias; the first term for instance corresponds to the all horizontal dimer configuration, and has indeed one pair of horizontal dimers in each column $b = -1, 0, 1$.

The recurrence (1.74) and the initial conditions (1.76) for $Q = 1$ have been considered in [48] as yet a further multiparameter generalization of the λ-Desnanot-Jacobi recurrence. The solution was viewed as a generalized, inhomogeneous λ-determinant, and denoted by $\det_{\boldsymbol{\lambda},\boldsymbol{\mu}}$.

The similarity with a λ-determinant follows from the recurrence itself, which implies that the $(\boldsymbol{\lambda}, \boldsymbol{\mu})$-determinant of a general square matrix A can be computed by using a modified condensation algorithm. The modification concerns the way connected 2×2 minors are computed: the value of a minor will depend on its position inside the matrix A that contains it. Let A be a matrix size $n+1$ (we will soon apply the algorithm to $A = P$ of size $n+1$); we label the diagonals of A by an integer a, ranging from $-n$ in the lower-left corner to n in the upper-right corner, so that $a = 0$ corresponds to the main diagonal ($i = j$). Similarly we label the antidiagonals of A by an integer b, with value $-n$ in the upper-left corner and value n in the lower-right corner, $b = 0$ being the label of the main antidiagonal ($i + j = n + 2$). Then the value of a connected 2×2 minor of a matrix X is (in the condensation algorithm, X will be one of the matrices A_k produced at intermediate steps)

$$\begin{vmatrix} x_{i,j} & x_{i,j+1} \\ x_{i+1,j} & x_{i+1,j+1} \end{vmatrix}_{\boldsymbol{\lambda},\boldsymbol{\mu}} = \mu_b\, x_{i,j}\, x_{i+1,j+1} + \lambda_a\, x_{i,j+1}\, x_{i+1,j}, \tag{1.78}$$

if the elements $x_{i,j}$, $x_{i+1,j+1}$ belong to the diagonal a in X and $x_{i,j+1}$, $x_{i+1,j}$ belong to the antidiagonal b. For such a minor, the values of a and b are between $-(s-1)$ and $s-1$ if X has size s. It follows that in the condensation algorithm recalled in the beginning of the chapter, the equation (1.4) is to be replaced by the following one (recall that A_k has size $n+2-k$),

$$(A_k)_{i,j} = \frac{\mu_{i+j-(n+3-k)}(A_{k-1})_{i,j}(A_{k-1})_{i+1,j+1} + \lambda_{j-i}(A_{k-1})_{i+1,j}(A_{k-1})_{i,j+1}}{(A_{k-2})_{i+1,j+1}}. \tag{1.79}$$

Starting from $A_0 = (1)_{1 \leqslant i,j \leqslant n+2}$ and $A_1 = A$ of size $n+1$, the recursive calculation of the sequence (A_k) terminates with $A_{n+1} = \det_{\boldsymbol{\lambda},\boldsymbol{\mu}} A$.

The following gives a combinatorial interpretation of the inhomogeneous determinants introduced in [48].

Theorem 1.3.1. *The partition function for perfect matchings of the Aztec graph of order n, with face weighting $(P, 1)$, extra bias $\sqrt{\lambda_a}$ on vertical dimers in row a and $\sqrt{\mu_b}$ on horizontal dimers in column b, is given by $T_n(P, 1|\boldsymbol{\lambda}, \boldsymbol{\mu}) = \det_{\boldsymbol{\lambda},\boldsymbol{\mu}} P$.*

Proof. We only have to show that the generalized recurrence (1.79) for $A = P$ leads to a Desnanot-Jacobi-type identity of the form (1.74) with

$Q = 1$. Let us observe, from (1.79), that the first matrix produced, A_2, of size n, depends on all parameters in $\boldsymbol{\lambda} = (\lambda_{-(n-1)}, \ldots, \lambda_{n-1})$ and $\boldsymbol{\mu} = (\mu_{-(n-1)}, \ldots, \mu_{n-1})$, and the same is true of the subsequent matrices $A_{k\geqslant 2}$, in particular of A_n (size 2) and $A_{n+1} = \det_{\boldsymbol{\lambda},\boldsymbol{\mu}} P$.

Let us now focus on the specific entry $(A_n)_{1,1}$. Following the recurrence backwards, we see that its value only depends on the UL restrictions of A_{n-1}, A_{n-2}, …, A_2, A_1, where the UL restriction means in each case omitting the last row and last column. As a consequence, $(A_n)_{1,1}$ only depends on the parameters in $\boldsymbol{\lambda}_{\mathrm{C}}$ and $\boldsymbol{\mu}_{\mathrm{L}}$ (let the indices i, j of A_2 vary between 1 and $n-1$) and is actually equal to $\det_{\boldsymbol{\lambda}_{\mathrm{C}},\boldsymbol{\mu}_{\mathrm{L}}} P_{\mathrm{UL}}$. The same argument applies to the three other entries A_n, namely $(A_n)_{1,2}$, $(A_n)_{2,1}$, $(A_n)_{2,2}$, with the appropriate restrictions UR, LL, LR, and also to the central entry $(A_{n-1})_{2,2}$ of A_{n-1}, for which the central restriction C is used (one omits the first and last rows and columns).

The relation (1.79) for $k = n+1$ (and $i = j = 1$) then implies the following relation,

$$\begin{aligned}\det_{\boldsymbol{\lambda},\boldsymbol{\mu}} P \cdot \det_{\boldsymbol{\lambda}_{\mathrm{CC}},\boldsymbol{\mu}_{\mathrm{CC}}} P_{\mathrm{C}} \;=\; & \mu_0 \det_{\boldsymbol{\lambda}_{\mathrm{C}},\boldsymbol{\mu}_{\mathrm{L}}} P_{\mathrm{UL}} \cdot \det_{\boldsymbol{\lambda}_{\mathrm{C}},\boldsymbol{\mu}_{\mathrm{R}}} P_{\mathrm{LR}} \\ & + \lambda_0 \det_{\boldsymbol{\lambda}_{\mathrm{L}},\boldsymbol{\mu}_{\mathrm{C}}} P_{\mathrm{LL}} \cdot \det_{\boldsymbol{\lambda}_{\mathrm{R}},\boldsymbol{\mu}_{\mathrm{C}}} P_{\mathrm{UR}}, \end{aligned} \tag{1.80}$$

identical to the recurrence satisfied by $T_n(P, 1|\boldsymbol{\lambda}, \boldsymbol{\mu})$. It follows that $T_n(P, 1|\boldsymbol{\lambda}, \boldsymbol{\mu}) = \det_{\boldsymbol{\lambda},\boldsymbol{\mu}} P$ for all n since, from (1.76), their values coincide for $n = 0$ and $n = 1$. □

Inhomogeneous bias allows one to focus on vertical or horizontal dimers in special rows or columns. For instance one may ask for the number $V_{n,k}$ of perfect matchings of the Aztec graph of order n which have exactly k pairs of vertical dimers in the zeroth (central) row. To compute its generating function $G_n(\lambda_0) = \sum_{k=0}^{n} V_{n,k}\, \lambda_0^k$, one simply sets all λ_a, μ_b to 1 except λ_0, takes $P = 1$, and evaluates

$$G_n(\lambda_0) = \det_{\boldsymbol{\lambda},\boldsymbol{\mu}}(p_{ij} = 1)_{1\leqslant i,j\leqslant n+1}, \tag{1.81}$$

while $\boldsymbol{\lambda} = (1, \ldots, 1, \lambda_0, 1, \ldots, 1)$ and $\boldsymbol{\mu} = (1, \ldots, 1)$. They can be easily computed for finite n. The first few are listed in the following.

Corollary 1.3.2. *For the first values of n, the generating functions $G_n(x)$ are given by*

$$G_1(x) = 1 + x, \tag{1.82a}$$
$$G_2(x) = 1 + 6x + x^2, \tag{1.82b}$$
$$G_3(x) = 1 + 47x + 15x^2 + x^3, \tag{1.82c}$$
$$G_4(x) = 1 + 572x + 390x^2 + 60x^3 + x^4, \tag{1.82d}$$
$$G_5(x) = 1 + 9197x + 17\,010x^2 + 5970x^3 + 589x^4 + x^5, \tag{1.82e}$$
$$G_6(x) = 1 + 173\,058x + 1\,118\,191x^2 + 661\,532x^3 + 135\,151x^4 + 9218x^5 + x^6. \tag{1.82f}$$

These polynomials seem to have a number of intriguing properties: (1) all their roots are real negative, (2) the roots of $G_n(x)$ and $G_{n+1}(x)$ are interlaced, (3) every $G_n(x)$ has a unique root which is, in norm, much larger that the others and which seems to be asymptotic to $-G'_{n-1}(0)$. For instance, the two largest, in norm, roots of $G_7(x)$ are $-173\,060.196$ and -9.9974, to be compared with $-G'_6(0) = -173\,058$. It follows that the coefficients $G_{n-1}(x)\big|_x$ and $G_n(x)\big|_{x^{n-1}}$ are close. Indeed we also observe: (4) the identity

$$G_n(x)\big|_{x^{n-1}} = G_{n-1}(x)\big|_x + 4n - 3 \tag{1.83}$$

appears to be exact, but remains to be properly understood.

Similarly to what we did at the end of Section 1.2.4, we can absorb the bias $\sqrt{\lambda_0}$ on the vertical edges of the central row in the redefinition of the matrices $P \to P_{\lambda_0}$ and $Q \to Q_{\lambda_0}$. Using the general Robbins-Rumsey formula (1.67), we can express the $(\boldsymbol{\lambda}, \boldsymbol{\mu})$-determinant in (1.81) as a single sum over alternating sign matrices. The result is the following,

$$G_n(\lambda_0) = \sum_{B \in \mathrm{ASM}_{n+1}} \lambda_0^{P_0(B)} \Big(\frac{1+\lambda_0}{2}\Big)^{N_-^0(B)} 2^{N_-(B)}, \tag{1.84}$$

where $P_0(B)$ and $N_-^0(B)$ are the restrictions of $P(B)$ and $N_-(B)$ to the main diagonal (thus $P_0(B)$ is the number of zeros on the main diagonal of B which have non-zero entries to the right and below, and such that the first non-zero entry in both directions is a one). For $n = 2$, the identity matrix contributes a factor 1, each of the other five permutation matrices a factor λ_0, whereas the seventh alternating sign matrix brings

a contribution $\lambda_0(1+\lambda_0)$. For general n however, this formula does not seem to help much to understand the structure of the polynomials $G_n(x)$.

1.A On elliptic curves related to biased two-periodic Aztec diamonds

The material presented in this Appendix owes much to exchanges with Alexei Borodin and Maurice Duits, and with Michael Somos for the last part.

In Section 1.2.2, we have discussed the problem of computing the partition function for tilings of two-periodic Azted diamonds, for which every vertical domino receives an extra weight $\sqrt{\lambda}$. The result, given in (1.27), can be written in terms of the first n terms of a sequence $(r_k)_{k\in\mathbb{Z}}$, defined recursively by

$$r_{k+1}\, r_{k-1} = \frac{\lambda + r_k^2}{1+\lambda\, r_k^2}, \qquad r_0 = 1, \quad r_1 = t. \tag{1.85}$$

We noted that when λ and t satisfy certain polynomial conditions, the sequence (r_k) is periodic with a certain periodicity $p \geqslant 3$, that is, satisfies $r_{k+p} = r_k$ for all k.

The surprising observation is that these polynomials are precisely those found in [39] to characterize when a certain point P of an elliptic curve is a torsion point, that is, when P has finite order p for the Abelian addition law on the elliptic curve. When P is a torsion point, it generates a periodic flow on the elliptic curve, given by $P_k = P_{k-1} + P$ for some initial point P_0. That flow encodes a sequence of Wiener-Hopf factorizations for a product of two-by-two matrices.

More specifically, the elliptic curve considered in [39] is given by (the two parameters α and a used in [39] are related to ours by $\alpha \leftrightarrow t$ and $a^2 \leftrightarrow \lambda$),

$$\mathcal{E}_1 \ : \ y^2 = x^2 + \frac{4x(x-\lambda)(x-1/\lambda)}{\left(\sqrt{\lambda}+1/\sqrt{\lambda}\right)^2 (t+1/t)^2}. \tag{1.86}$$

The specific point P generating the flow is $P = (\frac{1}{\lambda}, \frac{1}{\lambda})$. Thus P acts on the elliptic curve by translations, $(x, y) \to \sigma(x, y) = (x, y) + P$, with

$$\sigma(x,y) = \Big(\frac{(\lambda - x)(y - x)}{(1 - \lambda\, x)(x + y)}\,,\ \frac{\lambda(x^2 + y(\lambda - \lambda^{-1}) - 1)(y - x)}{(1 - \lambda\, x)^2 (x + y)} \Big). \quad (1.87)$$

The iteration of this transformation defines the flow, namely $P_k \equiv (x_k, y_k) = \sigma^k(P_0)$ for a given initial point P_0; in the context of [39], $P_0 = (-1, \frac{t^2-1}{t^2+1})$. Because P_0 and P are respectively on the negative and positive component of $\mathcal{E}_1$, all P_k are on the negative component, $x_k < 0$ for all k.

Although the recurrence (1.85) satisfied by the sequence (r_k) and the discrete flow $P_k = P_0 + k \cdot P$ on $\mathcal{E}_1$ do not have any apparent connection, the striking fact is the following,

The sequences $(r_k)_{k\geqslant 0}$ and $(P_k)_{k\geqslant 0}$ are simultaneously periodic with the same period, namely, in each case, the conditions ensuring their p-periodicity are identical.

This strongly suggests that the recurrence relation for the sequence (r_k) is intimately connected to the elliptic curve $\mathcal{E}_1$. Below we indeed exhibit a direct connection with $\mathcal{E}_1$, but surprisingly, the sequence (r_k) is more naturally connected to a translational flow on a different elliptic curve $\mathcal{E}_2$, which however shares the same periodicities as the flow on $\mathcal{E}_1$.

Element #1. On general grounds, a relation with the elliptic curve $\mathcal{E}_1$ used in [39] is expected, based on the following chains of connections. The recurrence (1.85) comes directly from the condensation algorithm applied to the computation of $\det_\lambda Q^{-1}$, where Q is the matrix with coefficients a and b alternating on rows and columns, see (1.21). As shown in Section 1.2.5, the condensation algorithm and the shuffling algorithm (or the urban renewal) applied to the q-faces work in the same way, reducing, at each step, the order of the Aztec graph by one unit at the price of a redefinition of the face weights. Finally, these successive redefinitions of the face weights and the translational flow on the elliptic curve $\mathcal{E}_1$ recalled above, were shown to be identical [59].

Element #2. One can exhibit a direct connection between the two sequences (r_k) and (P_k) as follows. By direct calculation, one finds from

(1.87) that $(x_k, y_k) = \sigma(x_{k-1}, y_{k-1})$ are related in such a way that the following identity holds,

$$\frac{1-\lambda\, x_k}{\lambda - x_k} \cdot \frac{y_k - x_k}{x_k + y_k} = \frac{1}{x_{k-1}}. \tag{1.88}$$

Using (1.87) once more, the terms x_k satisfy a second-order recurrence relation,

$$x_{k+1} = \frac{\lambda - x_k}{1-\lambda\, x_k} \cdot \frac{y_k - x_k}{x_k + y_k} = \Big(\frac{\lambda - x_k}{1-\lambda\, x_k}\Big)^2 \frac{1}{x_{k-1}}. \tag{1.89}$$

Multiplying both sides by -1 and taking the positive square root (all x_k are negative), we obtain

$$\sqrt{-x_{k+1}} = \frac{\lambda + (-x_k)}{1+\lambda\,(-x_k)}\, \frac{1}{\sqrt{-x_{k-1}}}, \tag{1.90}$$

which shows that $r_k > 0$ and $\sqrt{-x_k}$ satisfy the same recurrence relation. The initial conditions match since $x_0 = -1$ implies $r_0 = 1$, whereas $x_1 = -t^2$, which may be computed from (1.87) for $(x, y) = (x_0, y_0)$, yields $r_1 = t$. Therefore both sequences coincide, $x_k = -r_k^2$ for all $k \geqslant 0$.

The relation (1.88) can be solved for y_k in terms of x_k and x_{k-1}, themselves expressible in terms of the r_k's. The explicit expressions read

$$x_k = -r_k^2, \qquad y_k = r_k^2\, \frac{(\lambda + r_k^2) - (1+\lambda\, r_k^2)\, r_{k-1}^2}{(\lambda + r_k^2) + (1+\lambda\, r_k^2)\, r_{k-1}^2} = r_k^2\, \frac{r_{k+1} - r_{k-1}}{r_{k+1} + r_{k-1}}. \tag{1.91}$$

Because the terms r_k are positive, the two sequences (P_k) and (r_k) are simultaneously periodic with the same period.

Element #3. It turns out that the recurrence (1.85) belongs to a larger class of recurrence relations that have a fairly long history. Because it is of direct relevance for what follows, we will more specifically refer to [60] (see also [61]).

The basic but crucial observation is that the recurrence (1.85) is such that the map $\mu : (r_k, r_{k+1}) \to (r_{k+1}, r_{k+2})$ preserves the following bi-quadratic curve $\mathcal{E}_2$ (see Prop. 2.5 in [61] for a more general statement),

$$\mathcal{E}_2 \ : \ X^2\, Y^2 + \lambda^{-1}\, (X^2 + Y^2) + 1 = K\, XY, \tag{1.92}$$

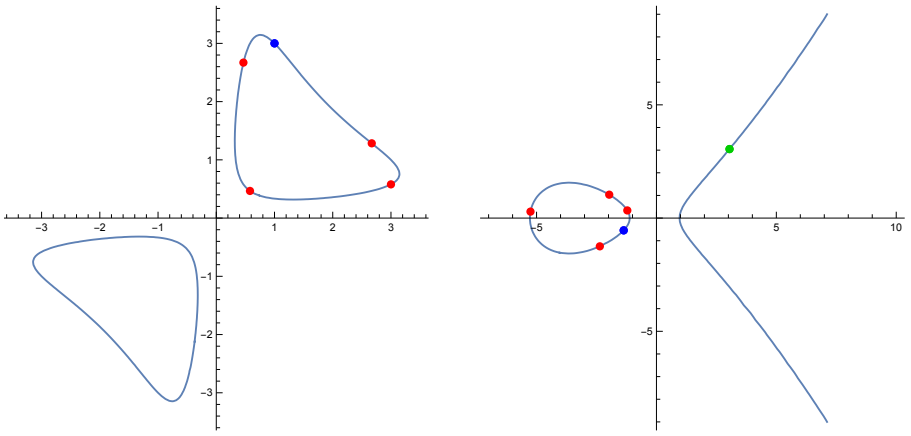

Figure 1.9: *Left*: real section of the biquadratic curve (1.92) for $\lambda = 2$ and $t = 3$ ($K = 5$). The red dots represent the points P_1, P_2, P_3, P_4 obtained from $P_0 = (1, 3)$, in blue, by the flow described in the text. *Right*: the same flow represented on the isomorphic cubic curve $\mathcal{E}_2'$; P_0 is the blue dot on the bounded component, whereas the green dot on the unbounded component is the point P in terms of which the flow can be viewed as a translational flow.

where K is a constant. For the initial conditions (1.85), namely $r_0 = 1$ and $r_1 = t$, it is given by $K = (1 + \frac{1}{\lambda})(t + \frac{1}{t})$. The real section of $\mathcal{E}_2$ has two bounded symmetric components related by $(X, Y) \leftrightarrow (-X, -Y)$, see Figure 1.9.

In a sense, $\mathcal{E}_2$ is already present in the relation (1.91) because the fact that the point (x_k, y_k) lies on the elliptic curve $\mathcal{E}_1$ implies that (r_{k-1}, r_k) satisfies the biquadratic relation (1.92). However the map $(r_{k-1}, r_k) \to (x_k, y_k)$ given in (1.91) is not birational (in particular, on the reals, its image only yields the negative component of $\mathcal{E}_1$).

The biquadratic curve $\mathcal{E}_2$ has genus 1 and is therefore an elliptic curve. The flow on $\mathcal{E}_2$ obtained by applying iteratively the map μ on the initial point $(r_0, r_1) = (1, t)$ is geometrically easy to describe [60]. Because $\mathcal{E}_2$ is symmetric under $X \leftrightarrow Y$, the two points $P_k = (r_k, r_{k+1})$ and $P_{k+1}^* = (r_{k+2}, r_{k+1})$, the diagonally reflected image of P_{k+1}, belong to $\mathcal{E}_2$ and are the only two intersection points of $\mathcal{E}_2$ with the horizontal line passing through P_k (for $Y = r_{k+1}$, (1.92) is quadratic in X with

roots equal to r_k and r_{k+2}). Thus P_{k+1} is found in three steps: draw a horizontal line through P_k, find the other intersection with $\mathcal{E}_2$, and diagonally reflect it. For λ and t positive, the flow remains on the positive component, see Figure 1.9. Moreover, similarly to the map σ discussed above, the flow induced by μ can be seen as the iterated addition on $\mathcal{E}_2$ of a specific point P [61].

Since $\mathcal{E}_1$ and $\mathcal{E}_2$ are both elliptic, the natural question is whether they are isomorphic. It turns out that the answer is negative. To see this, we first follow [60] where a sequence of birational transformations is defined that brings the biquadratic curve to an elliptic curve in standard, cubic form. We refer to [60] for the details and merely quote the final result.

Let u be the smallest positive root of $X^4 + (2\lambda^{-1} - K)X^2 + 1 = 0$. Then the biquadratic curve $\mathcal{E}_2$ is birationally equivalent to the following elliptic curve $\mathcal{E}_2'$ written in standard form as,

$$\mathcal{E}_2' \; : \quad \frac{4(K + 2\lambda^{-1} - 2u^2)}{q}\, y^2 = 4x^3 + b_2 x^2 + 2b_4 x + b_6, \tag{1.93}$$

where

$$\gamma = 2u^2 + \frac{2}{\lambda} - K, \quad p = -\frac{4u}{2 + \lambda K - 2\lambda u^2}, \quad q = p(\gamma + 4pu + 4p^2),$$

$$b_2 = -\frac{4}{q}(\gamma + 8pu + 12p^2), \qquad b_4 = \frac{8}{q}(u + 3p), \qquad b_6 = -\frac{16}{q}. \tag{1.94}$$

The point P on $\mathcal{E}_2'$ defining the translational flow is given by $P = (\frac{1}{p+u}, \frac{1}{p+u})$ and lies on the diagonal.

To check whether the elliptic curves $\mathcal{E}_1$ and $\mathcal{E}_2'$ are isomorphic, we merely compute their j-invariant. With respect to the standard form given in (1.93), into which $\mathcal{E}_1$ can easily be recast, the invariant is defined by [62]

$$j = \frac{(b_2^2 - 24b_4)^3}{9b_2b_4b_6 - \frac{1}{4}b_2^3 b_6 + \frac{1}{4}b_2^2 b_4^2 - 8b_4^3 - 27b_6^2}. \tag{1.95}$$

We find surprisingly close but definitely different values in terms of the two parameters λ and K,

$$j(\mathcal{E}_1) = \frac{\left(16\lambda^4 - 16\lambda^2 + \lambda^4K^4 - 8\lambda^4K^2 - 8\lambda^2K^2 + 16\right)^3}{\lambda^8\left[(K+2)^2 - 4\lambda^{-2}\right]\left[(K-2)^2 - 4\lambda^{-2}\right]}, \tag{1.96}$$

$$j(\mathcal{E}_2') = \frac{\left(16\lambda^4 + 224\lambda^2 + \lambda^4K^4 - 8\lambda^4K^2 - 8\lambda^2K^2 + 16\right)^3}{\lambda^{10}\left[(K+2)^2 - 4\lambda^{-2}\right]^2\left[(K-2)^2 - 4\lambda^{-2}\right]^2}. \tag{1.97}$$

It follows that the two curves are not isomorphic over $\mathbb{C}$ and therefore also not over $\mathbb{R}$. Yet the translational flows $P_k = P_0 + k \cdot P$ defined in terms of P_0 and P, and respectively different for $\mathcal{E}_1$ and $\mathcal{E}_2'$, are simultaneously periodic with the same period. Although this has been proved above, somewhat indirectly since the argument was made on the sequence $(-r_k^2)$, it remains to be properly understood.

Element #4. After submitting the manuscript [1], Michael Somos informed us of his observation that the two sequences (a_k) and (b_k) introduced in (1.25) are each generalized Somos-4 sequences, i.e. satisfy a quadratic recurrence relation of order 4,

$$s_k s_{k-4} = \alpha\, s_{k-1} s_{k-3} + \beta\, s_{k-2}^2. \tag{1.98}$$

The initial conditions s_0, s_1, s_2, s_3 are different for the a_k and b_k, but the coefficients α and β are identical for both sequences, and easily related to $a_0 = 1$, $a_1 = a^{-1}$, $b_0 = 1$ and $b_1 = b^{-1}$,

$$\alpha = \Big[\frac{a_0 b_1}{a_1 b_0} + \frac{a_1 b_0}{a_0 b_1} + \lambda \frac{a_0 a_1}{b_0 b_1} + \lambda \frac{b_0 b_1}{a_0 a_1}\Big]^2 = (1+\lambda)^2\,(t + t^{-1})^2, \tag{1.99a}$$

$$\beta = -\alpha + (1-\lambda^2)^2 = (1+\lambda)^2\big[(1-\lambda)^2 - (t+t^{-1})^2\big], \tag{1.99b}$$

with $t = \frac{a}{b}$.

Somos sequences are at the heart of the *elliptic realm*, and central in topics like elliptic divisibility and the Laurent phenomenon (see for instance the item A006720 on the On-line Encyclopedia of Integer Sequences [63] for a rich list of references). The intriguing observation made by Somos adds a layer of ellipticity to our problem, and in fact shed a new light on what we had already observed, as summarized above. Indeed there is a well-documented relation between Somos-4 sequences and elliptic curves, in particular translational flows on elliptic curves. In short, a Somos-4 sequence can be associated with a translational flow $P_0 + k \cdot P$, and vice-versa.

More precisely, let (x_k, y_k) be the coordinates of the points $P_0 + k \cdot P$ on an elliptic curve $\mathcal{E}$, for $P_0 = (x_0, y_0)$ and $P = (\overline{x}, \overline{y})$ non-singular points on $\mathcal{E}$. Then the sequence defined by

$$\frac{s_k}{s_{k-1}} = (\overline{x} - x_{k-1})\,\frac{s_{k-1}}{s_{k-2}}, \qquad \text{for } k \geqslant 1, \tag{1.100}$$

with s_{-1} and s_0 arbitrary, is a Somos-4 sequence [53].

Applying this to the elliptic flow on $\mathcal{E}_1$ discussed in [39] and recalled above, for which $\overline{x} = \frac{1}{\lambda}$, we readily obtain that the terms $\tilde{s}_k = \lambda^{k(k+1)/2} s_k$ form an equivalent Somos-4 sequence and satisfy

$$\frac{\tilde{s}_k}{\tilde{s}_{k-1}} = (1 - \lambda\, x_{k-1})\, \frac{\tilde{s}_{k-1}}{\tilde{s}_{k-2}} = (1 + \lambda\, r_{k-1}^2)\, \frac{\tilde{s}_{k-1}}{\tilde{s}_{k-2}}, \qquad \text{for } k \geqslant 1, \quad (1.101)$$

where the second equality follows from $x_{k-1} = -r_{k-1}^2$, see (1.91). Comparing with the recurrence satisfied by a_k, see (1.26), confirms that $a_k = \tilde{s}_k$ is a Somos-4 sequence. The same holds for the sequence (b_k). This clearly reinforces the tie with [39] since (a_k) and (b_k) are Somos-4 sequences that are associated in a natural way with the translational flow on $\mathcal{E}_1$ considered in [39].

1.B Generalized Somos-4 sequences

At the end of the previous appendix, we mentioned that (a_k) and (b_k) are generalized Somos-4 sequences and gave an argument for this in terms of the elliptic curve $\mathcal{E}_1$. In this appendix, we provide a combinatorial proof of this result and study the relation between Somos-4 recurrences,

$$s_k s_{k-4} = \alpha s_{k-1} s_{k-3} + \beta s_{k-2}^2, \quad (1.102)$$

for $\alpha, \beta \in \mathbb{C}$, $k \in \mathbb{Z}$, and coupled recurrence system of the kind

$$a_k = \frac{a_{k-1}^2 + \lambda b_{k-1}^2}{a_{k-2}}, \qquad b_k = \frac{b_{k-1}^2 + \lambda a_{k-1}^2}{b_{k-2}}, \quad (1.103)$$

with initial conditions a_0, a_1, b_0, b_1. In the above relations, λ can be taken as an arbitrary complex parameter, however, in the problem of interest (biased Aztec diamonds), $\lambda > 0$.

One can remark that this system is symmetric under the exchange $a_k \leftrightarrow b_k$ for all k. Hence, it suffices to proves that (a_k) is a Somos-4 and the result for (b_k) will follow. For this, we show that each of the sequences, (a_k) and (s_k), respect the same non-degenerate order 5 quartic recurrence relation for correctly chosen α and β.

From the Somos-4 recurrence

Let us consider the recurrence (1.102) at k and $k+1$,

$$\begin{cases} s_k s_{k-4} = \alpha s_{k-1} s_{k-3} + \beta s_{k-2}^2, \\ s_{k+1} s_{k-3} = \alpha s_k s_{k-2} + \beta s_{k-1}^2. \end{cases} \tag{1.104}$$

We want to rewrite the system in order to isolate α and β. For that, we multiply the first equation by s_{k-1}^2, the second by s_{k-2}^2, and subtract the two to cancel the term in β. Similarly, we can get rid of the term in α, and obtain

$$\begin{cases} s_k s_{k-1}^2 s_{k-4} - s_{k+1} s_{k-2}^2 s_{k-3} = \alpha(s_{k-1}^3 s_{k-3} - s_k s_{k-2}^3), \\ s_k^2 s_{k-2} s_{k-4} - s_{k+1} s_{k-1} s_{k-3}^2 = -\beta(s_{k-1}^3 s_{k-3} - s_k s_{k-2}^3). \end{cases} \tag{1.105}$$

Finally, we subtract these two equations in order to only keep the combination[6] $(\alpha+\beta)$, and find a quartic order 5 recurrence obeyed by the s_k,

$$\begin{aligned} s_{k+1} s_{k-3}(s_{k-1} s_{k-3} - s_{k-2}^2) - s_k s_{k-4}(s_k s_{k-2} - s_{k-1}^2) \\ = (\alpha+\beta)(s_{k-1}^3 s_{k-3} - s_k s_{k-2}^3). \end{aligned} \tag{1.106}$$

From the coupled recurrence system

Using the left relation in (1.103), we can isolate

$$b_{k-1} = \pm\sqrt{\frac{1}{\lambda}(a_k a_{k-2} - a_{k-1}^2)} \tag{1.107}$$

and insert the expression in the second relation, which yields

$$\sqrt{(a_{k+1}a_{k-1} - a_k^2)(a_{k-1}a_{k-3} - a_{k-2}^2)} = a_k a_{k-2} + (\lambda^2 - 1) a_{k-1}^2. \tag{1.108}$$

By taking the square and dividing both side by a_{k-1}, we find a cubic relation for (a_k),

$$a_k a_{k-2} a_{k-4} - a_k a_{k-3}^2 - a_{k-1}^2 a_{k-4} + 2(1-\lambda^2) a_{k-1} a_{k-2} a_{k-3} = (1-\lambda^2)^2 a_{k-2}^3. \tag{1.109}$$

[6] Numerical analysis of the sequences revealed that α and β separately may be complicated functions of the initial conditions while $(\alpha+\beta)$ seems to depend only on λ. This motivates our choice to isolate $(\alpha+\beta)$.

Let us consider the same relation with $k \mapsto k+1$, multiply the first one by a_k, the second by a_{k-3}, and subtract the two. In doing so, we can eliminate the term with the prefactor $2(1-\lambda^2)$, and obtain the quartic recurrence

$$a_{k+1}a_{k-3}(a_{k-1}a_{k-3} - a_{k-2}^2) - a_k a_{k-4}(a_k a_{k-2} - a_{k-1}^2) \\ = (1-\lambda^2)^2(a_{k-1}^3 a_{k-3} - a_k a_{k-2}^3). \quad (1.110)$$

Degeneracy of the quartic recurrence

Now that we proved that the sequences (a_k) and (s_k) both obey a similar quartic recurrence relation, we will verify it produces well-defined quantities. One can remark that (1.110) is non-degenerate (unequivocally determines all the a_k's) provided that $a_k \neq 0$ and $a_k^2 \neq a_{k+1}a_{k-1}$ for all $k \in \mathbb{Z}$. By inserting $a_k^2 = a_{k+1}a_{k-1}$ in the (a_k) recurrence, one remarks that the second condition is equivalent to $\lambda b_k^2 \neq 0$. In particular, both conditions are automatically satisfied if we restrict λ and the four initial conditions to be strictly positive numbers; in this case, $a_k, b_k > 0$ for all k due to (1.103).

Remark. In terms of elliptic curves, the values for which the recurrence is degenerate exactly correspond to the cases where the translational flow on the curve gives $P_0 + k \cdot P = O$ for some k, where O is the neutral element for the addition (i.e. the point at infinity). To see this, we can insert $a_k = 0$ in (1.103) and rewrite this as $(1 + \lambda r_{k-1}^2) = 0$, by defining $r_k = b_k/a_k$. According to [53] (chapter 7), this equation is the equivalent for Somos-4 sequences of the translational flow equation aforementioned.

Initial conditions

We have seen that the recurrence (1.110) is degenerate if and only if either one of the sequences (a_k) or (b_k) in (1.103) is. We then assume from now on that these sequences are well defined, and analyse the initial conditions. The objective is to verify that quantities defined by (1.103) also respect (1.102) for some α, β to be determined.

From one side, we have the four initial conditions (a_0, a_1, b_0, b_1). Using the recurrence, one can find the values for a_2 and a_3 in terms of these

initial conditions. On the other side, to obtain the correspondence, we have to choose $s_i = a_i$ for $i = 0, 1, 2, 3$, as initial values. We still have to determine α and β, which is done by solving the system of two equations $a_4 = s_4$ and $a_5 = s_5$, and provides

$$\alpha = \Big[\frac{a_0 b_1}{a_1 b_0} + \frac{a_1 b_0}{a_0 b_1} + \lambda\frac{a_0 a_1}{b_0 b_1} + \lambda\frac{b_0 b_1}{a_0 a_1}\Big]^2, \tag{1.111}$$

$$\beta = -\alpha + (1 - \lambda^2)^2. \tag{1.112}$$

We note that the equality $(\alpha+\beta) = (1-\lambda^2)^2$ ensures that the recurrences (1.106) and (1.110) coincide.

Summarizing, for the α, β given above, we have shown that the sequences (a_k) and (s_k) respect the same order 5 quartic recurrence, with the same four initial conditions. Since we assume (a_0, a_1, b_0, b_1) and λ to be strictly positive, the sequences are both unequivocally determined by this recurrence, and are identical for all $k \in \mathbb{Z}$.

Remark 1. Since α, β are invariant under $(a_0, a_1) \leftrightarrow (b_0, b_1)$, the sequence (b_k) respects the same Somos-4 recurrence as (a_k), only the initial conditions differ.

Remark 2. Our result easily generalizes to recurrence systems of the form

$$a_k = \frac{\lambda_1 a_{k-1}^2 + \lambda_2 b_{k-1}^2}{a_{k-2}}, \qquad b_k = \frac{\lambda_1 b_{k-1}^2 + \lambda_2 a_{k-1}^2}{b_{k-2}}. \tag{1.113}$$

For instance, we can produce the coefficient λ_1 by using transformations like $\tilde{a}_k = A^{k^2} a_k$ that are known to preserve Somos-4 recurrences [53] (section 6.3).

Chapter 2

Arctic curves in the elliptic SOS model at the free-fermion point

This chapter is part of an ongoing project [2] written with Philippe Ruelle, Hjalmar Rosengren and Christian Walmsley Hagendorf.

In this chapter, we compute the arctic curve of the elliptic solid-on-solid model at the free-fermion point using both the geometric (or one-refined) tangent method and the two-refined tangent method. The model shares the same arctic curve as the biased two-periodic Aztec diamond. The connections between the two models, at the level of configurations and partition functions, are also reviewed.

2.1 Generalities on the six-vertex model

The *square-ice model* was originally introduced by Linus Pauling in 1935 [64] to describe the molecular behaviour of ice crystals in an idealized two-dimensional framework, with the purpose to gain a better

understanding of the residual entropy observed experimentally. In this setup, water-ice is modelized by an arrangement of H_2O molecules on a square lattice $\mathbb{Z}^2$ where the oxygen atoms lie on the vertices of the lattice, and hydrogen atoms on the edges of the graph such that each O is surrounded by four H. Two of them are close, maintained by covalent bonds, and two are further away, bonded to a neighbouring oxygen atom. A hydrogen bond is formed between an oxygen atom and those two further hydrogen atoms such that it is a good approximation to assume that the hydrogen atoms take place on the edges of the graph. This description leads to six possible local configurations around each vertex that are depicted in Figure 2.1. One common representation of this model consists to replace the covalently bonded hydrogen atoms by incoming arrows (pointing toward their associated oxygen) and the others by outgoing arrows in each of these local configurations. As a direct consequence, each of these six vertices necessarily possesses two ingoing and outgoing arrows, what is referred to as the *ice-rule*, and the model is commonly known as the *six-vertex model* (6V).

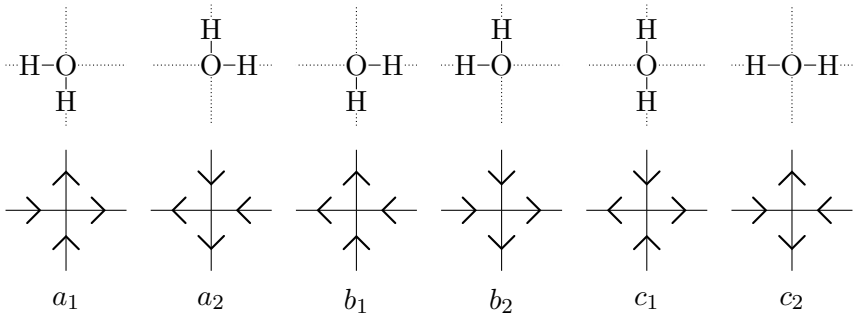

Figure 2.1: *Above*: six allowed local H_2O configurations respecting the ice-rule. *Below*: equivalent description in terms of arrows in the six-vertex model.

A configuration (or state) of size n is a coherent arrangement of these vertices on a $n \times n$ grid with prescribed boundary conditions. We decide to attach to each of these vertices a Boltzmann weight a_i, b_i, c_i, for $i = 1, 2$, as shown in Figure 2.1. We then associate to a configuration $\mathcal{C}$ the weight $w(\mathcal{C})$ given by the product of the vertex weights present in this

configuration. The probability to observe $\mathcal{C}$ is simply given by

$$\mathbb{P}(\mathcal{C}) = \frac{w(\mathcal{C})}{Z}, \qquad Z = \sum_{\mathcal{C}} w(\mathcal{C}) = \sum_{\mathcal{C}} a_1^{\#a_1}\, a_2^{\#a_2}\, b_1^{\#b_1}\, b_2^{\#b_2}\, c_1^{\#c_1}\, c_2^{\#c_2}, \tag{2.1}$$

where Z is the *partition function*.

It has been shown that the six-vertex model crucially depends on the choice of boundary conditions [24]. In the present work, we are mainly interested in the so-called *domain wall boundary conditions* (DWBC) for which an arctic phenomenon occurs (although other condition choices exist: open, (anti-)periodic, with reflecting end [65], etc.). In DWBC, all arrows on the left and right boundary sides point inward, while those on the top and bottom sides point outward. An example of a configuration with DWBC is shown in Figure 2.2.

In appearance, the model here described possesses six free parameters being the vertex weights. However, as shown in the next section, four conservation rules reduce the number of independent parameters to two.

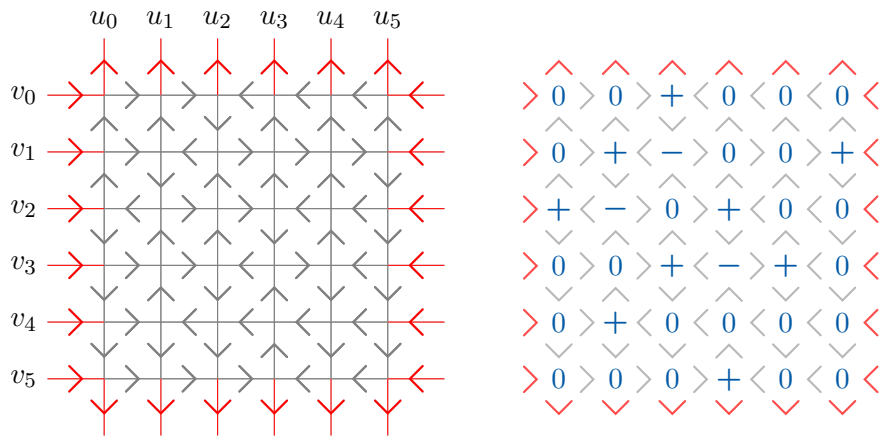

Figure 2.2: *Left*: example of a configuration of the six-vertex model on a lattice of size 6×6. The DWBC are highlighted in red. *Right*: the corresponding ASM with $+1$ and -1 respectively represented by $+$ and $-$.

The six-vertex model is known to exhibit several phases depending on the value of the parameter $\Delta = \frac{a^2+b^2-c^2}{2ab}$ [8, 24]. For the rest of this section, we set $a_1 = a_2 = a$, $b_1 = b_2 = b$, $c_1 = c_2 = c$. In the case of

DWBC, it is not restrictive since, as mentioned above, the model has only two free parameters. The phase diagram is identical for periodic boundary conditions or DWBC, however, V. Korepin and P. Zinn-Justin [24] showed that the bulk free energy could depend on this choice and they computed this energy in each phase for DWBC.

For $\Delta > 1$, the system is in the *ferroelectric phase*, and, in the thermodynamic limit, the model is *statistically frozen* in the most advantageous configurations. For periodic BC, it corresponds to the situation where all arrows are aligned (only a_1 or only a_2 vertices if $a > b$, and if $b > a$, only either b_1 or b_2 vertices). For DWBC, we necessarily have at least one c_2 vertex per row/column. These are solely located on the main diagonal if $b > a$ and on the main anti-diagonal if $a > b$. For $-1 < \Delta < 1$, the model is in the *disordered phase*; all vertex types appear in a disordered pattern. For DWBC, however, the arrows fixed on the edges of the grid have a macroscopic effect on the configurations so that, in the thermodynamic limit, the four corners of the lattice become statistically frozen and we observe an arctic phenomenon; with a probability that goes to 1 in the limit, each corner contains only one type of vertex, either a_1 (top-left), b_1 (top-right), a_2 (bottom-right) or b_2 (bottom-left) while the disorder accumulates in the center of the domain, similarly to what has been observed for Aztec diamonds in the previous chapter. In this disordered central region, the correlations between vertices decay algebraically (i.e. as an inverse power law) meaning that the model is *critical*. Finally, if $\Delta < -1$, the system is in the *anti-ferroelectric phase*. The weight c is dominant compared to the other two and the system will again freeze in the most advantageous configurations, consisting this time in an alternation of c_1 and c_2 in the central region (the corners remain frozen with a's and b's if the DWBC are imposed).

It is also well known that there exists an equivalence between the configurations of the six-vertex model with DWBC and alternating sign matrices (ASMs), already studied in Chapter 1. The correspondence is readily obtained by replacing the vertices a_i and b_i $(i = 1, 2)$ by 0's, vertices c_2 by 1's and vertices c_1 by -1's. An example of this correspondence is shown in Figure 2.2 and few more details are provided in Section 2.3.1.

Another interesting correspondence is obtained with Aztec diamonds when the parameter $\Delta = 0$, or more generally speaking, when $a_1a_2 + b_1b_2 = c_1c_2$. In this case, the six-vertex model is said to be *at the free-fermion point* [66]. This name comes from the fact that, for these parameters, there exists a transfer matrix of the model that can be written as the exponential of a free-fermionic Hamiltonian. Alternatively, it also means that there exists a determinantal point process describing the model. In Section 2.3.1, we study precisely this relation between the six-vertex model and Aztec diamonds in a more general context.

The six-vertex model defined in this section can be further generalized by letting the vertex weights depend on the location in the grid (row and column) of the vertices. It brings $2n$ new parameters $u_0, \dots, u_{n-1}$ and $v_0, \dots, v_{n-1}$ usually referred to as *spectral parameters* while the model then takes the name of *inhomogeneous six-vertex model*. What is particularly interesting with this generalization is that the model remains *exactly solvable* while these new parameters give us more control to analyse the statistical quantities.

2.2 The elliptic SOS model

In the rest of this chapter, we will consider a generalization of the six-vertex model described in the previous section called the *elliptic solid-on-solid model* (or *dynamical six-vertex model*), originally introduced by Baxter in 1973 [40–42] with the purpose to solve the eight-vertex model. The model is also called sometimes *eight-vertex solid-on-solid* (8VSOS) even though there are no additional vertices, contrary to the usual eight-vertex model.

Let us first introduce the height function defined on the faces of the square grid. For this, we choose a reference value, say 0, in the top left corner of the grid. The values of the height function are then controlled by the following rule: walking from one face to another (adjacent), the value increases by 1 if the crossed arrow is pointing to the left, according to the direction of the walk, or decreases by 1 if the arrow is pointing to the right. This rule unequivocally determines the values of the height function for a given configuration, and the set of height functions is in

1-to-1 correspondence with the configurations. An illustration is provided in Figure 2.3. The matrix containing as entries the value of the height function is easily related to the alternating sign matrix depicted in Figure 2.2, by replacing each 2×2 block $\left(\begin{smallmatrix} a_{11} & a_{12} \\ a_{21} & a_{22} \end{smallmatrix}\right)$ by the single value $(a_{12} - a_{11} + a_{21} - a_{22})/2$.

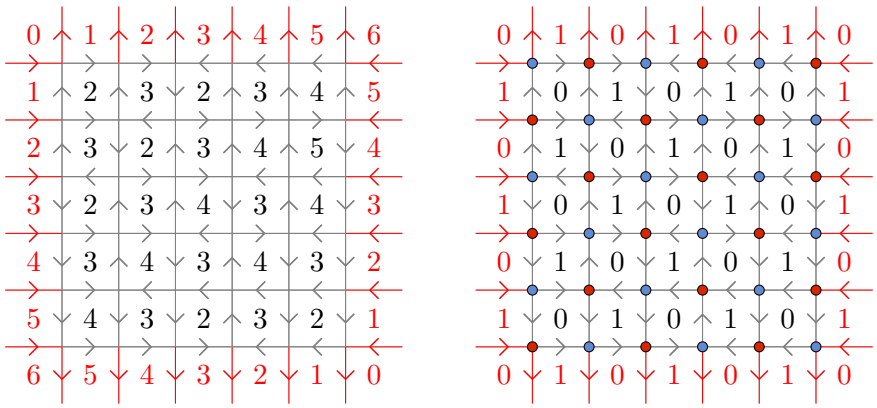

Figure 2.3: *Left*: example of a six-vertex configuration with the corresponding values of the heights written on the faces. *Right*: values of the height function modulo 2 and separation of the vertices in two classes; even/blue and odd/red. In both cases, by simplicity, the height function is represented with integer numbers h_{ij}. For general μ and η, these numbers are to be replaced by $\mu + h_{ij}\,\eta$.

We can slightly generalize this construction and choose the reference value and the step between two adjacent faces to be some complex number μ and η, parameters of the model. With the help of elliptic functions, it is then possible to parametrize the weights of each vertex to incorporate those new parameters and such that they respect the dynamical Yang-Baxter equation [67]. The specificity of this two-parameter generalization is that the vertex weights may vary according to the configuration itself (through the height-function). For this reason we call μ the *dynamical parameter*. We will not give the precise expression of these weights in the general setting (e.g. see [68]), but mention that they have a natural periodicity, say $a_1(\mu+1) = a_1(\mu)$, controlled by the parameter η. If one takes for instance $\eta = 1/3$ (or $\eta = \pi/3$ depending on the convention) only the values of the height function modulo 3 would matter, since in this case $a_1(\mu + 3\eta) = a_1(\mu)$ (the same stands for the other

vertices). Besides, at $\eta = 1/3$, the 8VSOS model is known to be related to the three-colouring of the square lattice (with arbitrary weights on each colour) [69].

The specialization of η in which we are interested in this work is $\eta = 1/2$, which corresponds to the free-fermion point in this generalized model. At this specific point, only the value modulo 2 of the height function is retained in the weights, and thus drastically simplifies the situation; since the height function mod 2 is just an alternation of 0 and 1 in a chessboard fashion, it becomes independent of the configuration (see Figure 2.3). In particular, one can distinguish two classes of vertices: writing (i, j) their locations with $(0, 0)$ in the top-left corner of the grid, either $i+j$ is even and the face-pattern around the vertex is $\left(\begin{smallmatrix} 0 & 1 \\ 1 & 0 \end{smallmatrix}\right)$ or else $i+j$ is odd and we find the values $\left(\begin{smallmatrix} 1 & 0 \\ 0 & 1 \end{smallmatrix}\right)$ around the vertex. One way to think about this model consists to view it as two interlaced copies of 6V model, taking place on the even and odd sublattices, resulting in a kind of twelve-vertex model or *two-periodic six-vertex (2p-6V) model*. In the following, we denote the weight attributed to the even vertices (the ones centered on the blue dots in Figure 2.3) with the usual letters $a_1, \dots, c_2$, and the odd ones (centered on the red dots) with the six capital letters $A_1, \dots, C_2$. Without loss of generality[1], let us set $a_1 = a_2 = a$, $b_1 = b_2 = b$, $A_1 = A_2 = A$ and $B_1 = B_2 = B$. Using a uniform spectral parameter u for the columns and 1 for the rows, we attribute the following weights to these vertices:

$$\begin{aligned} a = A &= \frac{\theta(-u)}{\theta(-1)}, & b &= \mathrm{i}\frac{\theta(u)\theta(-\mu)}{\theta(-1)\theta(\mu)}, & B &= \mathrm{i}\frac{\theta(u)\theta(\mu)}{\theta(-1)\theta(-\mu)}, \\ c_1 &= \frac{\theta(u\mu)}{\theta(\mu)}, & C_1 &= \frac{\theta(-u\mu)}{\theta(-\mu)}, & & \\ c_2 &= \frac{\theta(u/\mu)}{\theta(1/\mu)}, & C_2 &= \frac{\theta(-u/\mu)}{\theta(-1/\mu)}. & & \end{aligned} \tag{2.2}$$

We use the multiplicative convention for θ functions, such that

$$\theta(z) = \theta(z; p) = \prod_{j=0}^{\infty} (1 - z\,p^j)(1 - p^{j+1}/z), \quad \theta(pz) = \theta(z^{-1}) = -z^{-1}\theta(z). \tag{2.3}$$

[1] We show here after that these equalities does not truly constrain the model.

Appendix 2.A gives a brief review on theta functions and a summary of their main properties. The choice of weights (2.2) comes from [68]. From their notations to ours, after setting $\eta = 1/2$, we redefined $(e^{i\pi u}, e^{i\pi\mu}) \mapsto (u, \mu)$. We also multiplied all weights by $\sqrt{u}$, which only modifies the partition function by a global factor, and as well multiplied b_1 and B_1 by i and b_2 and B_2 by $-$i. This last operation has no effect on the partition function since only the products b_1B_1 and b_2B_2 matter, as we will see below. One can always convert uppercase vertices into lowercase ones by changing the sign of the dynamical parameter μ, as expected (in the additive convention it would be equivalent to transform $\mu \mapsto \mu + \eta$ which indeed inverts the two classes of vertices). This choice of weights respects the free-fermion rule for each class of vertices:

$$a_1a_2 + b_1b_2 = c_1c_2, \qquad A_1A_2 + B_1B_2 = C_1C_2. \tag{2.4}$$

These relations can be proved by using (2.125) from the appendix.

It is worth noting, although it is not apparent, that the 2p-6V model (always understood at the free-fermion point) with general weights $a_1, \ldots, C_2$ has only three free parameters, and is therefore in bijection with the 8VSOS at $\eta = 1/2$. This reduction in the number of parameters comes from several identities (or conservation laws) connecting the number of vertices of different classes. For instance, a first series,

$$\#a_1 = \#a_2, \qquad \#b_1 = \#b_2, \qquad \#A_1 = \#A_2, \qquad \#B_1 = \#B_2, \tag{2.5}$$

can be obtained by the following argument: the operation that reverses all the arrows around a given face (when allowed by the ice-rule) is transitive in the space of configurations (i.e. any configuration can be obtained from any other by a finite sequence of this arrow-reversing) [66]. By listing the different possibilities, it is not difficult to see that this operation preserves the numbers $\#x_1 - \#x_2$ for $x \in \{a, b, A, B\}$. It then suffices to inspect a single configuration and remark that these numbers are zero to obtain (2.5). Another, analogous, proof of this result is given in the next section, using the link with Aztec diamonds. Two more identities follow from the fact that the total number of vertices of each class is fixed by the size of the domain,

$$\#a_1 + \#a_2 + \cdots + \#c_2 = \left\lceil \frac{n^2}{2} \right\rceil, \qquad \#A_1 + \#A_2 + \cdots + \#C_2 = \left\lfloor \frac{n^2}{2} \right\rfloor. \tag{2.6}$$

Furthermore, by the link with ASM, it is immediate that each row (or column) contains exactly one more c_2/C_2 than c_1/C_1, and in particular $(\#c_2+\#C_2)-(\#c_1+\#C_1)=n$. Finally, the last two identities are the free-fermion rules given previously. It provides a total of 9 constraints on the 12 vertices, which indeed reduces the number of free parameters to 3. The chosen parametrization with theta functions is therefore indeed minimal with the parameters u, the *spectral parameter*, μ, the *dynamical parameter* and p, the *elliptic nome* of theta functions.

One can always recover the usual free-fermionic six-vertex model by taking the limit $p\to 0$, and then $\mu\to 0$. By the definition (2.3), we see that $\theta(x;p=0)=1-x$. Hence, it is easy to verify that the two classes of vertices coincide after taking these two limits. In doing so, u is the only remaining parameter, Δ being equal to zero due to the free-fermion condition, and controls the relative abundance of a and b vertices.

For the rest of the discussion, we now consider the system on a square grid of size $n+1$. As explained in the previous section, the model can be slightly generalized by introducing inhomogeneous spectral parameters in the columns and rows, $(u_0,u_1,\dots,u_n)$ and $(v_0,v_1,\dots,v_n)$, respectively. These are represented in Figure 2.2. The weights carried by the vertices (2.2) are consequently modified by changing $u\mapsto u_j/v_i$, where i and j are the row and column indices of the vertex.

To conclude this section, we give the general partition function with inhomogeneous weights [68, 70],

$$Z_{n+1}^{\text{2p-6V}}(\boldsymbol{u},\boldsymbol{v};\mu,p)=V^{-n}\frac{\theta((-1)^nU/V\mu)}{\theta(-1)^{n(n+1)}\theta((-1)^n/\mu)}\times\prod_{0\leqslant i<j\leqslant n}u_iv_i\theta\left(-\frac{u_j}{u_i}\right)\theta\left(-\frac{v_j}{v_i}\right),\tag{2.7}$$

where $U=\prod_{i=0}^n u_i$ and $V=\prod_{i=0}^n v_i$. We recover the homogeneous case by letting $u_i\to u$ and $v_i\to 1$ for all $i=0,\dots,n$,

$$Z_{n+1}^{\text{2p-6V}}(u;\mu,p)=u^{n(n+1)/2}\frac{\theta(-(-u)^{n+1}/\mu)}{\theta((-1)^n/\mu)}.\tag{2.8}$$

2.3 From the two-periodic 6V model to biased two-periodic Aztec diamonds

As mentioned in Section 2.1 and as we have seen in detail in Chapter 1, it is well known that $(n+1) \times (n+1)$ configurations of the 6V model with DWBC are bijective to ASM of size $n+1$, and that each one of the latter is in correspondence with a set of perfect matchings of an Aztec diamond (or graph) of order n. These associations allow one to transfer the weights of the 6V model to the edges of the AD, provided the 6V weights satisfy the free-fermion condition. The resulting weighting of the AD depends on one parameter, namely a vertical bias λ. By doubling the weights of the 6V model, defining a two-periodic six-vertex (2p-6V) model (equivalent to the 8VSOS model at the free-fermion point), the weights one obtains on the AD also become two-periodic. The first part of this section aims at explicitly recalling these constructions. Later on, we show how it is possible to obtain closed expressions for the partition functions of biased two-periodic Aztec diamonds and check explicitly that they correspond to the partition function of the 8VSOS at the free-fermion point.

2.3.1 Correspondence between partition functions

On a square grid of size $n+1$, a configuration of the 6V model gives rise to a matrix array of size $n+1$ in the following way: all four vertices of type a_i and b_i are replaced by a 0, the vertices of type c_1 are replaced by a -1, those of type c_2 are replaced by a 1. From the arrow flow of the six types of vertices, it is not difficult to see that the so-obtained array is an ASM, of size $n+1$. Because four vertices are mapped to 0, the correspondence is not manifestly bijective. However, one may observe that there are four different types of 0's in an ASM: indeed looking in the east, north, west and south directions from where the 0 is sitting, the first non-zero element is a 1 in exactly two (perpendicular) directions, either SE, NW, SW or NE. Each case corresponds to one and only one vertex of type a or b.

Let us look for instance at a 0 entry which has a 1 somewhere in the S direction and a 1 somewhere in the E direction, with (possibly) lots of

other 0's in between. Because the a and b vertices preserve the horizontal and vertical flows, and since the two 1's are c_2 vertices, the vertex associated to the 0 must have a left-right horizontal flow and a bottom-up vertical flow, that is, it must be a vertex of type a_1. Proceeding similarly for the other three cases, we obtain the following associations

$$\begin{array}{ccccc} \boxed{a_1} \cdots 0\ 1 & & 1 & & 1 \cdots 0\ \boxed{b_1} \\ \vdots & & 0 & & \vdots \\ 0 & & \vdots & & 0 \\ 1 & & \boxed{b_2} \cdots 0\ 1 & \quad 1\ 0 \cdots \boxed{a_2} & 1 \end{array}$$

In this way, one can assign each entry of the ASM the weight of its associated vertex, and then copy these weights on the p-faces (using the terminology of Section 1.1) of the Aztec graph of order n, to which the ASM entries are naturally associated, as indicated in Figure 2.4.

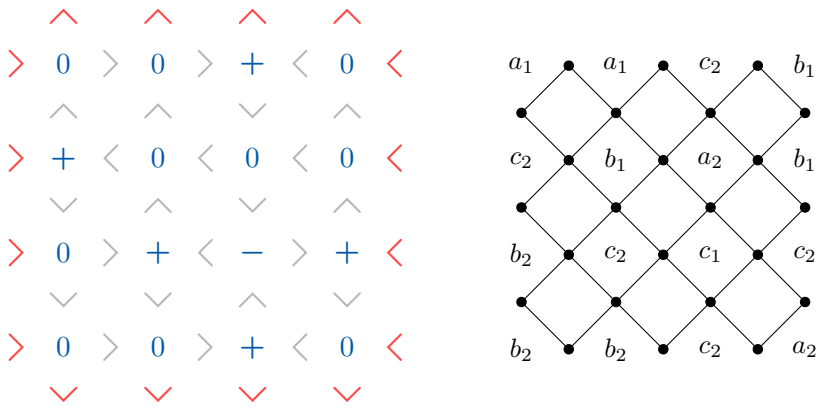

Figure 2.4: *Left*: a six-vertex configuration of size 4 with its associated ASM. The $+1$ and -1 are shortened by $+$ and $-$. *Right*: the vertex present in the left picture are written in the p-faces of an Aztec graph of size 3.

The relation between an ASM and perfect matchings of the Aztec graph is the usual one: an entry m_{ij} in an ASM means that the face p_{ij} is adjacent to $1 - m_{ij}$ dimers. When $m_{ij} = -1$, there are two possible local dimer configurations around the face p_{ij}, while if $m_{ij} = 0$, the local dimer configuration is unique, as we shall see now. Therefore,

there are 2^{N_-} perfect matchings associated with an ASM that contains N_- entries equal to -1.

In the last step, the weights were written in the p-faces, but they are not meant to be face weights. Instead these weights can actually be attached to edges in the following way.

A p-face with a weight a_i or b_i has only one adjacent dimer, because it has a 0 in the associated ASM. The weight itself completely determines which edge is covered by the single dimer around the face. The following figure illustrates the situation of a face with weight a_1.

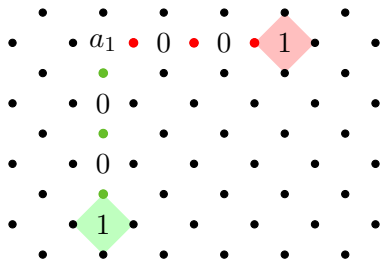

The two faces marked with a 1 have no dimer around them (type c_2), and those marked with a 0 have one. Starting from the face marked 1 on the same row as the one marked a_1 (shaded red), one sees that the eastern vertex of each face to its left (in red) must be covered by a dimer, oriented NE or SE. Likewise starting from the other face marked 1 (shaded green), all green vertices must be covered by a dimer, oriented SW or SE. This forces the unique dimer around the a_1 face to be oriented SE. Repeating the argument in the other three cases, we get the result depicted below.

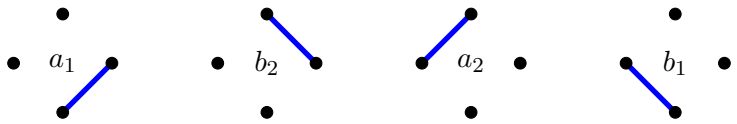

Figure 2.5: The vertex weights a_i and b_i lying on the p-faces completely determines the orientation of the dimers around these faces on the Aztec graph.

We can now transfer, in each of the four cases, the weight written on the face to the edge covered by the dimer. This consistently assigns a weight to the edges around the p-faces of the Aztec graph. If a p-face is adjacent

to two (parallel) dimers, it correctly brings a combined weight $a_1a_2 + b_1b_2 = c_1$ for the two possible cases (with $c_2 = 1$). This transposition on edge weights of the Aztec graph is depicted in Figure 2.6.

If c_2 is not equal to 1, we can in any case absorb its weight in the other vertices by dividing their weights by c_2; it would only affect the partition function by a constant factor. Similarly, in the two-periodic case, if c_2 and C_2 are not equal to 1, one can make use of the separate homogeneity of the 2p-6V model partition function in the small and in the large letter variables (see equation (2.6)) to absorb c_2 and C_2 into a redefinition of the other weights, by dividing these by c_2 and C_2 respectively.

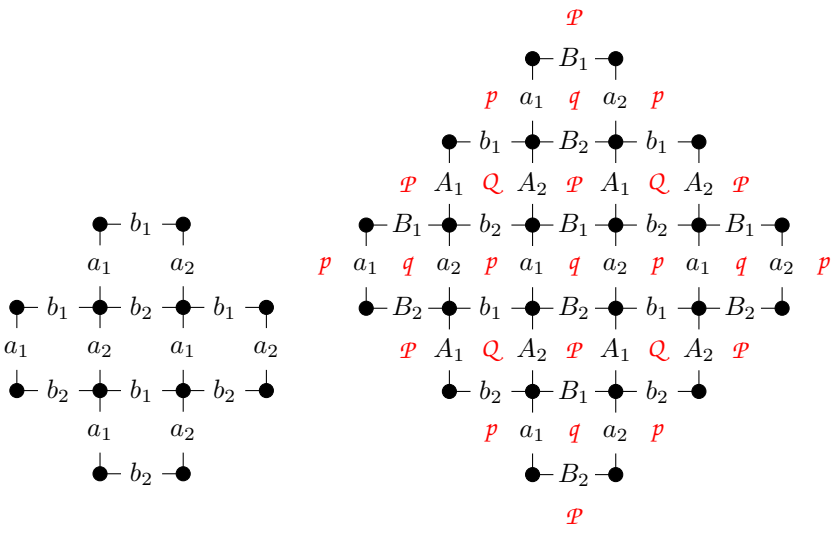

Figure 2.6: Rotating the Aztec graph by 45 degrees, we get the following edge weights coming from the 6V model: on the left picture, one set of weights is used; on the right, two sets of weights are used, alternating on the p-faces. Weights a_i, b_i on even faces ($p_{ij} = p$ for $i + j$ even), and weights A_i, B_i on odd faces ($p_{ij} = \mathcal{P}$ for $i + j$ odd).

The model on the left of the figure is equivalent to the standard biased Aztec diamonds: the vertical dimers have a weight $\sqrt{\lambda}$ while the horizontal dimers have weight 1. Indeed, in any configuration, the number of dimers on a_1 and a_2 edges are equal, as are those on b_1 and b_2 edges. Therefore the partition function depends only on the products a_1a_2 and

b_1b_2, and in fact, up to a global factor, only on the ratio $\frac{a_1a_2}{b_1b_2}$, which can be identified with λ.

The model on the right of the figure contains a two-periodicity and again a number of redundant parameters. The fully horizontal configuration has clearly an equal number of dimers on b_1 and b_2 edges, and on B_1 and B_2 edges. It is also well known that any other configuration can be obtained from that one by a finite sequence of flips, by which two parallel dimers around a single face are rotated. From the way the edges are weighted, one easily sees that a flip exchanges a pair of dimers as follows: $(a_1, a_2) \longleftrightarrow (b_1, b_2)$ if the flip acts on an even p-face, or $(A_1, A_2) \longleftrightarrow (B_1, B_2)$ (flip on an odd p-face), or $(a_1, a_2) \longleftrightarrow (B_1, B_2)$ (flip on an even q-face) or $(b_1, b_2) \longleftrightarrow (A_1, A_2)$ (flip on an odd q-face). It readily follows that $\#x_1 = \#x_2$ for $x \in \{a, b, A, B\}$ since, under a flip, x_1 and x_2 dimers appear or disappear simultaneously. As a consequence, the partition function then only depends on the four products x_1x_2.

To make contact with the two-periodic weighting on all faces, we assign the faces alternating weights, as shown in red in Figure 2.6 (in Chapter 1, we denoted q and $\mathcal{Q}$ by a and b resp., and set $p=\mathcal{P}=1$), and add an extra weight $\sqrt{\lambda}$ for each vertical dimer. For the face weights to reproduce the edges weights (under the assumption that an edge gets the product of the weights of its two adjacent faces, times $\sqrt{\lambda}$ if vertical), the former must satisfy the following identities,

$$\frac{a_1a_2}{c_2^2} = \lambda\,(pq)^2\,, \quad \frac{b_1b_2}{c_2^2} = (p\mathcal{Q})^2\,, \quad \frac{A_1A_2}{C_2^2} = \lambda\,(\mathcal{P}\mathcal{Q})^2\,, \quad \frac{B_1B_2}{C_2^2} = (\mathcal{P}q)^2\,. \tag{2.9}$$

The weights c_2 and C_2 in the denominator result from the absorption mentioned above. These identities do not include other contributions of the weights c_i and C_i, since they do not really make sense in terms of edge weights. The weights $\frac{c_1}{c_2}$ and $\frac{C_1}{C_2}$, associated to p-faces which are adjacent to two dimers, are correctly generated by the combinations $(a_1a_2 + b_1b_2)/c_2^2$ and $(A_1A_2 + B_1B_2)/C_2^2$. We mention the attribution of the weights in Figure 2.6 implicitly claims that $x_1 = x_2$ for $x \in \{a, b, A, B\}$. Thanks to the above discussion, we know it is not restrictive since only the product x_1x_2 matters for the partition function. If one desires to weight some vertices differently, it is always possible to multiply x_1 by a constant and x_2 by the inverse constant.

So far we are left with four parameters. There are different ways to see that this can be essentially reduced to three, either with the help of so-called gauge transformations or in the following way, by making use of the homogeneity with respect to the number of dimers.

The partition function for the 2p-6V model on a grid of size $n+1$ is given by

$$\begin{aligned}
Z_{n+1}^{\text{2p-6V}} &= \sum_{\text{configs 6V}} a_1^{\#a_1}\, a_2^{\#a_2}\, b_1^{\#b_1}\, b_2^{\#b_2}\, c_1^{\#c_1}\, c_2^{\#c_2} \\
&\qquad \times A_1^{\#A_1}\, A_2^{\#A_2}\, B_1^{\#B_1}\, B_2^{\#B_2}\, C_1^{\#C_1}\, C_2^{\#C_2} \\
&= c_2^{\lceil \frac{(n+1)^2}{2} \rceil}\, C_2^{\lfloor \frac{(n+1)^2}{2} \rfloor} \sum_{\text{configs 6V}} \big(\frac{a_1}{c_2}\big)^{\#a_1} \big(\frac{a_2}{c_2}\big)^{\#a_2} \big(\frac{b_1}{c_2}\big)^{\#b_1} \big(\frac{b_2}{c_2}\big)^{\#b_2} \big(\frac{c_1}{c_2}\big)^{\#c_1} \\
&\qquad \times \big(\frac{A_1}{C_2}\big)^{\#A_1} \big(\frac{A_2}{C_2}\big)^{\#A_2} \big(\frac{B_1}{C_2}\big)^{\#B_1} \big(\frac{B_2}{C_2}\big)^{\#B_2} \big(\frac{C_1}{C_2}\big)^{\#C_1} \\
&= c_2^{\lceil \frac{(n+1)^2}{2} \rceil}\, C_2^{\lfloor \frac{(n+1)^2}{2} \rfloor} \sum_{\text{configs 6V}} \big(\frac{a_1 a_2}{c_2^2}\big)^{\frac{1}{2}\#a} \big(\frac{b_1 b_2}{c_2^2}\big)^{\frac{1}{2}\#b} \big(\frac{a_1 a_2 + b_1 b_2}{c_2^2}\big)^{\#c_1} \\
&\qquad \times \big(\frac{A_1 A_2}{C_2^2}\big)^{\frac{1}{2}\#A} \big(\frac{B_1 B_2}{C_2^2}\big)^{\frac{1}{2}\#B} \big(\frac{A_1 A_2 + B_1 B_2}{C_2^2}\big)^{\#C_1} \\
&= c_2^{\lceil \frac{(n+1)^2}{2} \rceil}\, C_2^{\lfloor \frac{(n+1)^2}{2} \rfloor} \sum_{\text{configs 6V}} \big(\sqrt{\lambda}\, pq\big)^{\#a} \big(p\mathcal{Q}\big)^{\#b} \big(\sqrt{\lambda}\, \mathcal{P}\mathcal{Q}\big)^{\#A} \big(\mathcal{P}q\big)^{\#B} \\
&\qquad \times \big[\lambda\,(pq)^2 + (p\mathcal{Q})^2\big]^{\#c_1} \big[\lambda\,(\mathcal{P}\mathcal{Q})^2 + (\mathcal{P}q)^2\big]^{\#C_1} \\
&= c_2^{\lceil \frac{(n+1)^2}{2} \rceil}\, C_2^{\lfloor \frac{(n+1)^2}{2} \rfloor}\, Z_n^{\text{AD}}(p, \mathcal{P}, q, \mathcal{Q}|\lambda), \qquad (2.10)
\end{aligned}$$

namely the partition function for the biased two-periodic Aztec graphs, with face weights $p, q, \mathcal{P}, \mathcal{Q}$. Since $\#a+\#b+\#A+\#B+2\#c_1+2\#C_1 = n(n+1)$, the total number of dimers, we obtain

$$\begin{aligned}
Z_n^{\text{AD}}(p, \mathcal{P}, q, \mathcal{Q}|\lambda) &= (\mathcal{P}\mathcal{Q})^{n(n+1)} \sum_{\text{configs 6V}} (\sqrt{\lambda})^{\#a+\#A} \Big(\frac{pq}{\mathcal{P}\mathcal{Q}}\Big)^{\#a} \Big(\frac{p}{\mathcal{P}}\Big)^{\#b} \\
&\qquad \times \Big(\frac{q}{\mathcal{Q}}\Big)^{\#B} \Big[\lambda \Big(\frac{pq}{\mathcal{P}\mathcal{Q}}\Big)^2 + \Big(\frac{p}{\mathcal{P}}\Big)^2\Big]^{\#c_1} \Big[\lambda + \Big(\frac{q}{\mathcal{Q}}\Big)^2\Big]^{\#C_1} \\
&= (\mathcal{P}\mathcal{Q})^{n(n+1)}\, Z_n^{\text{AD}}\Big(\frac{p}{\mathcal{P}}, 1, \frac{q}{\mathcal{Q}}, 1|\lambda\Big), \qquad (2.11)
\end{aligned}$$

which explicitly shows the dependence on three parameters:

$$\lambda^2 = \frac{a_1 a_2 A_1 A_2}{b_1 b_2 B_1 B_2} = \left(\frac{\theta(-u)}{\theta(u)}\right)^4,$$
$$\left(\frac{p}{\mathcal{P}}\right)^4 = \frac{a_1 a_2 b_1 b_2 C_2^4}{A_1 A_2 B_1 B_2 c_2^4} = \left(\frac{\theta(-u/\mu)}{\theta(u/\mu)}\right)^4, \tag{2.12}$$
$$\left(\frac{q}{\mathcal{Q}}\right)^4 = \frac{a_1 a_2 B_1 B_2}{A_1 A_2 b_1 b_2} = \left(\frac{\theta(1/\mu)}{\theta(-1/\mu)}\right)^4,$$

while the global factor is given by

$$(\mathcal{P}\mathcal{Q})^4 = \frac{b_1 b_2\, A_1 A_2\, B_1 B_2}{a_1 a_2\, C_2^4} = \left(\frac{\theta(u)\theta(-1/\mu)}{\theta(-1)\theta(-u/\mu)}\right)^4. \tag{2.13}$$

We also write the vertex weights under their elliptic parametrization (2.2) to emphasize the 3-to-3 parameters relation. Let us note that, when one is interested to isolate, say $\mathcal{P}\mathcal{Q}$, and has to choose the correct fourth root in the above expression, the choice is usually guided by the domain in which we want the parameters to be. For instance, in Aztec diamonds, it is common to use real positive parameters to have a combinatorial interpretation and imposing $\mathcal{P}\mathcal{Q} > 0$ should indeed reduce to a single possibility the choice among the four roots.

Looking at the right-hand sides of (2.12) and (2.13), one can show that for u and μ on the unit circle and $0 \leqslant p < 1$, each ratio of theta functions is either real or pure imaginary. It means that for any fixed u, μ, p in these domains, there exists a choice of roots allowing the parameters of the Aztec diamonds to be real positive. The explicit description of this choice is nevertheless complicated and depends on the position of u and μ on the unit circle. There is also a more natural domain, $|u| = 1$, $|\mu| = \sqrt{p}$ and $0 \leqslant p < 1$, for which the positivity of AD parameters is guaranteed and the choice of root simpler (i.e. always the -1 root of unity for the 3 parameters $\lambda, \frac{p}{\mathcal{P}}, \frac{q}{\mathcal{Q}}$). In this domain, the quantity in the right-hand side of (2.13) is not real in general, but since this factor only concerns the relation between Aztec diamond partition functions, it is not important for it to be. In the rest of this chapter, we will refer to this second choice as the correct one to find positive parameters.

The above Aztec graph partition function uses the measure which makes a face with weight x contribute a term $x^{N_{\text{adj}}}$ (multiplied by the appropriate power of λ). If instead we use the measure for which a face

contributes a term $x^{1-N_{\mathrm{adj}}}$, we obtain the other partition function we have denoted by T in Chapter 1. The two are simply related through

$$Z_n^{\mathrm{AD}}(p,\mathcal{P},q,\mathcal{Q}|\lambda) = \\ p^{\lceil\frac{(n+1)^2}{2}\rceil}\,\mathcal{P}^{\lfloor\frac{(n+1)^2}{2}\rfloor}\,q^{\lceil\frac{n^2}{2}\rceil}\,\mathcal{Q}^{\lfloor\frac{n^2}{2}\rfloor}\,T_n^{\mathrm{AD}}(p^{-1},\mathcal{P}^{-1},q^{-1},\mathcal{Q}^{-1}|\lambda). \quad (2.14)$$

Combining with (2.10) and (2.11), we obtain,

$$Z_{n+1}^{\text{2p-6V}} = \left(\frac{c_2\,p}{\mathcal{P}}\right)^{\lceil\frac{(n+1)^2}{2}\rceil} c_2^{\lfloor\frac{(n+1)^2}{2}\rfloor}\left(\frac{q}{\mathcal{Q}}\right)^{\lceil\frac{n^2}{2}\rceil}(\mathcal{P}\mathcal{Q})^{n(n+1)}\times T_n^{\mathrm{AD}}\left(\tfrac{\mathcal{P}}{p},1,\tfrac{\mathcal{Q}}{q},1|\lambda\right). \quad (2.15)$$

When $p=\mathcal{P}=1$, so that the alternating non-trivial face weights are on the q-faces, the partition function $T_n^{\mathrm{AD}}(1,1,\frac{\mathcal{Q}}{q},1|\lambda)$ is then given by a λ-determinant. Alternatively we can keep the non-trivial weights on the p-faces, with corresponding partition function $T_n^{\mathrm{AD}}(\frac{\mathcal{P}}{p},1,1,1|\lambda)$, also given by a λ-determinant of size $n+1$. The two are easily related,

$$T_n^{\mathrm{AD}}\left(\tfrac{\mathcal{P}}{p},1,1,1|\lambda\right) = (1+\lambda)^{-(n+1)}\,T_{n+1}^{\mathrm{AD}}(1,1,\tfrac{p}{\mathcal{P}},1|\lambda). \quad (2.16)$$

As a final remark, let us note that the above correspondence started with a 6V model of size $n+1$. We could have as well started from a 6V model of size n, and the bijection with ASM of size n, themselves in correspondence with perfect matchings of Aztec graphs of order n (the 'inner' ASM whose entries are located on the q-faces, see Section 1.2.4). The same results would be obtained if we keep in mind that an entry m_{ij} in the inner ASM means that the face q_{ij} is adjacent to $1+m_{ij}$ dimers.

2.3.2 Condensation algorithm and Aztec diamond partition function

In this subsection, we show how to obtain the partition function of the biased two-periodic Aztec diamond on the basis of what has been achieved in Chapter 1.

Let us first recall some basic properties of the partition function T_n^{AD} as defined in the previous subsection (and in Chapter 1). One freedom

concerning the face weights on Aztec diamonds is the possibility to multiply all weights on an arbitrary diagonal or anti-diagonal by a constant factor. Since the underlying ASM on the p-faces has the property that the sum of the elements on each row (or column) is 1, this operation would only affect the partition function by the same amount. For the q-faces, looking at the quantity $1-N_{ij}$, with N_{ij} being the number of adjacent dimers around a face, gives rise to an ASM with interchanged $+1$ and -1. Consequently, the row (or column) sum is equal to -1. The multiplication of such a diagonal of q-faces by a constant factor would then affect the partition function by the inverse of this factor. From this remark, we deduce that

$$\begin{aligned} T_n^{\mathrm{AD}}(p,\mathcal{P},q,\mathcal{Q}|\lambda) &= \mathcal{P}\left(\frac{\mathcal{P}}{\mathcal{Q}}\right)^n T_n^{\mathrm{AD}}(\tfrac{p}{\mathcal{P}},1,\tfrac{q}{\mathcal{Q}},1|\lambda) \\ &= p\left(\frac{p}{q}\right)^n T_n^{\mathrm{AD}}(1,\tfrac{\mathcal{P}}{p},1,\tfrac{\mathcal{Q}}{q}|\lambda), \end{aligned} \tag{2.17}$$

which is actually nothing else than the equivalent of (2.11) for the function T_n^{AD}.

One of the main observations made in Section 1.2.5 was the identity between the partition function T_n^{AD} and the condensation of two matrices $\mathcal{P}$ and $\mathcal{Q}$ (of size $n+1$ and n resp.) containing as entries the weights p_{ij} and q_{ij}. Namely, the equation (1.71), that we recall here,

$$T_n^{\mathrm{AD}}\left(\mathcal{P},\mathcal{Q}|\lambda\right) = \mathrm{Cond}_\lambda\left(\overline{\mathcal{Q}},\mathcal{P}\right). \tag{2.18}$$

$\overline{\mathcal{Q}}$ can be any $(n+2)\times(n+2)$ matrix having $\mathcal{Q}$ as central $n\times n$ restriction. Using the weights $p,\mathcal{P},q,\mathcal{Q}$, the condensation algorithm produces a sequence of Toeplitz matrices (similarly to Section 1.2.2) of the form[2]

$$M_{-1}=\overline{\mathcal{Q}},\qquad M_0=\mathcal{P},\qquad M_k=\begin{pmatrix} a_k & b_k & a_k & \cdots \\ b_k & a_k & b_k & \cdots \\ a_k & b_k & a_k & \cdots \\ \vdots & \vdots & \vdots & \ddots \end{pmatrix}_{(n+1-k)\times(n+1-k)}, \tag{2.19}$$

[2]We chose to shift the indices of the sequence M_k from one unit in order to make easier the correspondence with the old sequences at $\frac{p}{\mathcal{P}}=1$ in Section 1.2.2.

where the entries satisfy the following recurrence relations, coming from the computation of 2×2 λ-minors in the condensation algorithm,

$$a_{k+1} = \frac{a_k^2 + \lambda b_k^2}{a_{k-1}}, \qquad b_{k+1} = \frac{b_k^2 + \lambda a_k^2}{b_{k-1}}, \qquad \text{with} \begin{cases} a_{-1} = q, \\ a_0 = p, \\ b_{-1} = \mathcal{Q}, \\ b_0 = \mathcal{P}. \end{cases} \tag{2.20}$$

The partition function is then given by the 1×1 matrix entry, after n iterations,

$$T_n^{\mathrm{AD}}(p, \mathcal{P}, q, \mathcal{Q}|\lambda) = \mathrm{Cond}_\lambda\left(M_{-1}, M_0\right) = (M_n)_{1\times 1} = a_n. \tag{2.21}$$

Compared to the case $\frac{p}{\mathcal{P}} = 1$, only the initial conditions have changed. This is due to the fact that the structure of the recurrence itself comes from the condensation algorithm and the Toeplitz structure of the matrices involved; it is therefore not affected by the generalization we consider here. In order to study the recurrence (2.20), it is useful to define, for $k \in \mathbb{Z}$,

$$r_k = \frac{b_k}{a_k}, \qquad r_{k+1} r_{k-1} = \frac{\lambda + r_k^2}{1 + \lambda r_k^2}, \qquad \text{with} \begin{cases} r_{-1} = \frac{\mathcal{Q}}{q}, \\ r_0 = \frac{\mathcal{P}}{p}. \end{cases} \tag{2.22}$$

Since $\frac{a_k}{a_{k-1}} = \frac{a_{k-1}}{a_{k-2}}(1+\lambda r_{k-1}^2)$, we can easily recover the partition function from the (r_k) sequence,

$$\begin{aligned} T_n^{\mathrm{AD}}(p, \mathcal{P}, q, \mathcal{Q}|\lambda) &= a_{-1} \prod_{k=0}^{n} \frac{a_k}{a_{k-1}} \\ &= a_{-1} \left(\frac{a_0}{a_{-1}}\right)^{n+1} \prod_{k=0}^{n} \prod_{\ell=0}^{k-1} (1 + \lambda r_\ell^2) \\ &= a_0 \left(\frac{a_0}{a_{-1}}\right)^{n} \prod_{k=0}^{n-1} (1 + \lambda r_k^2)^{n-k}. \end{aligned} \tag{2.23}$$

We note that the prefactor in the right-hand side is the same as in (2.17), which means that

$$T_n^{\mathrm{AD}}(1, \tfrac{\mathcal{P}}{p}, 1, \tfrac{\mathcal{Q}}{q}|\lambda) = \prod_{k=0}^{n-1} (1 + \lambda r_k^2)^{n-k}. \tag{2.24}$$

One can obtain the other relevant partition functions from this one by using the following observations:

(*i*) The exchange of the sequences $a_k \leftrightarrow b_k$ is equivalent to the exchange of $p \leftrightarrow \mathcal{P}$ and $q \leftrightarrow \mathcal{Q}$. Which means that

$$T_n^{\mathrm{AD}}(\mathcal{P}, p, \mathcal{Q}, q|\lambda) = b_n = r_n a_n = r_n T_n^{\mathrm{AD}}(p, \mathcal{P}, q, \mathcal{Q}|\lambda), \tag{2.25}$$

and, in particular,

$$T_n^{\mathrm{AD}}(\tfrac{\mathcal{P}}{p}, 1, \tfrac{\mathcal{Q}}{q}, 1|\lambda) = r_n T_n^{\mathrm{AD}}(1, \tfrac{\mathcal{P}}{p}, 1, \tfrac{\mathcal{Q}}{q}|\lambda). \tag{2.26}$$

(*ii*) Using (2.17), one can invert both fractions $\frac{\mathcal{P}}{p}$ and $\frac{\mathcal{Q}}{q}$,

$$\begin{aligned} T_n(\tfrac{p}{\mathcal{P}}, 1, \tfrac{q}{\mathcal{Q}}, 1|\lambda) &= \frac{p}{\mathcal{P}} \left(\frac{p}{\mathcal{P}}\frac{\mathcal{Q}}{q}\right)^n T_n(1, \tfrac{\mathcal{P}}{p}, 1, \tfrac{\mathcal{Q}}{q}|\lambda), \\ T_n(1, \tfrac{p}{\mathcal{P}}, 1, \tfrac{q}{\mathcal{Q}}|\lambda) &= \frac{p}{\mathcal{P}} \left(\frac{p}{\mathcal{P}}\frac{\mathcal{Q}}{q}\right)^n r_n T_n(1, \tfrac{\mathcal{P}}{p}, 1, \tfrac{\mathcal{Q}}{q}|\lambda). \end{aligned} \tag{2.27}$$

(*iii*) We could also have done all these developments in terms of b_n instead of a_n, and thus would have found

$$T_n(\mathcal{P}, p, \mathcal{Q}, q|\lambda) = b_n = b_0 \left(\frac{b_0}{b_{-1}}\right)^n \prod_{k=0}^{n-1} (1 + \lambda r_k^{-2})^{n-k}. \tag{2.28}$$

The recurrence on (r_k) ensures that this relation is equivalent to (2.23).

2.3.3 Elliptic parametrization and explicit check on the partition functions

It turns out that the recurrence on the (r_k) sequence can be solved explicitly with the use of theta functions (2.3). It is not totally surprising since we already observed that (a_k) and (b_k) were generalized Somos-4 sequences, and it is well known that such sequences are solved by elliptic functions [71].

Theorem 2.3.1. *For all $k \in \mathbb{Z}$ and $u, \mu, p \in \mathbb{C}$, with $|p| < 1$,*

$$r_k = -\frac{\theta(-(-u)^{k+1}/\mu; p)}{\theta(+(-u)^{k+1}/\mu; p)}, \quad \lambda = -\left(\frac{\theta(-u; p)}{\theta(u; p)}\right)^2, \quad r_{-1} = \frac{\mathcal{Q}}{q}, \quad r_0 = \frac{\mathcal{P}}{p}, \tag{2.29}$$

yields the unique solution to the recurrence (2.22). The theta function is defined in (2.3).

Proof. The three last equalities of the theorem give the relations between the six parameters $(\lambda, \frac{p}{\mathcal{P}}, \frac{q}{\mathcal{Q}}) \longleftrightarrow (u, \mu, p)$, and, in particular, the last two ensure that the initial conditions of (2.22) are fulfilled. In terms of the elliptic parametrization of $p/\mathcal{P}$ and $q/\mathcal{Q}$, given in (2.12), one can also verify that r_k at $k = -1, 0$ brings the expected values. For the elliptic parameters taken in the domain $0 \leqslant p < 1$, $|u| = 1$ and $|\mu| = \sqrt{p}$, one can verify the choice of fourth roots of unity given by the theorem ensures the positivity of $(\lambda, \frac{p}{\mathcal{P}}, \frac{q}{\mathcal{Q}})$ and of the (r_k) sequence for all $k \in \mathbb{Z}$. So that, it only remains to show that the r_k and λ defined above respect the recurrence relation for all k. For that, let us examine the quantities

$$\begin{aligned} \lambda + r_k^2 &= \frac{\theta(-(-u)^{k+1}/\mu)^2\theta(u)^2 - \theta((-u)^{k+1}/\mu)^2\theta(-u)^2}{\theta((-u)^{k+1}/\mu)^2\theta(u)^2} \\ &= -u\frac{\theta(-(-u)^{k+2}/\mu)\theta(-(-u)^k/\mu)\theta(-1)^2}{\theta((-u)^{k+1}/\mu)^2\theta(u)^2} \end{aligned} \tag{2.30}$$

and

$$\begin{aligned} 1 + \lambda r_k^2 &= \frac{\theta((-u)^{k+1}/\mu)^2\theta(u)^2 - \theta(-(-u)^{k+1}/\mu)^2\theta(-u)^2}{\theta((-u)^{k+1}/\mu)^2\theta(u)^2} \\ &= -u\frac{\theta((-u)^{k+2}/\mu)\theta((-u)^k/\mu)\theta(-1)^2}{\theta((-u)^{k+1}/\mu)^2\theta(u)^2}. \end{aligned} \tag{2.31}$$

These identities on theta functions are readily obtained using (2.125). We now take the ratio of the two and find, for all $k \in \mathbb{Z}$,

$$\frac{\lambda + r_k^2}{1 + \lambda r_k^2} = \frac{\theta(-(-u)^{k+2}/\mu)\theta(-(-u)^k/\mu)}{\theta(+(-u)^{k+2}/\mu)\theta(+(-u)^k/\mu)} = r_{k+1}r_{k-1}, \tag{2.32}$$

as desired. □

Remark. In terms of Jacobi theta function, the theorem would read

$$r_k = \frac{\vartheta_3(\tilde{\mu} + k\,\tilde{u}; \tilde{p})}{\vartheta_4(\tilde{\mu} + k\,\tilde{u}; \tilde{p})}, \qquad \lambda = \left(\frac{\vartheta_1(\tilde{u}; \tilde{p})}{\vartheta_2(\tilde{u}; \tilde{p})}\right)^2, \tag{2.33}$$

after an adequate change of variables between the tilde and non-tilde variables. This solution is real positive for $(\tilde{u}, \tilde{\mu}, \tilde{p}) \in \mathbb{R}$. The relations between multiplicative and additive conventions of theta functions are given in Appendix 2.A.

From the relations (2.24) and (2.31), the partition function T_n^{AD} immediately follows

$$T_n^{\mathrm{AD}}(1,\tfrac{\mathcal{P}}{p},1,\tfrac{\mathcal{Q}}{q}|\lambda)=\left(\frac{-u\,\theta(-1)^2}{\theta(u)^2}\right)^{\frac{n(n+1)}{2}}\left(\frac{\theta(1/\mu)}{\theta(-u/\mu)}\right)^n\frac{\theta((-u)^{n+1}/\mu)}{\theta(-u/\mu)}. \tag{2.34}$$

Or alternatively,

$$T_n^{\mathrm{AD}}(\tfrac{\mathcal{P}}{p},1,\tfrac{\mathcal{Q}}{q},1|\lambda)=\left(\frac{-u\,\theta(-1)^2}{\theta(u)^2}\right)^{\frac{n(n+1)}{2}}\left(\frac{\theta(1/\mu)}{\theta(-u/\mu)}\right)^n\frac{\theta(-(-u)^{n+1}/\mu)}{\theta(-u/\mu)}, \tag{2.35}$$

by using (2.26). These partition functions are real positive for all $n\in\mathbb{N}$, $0\leqslant p<1$, $|u|=1$ and $|\mu|=\sqrt{p}$.

The details about the relation between the two-periodic Aztec diamond and the 2p-6V model have been discussed in Section 2.3.1. We recall here the equation (2.15),

$$Z_{n+1}^{\text{2p-6V}}=\left(\frac{c_2\,p}{\mathcal{P}}\right)^{\lceil\frac{(n+1)^2}{2}\rceil}C_2^{\lfloor\frac{(n+1)^2}{2}\rfloor}\left(\frac{q}{\mathcal{Q}}\right)^{\lceil\frac{n^2}{2}\rceil}(\mathcal{P}\mathcal{Q})^{n(n+1)}\times T_n^{\mathrm{AD}}(\tfrac{\mathcal{P}}{p},1,\tfrac{\mathcal{Q}}{q},1|\lambda). \tag{2.36}$$

For the choice of weights (2.2), and by using the relations (2.12) and (2.13), one can verify that the factor in front of T_n^{AD} is equal to

$$\mathcal{A}_n=\left(\frac{\mathrm{i}\,\theta(u)}{\theta(-1)}\right)^{n(n+1)}\left(\frac{\theta(-u/\mu)}{\theta(1/\mu)}\right)^{n+1}\left(\frac{\theta(1/\mu)}{\theta(-1/\mu)}\right)^{\delta_{n,\mathrm{odd}}}. \tag{2.37}$$

Since $\mathcal{P}\mathcal{Q}$ appears with an even power for any n, we can take any of the two roots $\mathcal{P}\mathcal{Q}=\pm\mathrm{i}\frac{\theta(u)\theta(-1/\mu)}{\theta(-1)\theta(-u/\mu)}$ in (2.13). With this result at hands and with the partition function (2.35), we are now able to verify explicitly that the partition functions of both models coincide,

$$\mathcal{A}_nT_n^{\mathrm{AD}}(\tfrac{\mathcal{P}}{p},1,\tfrac{\mathcal{Q}}{q},1|\lambda)=u^{n(n+1)/2}\frac{\theta(-(-u)^{n+1}/\mu)}{\theta((-1)^n/\mu)}=Z_{n+1}^{\text{2p-6V}}(u;\mu,p). \tag{2.38}$$

2.4 One-refined tangent method

The purpose of this section is the computation of a parametric form for the arctic curve of the elliptic SOS model at the free-fermion point via

the geometric (or one-refined) tangent method, introduced by Colomo and Sportiello [43]. As we have seen in the previous section, the model is closely related to biased two-periodic Aztec diamonds. In particular, the relation between the partition functions of both models (and the way the configurations are weighted) allows one to verify that their arctic curves coincide. For this reason, in the following, we will focus our work on the 8VSOS for which we have the benefit to possess expressions for the fully inhomogeneous generalization. Although, we emphasize that it is not an imperative ingredient to compute the one-refined partition function, it greatly simplifies the derivation of its generating function[3].

Concerning the geometric tangent method, a detailed description is given in [52] and we mainly follow the same scheme. The strategy of this technique is briefly recalled in Section 2.4.3. In summary, to accomplish this task, we essentially need two quantities: $Z_{n+1,k}$, the one-refined partition function (i.e. the weighted sum on configurations while the position of the vertex c_2 (or C_2) on the first column is fixed at position k) and Z_1^{up}, the partition function of a single path on the elliptic SOS graph with no constrain. In the following subsection, we compute the first of these two quantities, while the path generating function is computed in the one after.

2.4.1 One-refined partition function

For this subsection, we consider the inhomogeneous extension of the model on a domain of size $n+1$ with domain wall boundary conditions and set the spectral parameters for the columns as $(u_0, u_1, \dots, u_n) = (t, u, \dots, u)$ and for the rows as $(v_0, v_1, \dots, v_n) = (1, 1, \dots, 1)$, as depicted in Figure 2.7. The parameter t is introduced to control the dependence on the zeroth column and compute the one-refined partition function, but the model that we really study is the one described at $t = u$.

[3] For instance, another possibility would be to use the elliptic solution of the (r_k) sequence together with the octahedron recurrence satisfied by the AD refined partition functions [52] to obtain a sum rule of the type (2.44).

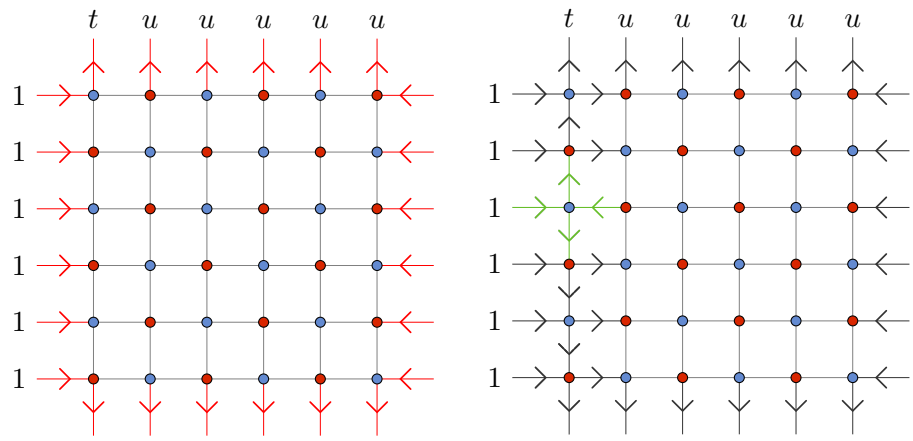

Figure 2.7: *Left*: grid of size 6 with DWBC (in red). The sites with $i+j$ even are represented in blue, the others in red. *Right*: the zeroth column is filled with a- and b-vertices with (necessarily) a unique c_2, drawn in green, marking the transition between them.

With our specialization, the partition function (2.7) reads

$$Z_{n+1}(t) = Z_{n+1}(t,u;\mu,p) = u^{n(n+1)/2}\frac{\theta((-u)^n t/\mu)}{\theta((-1)^n/\mu)}\left[\frac{\theta(-t/u)}{\theta(-1)}\right]^n, \tag{2.39}$$

and we also note that

$$Z_n(u) = u^{n(n-1)/2}\frac{\theta(-(-u)^n/\mu)}{\theta((-1)^{n+1}/\mu)}. \tag{2.40}$$

What we call a (one-)refined partition function (also called sometimes *one-point boundary correlation function* [43, 72]) is the weighted enumeration of configurations while the vertex content of the first column is prescribed. Due to the boundary conditions and the ice-rule, we know there is a unique vertex of type c_2 in this column and its position alone, let us call it[4] k ($0 \leqslant k \leqslant n$), fixes the remaining vertices of the column; the ones above are of type a_1, and those below are of type b_2.

On one hand, since by summing k over the whole column we have to recover the total state enumeration, the partition function must satisfy

[4] We count the position from 0 to n starting from the upper edge.

the decomposition

$$Z_{n+1}(t) = \sum_{k=0}^{n} Z_{n+1,k}(t). \tag{2.41}$$

On the other hand, once k is fixed, we know exactly the vertex content of the zeroth column, as explained above. We find either a c_2 or C_2 at position k (depending on k even or odd resp.), then essentially k vertices of type a and $n-k$ vertices of type b. This observation allows us to extract the dependence on t of $Z_{n+1,k}(t)$. More precisely, what we have is

$$\begin{aligned} Z_{n+1,k}(t) &= a^{\lceil k/2\rceil} A^{\lfloor k/2\rfloor} \left\{ \begin{array}{ll} b^{\lceil (n-k)/2\rceil} B^{\lfloor (n-k)/2\rfloor} & \text{if } n \text{ even} \\ b^{\lfloor (n-k)/2\rfloor} B^{\lceil (n-k)/2\rceil} & \text{if } n \text{ odd} \end{array} \right\} \\ &\qquad \times \left\{ \begin{array}{ll} c_2 & \text{if } k \text{ even} \\ C_2 & \text{if } k \text{ odd} \end{array} \right\} \mathbb{A}_{n,k}(u) \\ &= \left[\frac{\theta(-t)}{\theta(-1)}\right]^k \left[\frac{\mathrm{i}\,\theta(t)}{\theta(-1)}\right]^{n-k} \left[\frac{\theta((-1)^{n+1}\mu)}{\theta((-1)^n\mu)}\right]^{\delta_{n-k,\mathrm{odd}}} \left[\frac{\theta((-1)^k t/\mu)}{\theta((-1)^k/\mu)}\right] \mathbb{A}_{n,k}(u), \end{aligned} \tag{2.42}$$

where $\mathbb{A}_{n,k}(u)$ is the partition function on the domain with its zeroth column removed and with a reversed, that is, outgoing, arrow at position k (resulting from the presence of the c_2 or C_2 vertex at this position). Since $\mathbb{A}_{n,k}(u)$ does not depend on t, one can divide the above expression by $Z_{n+1,k}(u)$ and obtain the relation

$$Z_{n+1,k}(t) = \left[\frac{\theta(-t)}{\theta(-u)}\right]^k \left[\frac{\theta(t)}{\theta(u)}\right]^{n-k} \left[\frac{\theta((-1)^k t/\mu)}{\theta((-1)^k u/\mu)}\right] Z_{n+1,k}(u). \tag{2.43}$$

It would have been possible to obtain this relation faster by looking at the behaviour in t of the first column and by extracting directly the ratio of refined partition functions $Z_{n+1,k}(t)/Z_{n+1,k}(u)$, but we found it more pedagogical this way.

Let us define the $C_k = Z_{n+1,k}(u)/Z_n(u)$, the ratio of partition functions of interest for the tangent method, and $\xi(t) = \frac{\theta(-t)}{\theta(+t)}\frac{\theta(+u)}{\theta(-u)}$. We now insert (2.39) and (2.43) in the decomposition (2.41) and obtain, after

some simplifications,

$$F(t)=\frac{Z_{n+1}(t)}{Z_n(u)}\left[\frac{\theta(u)}{\theta(t)}\right]^n=u^n\frac{\theta((-1)^{n+1}/\mu)\theta((-u)^n t/\mu)}{\theta((-1)^n/\mu)\theta(-(-u)^n/\mu)}\left[\frac{\theta(-t/u)}{\theta(-1)}\frac{\theta(u)}{\theta(t)}\right]^n$$
$$=\sum_{k=0}^{n} C_k\,\xi^k\left[\frac{\theta((-1)^k t/\mu)}{\theta((-1)^k u/\mu)}\right]. \tag{2.44}$$

We can split the summations on k even and odd, and extract the oscillating factor $\left[\frac{\theta((-1)^k t/\mu)}{\theta((-1)^k u/\mu)}\right]$ from each term,

$$F(t)=\frac{\theta(t/\mu)}{\theta(u/\mu)}F_0(t)+\frac{\theta(-t/\mu)}{\theta(-u/\mu)}F_1(t), \tag{2.45}$$

where $F_0(t)$ and $F_1(t)$ are the terms in the sum $\sum_{k=0}^{n} C_k\,\xi^k$ corresponding to k even and odd respectively. Evaluating the expression at $t\mapsto t^{-1}$ and using $\xi(t^{-1})=-\xi(t)$ yields a second relation,

$$F(t^{-1})=\frac{\theta(1/t\mu)}{\theta(u/\mu)}F_0(t)-\frac{\theta(-1/t\mu)}{\theta(-u/\mu)}F_1(t). \tag{2.46}$$

These two relations can be viewed as a linear system which relates the two pairs of functions $\big(F(t),F(t^{-1})\big)\longleftrightarrow\big(F_0,F_1\big)$, and allow us to determine, for $k=0,1$,

$$F_k(t)=\theta((-1)^k u/\mu)\frac{F(t)\,\theta((-1)^{k+1}/t\mu)+(-1)^k F(t^{-1})\,\theta((-1)^{k+1}t/\mu)}{\theta(t/\mu)\theta(-1/t\mu)+\theta(-t/\mu)\theta(1/t\mu)}. \tag{2.47}$$

By the Cauchy theorem, we thus obtain an integral formula for the coefficients

$$C_k=\frac{1}{2\pi\mathrm{i}}\oint_0\frac{F_{k\bmod 2}}{\xi^{k+1}}\mathrm{d}\xi=\frac{1}{2\pi\mathrm{i}}\oint_{-1}\frac{F_{k\bmod 2}(t)}{\xi^{k+1}(t)}\xi'(t)\mathrm{d}t. \tag{2.48}$$

The numerator in (2.47) contains two terms, but for the second one, we may change the integration variable by $t\mapsto t^{-1}$ and remark that its contribution is the same as the first term:

(*i*) The change of variables $t\mapsto t^{-1}$ preserves the position of the pole at $t=-1$, and the orientation of the integration contour.

(*ii*) $F_k(t^{-1})=(-1)^k F_k(t)$.

(*iii*) $\xi^{k+1}(t^{-1}) = (-1)^{k+1}\xi^{k+1}(t)$.

(*iv*) $\mathrm{d}(t^{-1}) = -t^{-2}\mathrm{d}t$.

(*v*) $\frac{\mathrm{d}}{\mathrm{d}(t^{-1})}\xi(t^{-1}) = t^{-2}\frac{\mathrm{d}}{\mathrm{d}t}\xi(t)$.

We now let k scale with the size of the domain, $k = rn$ with $r \in [0,1]$, and use the above observation to rewrite

$$C_k = \frac{1}{\pi \mathrm{i}} \oint_{-1} B_k(t) \left[u \frac{\theta(u)\theta(-t/u)}{\theta(-1)\theta(t)\xi^r} \right]^n \mathrm{d}t = \frac{1}{\pi \mathrm{i}} \left[\frac{u\theta(u)}{\theta(-1)} \right]^n \oint_{-1} B_k(t) \mathrm{e}^{n\varphi(t,r)} \mathrm{d}t. \tag{2.49}$$

We set

$$\begin{aligned} B_k(t) &= \frac{\theta((-1)^k u/\mu)\theta((-1)^{k+1}/t\mu)}{\theta(t/\mu)\theta(-1/t\mu)+\theta(-t/\mu)\theta(1/t\mu)} \cdot \frac{\theta((-1)^{n+1}/\mu)\theta((-u)^n t/\mu)\xi'(t)}{\theta((-1)^n/\mu)\theta(-(-u)^n/\mu)\xi(t)} \\ &= \frac{(p^2;p^2)_\infty^2}{\theta(t^2;p^2)} \frac{\theta\left(\frac{(-1)^{k+1}}{\mu t}\right)\theta\left(\frac{(-1)^k u}{\mu}\right)\theta\left(\frac{t(-u)^n}{\mu}\right)}{\theta\left(\frac{(-1)^n}{\mu}\right)^2 \theta\left(-\frac{(-u)^n}{\mu}\right)}, \end{aligned} \tag{2.50}$$

with $(p;p)_\infty = \prod_{j=1}^\infty (1-p^j)$, the Euler function, which is itself related to a special evaluation of q-Pochhammer symbols, $(a;q)_\infty = \prod_{j=0}^\infty (1-aq^j)$. We may assume that $B_k(t)$ does not affect the leading order of the asymptotics since this factor can be bounded by quantities independent of n and is non-singular for generic values of the parameters[5]. In particular, for $0 \leqslant p < 1$, we can use the inequalities $|\theta(|z|)| \leqslant |\theta(z)| \leqslant |\theta(-|z|)|$ to obtain the following explicit bounds on B_k,

$$\left| \frac{\theta(|\frac{t}{\mu}|)\theta(|\frac{1}{t\mu}|)\theta(|\frac{1}{\mu}|)}{\theta(-|\frac{1}{\mu}|)^3} \right| \leqslant \left| \frac{\theta(t^2;p^2)}{(p^2;p^2)_\infty^2} B_k(t) \right| \leqslant \left| \frac{\theta(-|\frac{t}{\mu}|)\theta(-|\frac{1}{t\mu}|)\theta(-|\frac{1}{\mu}|)}{\theta(|\frac{1}{\mu}|)^3} \right|, \tag{2.51}$$

where we also assumed $|u| = 1$.

The function

$$\varphi(t,r) = \log \frac{\theta(-t/u)}{\theta(t)} - r \log \frac{\theta(-t)\,\theta(u)}{\theta(t)\,\theta(-u)} \tag{2.52}$$

thus controls the exponential rate of C_k and the integral (2.49) is well suited for applying the saddle point method. Let us define the function

[5] In fact, it is not difficult to see that the values of t, u, μ where $B_k = 0, \infty$ correspond to some choices where the vertex weights (2.2) themselves are singular.

$\phi(z) = z\theta'(z)/\theta(z)$. The saddle point equation reads[6]

$$\boldsymbol{t}\,\partial_t\varphi(\boldsymbol{t},r) = \phi(-\boldsymbol{t}/u) - \phi(\boldsymbol{t}) - r(\phi(-\boldsymbol{t}) - \phi(\boldsymbol{t})) = 0. \tag{2.53}$$

By isolating r in the equation,

$$r = \frac{\phi(\boldsymbol{t}) - \phi(-\boldsymbol{t}/u)}{\phi(\boldsymbol{t}) - \phi(-\boldsymbol{t})}, \tag{2.54}$$

we obtain an implicit solution for $\boldsymbol{t}(r)$, the position of the saddle point. We chose to call the saddle point $\boldsymbol{t} = \boldsymbol{t}(r)$ to emphasize the distinction with the initial spectral parameter t (which does not depend on r). We note that, for $\boldsymbol{t}$ and u on the unit circle (more precisely: either both on the upper half of the u.c. or both on its lower half), and $0 \leqslant p < 1$, we find $r \in [0,1]$. The asymptotics of the C_k's follows,

$$\lim_{n\to\infty} \frac{1}{n} \log C_k = \varphi(\boldsymbol{t}(r),r) + \log\left[\frac{u\,\theta(u)}{\theta(-1)}\right]. \tag{2.55}$$

The second term is not really important for our purpose since, for the tangent method, only the derivative in r of this quantity will matter; due to the saddle point equation, we find

$$\frac{\mathrm{d}}{\mathrm{d}r}\varphi(\boldsymbol{t}(r),r) = \frac{\partial}{\partial r}\varphi(\boldsymbol{t}(r),r) = -\log\xi(\boldsymbol{t}(r)). \tag{2.56}$$

Let us remark that in the limit $p,\mu \to 0$, in which we recover the usual free-fermionic six-vertex model, it is known that the coefficient $C_k = \frac{Z_{n+1,k}(u)}{Z_n(u)}$ are essentially given by binomial coefficients $\binom{n+1}{k}$ while the dependence on u factorizes. The coefficients C_k we studied in this section can therefore be seen as an elliptic generalization of these binomial coefficients. Unfortunately, we could not obtain any closed formula for them at finite n,k.

Another quantity that can be computed at this stage is the maximum in r of the exponential rate. It follows from (2.56) that this maximum r_{c} is given by

$$\frac{\mathrm{d}}{\mathrm{d}r}\varphi(\boldsymbol{t}(r_{\mathrm{c}}),r_{\mathrm{c}}) = -\log\xi(\boldsymbol{t}(r_{\mathrm{c}})) = 0. \tag{2.57}$$

[6] We suppose that, for some values of the parameters at least, a solution $\boldsymbol{t}(r)$ to this equation exist and that we can deform the contour integral into a suitable contour for the saddle point analysis (i.e. a contour $\gamma(t)$ around -1 that passes through $\boldsymbol{t}(r)$ and such that $\mathrm{Re}\,\gamma(t)$ has a unique global maximum at $\boldsymbol{t}(r)$).

It is easy to verify that $\xi(\boldsymbol{t}(r_{\mathrm{c}})) = 1$ when $\boldsymbol{t}(r_{\mathrm{c}}) = u$, and by inserting this result in (2.54), we find

$$r_{\mathrm{c}} = \frac{\phi(u) - \phi(-1)}{\phi(u) - \phi(-u)}. \tag{2.58}$$

In the regime of large n this quantity corresponds to the maximum in r of $Z_{n+1,rn}(u)$ and therefore describes the likeliest position of the vertex c_2 or C_2 in the zeroth column. In the scaling limit, it thus gives the position at which the arctic curve touches the edge of the domain. One can also verify that if we let[7] $p \to 0$, we find

$$r_{\mathrm{c}}(p = 0) = \frac{(1+u)^2}{4u} = \frac{\lambda}{1+\lambda}, \tag{2.59}$$

which indeed corresponds to the contact point in the usual 6V model at the free-fermion point.

2.4.2 Path generating function

In this subsection, we aim to compute the generating function for "paths" in this elliptic SOS grid. First, let us for this define a path representation of this vertex model. We do this by replacing at each vertex the arrow configuration by a specific path segment, as listed in Figure 2.8.

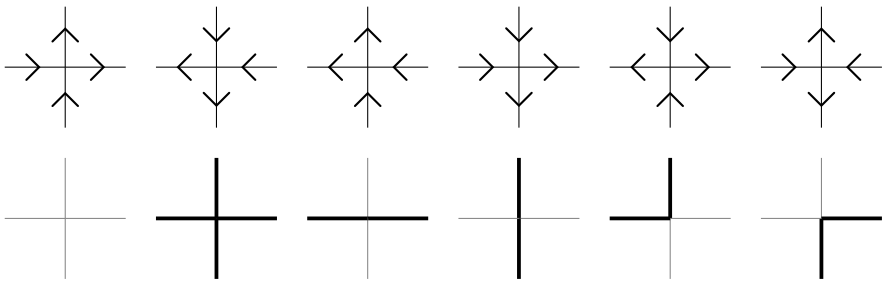

Figure 2.8: Dictionary between vertex and path representations: down and left arrows are replaced by thick lines while up and right arrows are replaced by thin gray lines.

[7] We recall that $\theta(z; p = 0) = 1 - z$ and $\phi(z; p = 0) = z/(z-1)$.

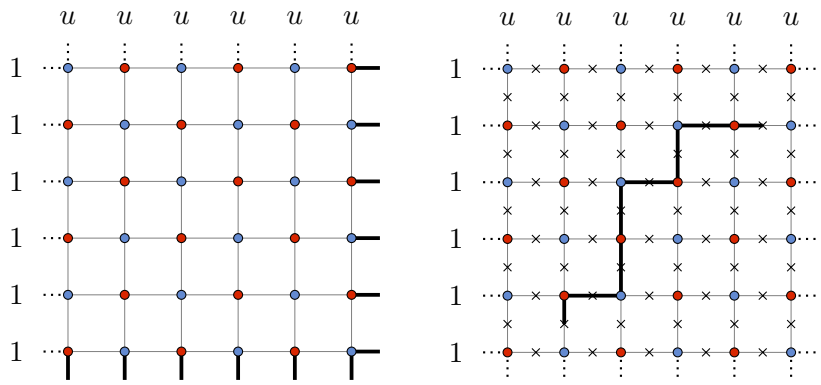

Figure 2.9: *Left*: representation of the domain with domain wall boundary conditions for the non-intersecting path representation. *Right*: example of an isolated path starting at $(i, j+\frac{1}{2})$ and ending at $(i'+\frac{1}{2}, j')$. The black crosses indicate the possible intermediate steps between each path fragment.

A consequence of the ice-rule is the conservation in the number of solid line passing through each vertex. The result on configurations is that the number of paths through the entire domain is conserved. Moreover, these paths cannot cross each other, only kissing points are allowed by a_2-type vertex. The domain wall boundary conditions impose to n paths to connect the bottom and right edges. We use the conventional orientation and consider they start at the bottom edge. Hence, due to the non-intersecting property, these paths necessarily end at the right edge in the same order as they entered the domain. An illustration of the lattice with DWBC as well as an example of paths are provided in Figure 2.9.

In order to compute the generating function of these paths, we start by listing all the different elementary lattice steps with their associated weights: for i, j positive integers, we have

$$w[(i-\tfrac{1}{2}, j) \to (i+\tfrac{1}{2}, j)] = \begin{cases} b_1 & \text{if } i+j \text{ even}, \\ B_1 & \text{if } i+j \text{ odd}, \end{cases} \tag{2.60a}$$

$$w[(i, j-\tfrac{1}{2}) \to (i, j+\tfrac{1}{2})] = \begin{cases} b_2 & \text{if } i+j \text{ even}, \\ B_2 & \text{if } i+j \text{ odd}, \end{cases} \tag{2.60b}$$

$$w[(i-\tfrac{1}{2},j)\to(i,j+\tfrac{1}{2})]=\begin{cases}c_1 & \text{if } i+j \text{ even},\\ C_1 & \text{if } i+j \text{ odd},\end{cases} \tag{2.60c}$$

$$w[(i,j-\tfrac{1}{2})\to(i+\tfrac{1}{2},j)]=\begin{cases}c_2 & \text{if } i+j \text{ even},\\ C_2 & \text{if } i+j \text{ odd}.\end{cases} \tag{2.60d}$$

To simplify the discussion, we suppose the blue vertices to be located at sites (i,j) such that $i+j$ is even. It is not difficult to change it to $i+j-n$ even in order to fit with our previous convention on the grid. We will not do it since it doesn't affect the final result anyway. We denote by $Z^{\text{path}}_{i,j}$ the partition function of the paths (i.e. the weighted sum over all possible paths) going from[8] $(0,\frac{1}{2})$ to $(i,j+\frac{1}{2})$ with i,j either both integers are both half-integers. Due to the nature of the lattice, we define, for $i,j\in\mathbb{N}$, the four quantities $Z^{\text{e}}_{i+\frac{1}{2},j}$, $Z^{\text{e}}_{i,j+\frac{1}{2}}$, $Z^{\text{o}}_{i+\frac{1}{2},j}$ and $Z^{\text{o}}_{i,j+\frac{1}{2}}$ according to $i+j$ being even or odd. Each of these functions enumerates the paths coming from $(0,\frac{1}{2})$ to the position corresponding to their indices. From the lattice steps above, we deduce the following recurrence relations on these path partition functions,

$$\begin{aligned}
Z^{\text{e}}_{i,j+\frac{1}{2}} &= b_2 Z^{\text{o}}_{i,j-\frac{1}{2}} + c_1 Z^{\text{o}}_{i-\frac{1}{2},j} + \delta_{i,0}\delta_{j,0} && \text{if } i+j \text{ even},\\
Z^{\text{o}}_{i,j+\frac{1}{2}} &= B_2 Z^{\text{e}}_{i,j-\frac{1}{2}} + C_1 Z^{\text{e}}_{i-\frac{1}{2},j} && \text{if } i+j \text{ odd},\\
Z^{\text{e}}_{i+\frac{1}{2},j} &= b_1 Z^{\text{o}}_{i-\frac{1}{2},j} + c_2 Z^{\text{o}}_{i,j-\frac{1}{2}} && \text{if } i+j \text{ even},\\
Z^{\text{o}}_{i+\frac{1}{2},j} &= B_1 Z^{\text{e}}_{i-\frac{1}{2},j} + C_2 Z^{\text{e}}_{i,j-\frac{1}{2}} && \text{if } i+j \text{ odd}.
\end{aligned} \tag{2.61}$$

Let us define the generating functions associated to these sequences, $G^{\alpha,\text{I}}(x,y)=\sum_{i,j\in\mathbb{N}} Z^{\alpha}_{i,j+\frac{1}{2}}x^iy^j$ and $G^{\alpha,\text{H}}(x,y)=\sum_{i,j\in\mathbb{N}+\frac{1}{2}} Z^{\alpha}_{i,j+\frac{1}{2}}x^iy^j$ with $\alpha=\text{e},\text{o}$. The letters I,H stand for integers and half-integers. The above recurrences induce a system of equation satisfied by these generating functions,

$$G^{\text{e,I}}(x,y)=b_2\,y\,G^{\text{o,I}}(x,y)+c_1\,\sqrt{xy}\,G^{\text{o,H}}(x,y)+1, \tag{2.62a}$$

$$G^{\text{o,I}}(x,y)=B_2\,y\,G^{\text{e,I}}(x,y)+C_1\,\sqrt{xy}\,G^{\text{e,H}}(x,y), \tag{2.62b}$$

[8] We could also have considered in addition the paths starting from $(1/2,0)$ by adding another $\delta_{i,0}\delta_{j,0}$ in the corresponding recurrence. It would have affected the numerator of the generating but not the denominator, which is the only part that contribute to the large deviation function.

$$G^{\mathrm{e,H}}(x,y) = b_1\, x\, G^{\mathrm{o,H}}(x,y) + c_2\, \sqrt{xy}\, G^{\mathrm{o,I}}(x,y), \tag{2.62c}$$

$$G^{\mathrm{o,H}}(x,y) = B_1\, x\, G^{\mathrm{e,H}}(x,y) + C_2\, \sqrt{xy}\, G^{\mathrm{e,I}}(x,y). \tag{2.62d}$$

This linear system can be solved easily and yields rational expressions (in the variables $x, y, \sqrt{xy}$) for each sub-generating function. By summing the four contributions, we obtain the total generating function

$$G(x,y) = \sum_{\substack{\alpha=\mathrm{e,o}\\ \beta=H,I}} G^{\alpha,\beta}(x,y) = \frac{1+y(B_2-xc_2C_1)-x^2b_1(B_1-yA_1A_2)+\sqrt{xy}(x(b_1C_2-yc_2A_1A_2)+B_2c_2y+C_2)}{1-xy(c_2C_1+c_1C_2)-x^2b_1B_1-y^2b_2B_2+x^2y^2(b_1b_2-c_1c_2)(B_1B_2-C_1C_2)}. \tag{2.63}$$

By using the free-fermion rule (2.4) mentioned in the introduction of the 8VSOS model, one can simplify the denominator (the numerator has already been simplified),

$$Q(x,y) = 1 - xy\,(c_2C_1 + c_1C_2) - x^2b_1B_1 - y^2b_2B_2 + x^2y^2a_1a_2A_1A_2. \tag{2.64}$$

Only the denominator is interesting for us since we don't need the subleading corrections to the exponential rate; $Z^{\mathrm{path}}_{r_1 n,\, r_2 n} \sim \mathrm{e}^{r_1 n L(\sigma)}$ where $\sigma = r_2/r_1 \in [0,\infty)$ is the slope of the straight line joining the endpoints of the path. This asymptotics can be obtained via the saddle point method, or by using the framework of [73]. Both yield the result $L(\sigma) = -\log \boldsymbol{x} - \sigma \log \boldsymbol{y}$ where $\boldsymbol{x}(\sigma)$ and $\boldsymbol{y}(\sigma)$ are the unique real positive solution of the system

$$\begin{cases} Q(\boldsymbol{x},\boldsymbol{y}) = 0, \\ \sigma\, \boldsymbol{x}\partial_x Q(\boldsymbol{x},\boldsymbol{y}) - \boldsymbol{y}\partial_y Q(\boldsymbol{x},\boldsymbol{y}) = 0. \end{cases} \tag{2.65}$$

By multiplying the first equation by $1-\sigma$ and taking the sum of the two, one can kill the terms in $\boldsymbol{xy}$ and $(\boldsymbol{xy})^2$, and find a quadratic equation for $\boldsymbol{x}$ with no linear term, from which we deduce

$$\boldsymbol{x}(s) = \frac{1}{\sqrt{b_1B_1}} \sqrt{\frac{s-z^2}{s\lambda^2 z^2 - 1}}, \tag{2.66}$$

with

$$z(s) = \boldsymbol{y}(s)\sqrt{b_2B_2} \qquad \text{and} \qquad s = \frac{\sigma-1}{\sigma+1} \in [-1,1]. \tag{2.67}$$

Inserting this result in the first equation allow us, in principle, to determine $z(s)$. However, the result is rather complicated and not useful anyway. It is actually easier for us to work with the inverse relation and use z as the independent variable for the parametrization of sigma,

$$s(z)=\Big[\alpha z\Big(1-\lambda^2z^4\Big)\sqrt{\alpha^2z^2+4(1-z^2)(1-\lambda^2z^2)}-\alpha^2z^2\Big(1+\lambda^2z^4\Big)$$
$$-2\Big(1-2z^2+\lambda^2z^4\Big)\Big(1-2\lambda^2z^2+\lambda^2z^4\Big)\Big]\frac{1}{2(1-2\lambda^2z^2+\lambda^2z^4)^2-2\alpha^2\lambda^2z^4}, \tag{2.68}$$

where we set $\alpha=\frac{c_1C_2+c_2C_1}{\sqrt{b_1b_2B_1B_2}}=-\frac{u\theta(-1)^3\theta(u^2)}{\theta(u)^3\theta(-u)}$ (using (2.122)). We note that since $\alpha(u)$ and $\lambda(u)$ are both independent of μ, the dynamical parameter, $s(z)$ also is. It was already the case in the previous subsection during the computation of the exponential rate of C_k, but it is quite surprising that the dependence on μ completely disappears from the leading order. We will come back to this observation in Section 2.6.

In the next subsection, we will need the values of $r_1L(\sigma(s))=r_1\tilde{L}(s)=-r_1\log\boldsymbol{x}-r_2\log\boldsymbol{y}$ when $\sigma=0,\infty$ or equivalently when $s=-1,1$ respectively. For that, let us remark that $s(z=0)=-1$, $s(z=1)=1$ and consequently $z(s=-1)=0$ and $z(s=1)=1$. Hence, we find in the case where $r_1=1,r_2=0$ that

$$r_1L(\sigma=0)=r_1\tilde{L}(s=-1)=-\log\boldsymbol{x}(s=-1)=\log\sqrt{b_1B_1}, \tag{2.69}$$

and when $r_1=0,r_2=1$,

$$r_1L(\sigma=\infty)=r_1\tilde{L}(s=1)=-\log\boldsymbol{y}(s=1)=\log\sqrt{b_2B_2}. \tag{2.70}$$

Intuitively, these quantities correspond to the exponential rate of a path following a horizontal (resp. vertical) straight line.

To conclude this subsection, let us also note that the derivative of the function $L(\sigma)$ is nicely given by

$$L'(\sigma)=\frac{\mathrm{d}}{\mathrm{d}\sigma}L(\sigma)=\frac{\partial}{\partial\sigma}L(\sigma)=-\log\boldsymbol{y}(\sigma). \tag{2.71}$$

This result is a simple consequence of the system (2.65) solved by $\boldsymbol{x},\boldsymbol{y}$. By taking the derivative of the first equation with respect to σ, one obtains the equality $\frac{\partial_yQ}{\partial_xQ}=-\frac{\boldsymbol{x}'(\sigma)}{\boldsymbol{y}'(\sigma)}$ and together with the second equation it yields $\frac{\boldsymbol{x}'(\sigma)}{\boldsymbol{y}'(\sigma)}=-\sigma\frac{\boldsymbol{x}(\sigma)}{\boldsymbol{y}(\sigma)}$, from which (2.71) readily follows.

2.4.3 One-refined parametrization of the arctic curve

The geometric tangent method as formulated in [43] can be described as follows. The quantity $Z_{n+1,k}$ retains only the configurations where the first path leaves the left edge at position $k = rn$ (measured from the upper-left corner), as depicted in Figure 2.10. This path is then free to proceed to the right and necessarily merges with the arctic curve at some point. Once the curve touches the upper edge, the path will eventually continue as a horizontal straight line until it reaches the right edge. In the scaling limit, the tangent method works under the two hypotheses: (i) the shape of the arctic curve is not affected by the uppermost path forced to leave the left boundary at k, and (ii) this uppermost path, after leaving the left edge, will continue toward the arctic curve as a straight line (with a probability that goes to 1 as n becomes large) and meets it tangentially before merging with the curve. In general, the hypothesis (i) is harder to control and has been made rigorous only in the context of the six-vertex model [74]. The second assumption can be deduced from the first one in a quite general framework [75].

In the following, we denote by $(x, h(x))$ the cartesian[9] parametrization of the (external) arctic curve and by $x_* = x_*(r)$ the abscissa where the uppermost path, in red in Figure 2.10, tangentially meets the arctic curve. Under the assumptions of the previous paragraph, the portion of the red path tangent to the arctic curve follows the straight line equation $y = \sigma_* x + (1 - r)$, where we denote by $\sigma_* = \sigma_*(r) = h'(x_*)$ its slope. By varying r, we obtain a family of straight lines which reproduces the arctic curve as an envelope. This latter is therefore immediately given by the system

$$\begin{cases} x(r) = \left(\frac{\mathrm{d}\sigma_*}{\mathrm{d}r}\right)^{-1}, \\ y(r) = \sigma_* x + (1 - r). \end{cases} \tag{2.72}$$

Our objective is now to understand the relation between σ_* and r. Here again, the assumptions of the tangent method help us. Since the first path is supposed to have no effect on the arctic curve and thus on the other paths, we expect, at the leading order in n, that the refined partition function $Z_{n+1,rn}$ factorizes into the contribution of the single red

[9] The cartesian coordinates (x, y) are the usual ones, with the origin taken in the bottom-left corner in Figure 2.10, contrary to the previous convention for r, s.

path represented in Figure 2.10, let us called it Z_1^{up}, and the contribution from the remaining n paths, given by Z_n. Formally, this factorization reads,

$$\lim_{n\to\infty} \frac{1}{n} \log \frac{Z_{n+1,rn}}{Z_n} = \lim_{n\to\infty} \frac{1}{n} \log Z_1^{\mathrm{up}}. \tag{2.73}$$

This factorization property has been conjectured and tested in a number of cases in [76]. It was then shown in [52] (Section 6.1) to follow from the tangent method itself. The quantity on the left-hand side of (2.73) corresponds to the large deviation function of C_k which has been computed in Section 2.4.1, while in Section 2.4.2, we gathered all the elements to compute Z_1^{up}. It is not difficult to see that this relation provides exactly what we seek, since the left part depend explicitly on r and the right part will show a dependence on the slope of the path as we will see immediately.

As shown in [75], in the scaling limit, the behaviour of Z_1^{up} is dominated by

$$Z_1^{\mathrm{up}} \sim \mathrm{e}^{nS[f]}, \qquad S[f] = \int_0^1 L(f'(x))\mathrm{d}x, \tag{2.74}$$

where $(x, f(x))$ are the cartesian coordinates of the red path and $L(\sigma)$ the large deviation function that leads the asymptotics of a path of slope σ, computed in the previous subsection. The trajectory of the red path can be fragmented into four parts, namely, $S[f]$ is equal to

$$\begin{aligned}&(1-r)\log\sqrt{b_2B_2} + \int_0^{x_*} L(h'(x_*))\mathrm{d}x + \int_{x_*}^{r_{\mathrm{c}}} L(h'(x))\mathrm{d}x + \int_{r_{\mathrm{c}}}^1 L(0)\mathrm{d}x \\ =&(1-r)\log\sqrt{b_2B_2} + x_* L(h'(x_*)) + \int_{x_*}^{r_{\mathrm{c}}} L(h'(x))\mathrm{d}x + (1-r_{\mathrm{c}})\log\sqrt{b_1B_1}.\end{aligned} \tag{2.75}$$

The first terms account for the vertical part of the path. It simplifies the discussion to rather consider the derivative of (2.73) with respect to r, and thus the quantity

$$\frac{\mathrm{d}}{\mathrm{d}r} S[f] = -\log\sqrt{b_2B_2} + L'(h'(x_*))x_* h''(x_*)\frac{\mathrm{d}x_*}{\mathrm{d}r}. \tag{2.76}$$

In order to compute $\frac{\mathrm{d}x_*}{\mathrm{d}r}$, we use the equation of the straight line going from $(0, 1-r)$ to $(x_*, h(x_*))$, namely, $y = h'(x_*)x + (1-r)$. Evaluating

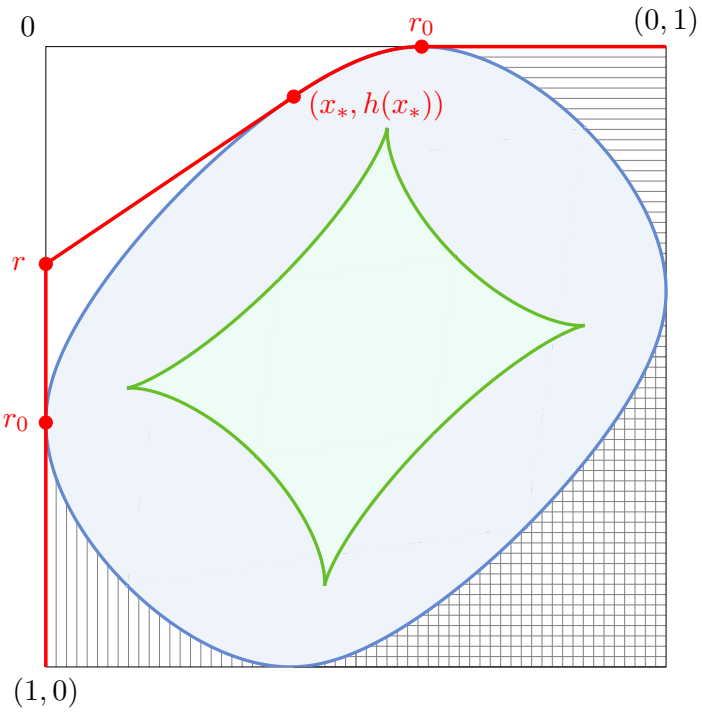

Figure 2.10: Illustration of the one-refined tangent method in the rescaled domain. Frozen regions in each corners are represented with the corresponding kind of vertices they contain. The external (resp. internal) arctic curve and the rough (resp. smooth) disordered region are in blue (resp. green). We force the first path (in red) to leave the left edge at position r. For large n, we claim that the red path follows a straight trajectory and meets the arctic curve tangentially at a certain point, $(x_*, h(x_*))$, it then accompanies the curve until it touches the upper edge of the domain. The position of the contact point r_c in the first column and row are equal due to the symmetries of the model.

this relation at $(x, y) = (x_*, h(x_*))$ and taking the derivative with respect to x_* yields

$$\frac{\mathrm{d}r}{\mathrm{d}x_*} = x_* h''(x_*). \tag{2.77}$$

As previously, let us denote by $\sigma_* = h'(x_*)$ the slope of the straight line tangent to the arctic curve and set $s_* = s(\sigma_*) = \frac{\sigma_*-1}{\sigma_*+1}$. By recalling that

$L'(\sigma(s)) = -\log \frac{z(s)}{\sqrt{b_2 B_2}}$, we finally obtain

$$\frac{\mathrm{d}}{\mathrm{d}r} S[f] = -\log z(s_*). \tag{2.78}$$

Used with the previous result (2.56), the identity (2.73) provides a relation between the slope σ_* and r,

$$\frac{\mathrm{d}}{\mathrm{d}r}\varphi(\boldsymbol{t}(r)) = \frac{\mathrm{d}}{\mathrm{d}r} S[f] \quad \Leftrightarrow \quad z(s(\sigma_*)) = \xi(\boldsymbol{t}(r)). \tag{2.79}$$

Rather than using r as the parameter to describe the curve, it seems more natural to use $\boldsymbol{t}$ instead. The relation (2.79) then provides an expression for s_* in terms of $\boldsymbol{t}$, namely, $s_* = s(z = \xi(\boldsymbol{t}))$ with $s(z)$ given by (2.68). The parametrization of the arctic curve can also be recast in terms of $\boldsymbol{t}$,

$$\begin{cases} x(\boldsymbol{t}) = \left(\frac{\mathrm{d}\sigma_*}{\mathrm{d}r}\right)^{-1} = \frac{\mathrm{d}r}{\mathrm{d}\boldsymbol{t}} \left(\frac{\mathrm{d}\sigma_*}{\mathrm{d}\boldsymbol{t}}\right)^{-1}, \\ y(\boldsymbol{t}) = \sigma_* x + (1 - r), \end{cases} \tag{2.80}$$

while the relation between r and $\boldsymbol{t}$ is given by (2.54). In the next section, we use an alternative method to derive the same parametrization, and continue in Section 2.6 the study of the arctic curve; in particular, the domain of the parameter $\boldsymbol{t}$ that produces a real curve in the (x, y) plane.

2.5 Two-refined tangent method

In this section, we show how to rederive the parametrization of the arctic curve by using the two-refined tangent method introduced by Sportiello [77]. This method relies on a change of behaviour in the exponential rate of the two-refined partition function [76]. In the limit where $n \to \infty$, it causes a 0–1 transition that allows one to probe the arctic curve.

The idea of the method is the following. Similarly to the one-refined case, we condition the first path to leave the left edge at position $k = rn$ and at the same time to join the upper edge at position $\ell = sn$, see Figure 2.11. As n becomes large, the sum over all possible paths is exponentially dominated by the trajectory of a single (classical) straight path joining the two edges.

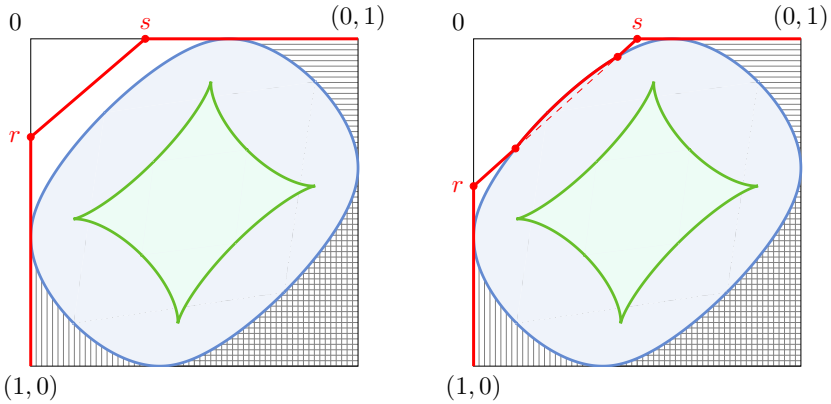

Figure 2.11: Illustration of the two-refined tangent method in the rescaled domain. We force the first path (in red) to leave the left edge at position r and the top edge at position s. For large n, we claim that the red path will follow a straight trajectory between these two points unless it meets the arctic curve in which case its trajectory is deviated as represented on the second picture.

This description leads to the presence of two regimes. In the first one, r and s are small enough, and the uppermost path, in red in the left picture of Figure 2.11, condenses almost surely to a straight trajectory between the two edges. In the second, for bigger (r, s) as depicted on the right picture of the same figure, the straight trajectory is forbidden since it would cross the arctic curve (and thus the other paths). The smallest possible deformation thus consists in two straight segments with in between a piece that follows the arctic curve. The special case exactly between those two regimes happens precisely when the first path is tangent to the arctic curve.

Let us denote by Z_1 the path partition function with starting point $(1, 0)$ and endpoint $(0, 1)$ with the only constraint of passing through $(r, 0)$ and $(0, s)$. In the first regime, since the first path does not interact with the arctic curve, we expect at the dominant order in n that the two-refined partition function behaves like $Z_{n+1,rn,sn} \simeq Z_n Z_1$. This function is properly defined below. In the second regime, the deviation of the first path by the arctic curve directly affects the exponential rate of this partition function, which decreases drastically. Hence, we expect in this case an inequality of the type $Z_{n+1,rn,sn} \simeq Z_n Z_1^{\text{def}} \ll Z_n Z_1$, where Z_1^{def}

is the path Z_1 deflected by the arctic curve. By normalizing correctly the refined partition function, it is then expected to observe a discontinuity in the large n limit,

$$\lim_{n\to\infty} \frac{Z_{n+1,rn,sn}}{Z_n Z_1} = \begin{cases} 1 & \text{if } (r,s) \text{ below } \mathcal{C}_{r,s}, \\ 0 & \text{if } (r,s) \text{ above } \mathcal{C}_{r,s}. \end{cases} \tag{2.81}$$

The relation between r and s that determines the regime of $Z_{n+1,rn,sn}$ forms a curve in the (r,s) plane, denoted above by $\mathcal{C}_{r,s}$, along which occurs the discontinuity.

It is important to mention that the actual discontinuity only occurs for this ratio of partition functions and in the limit $n \to \infty$, however, the change of behaviour itself between the two regimes is solely contained in $Z_{n+1,rn,sn}$.

The concrete application of the two-refined tangent method consists to determine the curve $\mathcal{C}_{r,s}$ by probing the discontinuity in (2.81). As explained, taking (r,s) on this curve provides a family of straight lines, tangent to the arctic curve that we can eventually retrieve as their envelope, similarly to the one-refined case.

The two-refined tangent method compared to the one-refined presents the advantages to rely on less hypotheses (e.g. the tangency assumption) and, as we will see, doesn't need the path generating function computed in Section 2.4.2. However, the downside is that the quantity $Z_{n+1,rn,sn}$ is both harder to obtain than $Z_{n+1,rn}$, and more complicated to analyse asymptotically. For these reasons, we personally think that both methods are nicely complementary.

2.5.1 Two-refined partition function

Similarly to Section 2.4.1, we will use the inhomogeneous extension of the model to compute the two-refined partition function and set this time the spectral parameters for the columns as $(u_0, u_1, \dots, u_n) = (t, u, \dots, u)$ and for the rows as $(v_0, v_1, \dots, v_n) = (v, 1, \dots, 1)$, as depicted in Figure 2.12. With this specialization, the partition function (2.7) reads

$$Z_{n+1}(t,v) = \frac{u^{n(n+1)/2}}{v^n} \frac{\theta\big((-u)^n t/v\mu\big)}{\theta\big((-1)^n/\mu\big)} \left[\frac{\theta(-t/u)\theta(-v)}{\theta(-1)^2}\right]^n. \tag{2.82}$$

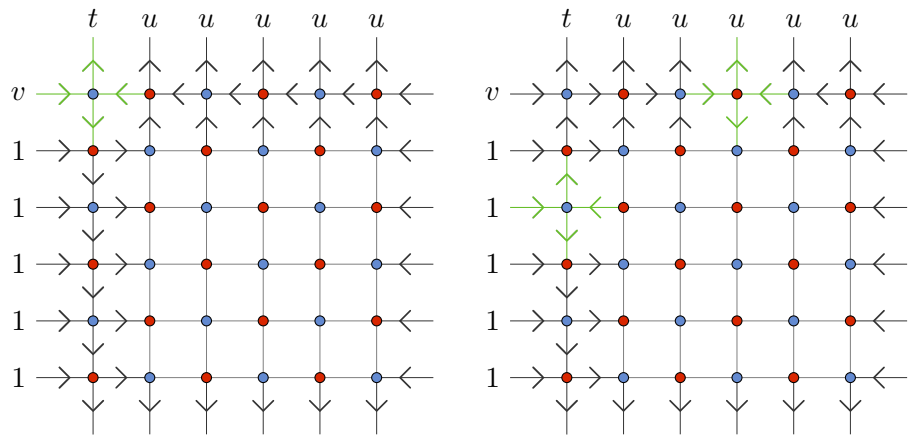

Figure 2.12: Grid of size 6 with DWBC. The sites with $i+j$ even are represented in blue, the others in red. On the left, a unique c_2 vertex (in green) is located on the site $(0,0)$. On the right, the c_2 of the first column is located at $(2,0)$ and the one of the first row at $(0,3)$.

We define here the two-refined partition function $Z_{n+1,k,\ell}$ as the weighted enumeration of configurations while the position of the single c_2-type vertex in the first column is located at position k and the c_2 vertex in the first row is at position ℓ. In most configurations, we have $1 \leqslant k, \ell \leqslant n$, and these two vertices are therefore necessarily distinct. But in few of them, a c_2 vertex occupies the position $(0,0)$, in which case this single vertex account for the first column and row at the same time. Example of both situations are given in Figure 2.12.

By its definition, the refined partition function summed on all possible k, ℓ must reproduce the total partition function,

$$Z_{n+1}(t,v) = Z_{n+1,0,0}(t,v) + \sum_{k,\ell=1}^{n} Z_{n+1,k,\ell}(t,v). \tag{2.83}$$

For $k, \ell = 0$, we can easily extract the weight of the vertex content of the first row and column,

$$\begin{aligned} Z_{n+1,0,0}(t,v) &= c_2(t/v)[b_2(t)b_1(u/v)]^{\lfloor n/2 \rfloor}[B_2(t)B_1(u/v)]^{\lceil n/2 \rceil} Z_n(u,1) \\ &= \frac{\theta(t/v\mu)}{\theta(-1/\mu)} \frac{\theta((-1)^{n+1}/\mu)}{\theta((-1)^n/\mu)} \left(-\frac{\theta(t)\theta(u/v)}{\theta(-1)^2}\right)^n Z_n(u,1). \end{aligned} \tag{2.84}$$

$Z_n(u,1)$ is the partition function of the n-sized grid that is left after the extraction of the first column and row.

For arbitrary k,ℓ, we can play the same game as in (2.42), and track the number of each vertex according to the parity of k,ℓ and n, however, it is easier to directly work with the elliptic weights and extract the ratio

$$\frac{Z_{n+1,k,\ell}(t,v)}{Z_{n+1,k,\ell}(u,1)} = \left[\frac{\theta(-t)}{\theta(-u)}\right]^{k-1}\left[\frac{\theta(-u/v)}{\theta(-u)}\right]^{\ell-1}\left[\frac{\theta(t)}{\theta(u)}\right]^{n-k}\left[\frac{\theta(u/v)}{\theta(u)}\right]^{n-\ell} \times \frac{\theta(-t/v)}{\theta(-u)}\frac{\theta((-1)^k t/\mu)}{\theta((-1)^k u/\mu)}\frac{\theta((-1)^\ell u/v\mu)}{\theta((-1)^\ell u/\mu)}. \quad (2.85)$$

Let us define the ratios of partition functions $C_{k,\ell} = \frac{Z_{n+1,k,\ell}(u,1)}{Z_n(u,1)}$,

$$F(t,v) = \frac{Z_{n+1}(t,v) - Z_{n+1,0,0}(t,v)}{Z_n(u,1)}\frac{\theta(-u)}{\theta(t/v)}\left(\frac{\theta(u)^2}{\theta(t)\theta(u/v)}\right)^{n-1}, \quad (2.86)$$

and the variables

$$\xi(t) = \frac{\theta(-t)}{\theta(+t)}\frac{\theta(+u)}{\theta(-u)}, \qquad \eta(v) = \frac{\theta(-u/v)}{\theta(+u/v)}\frac{\theta(+u)}{\theta(-u)}. \quad (2.87)$$

We can now insert the different results in the decomposition (2.83) in order to obtain, after some simplifications,

$$\begin{aligned} F(t,v) &= \sum_{k,\ell=1}^{n} C_{k,\ell}\,\xi^{k-1}\eta^{\ell-1}\left[\frac{\theta((-1)^k t/\mu)}{\theta((-1)^k u/\mu)}\right]\left[\frac{\theta((-1)^\ell u/v\mu)}{\theta((-1)^\ell u/\mu)}\right] \\ &= \left(\frac{-\theta(u)^2}{\theta(-1)^2}\right)^n \frac{\theta(t)\theta(-u/v)\theta(-u)\theta\left(\frac{t}{\mu v}\right)\theta\left(\frac{1}{\mu}\right)}{\theta(u)^2\theta\left(-\frac{t}{v}\right)\theta\left(\frac{(-1)^n}{\mu}\right)^2}\left[\left(\frac{\theta(-v)\theta\left(-\frac{t}{u}\right)}{\theta(t)\theta\left(\frac{v}{u}\right)}\right)^n \frac{\theta\left(-\frac{1}{\mu}\right)\theta\left(\frac{t(-u)^n}{\mu v}\right)}{\theta\left(\frac{t}{\mu v}\right)\theta\left(-\frac{(-u)^n}{\mu}\right)} - 1\right] \\ &= F_{0,0}\frac{\theta\left(\frac{t}{\mu}\right)\theta\left(\frac{u}{\mu v}\right)}{\theta\left(\frac{u}{\mu}\right)^2} + F_{1,0}\frac{\theta\left(-\frac{t}{\mu}\right)\theta\left(\frac{u}{\mu v}\right)}{\theta\left(-\frac{u}{\mu}\right)\theta\left(\frac{u}{\mu}\right)} + F_{0,1}\frac{\theta\left(\frac{t}{\mu}\right)\theta\left(-\frac{u}{\mu v}\right)}{\theta\left(-\frac{u}{\mu}\right)\theta\left(\frac{u}{\mu}\right)} + F_{1,1}\frac{\theta\left(-\frac{t}{\mu}\right)\theta\left(-\frac{u}{\mu v}\right)}{\theta\left(-\frac{u}{\mu}\right)^2}. \end{aligned} \quad (2.88)$$

$F_{0,0}(t,v)$ is the generating function of the subsequence of $C_{k,\ell}$ for k,ℓ even, respectively, the three others correspond the other classes of parity. We note that compared to (2.44), the exponent of ξ and η are shifted by one unit which will affect some signs. We can nevertheless apply the same trick as for the one-refined case, and evaluate $F(t^{-1},v), F(t,u^2/v)$ and $F(t^{-1},u^2/v)$. Since $\xi(t^{-1}) = -\xi(t)$ and $\eta(u^2/v) = -\eta(v)$, it produces a four-equation (linear) system allowing us to express $F_{k,\ell}(t,v)$ in

terms of $F(t,v)$. To write the result in a synthetic way, let us define the intermediate function

$$\tilde{F}(t,v) = F(t,v)\,\theta\left(\tfrac{(-1)^{k+1}}{\mu t}\right)\theta\left(\tfrac{(-1)^{\ell+1}v}{\mu u}\right)\theta\left(\tfrac{(-1)^{k}u}{\mu}\right)\theta\left(\tfrac{(-1)^{\ell}u}{\mu}\right). \quad (2.89)$$

The four-equation system then yields the following solution, for $k,\ell = 0,1$,

$$F_{k,\ell}(t,v) = \frac{\tilde{F}(t,v)+(-1)^{k+1}\tilde{F}\left(\frac{1}{t},v\right)+(-1)^{\ell+1}\tilde{F}\left(t,\frac{u^2}{v}\right)+(-1)^{k+\ell}\tilde{F}\left(\frac{1}{t},\frac{u^2}{v}\right)}{\left[\theta\left(-\frac{t}{\mu}\right)\theta\left(\frac{1}{\mu t}\right)+\theta\left(\frac{t}{\mu}\right)\theta\left(-\frac{1}{\mu t}\right)\right]\left[\theta\left(-\frac{v}{\mu u}\right)\theta\left(\frac{u}{\mu v}\right)+\theta\left(\frac{v}{\mu u}\right)\theta\left(-\frac{u}{\mu v}\right)\right]}. \quad (2.90)$$

The denominator can be factorized using formulas of Appendix 2.A.

Using the Cauchy theorem, we find an integral expression for the coefficients, for $1 \leqslant k,\ell \leqslant n$,

$$C_{k,\ell} = \frac{1}{(2\pi\mathrm{i})^2}\oiint_0 F_{k,\ell}\frac{\mathrm{d}\xi\,\mathrm{d}\eta}{\xi^k\,\eta^\ell} = \frac{1}{(2\pi\mathrm{i})^2}\oint_{-1}\oint_{-u} F_{k,\ell}(t,v)\frac{\xi'(t)\eta'(v)}{\xi^k(t)\eta^\ell(v)}\mathrm{d}v\,\mathrm{d}t. \quad (2.91)$$

Similarly to the one-refined case, we can reduce the four terms in the numerator of (2.90) to one by considering the changes of variables $t \mapsto t^{-1}$ and $v \mapsto u^2/v$. They both respect the same set of properties listed before the equation (2.49) (with a slight, and inconsequential, change of signs in the first two). In doing so, we rewrite

$$\begin{aligned} C_{k,\ell} &= \frac{1}{(\pi\mathrm{i})^2}\oiint F(t,v)\frac{\theta\left(\frac{(-1)^k u}{\mu}\right)\theta\left(\frac{(-1)^\ell u}{\mu}\right)\theta\left(\frac{(-1)^{k+1}}{\mu t}\right)\theta\left(\frac{(-1)^{\ell+1}v}{\mu u}\right)}{\theta(-1)^2\theta\left(-\frac{1}{\mu}\right)^2\theta\left(\frac{1}{\mu}\right)^2\theta(pt^2;p^2)\theta\left(p\frac{u^2}{v^2};p^2\right)}\frac{\xi'(t)\eta'(v)}{\xi^k(t)\eta^\ell(v)}\mathrm{d}v\,\mathrm{d}t \\ &= \frac{1}{(\pi\mathrm{i})^2}\left(\frac{-\theta(u)^2}{\theta(-1)^2}\right)^n\oint_{-1}\oint_{-u}\left[\left(\frac{\theta(-v)\theta\left(-\frac{t}{u}\right)}{\theta(t)\theta\left(\frac{v}{u}\right)}\right)^n\frac{\theta\left(-\frac{1}{\mu}\right)\theta\left(\frac{t(-u)^n}{\mu v}\right)}{\theta\left(\frac{t}{\mu v}\right)\theta\left(-\frac{(-u)^n}{\mu}\right)}-1\right] \\ &\quad\times\frac{B_{k,\ell}(t,v)}{\theta\left(-t/v\right)}\left(\frac{\theta(-t)\theta(u)}{\theta(t)\theta(-u)}\right)^{-rn}\left(\frac{\theta(-u/v)\theta(u)}{\theta(u/v)\theta(-u)}\right)^{-sn}\mathrm{d}v\,\mathrm{d}t, \end{aligned} \quad (2.92)$$

where we set $k = rn$, $\ell = sn$ and

$$B_{k,\ell}(t,v) = \frac{u\left(p^2;p^2\right)_\infty^4\theta\left(\frac{t}{\mu v}\right)}{v^2\theta(t)\theta\left(\frac{u}{v}\right)}\frac{\theta\left(\frac{(-1)^k u}{\mu}\right)\theta\left(\frac{(-1)^\ell u}{\mu}\right)\theta\left(\frac{(-1)^{k+1}}{\mu t}\right)\theta\left(\frac{(-1)^{\ell+1}v}{\mu u}\right)}{\theta(-u)\theta\left(-\frac{1}{\mu}\right)^2\theta\left(\frac{1}{\mu}\right)\theta\left(\frac{(-1)^n}{\mu}\right)^2}. \quad (2.93)$$

As before, $B_{k,\ell}(t,v)$ is non-singular for generic parameters and can be bounded by a quantity independent of n,k,ℓ. We may then assume it does not contribute to the leading order of the exponential rate. The

behaviour of this integral is however much more complicated than in the previous case, and we will here analyse it heuristically. For the details of the saddle point analysis, we refer to Appendix 2.B.

As one can see, a first difficulty comes from the function $\theta(-t/v)$ in the denominator, which causes a pole[10] at $v = -t$ that could be inside (or not) the steepest descent contours. When it is the case, we have to account for this pole by subtracting its residue, however, since the pole depends on both variables (and thus on both integration contours), it is not always clear when we do have to account for it.

Besides, there are now two terms in the square parentheses which are in competition. It is possible to show that the second one (i.e. the 1 term) dominates the integral in general with an exponential rate that we call φ_1. This term is in fact not difficult to approximate since one can compute one of the two integrals by residue computation and approximate the other using the saddle point method (see Appendix 2.B). However, the interesting behaviour hides in the other term in the square parentheses, which has to be evaluated by a double saddle point analysis. We claim that for small r, s, the exponential rate of this term is smaller than φ_1 in which case φ_1 governs the asymptotic behaviour of $C_{k,\ell}$. For r, s close to 1 however, the steepest descent contours enlarge and encompass the pole at $v = -t$. The residue subtracted to account for this pole produces a term with exponential rate equal to φ_1 (and with the same coefficient as the second term in the integral). This leads to a cancellation of the dominant order and the behaviour of $C_{k,\ell}$ is then described by the second leading order given by the double saddle points with an exponential rate smaller than φ_1.

This description matches with what is expected from the two-refined tangent method and since the change of behaviour in $C_{k,\ell}$ is solely contained in the first among the two terms in the square parentheses, we may focus on its description only and ignore the rest of the integral content. For the two-refined tangent method, we do not actually need the exact exponential rate of $C_{k,\ell}$, what matters is the curve $\mathcal{C}_{r,s}$ in the r, s

[10] To be precise, the integrand is not singular at $v = -t$ since the numerator and the denominator both vanish at this point. However, since the two terms in the numerator are analysed separately, we have to consider for both of them that there is a pole $v = -t$.

plane along which the discontinuity occurs. Similarly to $B_{k,\ell}(t,v)$, the factor

$$\frac{\theta\left(-\frac{1}{\mu}\right)\theta\left(\frac{t(-u)^n}{\mu v}\right)}{\theta\left(\frac{t}{\mu v}\right)\theta\left(-\frac{(-u)^n}{\mu}\right)} \tag{2.94}$$

does not contribute to the exponential rate, and may be ignored as well. After eliminating all the unimportant factors, and gathering only the essential dependence on n, we can summarize the term containing the discontinuity as

$$\oint_{-1}\oint_{-u}\frac{\mathrm{e}^{n\varphi(t,v)}}{\theta(-t/v)}\mathrm{d}v\,\mathrm{d}t, \tag{2.95}$$

with

$$\varphi(t,v)=\log\frac{\theta(-t/u)\theta(-v)}{\theta(t)\theta(v/u)}-r\log\frac{\theta(-t)\,\theta(u)}{\theta(t)\,\theta(-u)}-s\log\frac{\theta(-u/v)\,\theta(u)}{\theta(u/v)\,\theta(-u)}. \tag{2.96}$$

Assuming that n is large, the saddle point equations read

$$\begin{aligned}&\boldsymbol{t}\,\partial_t\varphi(\boldsymbol{t},\boldsymbol{v})=r[\phi(\boldsymbol{t})-\phi(-\boldsymbol{t})]-[\phi(\boldsymbol{t})-\phi\,(-\boldsymbol{t}/u)]=0,\\&\boldsymbol{v}\,\partial_v\varphi(\boldsymbol{t},\boldsymbol{v})=s[\phi\,(\boldsymbol{v}/u)-\phi\,(-\boldsymbol{v}/u)]-[\phi\,(\boldsymbol{v}/u)-\phi(-\boldsymbol{v})]=0,\end{aligned} \tag{2.97}$$

where $\boldsymbol{t}=\boldsymbol{t}(r)$ and $\boldsymbol{v}=\boldsymbol{v}(s)$. As one can see, the coefficient of the exponential rate, proportional to $\theta(-\boldsymbol{t}/\boldsymbol{v})^{-1}$, blows up at $\boldsymbol{v}=-\boldsymbol{t}$. It does not mean $C_{k,\ell}$ is singular at this point, but rather that the saddle point method does not yield the correct asymptotics because of the pole that is located on the steepest descent contour. If we were interested in the exponential rate of this integral, we would have to carefully study when is the pole inside or outside the contours and compute its residue. However, since it is a relation between r,s that we are looking for, we can merely insert the relation $\boldsymbol{v}(s)=-\boldsymbol{t}(r)$ in the saddle point equations to probe the discontinuity in the (r,s) plane,

$$r=\frac{\phi(\boldsymbol{t})-\phi\,(-\boldsymbol{t}/u)}{\phi(\boldsymbol{t})-\phi(-\boldsymbol{t})},\qquad s=\frac{\phi(\boldsymbol{t})-\phi\,(-\boldsymbol{t}/u)}{\phi(\boldsymbol{t}/u)-\phi(-\boldsymbol{t}/u)}. \tag{2.98}$$

These identities provide a parametrization $(r(\boldsymbol{t}),s(\boldsymbol{t}))$ of the change of exponential rate in $C_{k,\ell}$. This parametric form is enough for our purpose if we accept to continue to use $\boldsymbol{t}$ as parameter instead of r,s.

2.5.2 Two-refined parametrization of the arctic curve

In this subsection, our objective is two-fold. First, we use (2.98) to find a parametrization for the arctic curve. In second, we show that this parametrization is exactly the same as the one provided by the one refined tangent method (2.80); something already observed in [52].

The straight line joining the points $(0, 1-r)$ and $(s, 1)$ in the (x, y) plane (see Figure 2.11) obeys the equation $y = \frac{r}{s}x + (1-r)$. By taking the derivative with respect to $\boldsymbol{t}$, one obtains a second equation that can be interpreted as a tangency conditions. The following system then provides the envelope of the family of straight lines thus described,

$$\begin{cases} x(\boldsymbol{t}) = \frac{\mathrm{d}r}{\mathrm{d}\boldsymbol{t}} \left(\frac{\mathrm{d}}{\mathrm{d}\boldsymbol{t}} \frac{r}{s}\right)^{-1} & \text{(tangency)}, \\ y(\boldsymbol{t}) = \frac{r}{s}x + (1-r) & \text{(intersection)}. \end{cases} \tag{2.99}$$

In order to symmetrize the expression, let us make the change of variables $\boldsymbol{t} \mapsto \bar{\boldsymbol{t}}\sqrt{u}$. The equation (2.98) then reads

$$r = \frac{\phi(\bar{\boldsymbol{t}}\sqrt{u}) - \phi\left(-\bar{\boldsymbol{t}}/\sqrt{u}\right)}{\phi(\bar{\boldsymbol{t}}\sqrt{u}) - \phi(-\bar{\boldsymbol{t}}\sqrt{u})}, \qquad s = \frac{\phi(\bar{\boldsymbol{t}}\sqrt{u}) - \phi\left(-\bar{\boldsymbol{t}}/\sqrt{u}\right)}{\phi(\bar{\boldsymbol{t}}/\sqrt{u}) - \phi\left(-\bar{\boldsymbol{t}}/\sqrt{u}\right)}. \tag{2.100}$$

Whereas the ratio of the two, $\frac{r}{s}$, can be simplified using (2.128) and (2.126) and reads

$$\frac{r}{s} = \frac{1}{u} \frac{\theta(\bar{\boldsymbol{t}}^2 u; p^2)\theta(p\,\bar{\boldsymbol{t}}^2/u; p^2)}{\theta(p\,\bar{\boldsymbol{t}}^2 u; p^2)\theta(\bar{\boldsymbol{t}}^2/u; p^2)}. \tag{2.101}$$

Comparing (2.80) and (2.99), one sees that the parametrizations coincide if and only if $\frac{r}{s} = \sigma_*$. And since the second parametrization seems simpler, we propose to start by simplifying the other one. We observe that the parameter s_* can be remarkably simplified using the properties of theta functions and we obtained that the factorization

$$s_*(\bar{\boldsymbol{t}}) = \frac{\theta(-\bar{\boldsymbol{t}}^2)}{\theta(\bar{\boldsymbol{t}}^2)} \frac{\theta(u)}{\theta(-u)} \tag{2.102}$$

holds up to $\mathcal{O}(p^{10})$ (we thus conjecture this equality holds in general). From this expression, it is not difficult to compute

$$\sigma_* = \frac{1+s_*}{1-s_*} = \frac{1}{u} \frac{\theta(\bar{\boldsymbol{t}}^2 u; p^2)\theta(p\,\bar{\boldsymbol{t}}^2/u; p^2)}{\theta(p\,\bar{\boldsymbol{t}}^2 u; p^2)\theta(\bar{\boldsymbol{t}}^2/u; p^2)} = \frac{r}{s} \tag{2.103}$$

by using the formulas in Appendix 2.A, which proves the equality between the two parametrizations.

2.6 Algebraic curve and limit cases

In this section, we study the parametrization of the arctic curve obtained previously and show how to deduce an algebraic equation for the curve out of it.

With the parametrization (2.99), it is already possible to plot the arctic curve, but let us first study the parameter ranges. We already observed the curious fact that the curve seems to depend only on $(u, p) \leftrightarrow (\lambda, \alpha)$ whereas the parameter μ has totally disappeared from the expressions. It is instructive to look at the expression of α (defined in Section 2.4.2) in terms of the Aztec diamond parameters (2.12) to understand which are the relevant degree of freedom. A quick computation yields $\alpha = \frac{pQ}{\mathcal{P}q} + \frac{\mathcal{P}q}{pQ} + \lambda\frac{pq}{\mathcal{P}Q} + \lambda\frac{\mathcal{P}Q}{pq}$. In particular, this form guarantees that α is real positive when the parameters of the Aztec diamonds are.

A similar phenomenon was already known for non-biased two-periodic Aztec diamonds with parameters $(\lambda = 1, \frac{p}{\mathcal{P}}, \frac{q}{Q})$, for which the arctic curve only depends on a particular combination of the two parameters, namely, $(\frac{p}{\mathcal{P}} + \frac{\mathcal{P}}{p})(\frac{q}{Q} + \frac{Q}{q})$ [78]. This case is recovered by setting $u = \mathrm{i}$ in the elliptic weights.

As already discussed in Section 2.3.1, taking $0 \leqslant p < 1$, $|u| = 1$ and $|\mu| = \sqrt{p}$ provides real positive values for the relevant parameters of the model. Due to the periodicity property of theta functions (2.118), taking u on the upper half of the unit circle is sufficient: for u on the first quadrant we find $\lambda \geqslant 1$, and on the second $0 \leqslant \lambda \leqslant 1$, so that in fact, using the symmetry of the model, even a single quadrant would be enough.

Looking at the expression for $r(\boldsymbol{t})$, it seems natural to take $\boldsymbol{t}$ on the unit circle as well and we indeed verified that for $\boldsymbol{t}$ on the unit circle between u and -1, the parameter $r(\boldsymbol{t})$ runs from 0 to 1 as it should be. We also find in this case that $\xi(\boldsymbol{t}, u, p) \in [0, 1]$ and $\sigma_* \in [0, \infty)$, as expected. Hence, for such a chosen $\boldsymbol{t}$, our parametrization produces the upper-left

portion of the curve probed by the family of tangent lines as depicted in Figure 2.11.

If now we let $\boldsymbol{t}$ run over the rest of the unit circle, it turns out that our parametrization produces the three other pieces of the external arctic curve. This phenomenon is well known for the tangent method and not so surprising due to the symmetries of the curve. In particular, the point where the curve tangentially touches the boundaries of the domain are $\boldsymbol{t} = 1, u, -1, -u$.

However, what is very surprising is that our parametrization produces another real component that is obtained by letting $\boldsymbol{t}$ run over a circle of radius $\sqrt{p}$ in the complex plane. We can expect this domain to produce a real curve since in additive convention for theta functions, it would be equivalent to exchange the Jacobi theta $(\vartheta_1, \vartheta_2) \leftrightarrow (\vartheta_4, \vartheta_3)$. This second real component seems to reproduce exactly the inner arctic curve (antarctic curve), separating the rough disordered and smooth disordered regions, as suggested in Figure 2.13. To our knowledge, this phenomenon has never been observed in the literature, at the level of the parametric form of the curve at least. In previous applications of the tangent method, the parametric form reproduced only the external curve while the inner one was hidden as a second real component in the algebraic equation satisfied by the parametric form.

Let us now simplify the system (2.99), and rewrite it as

$$x(\boldsymbol{t}) = \frac{r'}{(r/s)'}, \qquad y(\boldsymbol{t}) = 1 - \frac{s'}{(s/r)'}. \tag{2.104}$$

The prime symbol stands for the derivative with respect to $\boldsymbol{t}$. In order to take full advantage of the symmetries of the system, let us change the coordinates to

$$\begin{cases} X(\boldsymbol{t}) = x(\boldsymbol{t}) - y(\boldsymbol{t}) = \dfrac{r'}{(r/s)'} + \dfrac{s'}{(s/r)'} - 1, \\ Y(\boldsymbol{t}) = x(\boldsymbol{t}) + y(\boldsymbol{t}) - 1 = \dfrac{r'}{(r/s)'} - \dfrac{s'}{(s/r)'}. \end{cases} \tag{2.105}$$

In these variables, the arctic curve is centered at $(0, 0)$ and the axes of symmetry of the curve coincide with the coordinate axes.

One can remark that it is possible the go from (X, Y) to $(-Y, -X)$ by the simple transformation $u \mapsto -u$ (after the rescaling of $\boldsymbol{t}$, it would read

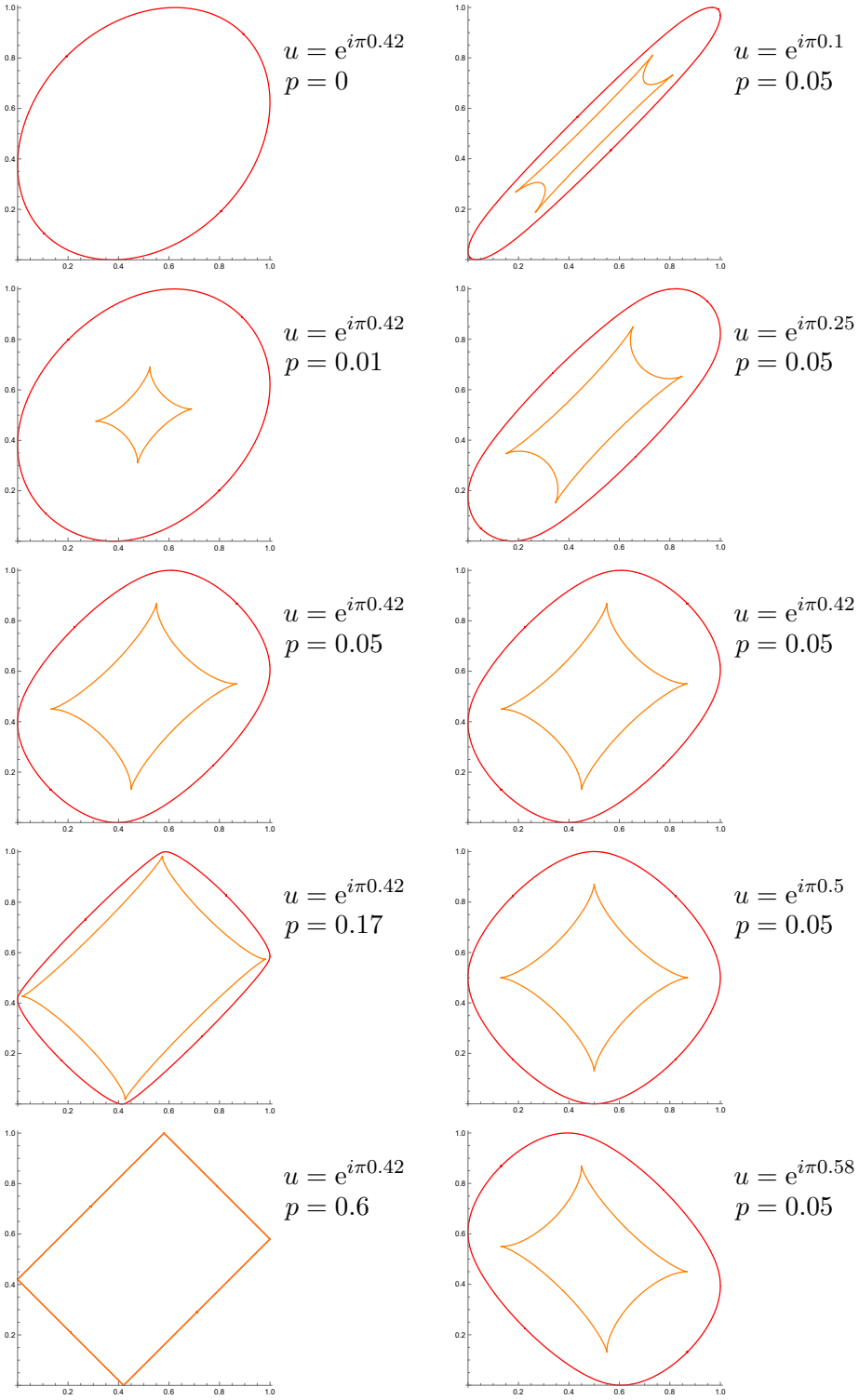

Figure 2.13: Arctic curves in (x, y) coordinates for different (u, p).

$(\bar{\boldsymbol{t}}, u) \mapsto (-\mathrm{i}\bar{\boldsymbol{t}}, -u)$). Taking back the expression (2.98), we find that this transformation sends $(r, s) \mapsto (r - \frac{r}{s}, 1 - s)$. Inserting this result in the above expression for X, Y readily proves our remark. Besides, this transformation has a clear interpretation in terms of the parameters $(\lambda, \frac{p}{\mathcal{P}}, \frac{q}{\mathcal{Q}})$ defined in (2.12). By including $\mu \mapsto (-1)^{n+1}\mu$ in the transformation, it inverts λ and either $\frac{p}{\mathcal{P}}$ or $\frac{q}{\mathcal{Q}}$ depending on the parity of n. On the Aztec graph of size n, this transformation, once combined with a reversal symmetry on the lattice (by a diagonal), preserves the weight structure and thus forms a symmetry of the system[11]. This symmetry gives a visual interpretation of how the transformation $(u, \mu) \mapsto (-u, \pm\mu)$ acts on the arctic curve, but it also simplifies our work by providing a simple relation between X and Y.

We verified by a series expansion in the nome p the following identities concerning the parametrization and conjecture their validity in general,

$$\begin{cases} V(T) = \dfrac{X(T)^2}{\mathcal{A}} = \dfrac{T(T\mathcal{Z}-1)(\mathcal{C}+\mathcal{D}(T-2\mathcal{Z}))^2}{(T^2-2T\mathcal{Z}+1)^2}, \\ W(T) = \dfrac{Y(T)^2}{\mathcal{B}} = \dfrac{(T-\mathcal{Z})(\mathcal{C}(1-2T\mathcal{Z})+\mathcal{D}T)^2}{(T^2-2T\mathcal{Z}+1)^2}, \end{cases} \tag{2.106}$$

where

$$\begin{aligned} T &= \frac{\theta(\bar{\boldsymbol{t}}^2, p^2)^2}{\theta(-\bar{\boldsymbol{t}}^2, p^2)^2}, & \mathcal{Z} &= \frac{(p^2;p^2)_\infty^{12}}{(p;p)_\infty^8 (p^4;p^4)_\infty^4} = \frac{\theta(-p;p^2)^2}{\theta(p;p^2)^2}, \\ \mathcal{A} &= \frac{u(p;p)_\infty^{12} (p^4;p^4)_\infty^4}{4(p^2;p^2)_\infty^{20}\theta(-u,p)^2}, & \mathcal{C} &= \frac{i}{u}\theta(u,p^2)^2(2\phi(u,p^2)-1), \\ \mathcal{B} &= \frac{u(p;p)_\infty^{12} (p^4;p^4)_\infty^4}{4(p^2;p^2)_\infty^{20}\theta(u,p)^2}, & \mathcal{D} &= \frac{i}{u}\theta(-u,p^2)^2(2\phi(-u,p^2)-1). \end{aligned} \tag{2.107}$$

In this parametrization, the values of $T \in (-\infty, 0]$ produce the external component of the arctic curve and $T \in [\frac{1}{\mathcal{Z}}, \mathcal{Z}]$ the inner one. A necessary condition for a cusp to occur is that both derivatives of $X(\boldsymbol{t})$ and $Y(\boldsymbol{t})$ are simultaneously equal to zero which happens when

[11] To see that, we recall that one can always report the weight $\sqrt{\lambda^{-1}}$ carried by vertical dimers to a weight $\sqrt{\lambda}$ on horizontal ones. This would only affect the partition function (and other statistical quantities) by an unimportant global factor. Similarly, an inversion of $\frac{p}{\mathcal{P}}$ can be seen as exchanging the two variables $p \leftrightarrow \mathcal{P}$.

$r''(\boldsymbol{t})\sigma'_*(\boldsymbol{t}) = r'(\boldsymbol{t})\sigma''_*(\boldsymbol{t})$. In terms of the variable T, the cusps occur when the following equation is satisfied,

$$(2\mathcal{C}\mathcal{Z} - \mathcal{D})\,T^3 - 3\mathcal{C}\,T^2 + 3\mathcal{D}\,T + (\mathcal{C} - 2\mathcal{D}\mathcal{Z}) = 0. \tag{2.108}$$

Since in the new parametrization, the dependence on $\boldsymbol{t}$ has been fully absorbed in the variable T, the rational form of these expressions allows us to obtain an algebraic equation for the arctic curve. This is done by eliminating T from this system, for what MATHEMATICA possesses the command `Eliminate` that yields the following result:

$$\begin{aligned}
0 = {} & -16\mathcal{C}^4\mathcal{D}^4\mathcal{Z}^6+32\mathcal{C}^5\mathcal{D}^3\mathcal{Z}^7+32\mathcal{C}^3\mathcal{D}^5\mathcal{Z}^7-16\mathcal{C}^6\mathcal{D}^2\mathcal{Z}^8-64\mathcal{C}^4\mathcal{D}^4\mathcal{Z}^8-16\mathcal{C}^2\mathcal{D}^6\mathcal{Z}^8+32\mathcal{C}^5\mathcal{D}^3\mathcal{Z}^9 \\
& +32\mathcal{C}^3\mathcal{D}^5\mathcal{Z}^9-16\mathcal{C}^4\mathcal{D}^4\mathcal{Z}^{10}+8\mathcal{C}^3\mathcal{D}^3\mathcal{Z}^4V+8\mathcal{C}^4\mathcal{D}^2\mathcal{Z}^5V-32\mathcal{C}^2\mathcal{D}^4\mathcal{Z}^5V-32\mathcal{C}^5\mathcal{D}\mathcal{Z}^6V+16\mathcal{C}^3\mathcal{D}^3\mathcal{Z}^6V \\
& +8\mathcal{C}\mathcal{D}^5\mathcal{Z}^6V+16\mathcal{C}^6\mathcal{Z}^7V+48\mathcal{C}^4\mathcal{D}^2\mathcal{Z}^7V+24\mathcal{C}^2\mathcal{D}^4\mathcal{Z}^7V-32\mathcal{C}^5\mathcal{D}\mathcal{Z}^8V-64\mathcal{C}^3\mathcal{D}^3\mathcal{Z}^8V+32\mathcal{C}^4\mathcal{D}^2\mathcal{Z}^9V \\
& -\mathcal{C}^2\mathcal{D}^2\mathcal{Z}^2V^2-8\mathcal{C}^3\mathcal{D}\mathcal{Z}^3V^2+10\mathcal{C}\mathcal{D}^3\mathcal{Z}^3V^2+8\mathcal{C}^4\mathcal{Z}^4V^2+24\mathcal{C}^2\mathcal{D}^2\mathcal{Z}^4V^2-\mathcal{D}^4\mathcal{Z}^4V^2-48\mathcal{C}^3\mathcal{D}\mathcal{Z}^5V^2 \\
& -16\mathcal{C}\mathcal{D}^3\mathcal{Z}^5V^2+16\mathcal{C}^4\mathcal{Z}^6V^2+32\mathcal{C}^3\mathcal{D}\mathcal{Z}^7V^2-16\mathcal{C}^4\mathcal{Z}^8V^2+\mathcal{C}^2\mathcal{Z}V^3-\mathcal{D}^2\mathcal{Z}V^3-10\mathcal{C}\mathcal{D}\mathcal{Z}^2V^3+8\mathcal{C}^2\mathcal{Z}^3V^3 \\
& +2\mathcal{D}^2\mathcal{Z}^3V^3+8\mathcal{C}\mathcal{D}\mathcal{Z}^4V^3-8\mathcal{C}^2\mathcal{Z}^5V^3+V^4-\mathcal{Z}^2V^4-8\mathcal{C}^3\mathcal{D}^3\mathcal{Z}^4W+32\mathcal{C}^4\mathcal{D}^2\mathcal{Z}^5W-8\mathcal{C}^2\mathcal{D}^4\mathcal{Z}^5W \\
& -8\mathcal{C}^5\mathcal{D}\mathcal{Z}^6W-16\mathcal{C}^3\mathcal{D}^3\mathcal{Z}^6W+32\mathcal{C}\mathcal{D}^5\mathcal{Z}^6W-24\mathcal{C}^4\mathcal{D}^2\mathcal{Z}^7W-48\mathcal{C}^2\mathcal{D}^4\mathcal{Z}^7W-16\mathcal{D}^6\mathcal{Z}^7W \\
& +64\mathcal{C}^3\mathcal{D}^3\mathcal{Z}^8W+32\mathcal{C}\mathcal{D}^5\mathcal{Z}^8W-32\mathcal{C}^2\mathcal{D}^4\mathcal{Z}^9W-2\mathcal{C}^2\mathcal{D}^2\mathcal{Z}^2VW+2\mathcal{C}^3\mathcal{D}\mathcal{Z}^3VW+2\mathcal{C}\mathcal{D}^3\mathcal{Z}^3VW \\
& -20\mathcal{C}^4\mathcal{Z}^4VW+54\mathcal{C}^2\mathcal{D}^2\mathcal{Z}^4VW-20\mathcal{D}^4\mathcal{Z}^4VW-16\mathcal{C}^3\mathcal{D}\mathcal{Z}^5VW-16\mathcal{C}\mathcal{D}^3\mathcal{Z}^5VW+40\mathcal{C}^4\mathcal{Z}^6VW \\
& +40\mathcal{D}^4\mathcal{Z}^6VW-64\mathcal{C}^3\mathcal{D}\mathcal{Z}^7VW-64\mathcal{C}\mathcal{D}^3\mathcal{Z}^7VW+64\mathcal{C}^2\mathcal{D}^2\mathcal{Z}^8VW+3\mathcal{C}^2\mathcal{Z}V^2W-3\mathcal{D}^2\mathcal{Z}V^2W \\
& -10\mathcal{C}\mathcal{D}\mathcal{Z}^2V^2W-22\mathcal{C}^2\mathcal{Z}^3V^2W+32\mathcal{D}^2\mathcal{Z}^3V^2W-16\mathcal{C}\mathcal{D}\mathcal{Z}^4V^2W+48\mathcal{C}^2\mathcal{Z}^5V^2W-32\mathcal{D}^2\mathcal{Z}^5V^2W \\
& +32\mathcal{C}\mathcal{D}\mathcal{Z}^6V^2W-32\mathcal{C}^2\mathcal{Z}^7V^2W+4V^3W-12\mathcal{Z}^2V^3W+8\mathcal{Z}^4V^3W-\mathcal{C}^2\mathcal{D}^2\mathcal{Z}^2W^2+10\mathcal{C}^3\mathcal{D}\mathcal{Z}^3W^2 \\
& -8\mathcal{C}\mathcal{D}^3\mathcal{Z}^3W^2-\mathcal{C}^4\mathcal{Z}^4W^2+24\mathcal{C}^2\mathcal{D}^2\mathcal{Z}^4W^2+8\mathcal{D}^4\mathcal{Z}^4W^2-16\mathcal{C}^3\mathcal{D}\mathcal{Z}^5W^2-48\mathcal{C}\mathcal{D}^3\mathcal{Z}^5W^2+16\mathcal{D}^4\mathcal{Z}^6W^2 \\
& +32\mathcal{C}\mathcal{D}^3\mathcal{Z}^7W^2-16\mathcal{D}^4\mathcal{Z}^8W^2+3\mathcal{C}^2\mathcal{Z}VW^2-3\mathcal{D}^2\mathcal{Z}VW^2+10\mathcal{C}\mathcal{D}\mathcal{Z}^2VW^2-32\mathcal{C}^2\mathcal{Z}^3VW^2 \\
& +22\mathcal{D}^2\mathcal{Z}^3VW^2+16\mathcal{C}\mathcal{D}\mathcal{Z}^4VW^2+32\mathcal{C}^2\mathcal{Z}^5VW^2-48\mathcal{D}^2\mathcal{Z}^5VW^2-32\mathcal{C}\mathcal{D}\mathcal{Z}^6VW^2+32\mathcal{D}^2\mathcal{Z}^7VW^2 \\
& +6V^2W^2-22\mathcal{Z}^2V^2W^2+32\mathcal{Z}^4V^2W^2-16\mathcal{Z}^6V^2W^2+\mathcal{C}^2\mathcal{Z}W^3-\mathcal{D}^2\mathcal{Z}W^3+10\mathcal{C}\mathcal{D}\mathcal{Z}^2W^3 \\
& -2\mathcal{C}^2\mathcal{Z}^3W^3-8\mathcal{D}^2\mathcal{Z}^3W^3-8\mathcal{C}\mathcal{D}\mathcal{Z}^4W^3+8\mathcal{D}^2\mathcal{Z}^5W^3+4VW^3-12\mathcal{Z}^2VW^3+8\mathcal{Z}^4VW^3+W^4-\mathcal{Z}^2W^4.
\end{aligned}$$

This algebraic curve is of degree 8 in the variables X, Y similarly to the un-biased case at $u = \mathrm{i}$ [52] and to the 6-periodic case (in the sense of the sequence r_k) obtained at $u = \mathrm{e}^{2\pi\mathrm{i}/3}$ [39].

One of our objectives is to understand the relations between the parameters $\mathcal{A}$, $\mathcal{B}$, $\mathcal{C}$, $\mathcal{D}$, $\mathcal{Z}$ characterizing the curve, and

$$\lambda = \frac{aA}{bB} = -\left(\frac{\theta(-u)}{\theta(u)}\right)^2, \tag{2.109}$$

$$\alpha = \frac{pQ}{\mathcal{P}q} + \frac{\mathcal{P}q}{pQ} + \lambda\frac{pq}{\mathcal{P}Q} + \lambda\frac{\mathcal{P}Q}{pq} = \frac{c_1C_2 + c_2C_1}{bB} = -\frac{u\theta(-1)^3\theta\left(u^2\right)}{\theta(u)^3\theta(-u)}, \tag{2.110}$$

the relevant parameters of the model in terms of the vertex/domino weights.

At the time this thesis is being written, this project is still ongoing and the general case is not properly understood yet. So far, we obtained two (among the five theoretically needed) relations between the parameters. The first is straightforwardly obtained from the comparison between $\mathcal{A}$ and $\mathcal{B}$ and reads $-\mathcal{B}/\mathcal{A} = \lambda$. A second one can be conjectured by a geometric argument. Since the arctic curve is supposed to touch the edge tangentially at the value $\tilde{T} = \frac{\theta(u;p^2)^2}{\theta(-u;p^2)^2}$ of the parameter, it means that the equation $X'(\tilde{T}) = Y'(\tilde{T})$ is satisfied. Using (2.106), and solving this equation on $\tilde{T}$ yields the result

$$\tilde{T} = \frac{\mathcal{A}+\mathcal{B}+\sqrt{(\mathcal{A}+\mathcal{B})^2 - 4\mathcal{A}\mathcal{B}\mathcal{Z}^2}}{2\mathcal{B}\mathcal{Z}} = -\frac{1+\lambda+\sqrt{(1-\lambda)^2+4\lambda\mathcal{Z}^2}}{2\lambda\mathcal{Z}}. \tag{2.111}$$

On the other hand, the curve touches the edge at $T = \tilde{T}$ and the contact point has been computed previously, see (2.58), so that

$$\begin{cases} X(\tilde{T}) = \sqrt{\mathcal{A}\tilde{T}(\tilde{T}\mathcal{Z}-1)}\,\dfrac{\mathcal{C}+\mathcal{D}(\tilde{T}-2\mathcal{Z})}{\tilde{T}^2-2\tilde{T}\mathcal{Z}+1} = r_{\mathrm{c}} - 1, \\ Y(\tilde{T}) = \sqrt{\mathcal{B}(\tilde{T}-\mathcal{Z})}\,\dfrac{\mathcal{C}(1-2\tilde{T}\mathcal{Z})+\mathcal{D}\tilde{T}}{\tilde{T}^2-2\tilde{T}\mathcal{Z}+1} = r_{\mathrm{c}}. \end{cases} \tag{2.112}$$

One can eliminate the parameter r_{c} by subtracting the two equations and use the above value of $\tilde{T}$ to obtain a relation between $\mathcal{A}$, $\mathcal{B}$, $\mathcal{C}$, $\mathcal{D}$, $\mathcal{Z}$. After simplifying all square roots, it reads

$$\begin{aligned} \mathcal{Z}^2\big(\mathcal{A}\mathcal{D}(\mathcal{C}-\mathcal{D}\mathcal{Z}) - \mathcal{B}\mathcal{C}(\mathcal{C}\mathcal{Z}-\mathcal{D})\big)^2 + 2\mathcal{Z}^2\big(\mathcal{A}\mathcal{D}(\mathcal{C}-\mathcal{D}\mathcal{Z}) - \mathcal{B}\mathcal{C}(\mathcal{C}\mathcal{Z}-\mathcal{D})\big) \\ + \mathcal{Z}(\mathcal{A}+\mathcal{B})(\mathcal{D}^2-\mathcal{C}^2) + \mathcal{Z}^2 = 1. \end{aligned} \tag{2.113}$$

In practice, the system (2.112) provides two relations, but for that, one needs to express $r_{\mathrm{c}} = \frac{\phi(u)-\phi(-1)}{\phi(u)-\phi(-u)}$ in terms of the parameters.

In the rest of this section, we review some well-known limiting cases for which the situation is simpler.

Non-elliptic case

In the limit $p, \mu \to 0$, we recover the usual free-fermionic 6V model. In this limit, we find that $\alpha = 2(1+\lambda)$, and the parameters of the curve drastically simplifies,

$$\mathcal{A} = \frac{1+\lambda^{-1}}{16}, \quad \mathcal{B} = -\frac{1+\lambda}{16}, \quad \mathcal{C} = \mathcal{D} = \frac{4\sqrt{\lambda}}{1+\lambda}, \quad \mathcal{Z} = 1, \tag{2.114}$$

leading to the equation of an ellipse for $\lambda > 0$,

$$(1+\lambda)X^2 + (1+\lambda^{-1})Y^2 = 1. \tag{2.115}$$

Un-biased case

The case $\lambda = \frac{p}{\mathcal{p}} = 1$ was studied in [52, 78] and the curve is also well known in this case. Taking[12] $u = \mathrm{i}$, it is not difficult to see that $\alpha = 2(\frac{q}{\mathcal{Q}} + \frac{\mathcal{Q}}{q}) = 4\mathcal{Z}$. Moreover, the parameters of the curve simplify to

$$\mathcal{B} = -\mathcal{A}, \qquad \mathcal{C} = \mathcal{D}, \qquad \mathcal{A} = \frac{1+\mathcal{Z}}{4\mathcal{C}^2\mathcal{Z}^2}, \tag{2.116}$$

allowing us to rewrite the curve in terms of $\mathcal{C}$ and $\mathcal{Z}$. It turns out the dependence on $\mathcal{C}$ factorizes and may be eliminated from the equation, leaving $\mathcal{Z}$ as the last parameter. It can be verified that the resulting curves reduces to the known result.

6-periodic case

The case $\frac{p}{\mathcal{p}} = 1$, $\lambda = 1 + \frac{q}{\mathcal{Q}} + \frac{\mathcal{Q}}{q}$ was studied by Borodin and Duits [39] and is known to correspond to a special case where the (r_k) sequence

[12] To obtain $\frac{p}{\mathcal{p}} = 1$, it is sufficient to set $\mu = \pm \mathrm{i}u\sqrt{p}$, however since μ does not affect the arctic curve, connecting the parameters $\mathcal{Z}$ and α is enough.

has a periodicity equal to six, $r_k = r_{k+6}$ for all $k \in \mathbb{Z}$ (see Section 1.2.2 and 2.3.2). The value of λ taken above implies that $\alpha = \lambda^{-1} - \lambda$. In this case, the algebraic equation of the curve in terms of λ is known explicitly, and given in [39] (Appendix A). It would be desirable to verify that our equation indeed reproduces their result. Unfortunately, at the time being, we failed to determine the relations between $\mathcal{A}$, $\mathcal{B}$, $\mathcal{C}$, $\mathcal{D}$, $\mathcal{Z}$ and λ, even in this special case.

2.7 Numerical simulations

In this section, we compare the arctic curve obtained from the parametric form with randomly generated tilings of an Aztec diamond of order $n = 1000$. The results are depicted in Figure 2.14. The tilings were generated by the shuffling algorithm using the implementation of Christophe Charlier [79].

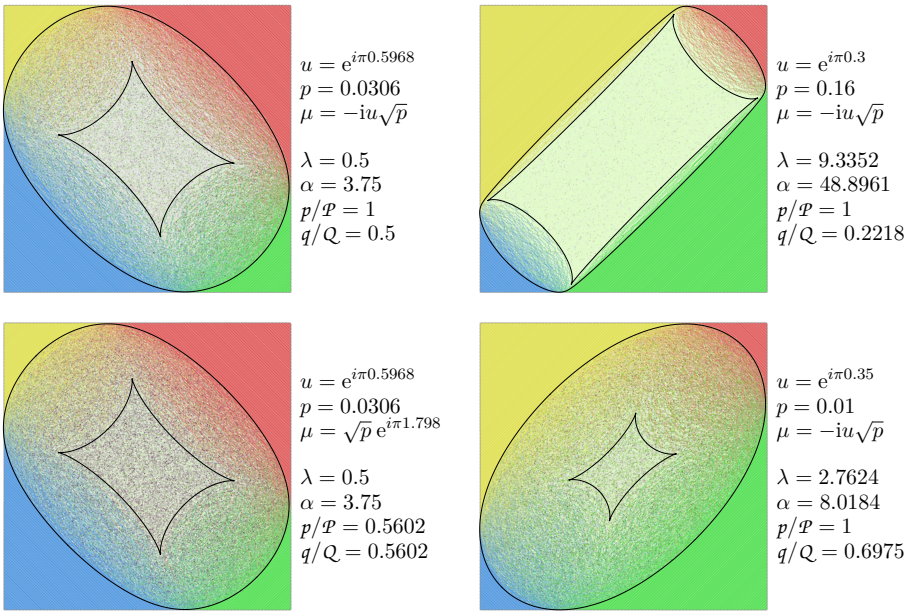

Figure 2.14: Comparison between the algebraic arctic curve and numerical simulations for some values of the parameters.

The dominos are coloured in red, green, blue, and yellow, following the same convention as in the introduction. The colours are then darkened

or lightened depending on whether the domino is adjacent to a face q or $\mathcal{Q}$, respectively. These colours typically highlight the smooth disordered region when $p/\mathcal{P} = 1$ and $q/\mathcal{Q} \neq 1$.

In the four pictures, we find good agreement between the algebraic curve and the separation of the various phases at finite size. This observation seems to indicate that the second real component of the curve that we have found indeed characterizes the inner arctic curve, as one would expect; even though the separation between the rough and smooth regions is not as clear as the other separation.

The first column in the figure illustrates two different choices of parameters that yield the same arctic curve. In the first case, most dominos gather around the $\mathcal{Q}$ faces, making the gaseous region mostly light shaded, with a favoured horizontal orientation. In the second case, the situation appears more ambiguous. By looking at the four possible plaquettes – red-blue and yellow-green, in either dark or light shades – one can observe that three of them carry roughly the same weight. As a consequence, they appear in similar proportions inside the central region, whereas the last type of plaquette (i.e. dark yellow–green), which carries a much smaller weight, indeed are in the minority.

Another noticeable feature of the gaseous region is that it appears to be much more homogeneous than the liquid one, in the sense that the density of each kind of domino seems not to depend on the location, or at least not as strongly as in the liquid region. This remark (if verified) would suggest that the behaviour inside the smooth region could possibly be approximated by a two-periodic dimer model on an infinite plane.

2.8 Conclusion and outlook

In this chapter, we established a connection between the 8VSOS model at the free-fermion point and biased two-periodic Aztec diamonds and obtained explicit relations between the partition functions of both models. The main results are the analytic expressions for the arctic curve: the parametric form and the algebraic equation, given in terms of elliptic parameters (u, p). It remains to see whether one could reparametrize the curve in terms of the vertex/domino weights relevant parameters

(λ, α). We have some reasons to believe that it is possible, however the complexity lies in the tremendous amount of theta function identities at hand which, in theory, should relate the parameters but, in practice, are difficult to manipulate.

What is remarkable with our approach is the simplicity with which we extracted the one- and two-refined partition functions using the spectral parameters of the 8VSOS model. Even though the theta functions make difficult a rigorous asymptotic analysis, the method proves to be very efficient in establishing primary conjectures on the parametric form of the arctic curve. We strongly believe this strategy could be extended to further generalizations of the model or other versions of it. For instance, in the case of domain wall and a (partially) reflecting end boundary conditions [80].

The case $\eta = 1/3$ would also be very interesting to investigate. Rather than the free-fermion point, showing connections with Aztec diamonds, the 8VSOS model at $\eta = 1/3$ has a combinatorial interpretation in terms of three-colourings of the square lattice, and the one-enumeration of alternating sign matrices. For general η however, the expression of the partition function [68,70] is only given in terms of a sum of determinants, and it is difficult to predict whether the method would still be applicable or not.

2.A Some identities on theta functions

This appendix aims to gather some routine identities concerning theta functions in multiplicative convention. We first recall its definition and the periodicity properties

$$\theta(z) = \theta(z;p) = \prod_{j=0}^{\infty}(1 - z\,p^j)(1 - p^{j+1}/z), \tag{2.117}$$

$$\theta(pz) = \theta(z^{-1}) = -z^{-1}\theta(z). \tag{2.118}$$

This function can alternatively be written in terms of q-Pochhammer symbols,

$$\theta(z;p) = (z;p)_\infty(\tfrac{p}{z};p)_\infty. \tag{2.119}$$

Relation to Jacobi theta functions

The theta function as defined above is related to the four Jacobi theta functions [81, 82] by the relations

$$\vartheta_1(z;p) = \theta(\mathrm{e}^{2\mathrm{i}z};p^2)\left(\mathrm{i}p^{1/4}\mathrm{e}^{-\mathrm{i}z}\right)\prod_{k=1}^{\infty}(1-p^{2k}), \tag{2.120a}$$

$$\vartheta_2(z;p) = \theta(-\mathrm{e}^{2\mathrm{i}z};p^2)\left(p^{1/4}\mathrm{e}^{-\mathrm{i}z}\right)\prod_{k=1}^{\infty}(1-p^{2k}), \tag{2.120b}$$

$$\vartheta_3(z;p) = \theta(-p\,\mathrm{e}^{2\mathrm{i}z};p^2)\prod_{k=1}^{\infty}(1-p^{2k}), \tag{2.120c}$$

$$\vartheta_4(z;p) = \theta(p\,\mathrm{e}^{2\mathrm{i}z};p^2)\prod_{k=1}^{\infty}(1-p^{2k}). \tag{2.120d}$$

All the formulas presented in this appendix can be found in additive convention in the references aforementioned. We refer to the function ϑ_i $(i = 1, 2, 3, 4)$ as the additive convention, and to the function θ as the multiplicative convention because of the exponentiation of the argument, which converts sums into products, in the above four relations.

Weierstass identity

The Weierstass identity is a three-term identity relating theta functions with the same nome. For general variables $a, b, c, x \in \mathbb{C}$, it stands

$$\begin{aligned}\theta(ax)\theta(a/x)\theta(bc)\theta(b/c) - \theta(ac)\theta(a/c)\theta(bx)\theta(b/x)\\ = \frac{a}{c}\theta(ab)\theta(b/a)\theta(cx)\theta(c/x).\end{aligned} \tag{2.121}$$

By fixing some of these variables, diverse sub-identities can be obtained. For instance, if one takes $a = z/\sqrt{w}$, $b = z\sqrt{w}$, $c = \sqrt{w}$, $x = -\sqrt{w}$, we find

$$\theta(z)\theta(-z)\Big(\theta(zw)\theta(-z/w)-\theta(-zw)\theta(z/w)\Big) = \frac{z}{w}\theta(z^2)\theta(w)\theta(-w)\theta(-1). \tag{2.122}$$

And since, for all $x \in \mathbb{C}$, we have $\theta(x) = -x\theta(x^{-1})$, we also find the alternative form

$$\theta(z)\theta(-z)\Big(\theta(zw)\theta(-w/z) + \theta(-zw)\theta(w/z)\Big) = \theta(z^2)\theta(w)\theta(-w)\theta(-1). \tag{2.123}$$

By exchanging z and w and this last equality and multiplying it with (2.122), we obtain another Weierstrass identity,

$$\theta(zw)^2\theta(-z/w)^2 - \theta(-zw)^2\theta(z/w)^2 = \frac{z}{w}\theta(z^2)\theta(w^2)\theta(-1)^2, \quad (2.124)$$

or equivalently

$$\theta(a)^2\theta(-b)^2 - \theta(-a)^2\theta(b)^2 = b\,\theta(ab)\theta(a/b)\theta(-1)^2. \quad (2.125)$$

These three identities are the ones that appear the most in the computations of this chapter.

Identities on the elliptic nome

Another class of identities relates theta functions of nome p and p^2. For instance, the ones that we use in Section 2.5.2 are

$$\theta(z;p) = \theta(z;p^2)\theta(zp;p^2), \quad (2.126a)$$

$$\theta(z^2;p^2) = \theta(z;p)\theta(-z;p), \quad (2.126b)$$

which can be obtained directly from the product expansion (2.117). In the same manner, it is not difficult to obtain some identities between theta functions evaluated at specific values, and the Euler function, $(p;p)_\infty = \prod_{k=1}^{\infty}(1-p^k)$,

$$\theta(-1;p) = 2\frac{(p^2;p^2)_\infty^2}{(p;p)_\infty^2}, \quad (2.127a)$$

$$\theta(p;p^2) = \frac{(p;p)_\infty^2}{(p^2;p^2)_\infty^2} = \frac{2}{\theta(-1;p)}, \quad (2.127b)$$

$$\theta(-p;p^2) = \frac{\theta(-1;p)}{\theta(-1;p^2)}, \quad (2.127c)$$

$$\theta(\mathrm{i};p)\theta(-\mathrm{i};p) = \mathrm{i}\,\theta(i;p)^2 = \theta(-1;p^2). \quad (2.127d)$$

Identities on the derivatives

A last kind of identities are those that relate the derivative of theta functions to theta functions themselves. For these, it is convenient to

work with the function $\phi(z) = \frac{z\theta'(z)}{\theta(z)}$ and some notable identities are, for instance,

$$\frac{\mathrm{d}}{\mathrm{d}z}\frac{\theta(z)}{\theta(-z)} = \frac{\theta(z)}{z\theta(-z)}\Big(\phi(z) - \phi(-z)\Big)$$
$$= \frac{\theta(z)}{\theta(-z)}\Big(-\frac{(p;p)_\infty^2}{2}\frac{\theta(-1)^2\theta(z\sqrt{p})\theta(-z\sqrt{p})}{\theta(z)\theta(-z)}\Big), \qquad (2.128a)$$

$$\frac{\mathrm{d}}{\mathrm{d}z}\frac{\theta(z)}{\theta(z\sqrt{p})} = \frac{\theta(z)}{z\theta(z\sqrt{p})}\Big(\phi(z) - \phi(z\sqrt{p})\Big)$$
$$= \frac{1}{2z}\frac{\theta(z)}{\theta(z\sqrt{p})}\Big(1 - \frac{(\sqrt{p};\sqrt{p})_\infty^4}{(p;p)_\infty^2}\frac{\theta(-z)\theta(-z\sqrt{p})}{\theta(z)\theta(z\sqrt{p})}\Big). \qquad (2.128b)$$

A significant number of other identities involving ϕ can be obtained by taking the derivative of previous relations shown in this appendix. To conclude this section, we merely write the equivalent of (2.118) for ϕ and the value at $p = 0$,

$$\phi(z^{-1}) = 1 - \phi(z), \qquad \phi(z; p = 0) = \frac{z}{z-1}. \qquad (2.129)$$

2.B Details of the saddle point analysis

In this appendix, we attempt to give a more rigorous treatment of the double integral appearing in Section 2.5.1. As we do not have, for the time being, a definitive proof of the result, and besides, since the tangent method is not fully rigorous either, we will mostly gather arguments to justify this integral indeed behaves as described in the text.

The appendix is structured as follows: we first consider the non-periodic case by taking the limit $p, \mu \to 0$ on $C_{k,\ell}$. This situation is much simpler since explicit solutions for the saddle points can be found. It serves the double purpose to build an intuition on the nature of the discontinuity and to consolidate the assumptions that we could make in the elliptic case. In a second time, we analyse the concrete situation at hands, with the elliptic form of $C_{k,\ell}$. We discuss the complications and argue that the nature of the cancellation in the integral should remain the same as in the previous case.

Before we begin, let us rewrite the integral in a more convenient form for our analysis. Rather than tracking the position of the pole[13] relatively to the integration contours, we find it easier to expand the denominator in series around the pole and then approximate the series by an integral over the real axis. At the leading order, this approximation yields the exact same result, but as we will see, it allows one to look at the cancellation between the two terms from another perspective. To do this, we use the Weierstrass formula (with $a = -\sqrt{v/\mu}$, $b = t/\sqrt{v\mu}$, $c = -u/\sqrt{v\mu}$, $x = \sqrt{v\mu}$) presented in the previous appendix to rewrite

$$\theta(-t/v) = \left(\left[\frac{\theta(-v,-t/u,-1/\mu,-tu/v\mu)}{\theta(t,v/u,t/v\mu,u/\mu)} \right] - 1 \right) \frac{\theta(t,v/u,t/v\mu,u/\mu)}{\theta(-u,-u/v\mu,-t/\mu)} \frac{u}{v}, \tag{2.130}$$

where $\theta(x_1,\dots,x_n) = \theta(x_1)\dots\theta(x_n)$. Inserting this expression in (2.92) and forgetting about all the unimportant factors[14] yields

$$C_{k,\ell} \sim \oint_{-1} \oint_{-u} \frac{1 - \left[\frac{\theta(-v)\theta(-t/u)}{\theta(t)\theta(v/u)} \right]^n \left(\frac{\theta(-1/\mu)\theta(t(-u)^n/v\mu)}{\theta(t/v\mu)\theta(-(-u)^n/\mu)} \right)}{1 - \left[\frac{\theta(-v)\theta(-t/u)\theta(-1/\mu)\theta(-tu/v\mu)}{\theta(t)\theta(v/u)\theta(t/v\mu)\theta(u/\mu)} \right]} \xi^{-rn}\eta^{-sn} \mathrm{d}v\,\mathrm{d}t, \tag{2.131}$$

where we recall the values of ξ and η,

$$\xi(t) = \frac{\theta(-t)\theta(u)}{\theta(t)\theta(-u)}, \qquad \eta(v) = \frac{\theta(-u/v)\theta(u)}{\theta(u/v)\theta(-u)}. \tag{2.132}$$

2.B.1 Non-elliptic case

As described above, we take the limit $p, \mu \to 0$ on $C_{k,\ell}$ and to symmetrize the expression in t, v, we also make the change of variables $v \mapsto u/v$,

$$C_{k,\ell} \sim \oiint_{-1} \frac{1-\rho^n}{1-\rho} \xi^{-rn}\eta^{-sn} \mathrm{d}v\,\mathrm{d}t = \oiint_{-1} \sum_{m=0}^{n-1} \rho^m \xi^{-rn}\eta^{-sn} \mathrm{d}v\,\mathrm{d}t. \tag{2.133}$$

[13] Let us remark that the integral does not have an actual pole at $v = -t$ since the two terms in the numerator cancel each other at this point. We nevertheless call it a pole because if one splits the integral in two part and analyse both terms separately, then the integrand indeed diverges at this point.

[14] Apart for $\left[\frac{-\theta(u)^2}{\theta(-1)^2} \right]^n$ that brings a constant, the neglected factors do not contribute to the exponential rate.

where

$$\rho(t,v)=-\frac{(t+u)(u+v)}{u(t-1)(v-1)},\quad \xi(t)=\frac{(t+1)(u-1)}{(t-1)(u+1)},\quad \eta(v)=\frac{(v+1)(u-1)}{(v-1)(u+1)}. \tag{2.134}$$

The advantage of this approach is that we get rid of the virtual singularity at $\rho=1$ (or $v=-u/t$) and are able to analyse the whole expression at once, rather than splitting the integral into two parts. Since the sum is finite, we may interchange it with the two integrals and by setting $m=n\tau$, we further approximate this sum by an integral,

$$C_{k,\ell}\sim\int_0^1\oint_{-1}\mathrm{e}^{n\varphi(t,v,\tau)}\mathrm{d}v\,\mathrm{d}t\,\mathrm{d}\tau, \tag{2.135}$$

with

$$\varphi(t,v,\tau)=\tau\log\rho(t,v)-r\log\xi(t)-s\log\eta(v). \tag{2.136}$$

This approximation could be made more accurate by including the corrections form Euler-Maclaurin formula, however, these terms contribute only to the coefficients of subleading exponential rates. For instance, if we look at the first correction from Euler-Maclaurin formula,

$$\frac{1}{2}\oint\oint\mathrm{e}^{n\varphi(t,v,\tau=1)}\mathrm{d}v\,\mathrm{d}t, \tag{2.137}$$

we see that this term have an exponential rate smaller than or equal to the one of (2.135). This contribution can nevertheless affect the coefficient in front of the exponential if $\tau=1$ is the global maximum of φ in the integration domain.

In the initial description, we had two terms in the integral, their difference has no pole, but separately they have one at $\rho=1$. In particular, for the term in ρ^n, there is the the question of whether or not the pole is inside the steepest descent contours. As we will see in a moment, this question reduces in the τ-integral to whether the saddle point (or maximum in this case) lies inside the integration interval. We start by computing the stationary points $t(\tau),v(\tau)$ of the contour integrals,

$$\begin{cases}\dfrac{r}{\tau}=\dfrac{(t+1)(u+1)}{2(t+u)},\\[2ex]\dfrac{s}{\tau}=\dfrac{(v+1)(u+1)}{2(v+u)},\end{cases}\quad\Leftrightarrow\quad\begin{cases}t(\tau)=-\dfrac{\tau(u+1)-2ru}{\tau(u+1)-2r},\\[2ex]v(\tau)=-\dfrac{\tau(u+1)-2su}{\tau(u+1)-2s}.\end{cases} \tag{2.138}$$

We studied the existence of the steepest descent contour on MATHEMATICA, see Figure 2.15. We only show the contour for t, the situation being very similar for v due to the symmetry between the variables. We used the function `RegionPlot` to obtain the regions where $\operatorname{Re}\varphi$ is greater than its value on the saddle point and the function `StreamPlot` with the vector field $(\operatorname{Re}\partial_t\varphi, -\operatorname{Im}\partial_t\varphi)$ to obtain the level lines of $\operatorname{Im}\varphi$. Even though there are logarithms in φ, we did not study the branch cuts since the integrand is originally defined with integer exponents n, k, ℓ and no logarithms. As mentioned in Section 2.6, it is enough to consider u in the first quadrant of the unit circle; for u in the other quadrants the plots change and the discussion would be more involving. The Figure 2.15 suggests that suitable steepest descent contour exist for $\tau > r, s$ but not for $\tau < r, s$. In this second case, we slightly anticipate the result of Proposition 2.B.1, and conjecture that there always exist a contour γ around -1 in the complex plane such that $\max_{t\in\gamma} \operatorname{Re}\varphi(t, v, \tau) < \operatorname{Re}\varphi(t(\tau_+), v(\tau_+), \tau_+)$ (we assume the contour in the v plane to be suitably chosen). In particular, it means that the contribution of the τ-integral in the domain $\tau < r, s$ is necessarily subdominant and can be neglected. Our conjecture is supported by a numerical analysis on MATHEMATICA. We also mention that we will not compute the imaginary phase factor coming from the saddle point analysis since it do not contributes to the absolute value of $C_{k,\ell}$.

One can verify that for all $|u| = 1$, $r, s, \tau > 0$, the saddle points $t(\tau), v(\tau)$ are on the unit circle and $\xi(t(\tau))$, $\eta(v(\tau))$, $\rho(t(\tau), v(\tau))$ are positive for $\tau > r, s$. Hence, the function $\varphi(\tau) = \varphi(t(\tau), v(\tau), \tau)$ is smooth and real-valued in this domain and we have the following proposition.

Proposition 2.B.1. *The function $\varphi(\tau)$ has two extrema, $\tau_+ \geqslant \max(r, s)$ and $\tau_- \leqslant \min(r, s)$ and is strictly concave on $\tau \geqslant r, s$.*

Proof. By differentiation, we obtain

$$\frac{\mathrm{d}}{\mathrm{d}\tau}\varphi(\tau) = \frac{\partial}{\partial\tau}\varphi(\tau) = \log\rho(t(\tau), v(\tau)). \tag{2.139}$$

Consequently, the extrema are given by the equation $\rho(t(\tau), v(\tau)) = 1$ or equivalently $v(\tau) = -u/t(\tau)$. The fact that this equation reproduces the pole of the initial integrand is not a coincidence; it brings the same

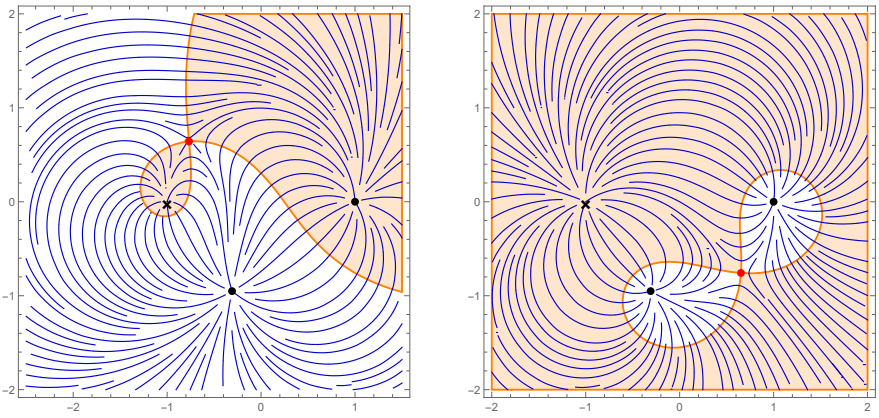

Figure 2.15: Representation of the complex plane in the variable t. The black crosses and the black dots are respectively the poles and zeros of the integrand, the red dot is the saddle point $t(\tau)$. The region where $\mathrm{Re}\,\varphi$ is greater than its value on the saddle point is shaded in orange, and the level line of $\mathrm{Im}\,\varphi$ are represented in blue. We fixed the parameters as $\arg u = 0.4\pi$, $\arg v = 0.3\pi$, $r = 0.3$, $s = 0.1$ and $\tau = 0.9$ (left), $\tau = 0.2$ (right). On the left picture, the steepest descent contour is obtained by following the stream lines passing through the saddle point and circling around the pole. In some in-between cases, following the stream lines provide a steepest descent contour that does not encircle the pole, but it is then possible to chose another suitable contour, around the pole and avoiding the orange region by relaxing the constant imaginary part condition to a neighbourhood of the pole, which is enough for our approximation.

contribution as the residue would have. In the present case, we can solve explicitly this equation for τ and find

$$\tau_\pm = s\frac{2u}{(u+1)^2}\left(1+\frac{r}{s} \pm \sqrt{\left(\frac{r}{s}-u\right)\left(\frac{r}{s}-\frac{1}{u}\right)}\right). \tag{2.140}$$

To obtain the inequalities with r, s, it is convenient to set $u \mapsto \mathrm{e}^{\mathrm{i}\tilde{u}}$,

$$\tau_\pm = \frac{s}{1+\cos\tilde{u}}\left(1+\frac{r}{s} \pm \sqrt{1+\left(\frac{r}{s}\right)^2 - \frac{2r}{s}\cos\tilde{u}}\right). \tag{2.141}$$

The inequality $\tau_+ \geqslant \max(r,s)$ is trivially obtained by taking the lower bounds on trigonometric functions. For the other, we can show that

$\tilde{u} = 0$ is the global maximum of the function $\tau_-(\tilde{u})$ by looking at its two first derivatives, and deduce that $\tau_- \leqslant \tau_-(\tilde{u} = 0) = \min(r, s)$.

It remains to prove the concavity of the function $\varphi(\tau)$. For that, we compute its second derivative,

$$\frac{\mathrm{d}^2}{\mathrm{d}\tau^2}\varphi(\tau) = \frac{1}{r-\tau} + \frac{1}{s-\tau} + \frac{2}{\tau}, \tag{2.142}$$

and remark it is strictly negative for $\tau \geqslant r, s$. In particular, it proves that τ_+ is the global maximum of $\varphi(\tau)$ in this domain. □

Since we restricted our analysis to the integration domain $[\max(r, s), 1]$ for τ, there are now two possible scenarios:

(I) The global maximum τ_+ is in the integration domain and the integral is dominated by $\varphi_{\mathrm{I}} = \varphi(t(\tau_+), v(\tau_+), \tau_+)$. The exact value of τ_+, given by the equation $\rho(t(\tau_+)), v(\tau_+) = 1$ does not really matter since this equation ensures in particular that τ_+ does not appear explicitly in the exponential rate. It is in fact more convenient to see the parameter τ_+ as a condition relating t and v: $v(\tau_+) = -u/t(\tau_+)$. By using the equations on the left of (2.138), we can extract an equation for $t = t(\tau_+)$,

$$\frac{r}{s} = \frac{(t+1)(v+u)}{(t+u)(v+1)} = u\frac{(t+1)(t-1)}{(t+u)(t-u)}, \qquad t = \pm u\sqrt{\frac{\frac{r}{s} - \frac{1}{u}}{\frac{r}{s} - u}} \tag{2.143}$$

relating t to r/s. Among the two solutions for t, the plus sign corresponds to $t(\tau_+)$ and the other to $t(\tau_-)$. The rate φ_{I} is thus given by

$$\begin{aligned}\varphi_{\mathrm{I}} &= -r\log\xi(t(\tau_+)) - s\log\eta(-\tfrac{u}{t(\tau_+)}) \\ &= -r\log\left(-\mathrm{i}\,\frac{\sqrt{\frac{r}{s}-u} + u\sqrt{\frac{r}{s}-\frac{1}{u}}}{\sqrt{\frac{r}{s}-u} - u\sqrt{\frac{r}{s}-\frac{1}{u}}}\right) - s\log\left(\mathrm{i}\,\frac{\sqrt{\frac{r}{s}-u} - \sqrt{\frac{r}{s}-\frac{1}{u}}}{\sqrt{\frac{r}{s}-u} + \sqrt{\frac{r}{s}-\frac{1}{u}}}\right) \\ &\qquad + (r+s)\log\sqrt{\lambda},\end{aligned} \tag{2.144}$$

with the parameter $\lambda = -\left(\frac{u+1}{u-1}\right)^2$.

(II) The global maximum τ_+ is greater than 1. By the concavity of $\varphi(\tau)$ and the fact there is no other extremum on $\tau > r, s$, the global maximum in $[\max(r,s),1]$ is therefore given by $\tau = 1$, the boundary of the domain. In such cases where the global maximum is on the boundary of the integration domain and $\varphi'(\tau = 1) \neq 0$, Laplace's method (i.e. the saddle point method on real intervals) still applies and gives the leading order of the exponential rate, but the coefficient preceding the exponential is slightly different and of order $1/n$ rather than $1/\sqrt{n}$ [83]. The large deviation function is thus given by $\varphi_{\text{II}} = \varphi(t(1), v(1), 1)$ where $t(1)$ and $v(1)$ are determined in terms of r, s by (2.138). After some simplifications, we obtain

$$\varphi_{\text{II}} = -r\log r - (1-r)\log(1-r) - s\log s - (1-s)\log(1-s) \\ - \log(1+\lambda) + (r+s)\log\lambda. \quad (2.145)$$

To be complete, we should include the contribution $\text{Re}\left[\frac{-\theta(u)^2}{\theta(-1)^2}\right]^n \xrightarrow[p\to 0]{} -n\log(1+\lambda)$ that we factored out at the beginning and which ensures that these exponential rates are negative in their respective regimes. These rates account for the real part of $C_{k,\ell}$ since we did not include the phase factor coming from the steepest descent method. Let us note that it is not expected for $C_{k,\ell}$ to be real anyway, since the partition function of the 2p-6V model, Z_{n+1}, generally is not. However, if one rewrite $C_{k,\ell}$ using the connection with Aztec diamonds, the imaginary part should vanish since T_n^{AD} is real.

The condition $\tau_+ < 1$ (or $\tau_+ > 1$) can be elegantly rewritten in terms of the derivative $\partial_\tau \varphi(\tau = 1) < 0$ which yields the explicit relation between r and s,

$$\rho(t(1), v(1)) = [(1-r)(1-s)(1+\lambda)]^{-1} < 1. \quad (2.146)$$

We can thus fully characterize the two regimes of the coefficient

$$C_{k,\ell} \sim \begin{cases} \frac{1}{\sqrt{n}} \mathrm{e}^{n\varphi_{\text{I}}} & \text{if } (1-r)(1-s)(1+\lambda) > 1 \qquad \text{(regime I)}, \\ \frac{1}{n} \mathrm{e}^{n\varphi_{\text{II}}} & \text{if } (1-r)(1-s)(1+\lambda) < 1 \qquad \text{(regime II)}. \end{cases} \quad (2.147)$$

The function φ_{I} is always greater than or equal to φ_{II}. Correctly normalized, the above two regimes will clearly lead to the 0–1 transition

discussed in Section 2.5. In particular, the regime (I) corresponds to the situation where the straight path does not touch the arctic curve, depicted on the left of Figure 2.11. The regime (II) corresponds to the case where the path is deflected by the arctic curve as shown in the right picture of the same figure.

2.B.2 Elliptic case

The objective is now to repeat the above analysis in the elliptic case. One of the major difficulties comes from the cancellation between the two terms in the integral which is not as clear anymore. In the previous case, the expansion around the pole (2.133) showed the cancellation happens even before the saddle point approximation which facilitated the analysis. In the present case, the cancellation happens only in the limit of large n and both terms have to be computed separately.

Other difficulties come from the fact that most equations are not solvable explicitly and we have to work with implicit solutions. We rely on the existence of such solutions at $p, \mu = 0$ and on the analyticity of theta functions to claim they still exist in the present case, at least in a neighbourhood of $p, \mu = 0$.

Let us begin with the expression (2.131). We make the change of variables $v \mapsto u/v$, to symmetrize the expression in t, v, and expand the denominator around the pole which yields after simplifications the approximated expression for $C_{k,\ell}$,

$$\oint\!\!\oint_{-1} \sum_{m=0}^{\infty} \frac{\rho^m}{\xi^{nr}\eta^{ns}} \Big\{1 - \Big[-u\tfrac{\theta(-v/u)\theta(-t/u)}{\theta(t)\theta(v)}\Big]^n \Big(\tfrac{\theta(-1/\mu)\theta(-tv(-u)^{n-1}/\mu)}{\theta(tv/u\mu)\theta(-(-u)^n/\mu)}\Big)\Big\}\,\mathrm{d}v\,\mathrm{d}t, \tag{2.148}$$

with

$$\rho(t,v) = -u\,\frac{\theta(-\frac{t}{u})\,\theta(-\frac{v}{u})\,\theta(-\frac{tv}{\mu})\,\theta(-\frac{1}{\mu})}{\theta(t)\,\theta(v)\,\theta(\frac{tv}{\mu u})\,\theta(\frac{u}{\mu})},$$

$$\xi(t) = \frac{\theta(-t)\theta(u)}{\theta(t)\theta(-u)}, \qquad \eta(v) = \frac{\theta(-v)\theta(u)}{\theta(v)\theta(-u)}. \tag{2.149}$$

The computation essentially resemble to (2.133) but the functions ρ in the numerator and denominator are not quite the same here and there is no cancellation in the series.

For the initial integration contours, which are supposed to be small loops around -1, it can be verified that $|\rho| \leqslant 1$ (with the equality only if $u = -1$ which corresponds to a singular choice of vertices). Hence, the series is absolutely convergent and we may interchange it with the integrals. Once it is done, we are allowed to deform the contours since the result of the integral does not depend on them. As before, we set $m = n\tau$ and approximate the series by an integral on τ,

$$C_{k,\ell} \sim \int_0^\infty \oiint_{-1} \mathrm{e}^{n\varphi_1} - \mathrm{e}^{n\varphi_2} \left(\tfrac{\theta(-1/\mu)\theta(-tv(-u)^{n-1}/\mu)}{\theta(tv/u\mu)\theta(-(-u)^n/\mu)} \right) \mathrm{d}v \, \mathrm{d}t \, \mathrm{d}(n\tau) = T_1 - T_2, \tag{2.150}$$

where the exponential rates are given by

$$\varphi_1(t, v, \tau) = \tau \log \rho(t, v) - r \log \xi(t) - s \log \eta(v), \tag{2.151}$$

$$\varphi_2(t, v, \tau) = \varphi_1(t, v, \tau) + \log \left[-u \frac{\theta(-v/u)\theta(-t/u)}{\theta(t)\theta(v)} \right]. \tag{2.152}$$

First term: T_1

Let us start our analysis with the first term having the exponential rate φ_1. The stationary point equations for $t(\tau), v(\tau)$ gives a system similar in form to the left part of (2.138) where it is possible to isolate the ratios r/τ and s/τ, however, the system is now coupled in the variables t and v and involves the derivative of theta functions,

$$\begin{aligned} \frac{r}{\tau} &= \frac{\phi(t) - \phi(-\frac{t}{u}) + \phi(\frac{tv}{\mu u}) - \phi(-\frac{tv}{\mu})}{\phi(t) - \phi(-t)}, \\ \frac{s}{\tau} &= \frac{\phi(v) - \phi(-\frac{v}{u}) + \phi(\frac{tv}{\mu u}) - \phi(-\frac{tv}{\mu})}{\phi(v) - \phi(-v)}. \end{aligned} \tag{2.153}$$

We expect the term T_1 to always produce the rate of the regime (I). It is thus not important to conserve the parameter τ to obtain the large deviation function, but it will be useful to understand the behavior of the second term T_2. On the basis of the previous analysis, we conjecture the following statement.

Conjecture 2.B.2. *For $\tau > r, s$ the saddle points $t(\tau), v(\tau)$ are accessible by the steepest descent contours, the function $\varphi_1(\tau) = \varphi_1(t(\tau), v(\tau), \tau)$ is concave and there exists a local maximum τ_+ which is also the global maximum of the function.*

In particular, these assumptions are sufficient to ensure the convergence of the integral for the part $\tau > r, s$. Similarly to the previous case, the equation determining the maximum τ_+ leads to $\rho(t(\tau_+), v(\tau_+)) = 1$ or equivalently $v(\tau_+) = -u/t(\tau_+)$. We can use this relation together with (2.153) to extract, for $t = t(\tau_+)$,

$$\frac{r}{s} = \frac{\phi(\frac{t}{u}) - \phi(-\frac{t}{u})}{\phi(t) - \phi(-t)}, \qquad \tau_+ = \frac{r\,[\phi(t) - \phi(-t)]}{\phi(t) - \phi(-\frac{t}{u}) + \phi(-\frac{1}{\mu}) - \phi(\frac{u}{\mu})}. \quad (2.154)$$

The first equation determines $t(\tau_+)$ in terms of r, s and the second tracks the position of the maximum τ_+. As the integration domain cover all the values $\tau > r, s$, we may assume for T_1 that τ_+ is always reached and dominate the integral. Consequently, the exponential rate is given by

$$\varphi_1(\tau_+) = \varphi_1(t(\tau_+), v(\tau_+), \tau_+) = -r \log \xi(t(\tau_+)) - s \log \eta(-\tfrac{u}{t(\tau_+)}). \quad (2.155)$$

To conclude the analysis of this first term, let us remark that it is possible to approximate the solution (t, τ_+) of the equations (2.154) by expanding ϕ in series in p and truncates at the desired order. The equations are then solvable numerically. In doing so, we verified that for generic parameters the first equation seems to always give two solutions[15] for t on the unit circle, opposite to each other. Among the corresponding two values for τ given by the second equation, we observed that one seems to be always greater than r, s (corresponding to τ_+) while the other lies between 0 and r, s (corresponding to τ_-), supporting the conjecture we have formulated. For this to be true however, we have to take $u = \mathrm{e}^{\mathrm{i}\tilde{u}}$ and $\mu = \sqrt{p}\,\mathrm{e}^{\mathrm{i}\tilde{\mu}}$ such that $\tilde{u} > \tilde{\mu}$; a condition that we do not understand completely.

Second term: T_2

The analysis of the second term is quite similar to the one of T_1. The presence of a new term in (2.152) slightly affects the saddle point equa-

[15] There are also other solutions in the complex plane, but their number and their positions depend on the order in p of the truncation. We think they are just artifacts of the approximation.

tions for φ_2,

$$\begin{aligned} r &= \frac{\tau\left[\phi(t)-\phi(-\frac{t}{u})+\phi(\frac{tv}{\mu u})-\phi(-\frac{tv}{\mu})\right]+\left[\phi(t)-\phi(-\frac{t}{u})\right]}{\phi(t)-\phi(-t)}, \\ s &= \frac{\tau\left[\phi(v)-\phi(-\frac{v}{u})+\phi(\frac{tv}{\mu u})-\phi(-\frac{tv}{\mu})\right]+\left[\phi(v)-\phi(-\frac{v}{u})\right]}{\phi(v)-\phi(-v)}. \end{aligned} \tag{2.156}$$

The solution $t(\tau), v(\tau)$ of this system is a priori different from the one of the previous system, we will however keep the same notation and add a lower index $i = 1, 2$ only when it is necessary to make the distinction. In the non-elliptic case, the terms containing μ in argument would vanish and these equations would be totally equivalent to the ones of T_1 after a shift $\tau \mapsto \tau - 1$. The situation here is slightly more complex, but we expect that the additional term does not affect to much the solutions.

If a local extremum $\overline{\tau}$ exists, it again fulfills the equation $\rho(t(\overline{\tau}), v(\overline{\tau})) = 1$ and consequently $v(\overline{\tau}) = -u/t(\overline{\tau})$. Inserting this result in (2.156) yields the following two equations for $\overline{\tau}$ and $t = t(\overline{\tau})$,

$$\frac{r}{s} = \frac{\phi(\frac{t}{u})-\phi(-\frac{t}{u})}{\phi(t)-\phi(-t)}, \qquad \overline{\tau} = \frac{r\left[\phi(t)-\phi(-t)\right]-\left[\phi(t)-\phi(-\frac{t}{u})\right]}{\phi(t)-\phi(-\frac{t}{u})+\phi(-\frac{1}{\mu})-\phi(\frac{u}{\mu})}. \tag{2.157}$$

Interestingly, the first equation is exactly the same as the one for T_1. The numerical analysis mentioned earlier therefore suggests there exist two solutions on the unit circle corresponding to $t(\overline{\tau}_-)$ and $t(\overline{\tau}_+)$, and as a direct consequence, we have that $t_2(\overline{\tau}_\pm) = t_1(\tau_\pm)$ (the lower indices stand to recall that the saddle points for φ_2 and φ_1 are different). Besides, together with $v(\overline{\tau}) = -u/t(\overline{\tau})$, it guarantees that $\varphi_2(\overline{\tau}_+) = \varphi_1(\tau_+)$.

The second equation gives the positions of $\overline{\tau}_\pm$ which are slightly different from the extrema of $\varphi_1(\tau)$. It is expected from what we observed in the non-elliptic case that the additional term shifts $\overline{\tau}_+$ outside of the integration domain for some values of r, s. We verified numerically with the same method described above that it was indeed the case. In particular, we observed that for r, s close to 1, we generally have $\overline{\tau}_+ > 0$, and for r, s close to 0, we rather have $\overline{\tau}_+ < 0$. In the first case, the maximum is in the integration domain and we may approximate the exponential rate by $\varphi_2(\overline{\tau}_+)$. However, when $\overline{\tau}_+ < 0$, we rather assume that the global maximum in the integration domain is located on the

boundary, at $\tau = 0$, which provides a different exponential rate given by $\varphi_2(0) = \varphi_2(t(0), v(0), 0)$ where $t = t(0)$ and $v = v(0)$ are determined by (2.156) at $\tau = 0$,

$$r = \frac{\phi(t) - \phi(-\frac{t}{u})}{\phi(t) - \phi(-t)}, \qquad s = \frac{\phi(v) - \phi(-\frac{v}{u})}{\phi(v) - \phi(-v)}. \tag{2.158}$$

Cancellation in $C_{k,\ell}$

In summary, we obtained that

$$T_1 \sim \frac{1}{\sqrt{n}} \mathrm{e}^{n\varphi_1(\tau_+)}, \qquad T_2 \sim \begin{cases} \frac{1}{n} \mathrm{e}^{n\varphi_2(0)} & \text{if } \overline{\tau}_+ < 0, \\ \frac{1}{\sqrt{n}} \mathrm{e}^{n\varphi_2(\overline{\tau}_+)} & \text{if } \overline{\tau}_+ > 0. \end{cases} \tag{2.159}$$

The transition between the two regimes in terms of r, s is not easy to describe. Hopefully, it is not essential if we decide to use t to parametrize the curve instead of r, s. As one can see, the discontinuity in the limit $n \to \infty$ is solely contained in the second term T_2, however, the correct description of the two regimes is given by the difference $T_1 - T_2$ in which a cancellation at the leading order is expected. To observe this cancellation, one has to verify that the first coefficients (in a $1/\sqrt{n}$ expansion) of both rates coincide. All the functions of t, v that we factored out at the beginning will be trivially equal due to the equality $t_1(\tau_\pm) = t_2(\overline{\tau}_\pm)$, and the additional coefficient appearing in (2.150) becomes equal to 1 due to the relation between t and v. It remains to verify that the coefficients produced by the steepest descent method [83] are also equal. For this, we have to prove that

$$\det \mathbf{H}_{\varphi_1}(t, v, \tau)\Big|_{t_1(\tau_+), v_1(\tau_+), \tau_+} = \det \mathbf{H}_{\varphi_2}(t, v, \tau)\Big|_{t_2(\overline{\tau}_+), v_2(\overline{\tau}_+), \overline{\tau}_+}, \tag{2.160}$$

where $\mathbf{H}_f$ is the Hessian matrix of the function f. Using the result of the stationary point equations, this equality is easily verified and ensures that the coefficient of the order $1/\sqrt{n}$ is the same in T_1 and T_2. This is all we need to observe the cancellation at the leading order, using the above expressions,

$$C_{k,\ell} = T_1 - T_2 \sim \begin{cases} \frac{1}{\sqrt{n}} \mathrm{e}^{n\varphi_{\mathrm{I}}} & \text{if } \overline{\tau}_+ < 0 \quad (r, s \simeq 0), \\ o(n^{-1/2}) \, \mathrm{e}^{n\varphi_{\mathrm{II}}} & \text{if } \overline{\tau}_+ > 0 \quad (r, s \simeq 1), \end{cases} \tag{2.161}$$

where $\varphi_{\text{I}} = \varphi_1(\tau_+) = \varphi_2(\overline{\tau}_+)$. Unlike the non-elliptic case, the function φ_{II} here is unknown; our analysis is not sufficient to determine this exponential rate. It may be possible that only the first coefficient, at order $1/\sqrt{n}$, vanishes in the cancellation and not the rest in which case $\varphi_{\text{II}} = \varphi_{\text{I}}$. But it is also possible that the cancellation occurs at all orders and thus a subdominant exponential rate (for instance the contribution from the boundary of the integral at $\tau = 0$) will lead the asymptotic behaviour. To settle this question, one could start by looking at the subleading coefficients in the expansions, for $i = 1, 2$,

$$T_i \sim \left(\frac{-2\pi}{n \det \mathbf{H}_{\varphi_i}(t_i(\tau_+), v_i(\tau_+), \tau_+)} \right)^{\frac{1}{2}} \mathrm{e}^{n\varphi_i(\tau_+)}(1 + \mathcal{O}(n^{-1})), \quad (2.162)$$

to see whether they seem to be equal for T_1 and T_2. Such a computation is however quite involving and in any case not useful for us since the expression (2.161) is already sufficient to observe the 0–1 transition in the large n limit. This semi-rigorous analysis supports the heuristic statement that we made in the text and corroborates the equations (2.98) parametrizing the curve in the (r, s) plane.

Another computation of T_1

To conclude this appendix, and to reinforce the validity of our analysis, we show it is possible to straightforwardly recover the approximation of T_1 by a residue computation. Taking the expression

$$T_1 \sim \oiint_{-1} \frac{1}{\theta(-tv/u)\xi(t)^{rn}\eta(v)^{sn}} \mathrm{d}v\, \mathrm{d}t, \quad (2.163)$$

one remarks the function $\theta(-tv/u)^{-1}$ is rapidly decreasing at infinity. We may then enlarge the contour in the v plane into a circle of large radius where the integrand decays sufficiently fast. The contour itself does not contribute to the integral but necessarily contains the pole at $v = -u/t$ and we have to include its contribution by subtracting its residue. A simple computation yields the result

$$T_1 \sim 2\pi\mathrm{i} \oint_{-1} \frac{u}{t\theta'(1)} \exp\{-nr \log \xi(t) - ns \log \eta(-u/t)\} \mathrm{d}t, \quad (2.164)$$

so that we are left with a unique integral that we can approximate using the steepest descent method. The stationary point equation immediately gives

$$\frac{r}{s} = \frac{\phi(\frac{t}{u}) - \phi(-\frac{t}{u})}{\phi(t) - \phi(-t)}, \tag{2.165}$$

From that, it is not difficult to verify that the exponential rates and the leading coefficients all coincide with the previous analysis. At $p, \mu = 0$, we also verified on Mathematica that a suitable steepest descent contour exists for generic parameters.

Chapter 3

GUE-corners process in two-periodic Aztec diamonds

This chapter uses material from [3] written with Philippe Ruelle.

Aztec diamonds (ADs) were originally introduced in 1992 [19, 20], and interest in the model rapidly grew in the following years. A main motivation to its study comes from the fact that it is one of the simplest cases where an arctic phenomenon (i.e. a spatial transition between statistically ordered and disordered regions, see Figure 3.1) takes place [21]. Moreover, ADs show connections with other statistical models such as the six-vertex model, Alternating Sign Matrices (ASMs), lozenge tilings of hexagons, etc.

Another remarkable feature is the relation between point processes occurring in Aztec diamonds and random matrix theory. In particular, it is known that near the contact point between the arctic curve and the edge of an Aztec diamond, the distribution of a certain subclass of dominos converges to the GUE-corners process [44, 45] in the case of uniformly weighted configurations. A similar phenomenon has been observed in

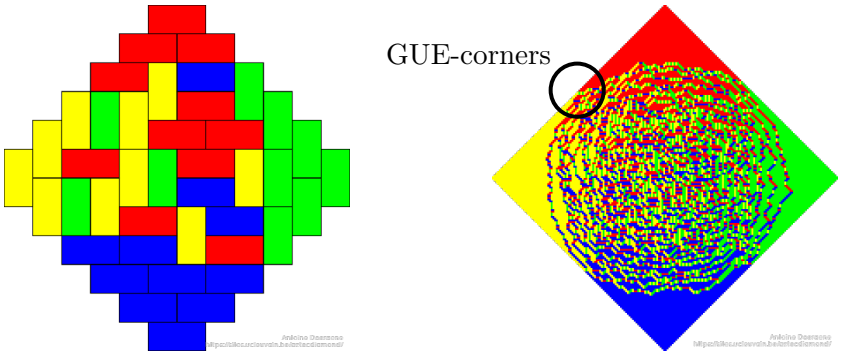

Figure 3.1: *Left*: Aztec diamond of order $n = 6$. *Right*: Aztec diamond of order $n = 100$ and arctic phenomenon. The order n of an Aztec diamond corresponds to the number of corners along one edge of the domain.

lozenge tilings [44, 84, 85], in plane partitions [86, 87], in the six-vertex model [88, 89], and in ASMs [90] for various probability measures.

In the present work, our main objective is to emphasize the universality of the GUE-corners process and prove that it continues to be the limiting process in *two-periodic Aztec diamonds* while the biased case serves more as an example to introduce the method. We also take advantage of the determinantal structure to obtain explicit expressions for the distribution of the point process in the discrete setting (before taking the large size limit).

The chapter is structured as follows: we start by describing our method in the simple (yet interesting) biased case. The first step consists in properly identifying the determinantal point process of interest. After that, we deduce the probability measure associated with this point process from the biased measure on Aztec diamonds. We show how it is possible to integrate recursively the probability density function of this process to obtain the distribution on a subset of points. Finally, we prove the convergence in distribution of this probability density to the GUE-corners process by extracting the dominant order in n of the distribution.

In Section 3.2, we repeat the same procedure in the case of two-periodic Aztec diamonds. For this measure, less is known about the model.

However, the determinantal structure is preserved, and this is sufficient for our purposes.

Finally, in Section 3.3, we connect the results and distributions that we obtained with other recent works on the subject [1, 52]. Connections with ASMs and the non-intersecting path description are also reviewed in this section.

3.1 Biased Aztec diamonds

The name *biased Aztec diamonds* refers to a specific choice of measure over the set of configurations where horizontal and vertical dominos do not necessarily carry the same weights. One can recover the *uniform* Aztec diamond by setting the same weight on all dominos. Biased ADs have been largely studied in the literature and are used here as a toy example both for reviewing the method in a simple case and for introducing most of the notation. The spirit of our method is mainly inspired by [45], yet some steps have been modified to better fit to the two-periodic case we analyse right after.

First of all, let us mention that it is not useful to consider weights on both horizontal and vertical dominos; since their total number is fixed, only the ratio between the two weights is relevant. We therefore associate a weight 1 to horizontal dominos and $\sqrt{\lambda}$ (called the bias) to the vertical ones. The weight of a configuration c is obtained by taking the product over all domino weights, $w(c) = \lambda^{N_v(c)/2}$ where $N_v(c)$ is the number of vertical dominos in the configuration (this number is always even). The probability of observing this configuration is defined as

$$\mathbb{P}(c) = \frac{w(c)}{Z_n}, \qquad Z_n = \sum_c w(c), \tag{3.1}$$

where n refer to the order of the Aztec diamond, Z_n is the partition function, and where the sum runs over all configurations.

3.1.1 Interlaced particles and adjacency

The main focus of this chapter is the study of an underlying (interlaced) particle system shown in Figure 3.2. In this picture, the dashed lines

give a coordinate system for the location of the cells with a given parity (e.g. if we think of the dominos as lying on a checkerboard-type domain, these would correspond, say, to the coordinates of the black cells). We choose to colour in white (resp. black) the dominos having their right (resp. left) part crossing the dashed lines. In the left part of each black domino, we also draw a red dot called *particle* in this description. We use the notation $x_i^{(\ell)} = 0, 1, \dots, n$ to designate the vertical position of the i-th particle on the *level*[1] ℓ. For instance, one can see in Figure 3.2 that there is one particle on the level $\ell = 1$ and $x_1^{(1)} = 4$. There are two particles on the second level with $x_1^{(2)} = 3$ and $x_2^{(2)} = 6$, etc. In addition, one can remark that the particle system is interlaced in the sense that, for all $1 \leqslant i \leqslant \ell \leqslant n$, we have $x_i^{(\ell+1)} \leqslant x_i^{(\ell)} \leqslant x_{i+1}^{(\ell+1)}$. More details about this observation are given at the beginning of Section 3.2.1. The notation $x^{(\ell)}$ has to be interpreted as the collection of all $x_i^{(\ell)}$ for $i = 1, \dots, \ell$. In what follows, we will slightly abuse notation, and will use $x_i^{(\ell)}$ to denote the particle at position $(\ell, x_i^{(\ell)})$.

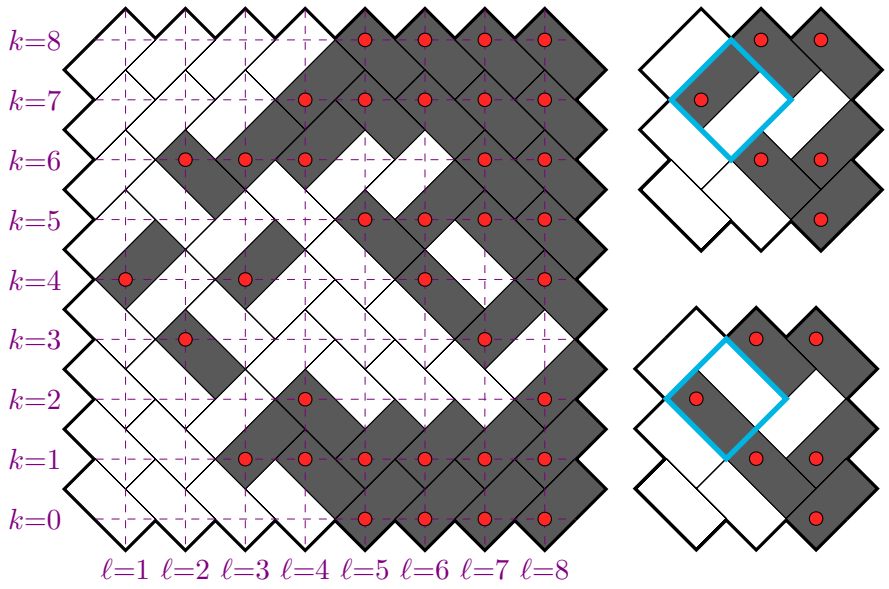

Figure 3.2: *Left*: interlaced particle description of an Aztec diamond of order 8. *Right*: example of two different AD configurations which lead to the same particle system. The local pattern in blue appear for each non-adjacent particle.

[1] We borrow this terminology from [91].

If all dominos have the same weight, all configurations are equiprobable. Then, the correspondence between the probability measure on the Aztec diamond and the interlaced particle system can be made solely by knowing how many AD configurations correspond to the same interlaced particle configuration. To answer this question, we use the notion of *adjacency* [45]. A particle $x_i^{(\ell)}$ is called *adjacent* if $x_i^{(\ell)} = x_j^{(\ell+1)}$ for $j = i$ or $i+1$, namely the particle $x_i^{(\ell)}$ has another particle directly to its right. We introduce the characteristic function

$$\alpha(x_i^{(\ell)}) = \delta_{x_i^{(\ell)},x_i^{(\ell+1)}} + \delta_{x_i^{(\ell)},x_{i+1}^{(\ell+1)}}, \tag{3.2}$$

which equals 1 if the particle at $x_i^{(\ell)}$ is adjacent and 0 otherwise. It allows us to write the number of adjacent particles lying from level ℓ_1 to ℓ_2 as

$$\alpha(x^{(\ell_1)},\dots,x^{(\ell_2)}) = \sum_{\ell=\ell_1}^{\ell_2} \alpha(x^{(\ell)}) = \sum_{\ell=\ell_1}^{\ell_2}\sum_{i=1}^{\ell} \alpha(x_i^{(\ell)}). \tag{3.3}$$

Since $n(n+1)/2$ is the total number of particles from level 1 to n, the number of non-adjacent particles on the entire AD is given by

$$\frac{n(n+1)}{2} - \alpha(x^{(1)},\dots,x^{(n)}). \tag{3.4}$$

Because of the remark made below about non-adjacent particles, we fix for consistency that all particles lying on the n-th level are adjacent, $\alpha(x^{(n)}) = n$, as if there was an imaginary $(n+1)$-th level completely fulfilled.

For further purposes, we split our definition of α into two distinct subclasses

$$\alpha_{\text{inf}}(x_i^{(\ell)}) = \delta_{x_i^{(\ell)},x_i^{(\ell+1)}}, \qquad \alpha_{\text{sup}}(x_i^{(\ell)}) = \delta_{x_i^{(\ell)},x_{i+1}^{(\ell+1)}}. \tag{3.5}$$

These functions encode the information of whether an adjacent particle on the level ℓ lies next to its superior or inferior neighbouring particle on the level $\ell+1$. When α functions are written with several arguments, it means that we take the sum over contributions of each individual particle, similarly to (3.3). We note that, for convenience, only $x_i^{(\ell)}$ appears in the arguments of the adjacency functions, although these functions formally depend on the particle on the next level also.

As one can see in Figure 3.2, whenever a particle is non-adjacent, its domino is contained in a plaquette made of two parallel dominos (framed in blue on the picture) which can be flipped without modifying the particle positions. As a consequence, we have two AD configurations for the same particle configuration. This observation is crucial to make the link between the probability distribution of the Aztec diamond and the density of the particle system. It is also reminiscent of the relation between Aztec diamond tilings and *Alternating Sign Matrices* or, equivalently, the *six-vertex model*. In fact, it can be shown that the freedom in those plaquette orientations is exactly the same one that appears when we relate AD configurations to ASMs, such that our particle system is in one-to-one correspondence with alternating sign matrices, see Section 3.3 for more details.

3.1.2 Probability density function

The probability distribution of the particle system is induced by the measure on AD configurations through the general relation

$$\rho(x^{(1)},\dots,x^{(n+1)}) = \left(\sum_{c\in\mathcal{C}} \mathbb{P}(c)\right) \chi(x^{(1)} \prec \cdots \prec x^{(n+1)}), \tag{3.6}$$

where $\mathcal{C} = \mathcal{C}(x^{(1)},\dots,x^{(n+1)})$ is the subset of all AD configurations which produces the same interlaced x-particle system. The notation $x^{(\ell)} \prec x^{(\ell+1)}$ means that the particles on levels ℓ and $\ell+1$ are interlaced, namely, we have for all i,

$$\begin{aligned} &x_i^{(\ell)} \in \{0,1,\dots,n\},\\ &x_i^{(\ell)} < x_{i+1}^{(\ell)},\\ &x_i^{(\ell+1)} \leqslant x_i^{(\ell)} \leqslant x_{i+1}^{(\ell+1)}, \end{aligned} \tag{3.7}$$

whereas $\chi(x^{(\ell)} \prec x^{(\ell+1)}) = 1$ if $x^{(\ell)} \prec x^{(\ell+1)}$ and 0 otherwise.

Based on the remark made in the previous section, it is not difficult to see that, in the uniform case [45],

$$\sum_{c\in\mathcal{C}} \mathbb{P}(c) = \frac{2^{n(n+1)/2-\alpha(x^{(1)},\dots,x^{(n)})}}{Z_n}. \tag{3.8}$$

Here, $Z_n = 2^{n(n+1)/2}$ is the partition function in the uniform case (i.e. the number of domino tilings of an Aztec diamond of order n).

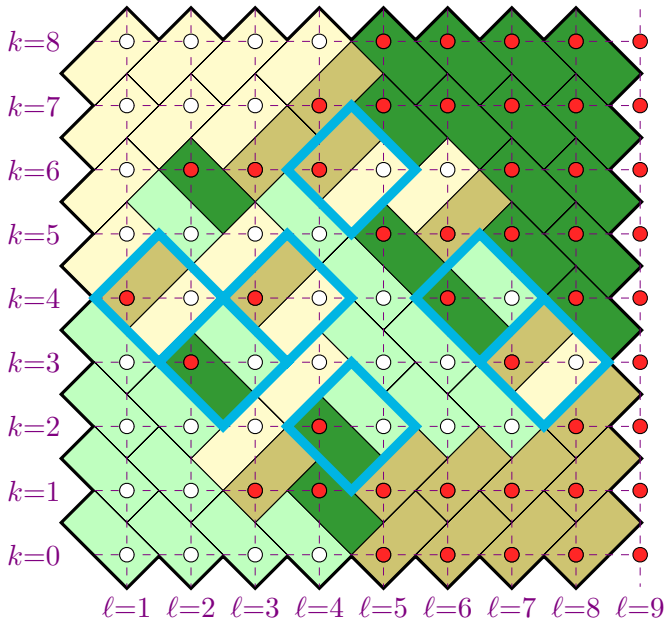

Figure 3.3: Weighted Aztec diamond of order $n = 8$ described in terms of interlaced particles. Vertical dominos are drawn in green and horizontal ones in yellow. We kept dark shades for previously black dominos, and light ones for dominos previously in white. The blue squares around non-adjacent particles indicate that we can flip a pair of yellow dominos into a pair of green ones (and conversely) without modifying the particle system. All the other dominos are entirely fixed by the particle positions. As well as the particles in red, their complement, the holes, are drawn in white. The additional level $\ell = n + 1$ is also represented.

In the biased case, one needs to distinguish the contribution from vertical and horizontal dominos in terms of the position of each particle. In Figure 3.3, we coloured the vertical and horizontal dominos in green and yellow respectively, and in two different intensities, the darker ones are those containing a particle. A striking remark is that the orientation of a domino lying on an adjacent particle is fully determined by the neighbouring particle to its right[2]. If it is adjacent to its supe-

[2]We give a detailed explanation for this in Section 3.2.1 in the two-periodic case.

rior neighbour (i.e. $x_i^{(\ell)} = x_{i+1}^{(\ell+1)}$) then the domino has to be vertical, if it is adjacent to its inferior neighbour (i.e. $x_i^{(\ell)} = x_i^{(\ell+1)}$) then the domino is horizontal. In addition, we know that the number of horizontal/vertical light shaded dominos is the same as their dark shaded version[3]. The number of vertical (resp. horizontal) dominos completely fixed by the particle configuration is then given by $2\alpha_{\sup}(x^{(1)}, \dots, x^{(n)})$ (resp. $2\alpha_{\inf}(x^{(1)}, \dots, x^{(n)})$). The remaining dominos are the ones in the blue plaquettes. Each plaquette contributes a factor 1 if the dominos are both horizontal, or λ if they are both vertical; their sum is raised to a power equal to the number of non-adjacent particles. From this observation, we finally obtain the total probability density

$$\rho(x^{(1)}, \dots, x^{(n+1)}) = \frac{(1+\lambda)^{\frac{n(n+1)}{2}}}{Z_n} \cdot \Omega(x^{(1)}, \dots, x^{(n)}) \cdot \cdot \chi(x^{(1)} \prec \cdots \prec x^{(n+1)}), \quad (3.9)$$

where

$$\Omega(x^{(1)}, \dots, x^{(n)}) = \frac{\lambda^{\alpha_{\sup}(x^{(1)}, \dots, x^{(n)})}}{(1+\lambda)^{\alpha(x^{(1)}, \dots, x^{(n)})}}. \quad (3.10)$$

In the distribution, we chose to include the $(n+1)$-th level, completely filled with particles. The variables $x^{(n+1)}$ are deterministic and have no effect on the distribution, but they turn out to be useful for computations. By summing over the positions of the particles in the $(m-1)$ first levels, we obtain the following result.

Proposition 3.1.1. *The joint probability density function (JPDF) over the subset of particles on levels m to $n+1$ is given by*

$$\rho(x^{(m)}, \dots, x^{(n+1)}) = \frac{(1+\lambda)^{\frac{n(n+1)}{2}}}{Z_n} \cdot \frac{\Delta(x^{(m)})}{\prod_{i=1}^{m-1} i!} \cdot \Omega(x^{(m)}, \dots, x^{(n)}) \cdot \cdot \chi(x^{(m)} \prec \cdots \prec x^{(n+1)}), \quad (3.11)$$

where

$$\Delta(x^{(m)}) = \det_{1 \leqslant i,j \leqslant m} \left[(x_i^{(m)})^{j-1} \right] = \prod_{1 \leqslant i < j \leqslant m} (x_j^{(m)} - x_i^{(m)}) \quad (3.12)$$

is a Vandermonde determinant.

[3] It is a direct consequence of the fact that any configuration can be obtained from another by a finite sequence of flips of two parallel dominos.

In particular, we can recover the partition function from this formula by integrating over all particle positions (i.e. considering the above formula for $m = n + 1$). Because $x_i^{(n+1)} = i - 1$, we have $\Delta(x_i^{(n+1)}) = \prod_{i=1}^{n} i!$ and since the probability density is normalized, we find

$$Z_n = (1+\lambda)^{\frac{n(n+1)}{2}}, \tag{3.13}$$

as expected [19]. We now prove Proposition 3.1.1.

Proof. From (3.9), the formula (3.11) is correct for $m = 1$. Assuming it is also the case for m, we show that it holds for $m + 1$ by verifying the following identity,

$$\sum_{x^{(m)}} \Delta(x^{(m)})\Omega(x^{(m)})\chi(x^{(m)} \prec x^{(m+1)}) = \frac{1}{m!}\Delta(x^{(m+1)}). \tag{3.14}$$

To lighten the notations, let us set $x_i \equiv x_i^{(m)} \quad (1 \leqslant i \leqslant m)$ and $y_i \equiv x_i^{(m+1)} \quad (1 \leqslant i \leqslant m+1)$. Since the Vandermonde determinant in the left-hand side (l.h.s.) depends on each variable separately row by row, we can factorize $\Omega(x^{(m)}) = \prod_i \Omega(x_i^{(m)})$ and insert it inside the determinant as well as the summations,

$$\sum_{x_1=y_1}^{y_2} \cdots \sum_{x_m=y_m}^{y_{m+1}} \det_{1\leqslant i,j\leqslant m} \left[x_i^{j-1}\Omega(x_i)\right] = \det_{1\leqslant i,j\leqslant m} \left[\sum_{x_i=y_i}^{y_{i+1}} x_i^{j-1}\Omega(x_i)\right]. \tag{3.15}$$

The factor $\Omega(x_i)$ only affect the boundary terms of the sum and can be written as

$$\Omega(x_i) = \frac{\lambda^{\alpha_{\sup}(x_i)}}{(1+\lambda)^{\alpha(x_i)}} = \begin{cases} \Omega_{\sup} \equiv \frac{\lambda}{(1+\lambda)} & \text{if } x_i = y_{i+1}, \\ \Omega_{\inf} \equiv \frac{1}{(1+\lambda)} & \text{if } x_i = y_i, \\ 1 & \text{otherwise.} \end{cases} \tag{3.16}$$

Such sums of powers can easily be computed using Euler-Maclaurin or Faulhaber's formula, for $j \geqslant 1$,

$$\begin{aligned} \sum_{x_i=y_i}^{y_{i+1}} x_i^{j-1}\Omega(x_i) &= \sum_{x_i=y_i+1}^{y_{i+1}} x_i^{j-1} + y_{i+1}^{j-1}(\Omega_{\sup} - 1) + y_i^{j-1}\,\Omega_{\inf} \\ &= \sum_{x_i=0}^{y_{i+1}} x_i^{j-1} - \sum_{x_i=0}^{y_i} x_i^{j-1} - \frac{y_{i+1}^{j-1}}{(1+\lambda)} + \frac{y_i^{j-1}}{(1+\lambda)} \\ &= p_j(y_{i+1}) - p_j(y_i), \end{aligned} \tag{3.17}$$

where

$$p_j(y) = \frac{y^j}{j} + \frac{\lambda-1}{\lambda+1}\frac{y^{j-1}}{2} + \sum_{k=2}^{j-1} \frac{B_k}{j}\binom{j}{k} y^{j-k}, \tag{3.18}$$

with B_k the Bernoulli numbers. As all entries of the determinant are proportional to the difference of polynomials in each variable, we can extend this determinant of size m into a determinant of size $(m+1)$ using the relation

$$\begin{aligned}\det_{1\leqslant i,j\leqslant m}\left[p_j(y_{i+1}) - p_j(y_i)\right] &= \det_{1\leqslant i,j\leqslant m+1}\left[p_{j-1}(y_i)\right] \\ &= \det_{1\leqslant i,j\leqslant m+1}\left[\frac{y_i^{j-1}}{j-1}\right] = \frac{1}{m!}\Delta(x^{(m+1)}),\end{aligned} \tag{3.19}$$

where we set $p_0(y) = 1$. The first equality is obtained by row operations and actually holds for more general functions than polynomials. The second is obtained by column operations and is a standard property of Vandermonde determinants. The last relation finally yields the desired result and concludes the proof. □

3.1.3 Distribution on first levels

In this section, we obtain the distribution $\rho(x^{(1)}, \dots, x^{(m)})$ by integrating from the right side of the particle system. Another possible approach to obtain this result, similar to [45], consists in the introduction of the holes (the complement of the particle set, see Figure 3.3) and the use of the symmetries of the Aztec diamond. It is how we initially obtained the distribution, however, the method described here after is slightly more direct.

Proposition 3.1.2. *The probability density of the particle process on the first m levels is given by*

$$\begin{aligned}\rho(x^{(1)}, \dots, x^{(m)}) = A_{n,m} \det_{1\leqslant i,j\leqslant m}\left[L_{n-m+i, x_j^{(m)}}\right] \cdot \Omega(x^{(1)}, \dots, x^{(m-1)}) \cdot \\ \cdot \chi(x^{(1)} \prec \cdots \prec x^{(m)}),\end{aligned} \tag{3.20}$$

where the $L_{i,j} = \lambda^j \binom{i}{j}$ *can be defined by the initial condition* $L_{0,j} = \delta_{0,j}$, *and the recurrence, for* $i \geqslant 0$,

$$L_{i+1,j} = L_{i,j} + \lambda\, L_{i,j-1}, \qquad \textit{while} \qquad A_{n,m} = \frac{\lambda^{-m(m-1)/2}}{(1+\lambda)^{m(n+1-m)}}. \tag{3.21}$$

Proof. We proceed by induction starting from $m = n+1$ (or indeed $m = n$ as both values yields the same distribution as it should do). In this case, we recover directly (3.9) due to $\det_{1\leqslant i,j\leqslant n+1} L_{i-1,j-1} = \lambda^{n(n+1)/2}$. For the induction step, we need to prove that the distribution integrated over its $(m+1)$-th level yields the correct density for the m first levels. This is equivalent to show that

$$\sum_{x^{(m+1)}} \det_{1\leqslant i,j\leqslant m+1} \left[L_{n-m+i-1,x_j^{(m+1)}} \right] \cdot \Omega(x^{(m)}) \cdot \chi(x^{(m)} \prec x^{(m+1)}) = \frac{A_{n,m}}{A_{n,m+1}} \det_{1\leqslant i,j\leqslant m} \left[L_{n-m+i,x_j^{(m)}} \right]. \tag{3.22}$$

As before, let us set $x_j \equiv x_j^{(m)} \quad (1 \leqslant j \leqslant m)$ and $y_j \equiv x_j^{(m+1)} \quad (1 \leqslant j \leqslant m+1)$. The adjacency factor $\Omega(x^{(m)})$ weighs the distribution when particles of levels m and $m+1$ have the same position. Until now, we wrote it as a function of the level m, but here, it is convenient to interpret this factor as a function $\overleftarrow{\Omega}(x^{(m+1)}) = \Omega(x^{(m)})$ of the level $m+1$ instead, such that

$$\overleftarrow{\Omega}(y_j) = \begin{cases} \frac{1}{(1+\lambda)} & \text{if } y_j = x_j, \\ \frac{\lambda}{(1+\lambda)} & \text{if } y_j = x_{j-1}, \\ 1 & \text{otherwise.} \end{cases} \tag{3.23}$$

We rewrite the l.h.s. of (3.22) with the sums in the determinant,

$$\det_{1\leqslant i,j\leqslant m+1} \left[\sum_{y_j = x_{j-1}}^{x_j} L_{n-m+i-1,y_j}\, \overleftarrow{\Omega}(y_j) \right], \tag{3.24}$$

where we set $x_0 = 0$ and $x_{m+1} = n$. (Note that $\overleftarrow{\Omega}$ takes the value 1 in these special cases since it corresponds to the boundary of the AD and not to the presence of a particle.) We simplify this determinant

with the column operations: $C_j \mapsto \sum_{k=1}^{j} C_k$. Since we have $\overleftarrow{\Omega}(y_i = x_i) + \overleftarrow{\Omega}(y_{i+1} = x_i) = 1$, the entries become

$$\sum_{y_j=0}^{x_j} L_{n-m+i-1,y_j}\, \overleftarrow{\Omega}(y_j), \tag{3.25}$$

with $\overleftarrow{\Omega}$ affecting only the upper bound of the summation. In the last column, the expression simplifies further and we find $\sum_{y=0}^{n} L_{n-m+i-1,y} = (1+\lambda)^{n-m+i-1}$. Since we want to reduce the size of the determinant, we apply the row operations $L_i \mapsto L_i - (1+\lambda)L_{i-1}$ in order to obtain 0's in all the elements of the last column except for the top-right corner. The rest of the entries, for $i = 2, \dots, m+1$ and $j = 1, \dots, m$, are given by

$$\begin{aligned}\sum_{y_j=0}^{x_j} &(L_{n-m+i-1,y_j} - (1+\lambda)L_{n-m+i-2,y_j})\overleftarrow{\Omega}(y_j) \\ &= \sum_{y_j=0}^{x_j} \lambda(L_{n-m+i-2,y_j-1} - L_{n-m+i-2,y_j})\overleftarrow{\Omega}(y_j). \end{aligned} \tag{3.26}$$

The last summation, being telescopic, can be carried explicitly and, after some simplifications, using the recurrence relation of the $L_{i,j}$'s, one finds that these entries are equal to $\frac{-\lambda}{1+\lambda} L_{n-m+i-1,x_j}$. In summary, the determinant is now given by

$$\begin{aligned}&\left|\begin{array}{c|c} \sum_{x=0}^{x_j} L_{n-m,x}\, \overleftarrow{\Omega}(x) & (1+\lambda)^{n-m} \\ \hline & 0 \\ \frac{-\lambda}{1+\lambda} L_{n-m+i-1,x_j} & \vdots \\ & 0 \end{array}\right|_{(m+1)\times(m+1)} \\ &\qquad = \frac{\lambda^m}{(1+\lambda)^{2m-n}} \det_{1\leqslant i,j\leqslant m}\Big[L_{n-m+i,x_j}\Big], \end{aligned} \tag{3.27}$$

and the prefactor exactly corresponds to $A_{n,m}/A_{n,m+1}$. □

The determinant in (3.20) can be explicitly computed, providing the following result.

Corollary 3.1.3. *The probability density of the particle process on the first m levels is given by*

$$\rho(x^{(1)},\dots,x^{(m)}) = A_{n,m}\Delta(x^{(m)})\prod_{i=1}^{m}\frac{(n+1-i)!\,\lambda^{x_i^{(m)}}}{x_i^{(m)}!(n-x_i^{(m)})!}\cdot \\ \cdot\,\Omega(x^{(1)},\dots,x^{(m-1)})\cdot\chi(x^{(1)}\prec\cdots\prec x^{(m)}). \quad (3.28)$$

To see that this distribution is indeed equal to the one in Proposition 3.1.2, we only have to show that

$$\begin{vmatrix} \binom{n+1-m}{x_1^{(m)}} & \cdots & \binom{n+1-m}{x_m^{(m)}} \\ \vdots & \ddots & \vdots \\ \binom{n}{x_1^{(m)}} & \cdots & \binom{n}{x_m^{(m)}} \end{vmatrix} = \prod_{i=1}^{m}\frac{(n+1-i)!}{x_i^{(m)}!(n-x_i^{(m)})!}\prod_{1\leqslant i<j\leqslant m}(x_j^{(m)}-x_i^{(m)}), \quad (3.29)$$

since the factor $\lambda^{\sum_i x_i^{(m)}}$ accounts for the dependence on λ of the $L_{i,j}$'s. To compute this determinant, one can use techniques from [92], for instance. However, this computation is not very instructive and will not be detailed here. This expression also makes the link with the result in the uniform case as obtained in [45].

From this distribution, we can also obtain the JPDF of the particle positions on a single level by integrating over the first $m-1$ levels. Since all the dependence on these levels is contained solely inside the characteristic function χ and the adjacency functions Ω, the computation is identical to the proof of Proposition 3.1.1. Hence, we obtain[4]

$$\rho(x^{(m)}) = \frac{\lambda^{\sum_i x_i^{(m)}-\frac{m(m-1)}{2}}}{(1+\lambda)^{m(n+1-m)}}\frac{\left[\Delta(x^{(m)})\right]^2}{\prod_{i=1}^{m}x_i^{(m)}!(n-x_i^{(m)})!}\prod_{i=0}^{m-1}\frac{(n-i)!}{i!}. \quad (3.30)$$

This last distribution is particularly interesting since it describes how the positions of particles evolve when we look deeper inside the Aztec diamond. As no approximation has been made so far, it contains all the contributions coming from the edges of the domain and the finite size effects. For instance, it was shown in [45] that for $\lambda = 1$, it is possible to recover the shape of the arctic curve from it. In this case, it is well

[4] Similarly, it is not difficult to obtain the distribution $\rho(x^{(m)},\dots,x^{(m+k)})$ for $k+1$ consecutive levels.

known that this curve is a circle [21]. For $\lambda \neq 1$, the curve is an ellipse such that horizontal or vertical dominos are favoured according to $\lambda < 1$ or $\lambda > 1$ respectively. We could probably recover the elliptic arctic curve using the expression above, however, it is an already well-documented subject, and other techniques such as the tangent method [43] are more appropriate for that.

The distribution (3.30) is also known to correspond to the probability measure of the Krawtchouk ensemble [93, 94],

$$m!\,\mathbb{P}^{Kr}_{m,n,p}(x^{(m)}) = \frac{[\Delta(x^{(m)})]^2}{(n!)^m (pq)^{\frac{m(m-1)}{2}}} \prod_{i=1}^{m} \binom{n}{x_i^{(m)}} p^{x_i^{(m)}} q^{n-x_i^{(m)}} \prod_{i=0}^{m-1} \frac{(n-i)!}{i!}, \tag{3.31}$$

for $p = \frac{\lambda}{1+\lambda}$ and $q = 1-p$, and has been studied in detail by Johansson [94–97]. However, his formalism and approach to the problem differ from ours. More precisely, he studied the statistics of a certain class of "zig-zag paths", which can be shown to correspond exactly to the particle system we are considering, the difference is that he does not compute the distribution $\rho(x^{(1)}, \ldots, x^{(m)})$ (which is our main interest) but directly $\rho(x^{(m)})$ via the Lindström-Gessel-Viennot method.

3.1.4 Convergence to the GUE-corners process

In this section, our main purpose is to compute the scaling limit of the distribution for the $x_i^{(\ell)}$'s, and to show that they behave like the eigenvalues of GUE matrices. This correspondence is an impressive result in the study of Aztec diamonds and other tiling models [31, 98], obtained first at the level of correlation functions, by Johansson and Nordenstam [44], and later at the level of the probability distribution itself by Fleming and Forrester [45].

The GUE-corners process (sometimes also called under its original name: GUE minor) is a well-known *determinantal point process* in random matrix theory [44, 99]. GUE refers to the Gaussian Unitary Ensemble which is constituted by random complex $m \times m$ hermitian matrices with entries following Gaussian laws in both their real and imaginary part, while the GUE-corners process more precisely describes the eigenvalues of matrices from GUE as well as all the eigenvalues $z_i^{(\ell)}$ of the size ℓ principal

submatrix located in the upper-left corner ($1 \leqslant i \leqslant \ell$ and $1 \leqslant \ell \leqslant m$). As a property of hermitian matrices, these eigenvalues between two consecutive submatrices interlace themselves. In the present work, we are mainly interested in the probability distribution of this process,

$$\rho_{\text{GUE-corners}}(z^{(1)}, \dots, z^{(m)}) = \frac{1}{(2\pi)^{m/2}} \Delta(z^{(m)}) \prod_{i=1}^{m} \mathrm{e}^{-\frac{1}{2}(z_i^{(m)})^2} \cdot \\ \cdot \chi(z^{(1)} \prec \cdots \prec z^{(m)}). \quad (3.32)$$

Over the last 20 years, the GUE-corners process has exhibited many universal features and has been observed to be the correct limiting process in many models showing an interlaced particle system. In some cases, the initial (discrete) particle process can be shown to be already *determinantal* (as in the present case), which is very convenient to perform explicit calculations at finite size. In some other cases, however (as for the *Alternating Sign Matrices* uniformly weighted), the initial process is not determinantal, although it still converges to GUE-corners in a suitable limit [90].

The main goal of this work is to emphasize this universality aspect by showing that this limiting process does not depend directly on the probability measure that we consider, but only the rescaling on the particle system does. Meaning that for some specific classes of probability measures on Aztec diamonds, in the scaling limit, GUE-corners always gives the correct description in a certain neighbourhood of the contact point between the edge and the arctic curves.

Proposition 3.1.4. *If we define* $z_i^{(\ell)} = \frac{x_i^{(\ell)} - \mu}{\sigma}$ *to be the rescaling of the x-particle system, with* $\mu = \frac{n\lambda}{1+\lambda}$ *and* $\sigma^2 = \frac{n\lambda}{(1+\lambda)^2}$*, then the JPDF* $\rho(z^{(1)}, \dots, z^{(m)})$ *converges in distribution to* $\rho_{\text{GUE-corners}}(z^{(1)}, \dots, z^{(m)})$ *in the limit where* $n \to \infty$ *and* m *remains finite.*

What may seem surprising is the simplicity of the rescaling and the fact there is no dependence on the level of the particles. In Section 3.2.3, we give more details concerning this rescaling and get a better understanding on this apparent simplicity.

A remark about the limit that we consider: keeping m finite while n is growing is equivalent to zoom in a microscopic region around the

contact point between the arctic curve and the edge of the domain. We emphasize the fact that this limit disregards the global structure of Aztec diamonds and tells nothing about the shape of the arctic curve for instance. Let us now present the proof of the result.

Proof. The Jacobian determinant of the transformation $x_i^{(\ell)} \mapsto z_i^{(\ell)} = \frac{x_i^{(\ell)}-\mu}{\sigma}$ is equal to $\sigma^{m(m+1)/2}$ and the Vandermonde determinant transforms like $\Delta(x^{(m)}) = \sigma^{m(m-1)/2}\Delta(z^{(m)})$. Thus, we find the probability distribution of the z-particles to be

$$\rho(z^{(1)},\dots,z^{(m)}) = \sigma^{m^2}\cdot\frac{\lambda^{\sigma\sum_i z_i^{(m)}+m\mu-\frac{m(m-1)}{2}}}{(1+\lambda)^{m(n-m+1)}}\Delta(z^{(m)})\cdot \prod_{i=1}^{m}\frac{(n+1-i)!}{(z_i^{(m)}\sigma+\mu)!(n-z_i^{(m)}\sigma-\mu)!}\Omega(x^{(1)},\dots,x^{(m-1)})\chi(x^{(1)}\prec\ldots\prec x^{(m)}). \tag{3.33}$$

Since we keep the number of particles finite in this approximation while the number of possible positions grows with n, it is expected that the probability to find adjacent particles goes to zero as n increases. It implies that we can neglect the exponent α (and thus the effect of Ω) at the leading order in n. Finally, we use the Stirling approximation,

$$(an+b\sqrt{n}+c)! = \sqrt{2\pi}(an)^{an+b\sqrt{n}+c+\frac{1}{2}}\ e^{\frac{b^2}{2a}-an}(1+\mathcal{O}(n^{-1/2})), \tag{3.34}$$

to extract the dominant order of the distribution, and after some computations, we find

$$\rho(z^{(1)},\dots,z^{(m)}) = \frac{1}{(2\pi)^{m/2}}\Delta(z^{(m)})\prod_{i=1}^{m}\mathrm{e}^{-\frac{1}{2}(z_i^{(m)})^2}\cdot \cdot\chi(z^{(1)}\prec\cdots\prec z^{(m)})\ (1+\mathcal{O}(n^{-1/2})), \tag{3.35}$$

which ensures the convergence in distribution to the GUE-corners process in the limit $n\to\infty$. □

3.2 Two-periodic Aztec diamonds

In this section, we repeat the same procedure to obtain the distribution of particles for the two-periodic measure on Aztec diamonds. This measure can be defined on the dual graph as follows: we attribute weights a

and b on the faces of the graph as represented in Figure 3.4. The weight is then assigned to dimers according to whether they are adjacent to a face a or b. Following this rule, the weight of a configuration c is given by $w(c) = \prod_{\text{faces } x_{i,j}} x_{i,j}^{N_{i,j}}$, where $N_{i,j} = 0, 1, 2$ is the number of dimers adjacent to the face $x_{i,j}$ in the configuration. We take the convention that the face in the bottom-left corner of the graph is always a.

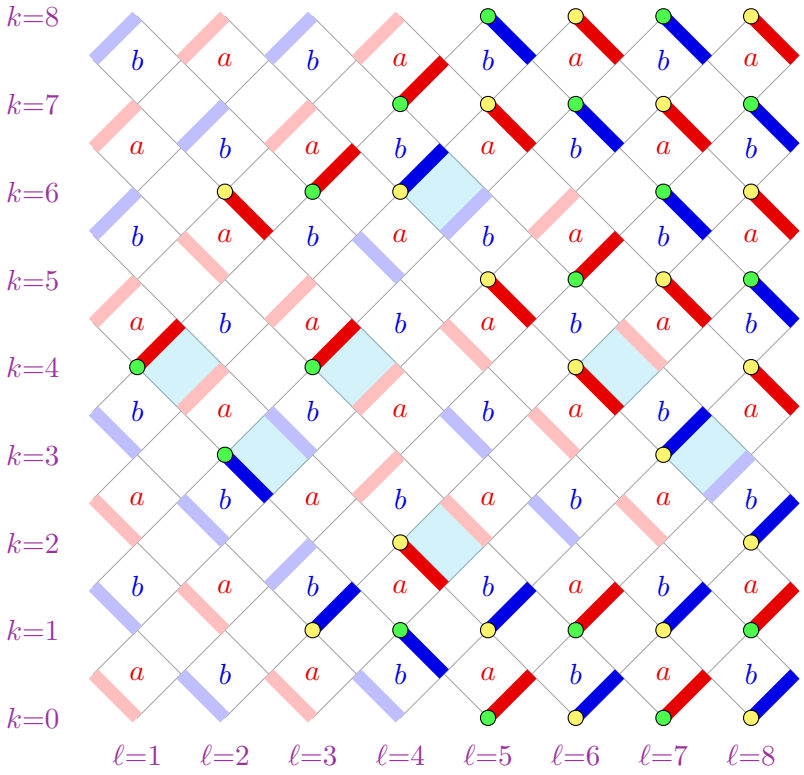

Figure 3.4: Same configuration as displayed in Section 3.1.2 shown on the dual lattice with the two-periodic weighting. We kept the light and dark shade with the same convention as previously and dimers are coloured according to the weight, a or b, they carry. Sky blue squares stand for the non-adjacent particles and the corresponding pair of dimers that can be flipped without modifying the particle configuration. Even particles are coloured in yellow and odd ones in green.

This probability measure on Aztec diamonds has been thoroughly studied in the literature recently [39, 52, 78, 91, 100, 101], partly due to the interesting phenomenology it brings to the model. Indeed, the disordered

region in this case is separated into two distinct zones with different behaviours. The external one is the usual rough/liquid region presenting the same characteristics as in the uniform case. While, in the very center, the disordered tiles are more likely to group themselves by pairs of parallel dominos around faces a or b depending on the favoured weight, see Figure 3.5. This region is usually called smooth or gaseous.

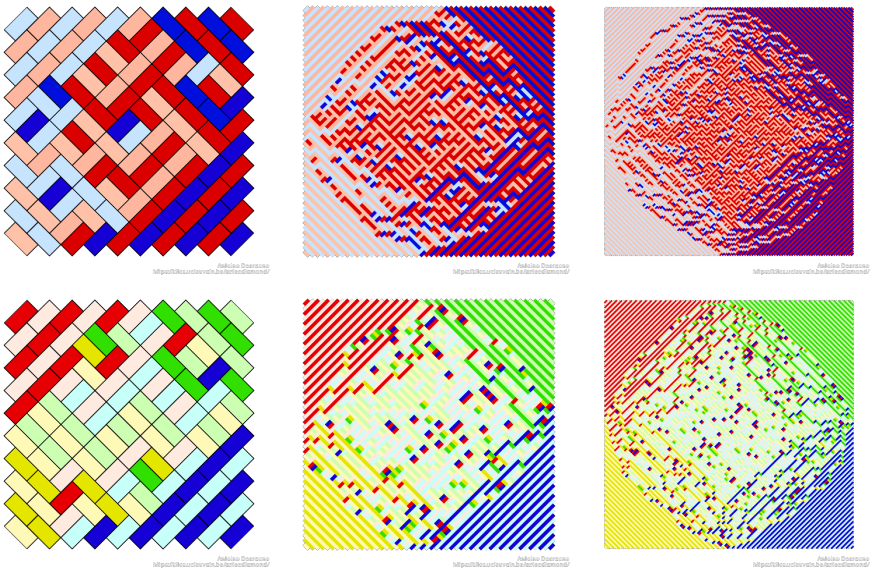

Figure 3.5: Two-periodic AD configurations with $a/b = 2$ and $n = 10, 50, 100$ from left to right. The first row uses the same colours as the previous figure while in the second eight different colours are used to highlight the gaseous region in the center. These eight colours are chosen as follows: first, we distinguish the four usual colours as in Figure 3.1. After that, we lighten the colours carried by dominos with weight a, and darken the ones carried by dominos with weight b.

We define the particle system in the same way as before. The main difference with the previous case is that we have now to account for the parity of the particles. For this purpose, we define the parity of a position $(\ell, x_i^{(\ell)})$ on the grid by

$$\varepsilon_\ell(x_i^{(\ell)}) = (-1)^{\ell + x_i^{(\ell)}}, \tag{3.36}$$

and assign a particle the parity of its position. It follows that the particles lying at the top of an a-face are even and those at the top of a b-face are odd.

According to this definition, we further split the adjacency functions into[5]:

$$\alpha^{\mathrm{e}}_{\mathrm{inf}}(x_i^{(\ell)}) = \delta_{x_i^{(\ell)},x_i^{(\ell+1)}}\delta_{\ell+x_i^{(\ell)},\,\mathrm{even}}, \qquad \alpha^{\mathrm{o}}_{\mathrm{inf}}(x_i^{(\ell)}) = \delta_{x_i^{(\ell)},x_i^{(\ell+1)}}\delta_{\ell+x_i^{(\ell)},\,\mathrm{odd}},$$
$$\alpha^{\mathrm{e}}_{\mathrm{sup}}(x_i^{(\ell)}) = \delta_{x_i^{(\ell)},x_{i+1}^{(\ell+1)}}\delta_{\ell+x_i^{(\ell)},\,\mathrm{even}}, \qquad \alpha^{\mathrm{o}}_{\mathrm{sup}}(x_i^{(\ell)}) = \delta_{x_i^{(\ell)},x_{i+1}^{(\ell+1)}}\delta_{\ell+x_i^{(\ell)},\,\mathrm{odd}}. \tag{3.37}$$

We also keep the convention that for α functions of several arguments, we take the sum over the contributions of each particle similarly to (3.3).

3.2.1 Probability density function

Referring to the equation (3.6), we need to determine the number of a- and b-dimers in terms of the particle positions. As claimed in Section 3.1.2, we provide an explanation for the interlacement as well as the equivalence in the number of dark shaded dimers of each weight, and the adjacency classes of their corresponding particles. In Figure 3.6, we construct iteratively a configuration of order $n = 4$ from level 1 to n. In the first of these pictures, we see there are n vertices to cover on the left edge of the graph, and $n + 1$ in the column right after ($\ell = 1$). Hence, one vertex of this column will not be covered by a dimer touching the left edge, and this is where the first particle will be located. For the three as yet uncovered vertices lying in between the levels $\ell = 1$ and $\ell = 2$, we see two groups of vertices separated by the red dimer: a group of one vertex above the red dimer, a group of two vertices below the red dimer. Therefore, the dimers covering these three vertices will leave two uncovered vertices, where the two particles at $\ell = 2$ will be located. Continuing this way explains the interlacing property. Moreover, by looking at the first two pictures of Figure 3.6, one sees that if two particles are sitting next to each other in two neighbouring levels,

[5] In practice, these adjacency functions need both particle coordinates $(\ell, x_i^{(\ell)})$ as arguments to be well-defined, but we decided to omit the level ℓ since it will be specified as upperscript of $x_i^{(\ell)}$ most of the time.

then we have $x_i^{(\ell)} = x_i^{(\ell+1)}$ if the dimer covering the vertex at $x_i^{(\ell)}$ is horizontal, and otherwise $x_i^{(\ell)} = x_{i+1}^{(\ell+1)}$ if that dimer is vertical. These observations repeat in the other pictures. The conclusion is that the weight of a dimer covering an adjacent particle located at $x_i^{(\ell)}$ gets a factor a if $\alpha^{\mathrm{o}}_{\mathrm{inf}}(x_i^{(\ell)}) = 1$ or $\alpha^{\mathrm{e}}_{\mathrm{sup}}(x_i^{(\ell)}) = 1$, and a factor b if $\alpha^{\mathrm{e}}_{\mathrm{inf}}(x_i^{(\ell)}) = 1$ or $\alpha^{\mathrm{o}}_{\mathrm{sup}}(x_i^{(\ell)}) = 1$.

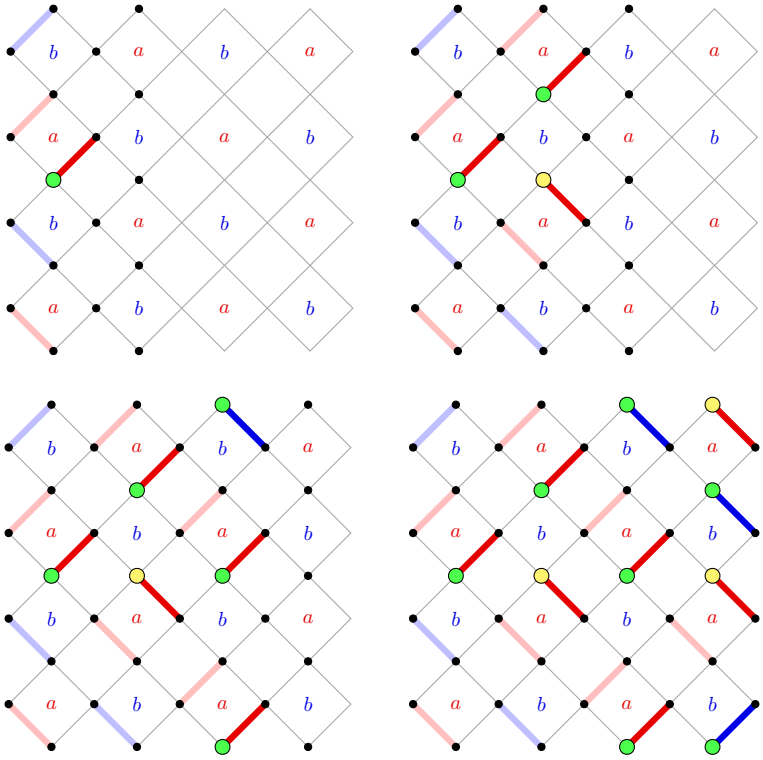

Figure 3.6: Construction level by level of a configuration of order 4.

In addition to that, the light and dark red dimers come in equal number and with the same weight by the same argument stated on page 142 (the same goes for the blue dimers), so that the weights of the light dimers can be included into those of the dark ones, by replacing the factors a and b by a^2 and b^2. Finally, each non-adjacent particle lies around a flippable plaquette and contributes a weight $a^2 + b^2$. Altogether, this

leads to the probability distribution for the total system

$$\rho(x^{(1)},\dots,x^{(n+1)}) = \frac{(a^2+b^2)^{\frac{n(n+1)}{2}}}{Z_n}\cdot\Omega(x^{(1)},\dots,x^{(n)})\cdot \\ \cdot\chi(x^{(1)}\prec\cdots\prec x^{(n+1)}), \quad (3.38)$$

where we define

$$\Omega(x^{(1)},\dots,x^{(n)}) = \\ \frac{(a^2)^{\alpha^{\mathrm{o}}_{\mathrm{inf}}(x^{(1)},\dots,x^{(n)})+\alpha^{\mathrm{e}}_{\mathrm{sup}}(x^{(1)},\dots,x^{(n)})}(b^2)^{\alpha^{\mathrm{e}}_{\mathrm{inf}}(x^{(1)},\dots,x^{(n)})+\alpha^{\mathrm{o}}_{\mathrm{sup}}(x^{(1)},\dots,x^{(n)})}}{(a^2+b^2)^{\alpha(x^{(1)},\dots,x^{(n)})}}. \quad (3.39)$$

This result is valid for n even or odd despite the fact that two-periodic ADs for n odd break the symmetry between the weight a and b. The total density found here looks very similar to the one for the biased case; only the factor Ω is different, reflecting the fact that particles are weighted differently when they are adjacent. In some sense, it is as if all the complexity of the probability measure is reduced into this notion of adjacency. We will see in the following that although the change in the distribution seems innocuous at this stage, it has a huge impact on the integration of the distribution and further computations.

Proposition 3.2.1. *The joint probability distribution over the subset of particles on levels m to $n+1$ is given by*

$$\rho(x^{(m)},\dots,x^{(n+1)}) = \frac{(a^2+b^2)^{\frac{n(n+1)}{2}}}{Z_n}\cdot\tilde{\Delta}(x^{(m)})\cdot\Omega(x^{(m)},\dots,x^{(n)})\cdot \\ \cdot\chi(x^{(m)}\prec\cdots\prec x^{(n+1)}) \quad (3.40)$$

with

$$\tilde{\Delta}(x^{(m)}) = \det_{1\leqslant i,j\leqslant m}\left[\frac{(x_i^{(m)})^{j-1}}{(j-1)!}+\varepsilon_m(x_i^{(m)})\sum_{k=0}^{j-2}\frac{(x_i^{(m)})^k}{k!}\alpha_{j-2-k}\right]. \quad (3.41)$$

The coefficients α_k for $k\in\mathbb{N}$ are given by

$$\alpha_0 = v, \qquad \alpha_k = \sum_{\ell=2}^{k}\left(v\,\alpha_{\ell-2}\,\alpha_{k-\ell}-\frac{2^\ell B_\ell}{\ell!}\,\alpha_{k-\ell}\right), \quad (3.42)$$

$$f(z) = \sum_{k=0}^{\infty}\alpha_k z^k = \frac{1}{2vz\tanh(z)}\left(1-\sqrt{1-4v^2\tanh^2(z)}\right), \quad (3.43)$$

with B_ℓ the Bernoulli numbers and $v = \frac{1}{2}\frac{b^2-a^2}{a^2+b^2} \in [-\frac{1}{2}, \frac{1}{2}]$.

One can remark that only odd powers of v appear in the determinant. As a consequence, the inversion of the weight $v \mapsto -v$ has exactly the same effect on the distribution as the inversion of the parity (even and odd) of the particles, as expected from (3.38). We also note that our definition of $\tilde{\Delta}$ differs slightly from the previous section; for convenience, we absorbed the factorials inside the determinant.

To lighten the notations, let us set $x_i \equiv x_i^{(m)} \quad (1 \leqslant i \leqslant m)$ and $y_i \equiv x_i^{(m+1)} \quad (1 \leqslant i \leqslant m+1)$. In anticipation of the proof, it is useful to rewrite the function $\Omega(x_i^{(m)})$ in terms of the level $m+1$,

$$\Omega(x_i) = \begin{cases} \Omega_{\text{sup}} = \frac{1}{2} + v\varepsilon_{m+1}(y_{i+1}) & \text{if } x_i = y_{i+1}, \\ \Omega_{\text{inf}} = \frac{1}{2} - v\varepsilon_{m+1}(y_i) & \text{if } x_i = y_i, \\ 1 & \text{otherwise.} \end{cases} \tag{3.44}$$

We also need the value of a sum of powers with modified boundary terms,

$$\sum_{x_i=y_i}^{y_{i+1}} x_i^{j-1}\Omega(x_i) = \frac{y_{i+1}^j - y_i^j}{j} + v(\varepsilon_{m+1}(y_{i+1})y_{i+1}^{j-1} - \varepsilon_{m+1}(y_i)y_i^{j-1}) + \sum_{k=2}^{j-1} \frac{B_k}{j}\binom{j}{k}(y_{i+1}^{j-k} - y_i^{j-k}), \tag{3.45}$$

as well as its alternating version,

$$\sum_{x_i=y_i}^{y_{i+1}} \varepsilon_m(x_i)x_i^{j-1}\Omega(x_i) = -v(y_{i+1}^{j-1} - y_i^{j-1}) - \sum_{k=2}^{j} \frac{B_k}{j}\binom{j}{k}(2^k-1)(\varepsilon_{m+1}(y_{i+1})y_{i+1}^{j-k} - \varepsilon_{m+1}(y_i)y_i^{j-k}), \tag{3.46}$$

for which a proof is given in Appendix 3.A. We note that, due to the presence of ε in the result of these summations, we no longer find polynomials. However, the result is still antisymmetric in the bounds of the summations, which is the important ingredient to extend the size of the determinant. We now present the proof for Proposition 3.2.1.

Proof. In the following, we proceed by induction. The case $m = 1$ is verified since $\tilde{\Delta}(x^{(1)}) = 1$. Supposing that the result holds for m, we have to show that

$$\sum_{x^{(m)}} \tilde{\Delta}(x^{(m)})\Omega(x^{(m)})\chi(x^{(m)} \prec x^{(m+1)}) = \tilde{\Delta}(x^{(m+1)}). \tag{3.47}$$

If we pull all functions and sums inside the determinant, it remains to evaluate the quantity

$$\det_{1\leqslant i,j\leqslant m}\left[\sum_{x_i=y_i}^{y_{i+1}}\left(\frac{x_i^{j-1}}{(j-1)!}+\varepsilon_m(x)\sum_{k=0}^{j-2}\frac{x_i^k}{k!}\alpha_{j-2-k}\right)\Omega(x_i)\right]. \tag{3.48}$$

We compute the summations inside the determinant by using the previous formulas and, by the argument of antisymmetry (3.19), extend the $m \times m$ determinant into a determinant of size $(m+1)$,

$$\begin{aligned}\det_{1\leqslant i,j\leqslant m+1}\Bigg[&\frac{y_i^{j-1}}{(j-1)!}+v\varepsilon_{m+1}(y_i)\frac{y_i^{j-2}}{(j-2)!}+\sum_{k=2}^{j-2}\frac{B_k}{k!}\frac{y_i^{j-1-k}}{(j-1-k)!}\\ &-\sum_{k=1}^{j-3}\alpha_{j-3-k}\left(v\frac{y_i^k}{k!}+\varepsilon_{m+1}(y_i)\sum_{\ell=2}^{k+1}\frac{B_\ell}{\ell!}\frac{y_i^{k+1-\ell}}{(k+1-\ell)!}(2^\ell-1)\right)\Bigg],\end{aligned} \tag{3.49}$$

where we used the convention that $(-1)! = \infty$. The shift in the index j is induced by the enlargement of the determinant. We want to find the column operations that simplify this determinant. First, let us suppose that the entries of the m first columns can be written as

$$C_j = \frac{y_i^{j-1}}{(j-1)!}+\varepsilon_{m+1}(y_i)\sum_{k=0}^{j-2}\frac{y_i^k}{k!}\alpha_{j-2-k}. \tag{3.50}$$

It is certainly true for $j = 1$, so that we only have to show that it is also correct for $m+1$. For this, we start by rearranging the summations in (3.49), and express the entries of the last column as

$$\begin{aligned}&\frac{y_i^m}{m!}+v\varepsilon_{m+1}(y_i)\frac{y_i^{m-1}}{(m-1)!}+\sum_{k=1}^{m-2}\frac{y_i^k}{k!}\left(\frac{B_{m-k}}{(m-k)!}-v\alpha_{m-2-k}\right)\\ &\qquad-\varepsilon_{m+1}(y_i)\sum_{k=0}^{m-3}\frac{y_i^k}{k!}\sum_{\ell=2}^{m-1-k}\frac{B_\ell}{\ell!}(2^\ell-1)\alpha_{m-1-k-\ell}.\end{aligned} \tag{3.51}$$

We apply the column operation

$$C_{m+1} \mapsto C'_{m+1} = C_{m+1} - \sum_{j=1}^{m-2} \left(\frac{B_{m-j}}{(m-j)!} - v\alpha_{m-2-j} \right) C_{j+1} \tag{3.52}$$

in order to cancel the terms which do not contain ε functions as prefactor (except the very first term). Note that, as B_j and α_j are equal to zero for j odd, only the columns of the same parity as C_{m+1} really appear in this transformation, although it is implicit in our notations. One can verify that after this operation the last column of the determinant becomes

$$\begin{aligned} C'_{m+1} = \frac{y_i^m}{m!} + v\varepsilon_{m+1}(y_i)\frac{y_i^{m-1}}{(m-1)!} \\ - \varepsilon_{m+1}(y_i) \sum_{k=2}^{m-1} \frac{y_i^{m-1-k}}{(m-1-k)!} \sum_{\ell=2}^{k} \left(\frac{2^\ell B_\ell}{\ell!} - v\,\alpha_{\ell-2} \right) \alpha_{k-\ell}. \end{aligned} \tag{3.53}$$

Comparing this expression with the last column of $\tilde{\Delta}(x^{(m+1)})$, we see that we have the equality between the two if and only if the coefficients α_k obey the following recurrence relation, for all $k \geqslant 1$,

$$\alpha_0 = v, \qquad \alpha_k = \sum_{\ell=2}^{k} \left(v\,\alpha_{\ell-2}\,\alpha_{k-\ell} - \frac{2^\ell B_\ell}{\ell!}\,\alpha_{k-\ell} \right), \tag{3.54}$$

which is indeed the case.

For the sake of completeness, we compute the generating function $f(z) = \sum_{k=0}^{\infty} \alpha_k z^k$ of these numbers. Multiplying each side of the recurrence relation by z^k and summing over k gives a quadratic equation for f,

$$v\,z^2 f(z)^2 - z\coth(z) f(z) + v = 0. \tag{3.55}$$

Among the two solutions, we select the one for which $f(0) = \alpha_0$, namely

$$f(z) = \frac{1}{2vz\tanh(z)} \left(1 - \sqrt{1 - 4v^2\tanh^2(z)} \right). \tag{3.56}$$

□

One may notice that, despite the complexity of the weighting system, the determinantal structure of the problem still allows us to perform

explicit computations. However, the drawback is that the determinant can no longer be evaluated in a closed form.

Remark 1. The similarity between the generating function of Catalan numbers $c(z) = \frac{1}{2z}\left(1-\sqrt{1-4z}\right) = \sum_{k=0}^{\infty} C_k z^k$ and the function f allows us to rewrite the α_k in term of the $C_k = \binom{2k}{k}\frac{1}{k+1}$ by using the expansion

$$f(z) = \frac{v\tanh(z)}{z}\, c(v^2\tanh^2(z)) = \sum_{k=0}^{\infty} z^k \sum_{\ell=0}^{\infty} \frac{C_\ell v^{2\ell+1}}{(k+1)!}\partial_w^{k+1}\tanh^{2\ell+1}(w)\Big|_{w=0}. \tag{3.57}$$

Remark 2. By taking $v = 0$ (equivalently $a = b$), one directly recovers the result on the uniform AD since in this case $\alpha_m = 0$ for all m, and the determinant in the density becomes a Vandermonde. Another interesting limit of these numbers is when $v \to \pm 1/2$. This is equivalent to taking extreme values for the weights; $a/b \to 0$ or $a/b \to \infty$. In this case, the α_m numbers also simplify. At the level of the generating function, we have

$$\frac{1}{2vz\tanh(z)}\left(1-\sqrt{1-4v^2\tanh^2(z)}\right)\Big|_{v=\pm 1/2} = \pm\frac{\tanh(z/2)}{z} = \mp g(z). \tag{3.58}$$

The function g is the exponential generating function for the Genocchi numbers (shifted by two units).

Remark 3. Similarly to the biased case, it is possible to find the partition function by evaluating the distribution (3.40) at $m = n+1$, which gives the equality

$$Z_n = (a^2+b^2)^{\frac{n(n+1)}{2}}\tilde{\Delta}(x_i^{(n+1)}). \tag{3.59}$$

It requires however to compute the determinant $\tilde{\Delta}(x_i^{(n+1)} = i-1)$ on the last particle level. The computation can be performed recursively where the induction step consists of a triangularization of the first two columns. The remaining determinant after this operation can be shown to be proportional to $\tilde{\Delta}(x_i^{(n-1)} = i) = \tilde{\Delta}(x_i^{(n-1)} = i-1; -v)$ which concludes the induction argument. Although seemingly not so complicated, the proof involves tedious computations and is not so much relevant for our purposes. We merely give the final result:

Proposition 3.2.2. *The determinant* $\tilde{\Delta}_{n+1} = \tilde{\Delta}(x_i^{(n+1)} = i-1)$ *can be computed exactly, and is given by*

$$\tilde{\Delta}_{n+1} = (1-4v^2)^{\frac{1}{2}\lfloor\frac{(n+1)^2}{4}\rfloor} \times \begin{cases} 1 & \text{if } n \neq 1 \mod 4, \\ \sqrt{\frac{1-2v}{1+2v}} & \text{if } n = 1 \mod 4. \end{cases} \tag{3.60}$$

The partition function follows directly form this proposition,

$$Z_n = (2ab)^{\lfloor\frac{(n+1)^2}{4}\rfloor}(a^2+b^2)^{\lfloor\frac{n^2}{4}\rfloor} \times \begin{cases} 1 & \text{if } n \neq 1 \mod 4, \\ a/b & \text{if } n = 1 \mod 4. \end{cases} \tag{3.61}$$

This quantity has been computed in [78] by using the relation between Aztec diamonds and the octahedron recurrence (see Section 3.3 for more details) and in [1] by using λ-determinants.

We note that the expression (3.60) is relatively simple, in the sense that it depends only on a certain power of factors $(1-2v)$ and $(1+2v)$. It means in particular that all the combinatorics hidden in the α_k coefficients seems to disappear when we compute the determinant on the last particle level, which is rather surprising.

3.2.2 Distribution on first levels

Similarly to the biased case, it is possible to guess the distribution for the first m levels and prove it to be correct by integrating from the higher to the lower levels. The strategy of the proof is the same as in Proposition 3.1.2, only the complexity of the expressions involved increases. The distribution may seem hard to guess in this case, but a part of the intuition on how we initially derived it is given at the end of the section.

Proposition 3.2.3. *The probability density of the particle process on the first* m *levels is given by*

$$\rho(x^{(1)},\dots,x^{(m)}) = A_{n,m} \det_{1\leqslant i,j\leqslant m}\left[L_{n-m+i,x_j^{(m)}}((-1)^m v)\right] \cdot \\ \cdot \Omega(x^{(1)},\dots,x^{(m-1)}) \cdot \chi(x^{(1)} \prec \cdots \prec x^{(m)}), \tag{3.62}$$

where, for $i \geqslant 0$, the $L_{i,j}$'s are defined by the initial condition $L_{0,j} = \delta_{0,j}$, and the recurrence

$$L_{i+1,j}(v) = (L_{i,j}(v) + L_{i,j-1}(-v))\beta_i(v),$$
$$\beta_i(v) = \begin{cases} (1-2v)^{-1} & \text{if } i = 0 \mod 4, \\ (1+2v)^{-1} & \text{if } i = 2 \mod 4, \\ 1 & \text{if } i = 1 \mod 2, \end{cases} \tag{3.63}$$

while

$$A_{n,m} = \left(\frac{1-4v^2}{4}\right)^{m(n+1-m)/2} \times$$
$$\times \begin{cases} \sqrt{\frac{1+2v}{1-2v}} & \text{if } n = 1 \pmod 4 \text{ and } m = 1 \pmod 2, \\ \sqrt{\frac{1-2v}{1+2v}} & \text{if } n = 3 \pmod 4 \text{ and } m = 1 \pmod 2, \\ 1 & \text{otherwise.} \end{cases} \tag{3.64}$$

Observe that, due to the initial conditions, it is immediate that $L_{i,j} = 0$ for $j < 0$ and $j > i$. Similarly to the biased case, the recurrence generalizes Pascal's triangular relation but here with a coefficient β_i, that depends on i mod 4, and a replacement $v \mapsto -v$ in $L_{i,j-1}$. An analogous recurrence for related quantities $S_{i,j}$ has been derived in [52] where refined partition functions of two-periodic Aztec diamonds were considered. The quantities introduced in [52] are in fact closely related to ours by the transformation $S_{i,j}\prod_{k=0}^{i-1}\beta_k = L_{i,j}$ (see Section 3.3 for more details). Before proving the proposition, we need the following results on the $L_{i,j}$ coefficients:

Lemma 3.2.4. *For $n \geqslant 0$, we have*

$$\sum_{k=0}^{n} L_{n,k} = A_{n,1}^{-1}(-v) = 2^n \prod_{k=1}^{n} \beta_k\beta_{k-1}. \tag{3.65}$$

Lemma 3.2.5. *For $i \geqslant 1$ and $j \in \mathbb{N}$, we have*

$$-2\overline{\beta}_i\overline{\beta}_{i-1}\sum_{k=0}^{j}(L_{i,k} - 2\beta_i\beta_{i-1}L_{i-1,k})\left[\frac{1}{2} - v(-1)^j\right]^{\delta_{k,j}} = \overline{L}_{i,j}. \tag{3.66}$$

The bar above some quantities is a shortcut notation to say that they are evaluated at $-v$ rather than v. In this section, we will also frequently need some properties on the β_k coefficients that we gather here:

$$\beta_k = \overline{\beta}_{k+2} = \beta_{k+4}, \qquad \beta_k + \overline{\beta}_k = 2\beta_k\overline{\beta}_k, \tag{3.67}$$

for all $k \in \mathbb{Z}$.

Proof of Lemma 3.2.4. In some sense, this lemma may appear trivial; if we assume the proposition to be true, it just ensures that the distribution at $m = 1$ is normalized,

$$A_{n,1}(v) \sum_{k=0}^{n} L_{n,k}(-v) = \sum_{k=0}^{n} \rho(x_1^{(1)} = k) = 1. \tag{3.68}$$

The lemma can nevertheless be obtained independently. Hereafter, we show that the left- and the right-hand side of (3.65) obey the same recurrence relation. For $n = 0$ it is clear that both sides are equal to 1, therefore, it only remains to show that

$$2\beta_{n+1}\beta_n \sum_{k=0}^{n} L_{n,k} = \sum_{k=0}^{n+1} L_{n+1,k}. \tag{3.69}$$

Using the recurrence of $L_{i,j}$ on the right-hand side and playing with the properties of β_k, this is equivalent to

$$\sum_{k=0}^{n+1} \frac{L_{n,k}}{\beta_{n-1}} - \frac{\overline{L}_{n,k-1}}{\overline{\beta}_{n-1}} = 0. \tag{3.70}$$

The expression inside the sum is equal to $L_{n-1,k} - L_{n-1,k-2}$ so that the summation on k indeed gives zero. □

Proof of Lemma 3.2.5. In this proof, we follow the same strategy as in the previous one, and show that the two sides of the equality obey the same recurrence relation. The case $i = 1$ is easy to prove and only relies on the values of $L_{0,k} = \delta_{0,k}$ and $L_{1,k} = (\delta_{0,k}+\delta_{1,k})\beta_0$. For the recurrence, we claim that both sides obey $(\overline{L}_{i,j} + L_{i,j-1})\overline{\beta}_i = \overline{L}_{i+1,j}$. For the right-hand side, it directly follows from the definition of the $L_{i,j}$, while for the

l.h.s., summed at j and $j-1$ with the replacement $v \mapsto -v$, we find

$$-2\overline{\beta}_i \sum_{k=0}^{j} \left[\overline{\beta}_i\overline{\beta}_{i-1}L_{i,k} + \beta_i\beta_{i-1}\overline{L}_{i,k-1} - 2\overline{\beta}_i\overline{\beta}_{i-1}\beta_i\beta_{i-1}(L_{i-1,k} + \overline{L}_{i-1,k-1})\right] \times \left[\frac{1}{2} - v(-1)^j\right]^{\delta_{k,j}}, \quad (3.71)$$

where we used that $L_{i,j} = 0$ for $j < 0$ and $j > i$. Using the recurrence on the $L_{i,j}$'s and (3.67), we rewrite this expression as

$$\begin{aligned} &-2\overline{\beta}_i\beta_i \sum_{k=0}^{j} \left[-\overline{\beta}_{i-1}L_{i,k} + \beta_{i-1}\overline{L}_{i,k-1}\right] \left[\frac{1}{2} - v(-1)^j\right]^{\delta_{k,j}} \\ &\quad = -2\overline{\beta}_{i+1}\overline{\beta}_i \sum_{k=0}^{j} \left[L_{i+1,k} - 2\beta_{i+1}\beta_i L_{i,k}\right] \left[\frac{1}{2} - v(-1)^j\right]^{\delta_{k,j}}. \quad (3.72) \end{aligned}$$

This last equality brings the expression back to its original form at $i+1$, which concludes the proof. □

Proof of Proposition 3.2.3. We proceed by induction starting from $m = n+1$. In this case, the determinant is lower triangular, and, in order to recover (3.38), we need to show that $\prod_{k=0}^{n} L_{k,k}\big((-1)^{n+1}v\big) = (a^2 + b^2)^{n(n+1)/2}/Z_n = [\tilde{\Delta}_{n+1}(v)]^{-1}$. The product can be computed by using

$$L_{k,k}(v) = (1-4v^2)^{-\lfloor \frac{k}{4} \rfloor} \times \begin{cases} 1 & \text{if } k = 0 \mod 4, \\ (1-2v)^{-1} & \text{if } k = 1 \mod 4, \\ (1+2v)^{-1} & \text{if } k = 2 \mod 4, \\ (1-4v^2)^{-1} & \text{if } k = 3 \mod 4, \end{cases} \quad (3.73)$$

and by separating each value of n mod 4. One can verify that it gives the claimed result by comparison with (3.60). For the induction step, we have to show that the distribution integrated over its level $m+1$ gives back the density at m. It is equivalent to verify that

$$\begin{aligned} &\sum_{x^{(m+1)}} \det_{1\leqslant i,j\leqslant m+1} \left[L_{n-m+i-1,x_j^{(m+1)}}\big((-1)^{m+1}v\big)\right] \cdot \Omega(x^{(m)}) \cdot \chi(x^{(m)} \prec x^{(m+1)}) \\ &\qquad = \frac{A_{n,m}}{A_{n,m+1}} \det_{1\leqslant i,j\leqslant m} \left[L_{n-m+i,x_j^{(m)}}\big((-1)^m v\big)\right]. \quad (3.74) \end{aligned}$$

As before, we set $x_j \equiv x_j^{(m)} \quad (1 \leqslant j \leqslant m)$ and $y_j \equiv x_j^{(m+1)} \quad (1 \leqslant j \leqslant m+1)$. Similarly to what we did in Section 3.1.3, we write $\Omega(x^{(m)}) = \overleftarrow{\Omega}(x^{(m+1)})$ as a function of $x^{(m+1)}$ such that

$$\overleftarrow{\Omega}(y_j) = \begin{cases} \frac{1}{2} + v\varepsilon_m(x_j) = \frac{1}{2} - v(-1)^{m+1+x_j} & \text{if } y_j = x_j, \\ \frac{1}{2} - v\varepsilon_m(x_{j-1}) = \frac{1}{2} + v(-1)^{m+1+x_{j-1}} & \text{if } y_j = x_{j-1}, \\ 1 & \text{otherwise.} \end{cases} \tag{3.75}$$

We rewrite the l.h.s. of (3.74) with the sums in the determinant,

$$\det_{1\leqslant i,j\leqslant m+1} \left[\sum_{y_j=x_{j-1}}^{x_j} L_{n-m+i-1,y_j}((-1)^{m+1}v)\, \overleftarrow{\Omega}(y_j) \right], \tag{3.76}$$

where we defined $x_0 = 0$ and $x_m = n$. (Note that $\overleftarrow{\Omega}$ takes the value 1 in these special cases since it corresponds to the boundary of the AD and not to the presence of a particle.) Without loss of generality, we absorb the sign $(-1)^{m+1}$ in a redefinition of $v \mapsto (-1)^{m+1}v$. We simplify this determinant with the following column operations: $C_j \mapsto \sum_{k=1}^{j} C_k$. Since we have $\overleftarrow{\Omega}(y_i = x_i) + \overleftarrow{\Omega}(y_{i+1} = x_i) = 1$, the entries become

$$\sum_{y_j=0}^{x_j} L_{n-m+i-1,y_j} \left[\frac{1}{2} - v(-1)^{x_j} \right]^{\delta_{y_j,x_j}}. \tag{3.77}$$

In the last column, the expression simplifies further and we find, due to Lemma 3.2.4, $\sum_{y=0}^{n} L_{n-m+i-1,y} = 2^{n-m+i-1} \prod_{k=1}^{n-m+i-1} \beta_k \beta_{k-1}$. Since we want to reduce the size of the determinant, we choose to apply the row operations $L_i \mapsto L_i - 2\beta_{n-m+i-1}\beta_{n-m+i-2}L_{i-1}$ in order to obtain 0's in the last column. The rest of the entries, for $i = 2, \ldots, m+1$ and $j = 1, \ldots, m$, are given by

$$\sum_{y_j=0}^{x_j} \left(L_{n-m+i-1,y_j} - 2\beta_{n-m+i-1}\beta_{n-m+i-2}L_{n-m+i-2,y_j} \right) \left[\frac{1}{2} - v(-1)^{x_j} \right]^{\delta_{y_j,x_j}}. \tag{3.78}$$

We can use Lemma 3.2.5 to simplify the expression and find something proportional to the desired entries. In summary, the determinant is now

given by

$$\begin{vmatrix} \sum_{y=0}^{x_j} L_{n-m,y}\, \overleftarrow{\Omega}(y;(-1)^{m+1}v) & 2^{n-m}\prod_{k=1}^{n-m}\beta_k\beta_{k-1} \\ -\dfrac{L_{n-m+i-1,x_j}}{2\overline{\beta}_{n-m+i-1}\overline{\beta}_{n-m+i-2}} & \begin{matrix}0\\ \vdots \\ 0\end{matrix} \end{vmatrix}_{(m+1)\times(m+1)}$$

$$\simeq \det_{1\leqslant i,j\leqslant m}\left[\overline{L}_{n-m+i,x_j}\right]. \quad (3.79)$$

After a tedious computation, the proportionality factor between the two determinants can be shown to correspond exactly to

$$A_{n,m}((-1)^{m+1}v)/A_{n,m+1}((-1)^{m+1}v). \quad (3.80)$$

□

Remark. In this proof, we used the knowledge of the partition function to slightly simplify the expression of $A_{n,m}$. However, it is not difficult to rewrite it while keeping Z_n implicit, by defining $\tilde{A}_{n,m} = A_{n,m}\frac{Z_n}{(a^2+b^2)^{n(n+1)/2}}$. The induction step would not change since we have $A_{n,m-1}/A_{n,m} = \tilde{A}_{n,m-1}/\tilde{A}_{n,m}$. In the end, it would be easy to deduce the partition function from the proposition, just by integrating the case $m = 1$.

By the same integration performed in Proposition 3.2.1, we can write down the one level density distribution[6]

$$\rho(x^{(m)}) = A_{n,m}\det_{1\leqslant i,j\leqslant m}\left[L_{n-m+i,x_j^{(m)}}((-1)^m v)\right]\cdot\tilde{\Delta}(x^{(m)}), \quad (3.81)$$

where $\tilde{\Delta}(x^{(m)})$ is still given by (3.41). It is a relatively simple formula given by the product of two determinants of identical sizes. We have not been able to evaluate these determinants in closed form and the product of the two does not seem to simplify the expression. The question of whether this last expression can be related to orthogonal or biorthogonal polynomials (similarly to the biased case with the Krawtchouk ensemble) remains open.

[6] Similarly, it is not difficult to obtain the distribution $\rho(x^{(m)},\dots,x^{(m+k)})$ for $k+1$ consecutive levels.

Another question is whether it is still possible to obtain the shape of the (outer) arctic curve by looking at the support of this distribution in the limit where n becomes large (method proposed by [45] in the uniform case). In practice, the above distribution contains all the necessary information; the problem rather lies in the feasibility of the computation from the determinantal expressions.

In the remainder of this section, we attempt to give a better understanding of the distribution (3.62). Originally, following the method proposed in [45], we deduced it from (3.40) by using the Jacobi identity, sometimes also referred to as Jacobi complementary minor theorem. For a square matrix M, the formula reads

$$\det M_{J,K} = (-1)^{\sum_i j_i + k_i} \det\left[(M^{-1})_{K^c,J^c}\right] \det M, \tag{3.82}$$

where $J = \{j_1, j_2, \dots\}, K = \{k_1, k_2, \dots\}$ are subsets of rows and columns of M, and J^c, K^c their complements. The above formula makes the bridge between the minors of a given matrix and the minors of its inverse. Interestingly, this formula can be used to connect the distribution of particles with the distribution of holes (the absence of particles). For instance, we can take M to be $\tilde{\Delta}_{n+1}(\pm v)$. In this case, the rows selected in J correspond to the particle positions, and consequently, J^c gives the hole positions.

The difficulty then lies in the inverse matrix, which can be hard to determine in principle, but since the equality holds at the determinant level, the exact inverse of M is not needed. Suppose that we have a lower triangular matrix L such that $LM = U$ with U an upper triangular matrix with ones on its diagonal. The inverse of M is given by $M^{-1} = U^{-1}L$, however, due to its triangular shape, U^{-1} do not contribute to the minors containing the last m rows of M^{-1} which are simply given by $|M^{-1}_{K^c,J^c}| = |L_{K^c,J^c}|$.

Our claim is that such a matrix $(L_{i,j})_{i,j=0}^{n}$ is actually given by the coefficients $L_{i,j}$ in (3.63) where the -1 prefactor in the Jacobi's formula has been absorbed inside the determinant. The exact sign of v in the different expressions depends on the parity of n and m. Once we have the distribution of holes, one can use the symmetries of the Aztec diamonds to exchange the roles of particles and holes and recover the distribution (3.62). It is also needed to know how to relate the adjacency of particles

and holes, but this can be done by explicitly counting the different kinds of dimers on a given level according to the particle positions.

3.2.3 Generating functions, asymptotics and convergence to the GUE-corners process

In this section, our first objective is to find an asymptotic formula for the $L_{i,j}$ coefficients, allowing us to understand the behaviour of the determinant near the edge in the large n limit. Such an analysis for a similar recurrence has been carefully realized in [52] so that we will not detail all the computations in the present document. Since the $L_{i,j}$'s obey a linear recurrence relation, their generating function is rational, and the tools developed in [73] are quite adapted. The only difficulty lies in the functions $\beta_i(v)$ that depends on the value of i modulo 4. It leads us to split the generating function into four functions, according to each subsequence. In the regime where i and j become large, the large deviation function leading to the asymptotics of these subsequences is the same; however, the prefactor and subleading terms may slightly differ for each of them.

The theorem 3.19 of [73] gives the asymptotics for large n of the coefficients

$$L_{sn,rn}(v) = \frac{1}{\sqrt{2\pi sn}} \mathrm{e}^{snF(\frac{r}{s})} \sum_{k=0}^{\infty} \frac{N_k^{[sn]}(\frac{r}{s})}{(sn)^{k/2}}, \tag{3.83}$$

for $s, r \in [0,1]$. $F(t)$ is the large deviation function and depends, in practice, only on the denominator of the generating function. The $N_k^{[sn]}(t)$ give the corrections at all orders in n and depend on derivatives of numerator and denominator of the generating function, they are therefore supposed to be smooth in t; these correction terms also depend implicitly on v. The exponent $[sn]$ reminds that the function may depend on sn but only on its value modulo 4 so that we have here four different functions $N_k^{[sn]}$ for each $k \in \mathbb{N}$. An explicit form of these corrections is not needed for our purposes[7]; however, since several cancellations occur in the determinant, we need to verify they do not interfere with the leading order. Once we have a clear knowledge of these cancellations, one can always truncate this series to only keep the necessary terms.

[7] A formula for $N_0^{[sn]}$ is given in [73].

Concerning the function F, it turns out that the discussion made in Section 4.1 of [52] applies almost verbatim in our case: in particular, it can be shown that $F(t) = F_1(t) - \frac{1}{2}\log\sqrt{1-4v^2}$, where F_1 is defined in the equation (4.12) of [52]. The function F can then be proven to be strictly concave with a unique maximum at $r_* = 1/2$ where $F(r_*) = \log\frac{2}{\sqrt{1-4v^2}}$ and $F''(r_*) = \frac{-4}{1-4v^2}$. We can now formulate the main result of this work.

Theorem 3.2.6. *If we define $z_i^{(\ell)} = \frac{x_i^{(\ell)}-\mu}{\sigma}$ to be the rescaling of the x-particle system, with $\mu = nr_*$ and $\sigma^2 = \frac{n}{-F''(r_*)}$, then the JPDF $\rho(z^{(1)},\dots,z^{(m)})$ converges in distribution to $\rho_{\text{GUE-corners}}(z^{(1)},\dots,z^{(m)})$ in the limit where $n\to\infty$ and m remains finite.*

Proof. We start by recalling the expression of the particle distribution at finite n, given in (3.62),

$$\rho(x^{(1)},\dots,x^{(m)}) = A_{n,m}\det_{1\leqslant i,j\leqslant m}\left[L_{n-m+i,x_j^{(m)}}\big((-1)^m v\big)\right]\cdot \\ \cdot\,\Omega(x^{(1)},\dots,x^{(m-1)})\cdot\chi(x^{(1)}\prec\cdots\prec x^{(m)}). \quad (3.84)$$

As in Section 3.1.4, we neglect the factor $\Omega(x^{(1)},\dots,x^{(m-1)})$ since the probability that some particles be adjacent decays to 0 in the large n limit. On level $m \ll n$, the particles are close to the contact point of the arctic curve with the boundary, located at $\mu = nr_* = \frac{n}{2}$. We set[8] $r_j = x_j^{(m)}/n$ and $s_i = 1 - \frac{m-i}{n}$ in order to make contact with the asymptotic form (3.83) for the $L_{sn,rn}$ coefficients. Thus the s_i are all close to 1, and the r_j are close to r_* and related to the z_j by the relation $r_j = r_* + z_j/\sqrt{-nF''(r_*)} + \dots$, where the dots refer to the fluctuations of r_j around r_* of scales larger than $\sqrt{n}$.

From (3.83), the coefficient L_{s_in,r_jn} contains the function $s_inF(r_j/s_i)$ which we can expand around $s_i = 1$ and $r_j = r_*$,

$$\begin{aligned} s_inF(r_j/s_i) &= nF(r_j) - (m-i)F(r_j) + (m-i)r_jF'(r_j) + \dots \\ &= nF(r_*) - \frac{1}{2}z_j^2 - (m-i)\big[F(r_j) - r_jF'(r_j)\big] + \dots \end{aligned} \quad (3.85)$$

[8] The superscript m is omitted in the definition of the r_j to keep the notation lighter.

where the dots are terms which go to 0 when n goes to infinity.

Using (3.83), we can now write the determinant as

$$\det_{1\leqslant i,j\leqslant m}\left[L_{s_i n, r_j n}\right] = (2\pi n)^{-m/2}\,\mathrm{e}^{mnF(r_*)}\prod_{j=1}^{m}\mathrm{e}^{-\frac{1}{2}z_j^2}\times\det_{1\leqslant i,j\leqslant m}\left[G_i(r_j)\right], \tag{3.86}$$

where the functions $G_i(r_j)$ are given by

$$G_i(r_j) = \frac{1}{\sqrt{s_i}}\,\mathrm{e}^{s_i nF(r_j/s_i)-nF(r_*)+z_j^2/2}\sum_{k=0}^{\infty}\frac{N_k^{[s_i n]}(r_j/s_i)}{(s_i n)^{k/2}}. \tag{3.87}$$

From (3.85), each function $G_i(r)$ has an expansion in inverse powers of n, whose dominant, order 0 term is

$$\tilde{N}_0^{[n-m+i]}(r) \equiv G_i(r)\Big|_{n^0} = N_0^{[n-m+i]}(r)\,\mathrm{e}^{(i-m)[F(r)-rF'(r)]}. \tag{3.88}$$

Before evaluating the asymptotic value of this determinant, we examine the other various factors depending on n that will enter the probability distribution in the scaling limit. There are four such terms: the $A_{n,m}$ factor, given in (3.64), the Jacobian of the change of variables $x_j \to z_j$, equal to $\sigma^{m(m+1)/2}$, and the terms $(2\pi n)^{-m/2}$ and $\mathrm{e}^{mnF(r_*)}$ in (3.86). Collecting their explicit values, we find

$$(2\pi n)^{-m/2}A_{n,m}\,\sigma^{m(m+1)/2}\,\mathrm{e}^{mnF(r_*)} = \frac{C_{n,m}(v)}{(2\pi)^{m/2}}\left(\frac{4}{1-4v^2}\right)^{m(m-3)/4} n^{m(m-1)/4}, \tag{3.89}$$

where $C_{n,m}(v)$ is the function on v, given in (3.64), which depends on n mod 4 and on m mod 2.

Collecting all terms, the scaling limit of the discrete distribution is given in terms of the remaining determinant as

$$\rho(z^{(1)},\dots,z^{(m)}) = \lim_{n\to\infty}\frac{C_{n,m}(v)}{(2\pi)^{m/2}}\left(\frac{4}{1-4v^2}\right)^{m(m-3)/4} n^{m(m-1)/4} \prod_{j=1}^{m}\mathrm{e}^{-\frac{1}{2}z_j^2}\det_{1\leqslant i,j\leqslant m}\left[G_i(r_j)\right]\cdot\chi(z^{(1)}\prec\cdots\prec z^{(m)}). \tag{3.90}$$

To evaluate the determinant, we expand the functions $G_i(r_j)$ around $r_j = r_* + \varepsilon_j$, to obtain

$$G_i(r_j) = G_i(r_*) + \varepsilon_j\, G_i'(r_*) + \frac{\varepsilon_j^2}{2}\, G_i''(r_*) + \ldots + \frac{\varepsilon_j^{m-1}}{(m-1)!}\, G_i^{(\geqslant m-1)}(r_*), \tag{3.91}$$

where $G_i^{(\geqslant m-1)}(r_*)$ contains the tail of the Taylor expansion, namely,

$$G_i^{(\geqslant m-1)}(r_*) = G_i^{(m-1)}(r_*) + \frac{\varepsilon_j}{m}\, G_i^{(m)}(r_*) + \frac{\varepsilon_j^2}{m(m+1)}\, G_i^{(m+1)}(r_*) + \ldots \tag{3.92}$$

The matrix inside the determinant factorizes so that, with $G_i^{(m-1)}(r_*)$ standing for $G_i^{(\geqslant m-1)}(r_*)$,

$$\begin{aligned} \det_{1\leqslant i,j\leqslant m} [G_i(r_j)] &= \det_{1\leqslant i,j\leqslant m} \left[\sum_{k=1}^{m} \frac{1}{(k-1)!}\, G_i^{(k-1)}(r_*)\, \varepsilon_j^{k-1} \right] \\ &= \det_{1\leqslant i,j\leqslant m} \left[\frac{1}{(j-1)!}\, G_i^{(j-1)}(r_*) \right] \det_{1\leqslant i,j\leqslant m} \left[\varepsilon_j^{i-1} \right]. \end{aligned} \tag{3.93}$$

The Vandermonde determinant yields, upon using $\varepsilon_j = z_j/\sqrt{-nF''(r_*)} + \ldots$,

$$\det_{1\leqslant i,j\leqslant m} [\varepsilon_j^{i-1}] = \Delta\Big(\frac{z_j^{(m)}}{\sqrt{-nF''(r_*)}} + \ldots \Big) = \big(-nF''(r_*)\big)^{-m(m-1)/4} \Delta(z_j^{(m)}) + \ldots \tag{3.94}$$

Thus its dominant order in n precisely cancels the power $n^{m(m-1)/4}$ in the expression (3.90), implying, in the large n limit, that the corrections in the previous equation will decay to zero, and that the contribution of the derivatives $G_i^{(j-1)}(r_*)$ will be given by the derivatives of their zeroth order in n, that is,

$$\begin{aligned} B_m^{[n]} &\equiv \lim_{n\to\infty} \det_{1\leqslant i,j\leqslant m} \left[\frac{1}{(j-1)!}\, G_i^{(j-1)}(r_*) \right] \\ &= \det_{1\leqslant i,j\leqslant m} \left[\frac{1}{(j-1)!}\, \frac{\mathrm{d}^{j-1} \tilde{N}_0^{[n-m+i]}(r)}{\mathrm{d}r^{j-1}} \Big|_{r_*} \right]. \end{aligned} \tag{3.95}$$

We obtain the following final result for the particle distribution in the scaling limit,

$$\rho(z^{(1)},\dots,z^{(m)}) = \frac{1}{(2\pi)^{m/2}}\,\Delta(z_j^{(m)})\,\prod_{j=1}^{m}\mathrm{e}^{-\frac{1}{2}(z_j^{(m)})^2}\,\chi(z^{(1)}\prec\ldots\prec z^{(m)})\times \\ \times\left\{C_{n,m}(v)\,B_m^{[n]}\left(\frac{1-4v^2}{4}\right)^{m/2}\right\}, \quad (3.96)$$

precisely the GUE-corners distribution except for the factor within the curly brackets. The proper normalizations of both the discrete distribution we started from and of the GUE-corners process ensure that this factor must be equal to 1. □

Remark. It would be clearly desirable to check explicitly that the factor within the brackets is actually equal to 1. Although the final result is surprisingly simple, the explicit calculation of $B_m^{[n]}((-1)^m v)$ looks awkward: it requires multiple derivatives of the functions $F(r)$ and $N_0^{[0]}(r),\dots,N_0^{[3]}(r)$, which are all rather complicated for $v\neq 0$. We have nevertheless checked that the factor is indeed equal to 1 for $m\leqslant 4$. For $v=0$ however the situation simplifies drastically. For any v, the arguments in the above proof indeed show that, in the large n limit, the determinant of the matrix $\big(G_i(r_j)\big)_{i,j}$ can be reduced to the determinant of its zeroth order $\big(\tilde{N}_0^{[n-m+i]}(r_j)\big)_{i,j}$. However, for $v=0$, the functions $N_0^{[n-m+i]}(r)=N_0(r)$ do not depend on i, and we obtain

$$\begin{aligned}&\det_{1\leqslant i,j\leqslant m}\Big[N_0^{[n-m+i]}(r_j)\,\mathrm{e}^{(i-m)[F(r_j)-r_jF'(r_j)]}\Big]\\ &\quad=\Big[\prod_{j=1}^{m}N_0(r_j)\Big]\,(-1)^{m(m-1)/2}\,\Delta\Big(\mathrm{e}^{-[F(r_j)-r_jF'(r_j)]}\Big)\\ &\quad=\big[N_0(r_*)\big]^m\,\Big[(-r_*F''(r_*))\mathrm{e}^{-F(r_*)}\Big]^{m(m-1)/2}\,\Delta\Big(\frac{z_j^{(m)}}{\sqrt{-nF''(r_*)}}\Big).\end{aligned} \quad (3.97)$$

As stated in Proposition 3.1.2, $L_{i,j}$ is given by a binomial coefficient, $L_{i,j}=\binom{i}{j}$. The asymptotic value relevant here is

$$L_{n,rn}\simeq\frac{r^{-rn}(1-r)^{-(1-r)n}}{\sqrt{2\pi n\,r(1-r)}}, \quad (3.98)$$

from which one obtains $F(r) = -r\log r - (1-r)\log(1-r)$ (implying, as announced above, $r_* = \frac{1}{2}$, $F(r_*) = \log 2$ and $F''(r_*) = -4$) and $N_0(r) = [r(1-r)]^{-1/2}$, with $N_0(r_*) = 2$. Then, the coefficient in front of the Vandermonde determinant, to be identified with $B_m^{[n]}$, yields $B_m^{[n]}(0) = 2^m$. With $C_{n,m}(0) = 1$, we obtain that the factor in the curly brackets in (3.96) is indeed equal to 1.

3.3 Connections with the octahedron recurrence

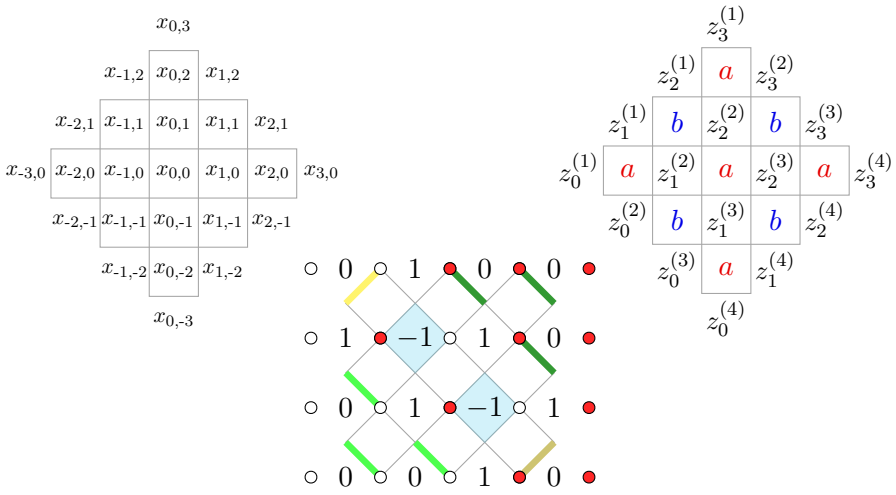

Figure 3.7: *Left*: general face weighting on the Aztec graph $\widehat{\mathcal{A}}_n$ for $n = 3$. *Right*: relabelling of the weights into the usual two-periodic ones with additional weights $z_k^{(\ell)}$. *Center*: example of a particle configuration and the corresponding alternating sign matrix of size $n+1$.

In this section, we make the connection between the probability density on the first m levels, $\rho(x^{(1)}, \ldots, x^{(m)})$, and the results obtained in [1, 52] and in Chapter 1 of this thesis. For this purpose, let us recall the notations used in Section 1.1 and denote the extended Aztec graph of order n by $\widehat{\mathcal{A}}_n$ and the face weight associated to a perfect matching M by $w_F(M) = \prod_{(i,j)\in\widehat{\mathcal{A}}_n} x_{i,j}^{1-N_{i,j}}$, where $N_{i,j} = 0, 1, 2$ is the number of dimers adjacent to the face $x_{i,j}$ of $\widehat{\mathcal{A}}_n$ (see Figure 3.7). We also consider a bias $\sqrt{\lambda}$ on the vertical edges of the graph such that the partition function T_n hence defined respects the octahedron recurrence (1.12) with initial

conditions (1.13). This measure differs from the one defined at the beginning of Section 3.2 but the corresponding partition functions are easily related by setting $\lambda = 1$ and by an inversion of the weights (only a global factor subsist). Another difference is that we now allow the external faces, on the edges of the graph, to also carry weights.

To make contact with the two-periodic measure, let us redefine the face weights as shown in the right picture of Figure 3.7. In addition to a and b, we keep the weights on the remaining faces (the p-faces in the notations of Section 1.2) and labelled them $z_k^{(\ell)}$; the reason will be clear in a moment. We easily recover the usual two-periodic AD by setting these latter variables to 1. In the central picture of Figure 3.7, we wrote the values $1-N_{k,\ell}$ inside each corresponding face $z_k^{(\ell)}$ for a given particle configuration. We have seen in Section 1.2.4 that this quantity corresponds to the entries of an alternating sign matrix of size $n+1$ [19]. Besides, one can see that the matrix is bijectively related to the particle system. A dictionary for this bijection is given in Figure 3.8. An alternating sign matrix possesses six different kinds of entries (directly related to the six-vertex model), namely $+1$, -1, and four different kinds of 0's, distinguishable according to the relative positions of the $+1$ entries in the same rows/columns of the matrix[9]. To each of these entries corresponds exactly one local particle configuration. The two first picture of the figure look similar from the particle point of view, but the underlying dimers indicate that in one case the left particle is adjacent to its inferior neighbour (i.e. $\alpha_{\text{inf}} = 1$) and in the other case the left particle is adjacent to its superior neighbour (i.e. $\alpha_{\text{sup}} = 1$). A similar notion of adjacency for holes enables us to distinguish between the third and the fourth picture. In terms of domino tilings however, the correspondence is not bijective; the non-adjacent particles (or equivalently the -1's) offer the possibility of two different local tilings (previously called the flippable plaquettes).

Let us define $\mathbf{x} = \{x^{(1)}, \dots, x^{(n+1)}\}$ to be the complete collection of particle positions in a given configuration. In the light of the connection

[9] Let us consider a 0 entry in an ASM. In the same row, this 0 is necessarily in between an entry $+1$ and -1 (or the edge of the matrix if there is no -1). There are two possibilities, the $+1$ can either be to the right of the 0 or to its left. The same goes for the column of the chosen 0 entry. The four possible cases are depicted in Figure 3.8.

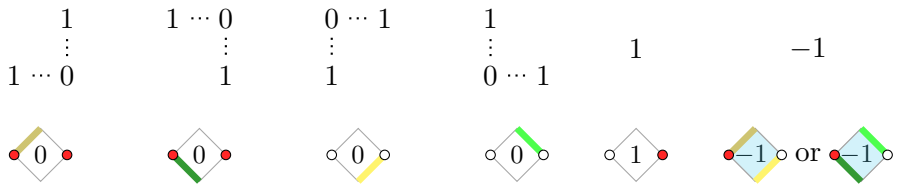

Figure 3.8: Dictionary between alternating sign matrix entries, local particle configurations and tilings.

with alternating sign matrices, we can decompose the function T_n (with the weighting specified in the right picture of Figure 3.7) as

$$T_n(a,b;z_k^{(\ell)}) = \sum_{\mathbf{x}} T_{n;\mathbf{x}}^{(n+1)}(a,b) \prod_{k,\ell=1}^{n+1} \left[z_{k-1}^{(\ell)}\right]^{B_{k,\ell}(\mathbf{x})}, \tag{3.99}$$

where $B(\mathbf{x})$ is the (unique) alternating sign matrix of size $n+1$ corresponding to the particle configuration $\mathbf{x}$. In this expression, the coefficients $T_{n;\mathbf{x}}^{(n+1)}(a,b)$ have a clear interpretation: they correspond to the (weighted) number of ways in which an AD of size n can be tiled while the positions of all particles are prescribed. By letting $z_k^{(\ell)} = 1$ for $\ell > m$, one can specialize the previous expression. Since all configurations having their particles on the m first levels at the same positions carry the same weight in $z_k^{(\ell)}$, we can write, for $\overline{\mathbf{x}} = \{x^{(1)}, \dots, x^{(m)}\}$,

$$T_n(a,b;z_k^{(\ell)}) = \sum_{\overline{\mathbf{x}}} T_{n;\overline{\mathbf{x}}}^{(m)}(a,b) \prod_{\substack{1\leqslant k\leqslant n+1\\ 1\leqslant \ell\leqslant m}} \left[z_{k-1}^{(\ell)}\right]^{B_{k,\ell}(\overline{\mathbf{x}})}. \tag{3.100}$$

In this expression, $B(\overline{\mathbf{x}})$ is not unique, only its first m columns are fixed by $\overline{\mathbf{x}}$, but the others do not contribute to the product anyway since $z_k^{(\ell)} = 1$ for $\ell > m$. The coefficients $T_{n;\overline{\mathbf{x}}}^{(m)}(a,b)$ keep the same interpretation, they give the total weight of AD configurations having particles at positions $\overline{\mathbf{x}}$. We now insert this expression in the octahedron recurrence (1.12) and find, for $\overline{\mathbf{x}} = \{x^{(1)}, \dots, x^{(m)}\}$ and $\overline{\mathbf{y}} = \{y^{(1)}, \dots, y^{(m-1)}\}$,

$$\sum_{\overline{\mathbf{x}},\overline{\mathbf{y}}} \left(T_{n;\overline{\mathbf{x}}}^{(m)}\, T_{n-2;\overline{\mathbf{y}}-1}^{(m-1)} - T_{n-1;\overline{\mathbf{x}}}^{(m)}\, T_{n-1;\overline{\mathbf{y}}-1}^{(m-1)} - \lambda\, \overline{T}_{n-1;\overline{\mathbf{x}}-1}^{(m)}\, \overline{T}_{n-1;\overline{\mathbf{y}}}^{(m-1)} \right) \times$$
$$\times \prod_{\substack{1\leqslant k\leqslant n+1\\ 1\leqslant \ell\leqslant m}} \left[z_{k-1}^{(\ell)}\right]^{B_{k,\ell}(\overline{\mathbf{x}})} \prod_{\substack{1\leqslant k\leqslant n+1\\ 1\leqslant \ell\leqslant m-1}} \left[z_{k-1}^{(\ell+1)}\right]^{B_{k,\ell}(\overline{\mathbf{y}})} = 0. \tag{3.101}$$

The summations run over all acceptable (i.e. interlaced in the sense of (3.7)) particle configurations for $\overline{\mathbf{x}}$ and $\overline{\mathbf{y}}$ independently and $\overline{T}_n$ stands for $T_n(b,a)$. It provides a system of equations which allows us to compute recursively the coefficients $T^{(m)}_{n;\overline{\mathbf{x}}}$ for any n, m and $\overline{\mathbf{x}}$ relying only on the initial values

$$T^{(0)}_0(a,b) = 1, \qquad T^{(0)}_1(a,b) = a^{-1}(1+\lambda). \tag{3.102}$$

However, due to the double summation on $\overline{\mathbf{x}}$ and $\overline{\mathbf{y}}$, several terms in these sums may have the same power in the variables $z^{(\ell)}_k$ which makes it difficult to extract generic equations for $T^{(m)}_{n;\overline{\mathbf{x}}}$. To simplify, let us examine the case $m = 2$, the equation then becomes

$$\sum_{\overline{\mathbf{x}},\overline{\mathbf{y}}} \Big(T^{(2)}_{n;\, x^{(1)}_1, x^{(2)}_1, x^{(2)}_2}\, T^{(1)}_{n-2;\, y^{(1)}_1 - 1} - T^{(2)}_{n-1;\, x^{(1)}_1, x^{(2)}_1, x^{(2)}_2} T^{(1)}_{n-1;\, y^{(1)}_1 - 1}$$

$$-\lambda\, \overline{T}^{(2)}_{n-1;\, x^{(1)}_1 - 1,\, x^{(2)}_1 - 1,\, x^{(2)}_2 - 1}\, \overline{T}^{(1)}_{n-1;\, y^{(1)}_1} \Big) z^{(1)}_{x^{(1)}_1}\, z^{(2)}_{x^{(2)}_1}\, z^{(2)}_{x^{(2)}_2}\, z^{(2)}_{y^{(1)}_1}\, \big[z^{(2)}_{x^{(1)}_1}\big]^{-1} = 0. \tag{3.103}$$

Already in this case, the generic coefficient of $z^{(1)}_k z^{(2)}_i z^{(2)}_j z^{(2)}_p [z^{(2)}_k]^{-1}$ would involve three different combinations of the expression in the parentheses. In some specific cases, for instance if $p = j$, it simplifies and only one combination appears, however, the equations thus extracted are not sufficient to obtain all the $T^{(m)}_{n;\overline{\mathbf{x}}}$.

What is interesting for us in this context is the function $T^{(m)}_{n;\overline{\mathbf{x}}}$ which is, by its definition, directly related to the distribution $\rho(\overline{\mathbf{x}})$ we computed. Indeed, as we said, this function counts the total weight of AD configurations having particles at positions $\overline{\mathbf{x}}$. If we divide this quantity by the partition function, it then gives the probability to observe the particle system in the state $\overline{\mathbf{x}}$, so that we have

$$\rho(\overline{\mathbf{x}}) = \frac{Z^{(m)}_{n;\overline{\mathbf{x}}}(a,b)}{Z_n(a,b)} = \frac{T^{(m)}_{n;\overline{\mathbf{x}}}(\frac{1}{a},\frac{1}{b})}{T_n(\frac{1}{a},\frac{1}{b})}, \tag{3.104}$$

where $Z^{(m)}_{n;\overline{\mathbf{x}}}$ is the equivalent of $T^{(m)}_{n;\overline{\mathbf{x}}}$ for the measure defined at the beginning of Section 3.2. As a consequence, the expression we found for $\rho(\overline{\mathbf{x}})$ in the previous sections must solve the octahedron system (3.101) at $\lambda = 1$. We verified this statement explicitly for $m = 2, 3$ and small

values of n on MATHEMATICA. However, for the general case, even with the solution at hand it is not obvious to us how to construct a direct proof that $T^{(m)}_{n;\overline{\mathbf{x}}}(a,b) = T_n(a,b)\,\rho(\overline{\mathbf{x}};-v)$ solves the equation (3.101). In [52], the system is studied at $m=1$ and the equation is linearized by considering the ratio

$$\begin{aligned} S_{n,k}(a,b) &= a\,\frac{T^{(1)}_{n,k}(a,b)}{T_{n-1}(a,b)} \\ &= S_{n-1,k}(a,b) + S_{n-1,k-1}(b,a) \times \begin{cases} 1 & \text{if } n = 0,1 \mod 4, \\ a^2/b^2 & \text{if } n = 2,3 \mod 4, \end{cases} \end{aligned} \tag{3.105}$$

with initial conditions $S_{0,k} = \delta_{0,k}$. These numbers are easily mapped to the $L_{n,k}$'s by the transformation $S_{n,k}\prod_{i=0}^{n-1}\beta_i = L_{n,k}$. In that work, the author is interested in computing the asymptotics of $T^{(1)}_{n,k}$ with the objective of finding the arctic curve of the model via the tangent method. This quantity is referred to as the *one-refined partition function* due to the fact that it counts the number of configurations while the position of the particle $x^{(1)}_1$ is prescribed. In this sense, the function $T^{(m)}_{n;\overline{\mathbf{x}}}$ can be seen as a *multi-refined partition function*. The octahedral recurrence then offers an explanation of why $T^{(m)}_{n;\overline{\mathbf{x}}}$ can be expressed solely in terms of $T^{(1)}_{n;k}$ itself being proportional to $L_{n,k}$.

Our last remark concerns the link between the interlaced particle system and the non-intersecting paths formulation of Aztec diamonds. Figure 3.9 shows a superposition of the two systems. We see in this picture that the particles appear on the beginning of steps $(2,0)$ and $(1,-1)$, which follows directly from their definition in terms of the dominos. The first particle $x^{(1)}_1$ is then related to the first bifurcation from the edge of the first path, and more generally, the particle $x^{(j)}_i$ is related to i-th bifurcation (i.e. steps $(2,0)$ and $(1,-1)$) of the $(j-i+1)$-th path.

3.4 Discussion

In this chapter, we showed that the GUE-corners distribution still appears as the limiting distribution in Aztec diamonds near the contact point between the arctic curve and the edge of the domain when the

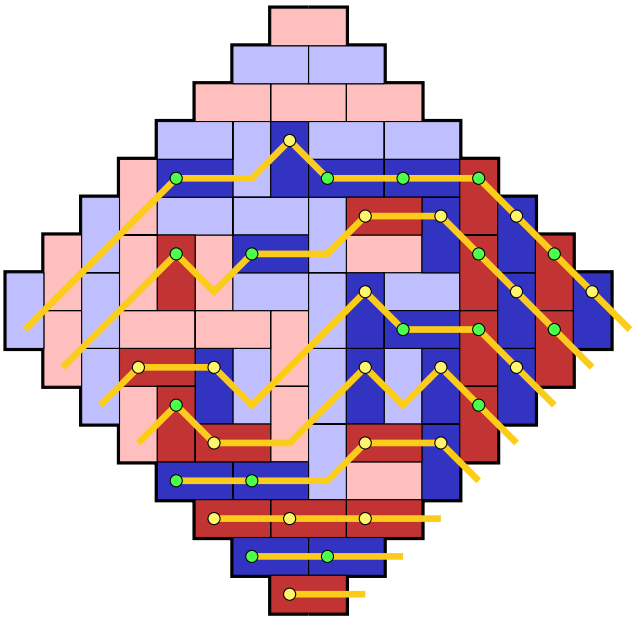

Figure 3.9: Superposition of the path description with the interlaced particles. We shifted by 1/2 unit to the right the usual paths to emphasize the correspondence. By definition, particles lie on starting points of steps $(2, 0)$ and $(1, -1)$.

probability measure on the configuration set is modified. More precisely, we examined the biased (or one-periodic) and the two-periodic measures. The main ingredients that we used are the determinantal structure of the particle process and the asymptotic Gaussian behaviour of the determinant entries. We believe these hypotheses to be sufficient to observe the convergence to the GUE-corners process in Aztec diamonds with any non-pathological probability measure, even though a deeper analysis would be required to settle this question. On the other hand, these hypotheses are certainly not necessary, since there exist discrete non-determinantal point processes (for instance, the uniformly weighted alternating sign matrices [90]) that also converge to GUE-corners. Under such considerations, it would not be surprising that further generalizations of the weighting system on Aztec diamonds continue to be associated with GUE, for instance, higher periodicity or two-periodic with an additional vertical bias, although fully explicit cal-

culations in these cases would probably become difficult to perform with our method.

It is also known that partition functions of Aztec diamonds are related to the octahedron recurrence [49,50], and one natural question would be to know whether the distribution of particles $\rho(x^{(1)},\dots,x^{(m)})$ also share connections with this recurrence. Since the density ρ gives the probability to observe a configuration while the position of a certain number of particle is prescribed, it is easily related to the notion of *refined partition functions* (enumeration of weighted configurations with the same constraints). These functions have to satisfy a modified octahedron system (as it is shown in [52] for the one-refined partition function). However, when one considers a refinement on several levels, the equations produced by the octahedron recurrence do not simplify very much, and although it effectively allows us to compute $\rho(x^{(1)},\dots,x^{(m)})$ recursively, the system of equations becomes rapidly complicated as m increases and it seems that no general formula for ρ can be extracted from it.

One last peculiarity that we observed is that *multi-refined partition functions* (in the sense that the particle positions on the m first levels are prescribed) appear to be proportional to the determinant of one-refined partition functions. In terms of the probability distribution, it is equivalent to observe that the m-level correlation function for Aztec diamonds of order n is proportional to a determinant of 1-level correlation functions of ADs of smaller size,

$$\rho_n(x^{(1)},\dots,x^{(m)}) \sim \det_{1\leqslant i,j\leqslant m}\left[\rho_{n-m+i}(x_j^{(m)})\right]\cdot\Omega(x^{(1)},\dots,x^{(m-1)})\cdot \\ \cdot\chi(x^{(1)}\prec\cdots\prec x^{(m)}). \quad (3.106)$$

The octahedron equation provide a partial answer to this observation since it shows that m-refined partition functions can always be related to the $m-1$ ones, but it does not really shed any light on the underlying structure. A similar construction has already been observed in a slightly different context [76], even though the details of this factorization remain unclear to us. It would be interesting to investigate whether there exists a general structure behind it.

3.A Alternating sum of powers

In this appendix, we prove the formula

$$\sum_{x=y_1}^{y_2} \varepsilon_\ell(x)\, x^{j-1}\, \Omega(x) = -v\left(y_2^{j-1} - y_1^{j-1}\right) - \sum_{k=2}^{j} \frac{B_k}{j}\binom{j}{k}(2^k-1)\left(\varepsilon_{\ell+1}(y_2)\, y_2^{j-k} - \varepsilon_{\ell+1}(y_1)\, y_1^{j-k}\right). \quad (3.107)$$

Lemma 3.A.1. *For y and j strictly positive integers, we have*

$$\sum_{x=0}^{y}(-1)^x x^{j-1} = (-1)^y\left[\frac{y^{j-1}}{2} + \sum_{k=2}^{j}\frac{B_k}{j}\binom{j}{k}(2^k-1)y^{j-k}\right] - \frac{B_j}{j}(2^j-1). \quad (3.108)$$

Proof. We compute the exponential generating function by multiplying by $z^{j-1}/(j-1)!$ both sides of the equality. The l.h.s. gives

$$\sum_{j=1}^{\infty}\sum_{x=0}^{y}(-1)^x\frac{(zx)^{j-1}}{(j-1)!} = \sum_{x=0}^{y}(-1)^x \mathrm{e}^{zx} = \frac{1-(-\mathrm{e}^z)^{y+1}}{1+\mathrm{e}^z}. \quad (3.109)$$

While we find for the right-hand side

$$\frac{(-1)^y}{2}\sum_{j=1}^{\infty}\frac{(zy)^{j-1}}{(j-1)!} + (-1)^y\sum_{k=2}^{\infty}\frac{B_k}{k!}(2^k-1)z^{k-1}\sum_{j=0}^{\infty}\frac{(zy)^j}{j!} - \sum_{j=1}^{\infty}\frac{B_j^-}{j!}(2^k-1)z^{j-1}$$

$$= \frac{(-1)^y}{2}\mathrm{e}^{zy}(1+\tanh(z/2)) + \frac{1}{2}(1-\tanh(z/2)). \quad (3.110)$$

Using the exponential definition of tanh, it is immediate to prove the equality between the two generating functions. □

We recall that $\varepsilon_\ell(x) = (-1)^{\ell+x} = -\varepsilon_{\ell+1}(x)$ and

$$\Omega(x) = \begin{cases} \Omega_{\sup} = \frac{1}{2} + v\varepsilon_{\ell+1}(y_2) & \text{if } x = y_2, \\ \Omega_{\inf} = \frac{1}{2} - v\varepsilon_{\ell+1}(y_1) & \text{if } x = y_1, \\ 1 & \text{otherwise.} \end{cases} \quad (3.111)$$

Finally, to evaluate the desired sum, one can separate the terms as

$$\sum_{x=y_1}^{y_2} \varepsilon_\ell(x)\, x^{j-1}\, \Omega(x) = \sum_{x=0}^{y_2} \varepsilon_\ell(x)\, x^{j-1} - \sum_{x=0}^{y_1} \varepsilon_\ell(x)\, x^{j-1} + \Omega_{\inf}\, \varepsilon_\ell(y_1)\, y_1^{j-1} + (\Omega_{\sup} - 1)\, \varepsilon_\ell(y_2)\, y_2^{j-1}, \quad (3.112)$$

and use the lemma above to obtain the claimed formula (3.107).

Chapter 4

Two-periodic dimer models on the plane

This chapter is part of an ongoing project [4] written with Philippe Ruelle.

We present in this chapter two different field-theoretic descriptions of the continuum limit of the two-periodic dimer model on the full plane, based on Majorana fermions for one, on symplectic fermions for the other. We start by revisiting the description of the dimer model in terms of Kasteleyn's Pfaffian formula, written as an integration over discrete fermions. The two-periodic measure is an off-critical extension of the usual uniform case by two relevant parameters. The continuum limit of the discrete action leads to four coupled and massive fermions forming a massive ghost system, and depends on a parameter which controls the scaling dimensions of the fermions. For a specific and natural value of this parameter, the ghost system can be recast as two pairs of uncoupled massive Majorana fermions (two uncoupled massive Ising models) with central charge $c = 1$ in the massless limit. The symplectic fermion alternative builds on the relations between the dimer model and the spanning tree and sandpile models. In this case, the two-periodic measure requires two pairs of uncoupled massive symplectic fermions,

which, in the critical case, underlie a conformal field theory with central charge $c = -4$.

4.1 The dimer model: Kasteleyn matrix and partition function

Given a graph G with a set of vertices V_G and a set of edges E_G, a perfect matching M of G is a subset of E_G such that all the vertices of V_G are adjacent to one and only one edge of M. An edge belonging to a perfect matching is viewed as a rod covering the edge and called a dimer. The dimer model on G considers the set of all perfect matchings of G and studies their statistical properties.

The simplest probability measure one can define on the set of perfect matchings is the uniform measure, by which all perfect matchings have the same weight. More generally, one may assign each edge of E_G a specific weight $w(e)$ and decide that a perfect matching has a weight which is the product of the weights of all the edges of M. The partition function is then the sum of the weights of all perfect matchings,

$$Z_G = \sum_M w(M) = \sum_M \prod_{e \in M} w(e). \tag{4.1}$$

For the uniform measure, $w(e) = 1$, the partition partition reduces to the mere number of perfect matchings on G.

When the graph G is a rectangular grid, namely a rectangular portion of $\mathbb{Z}^2$, Temperley and Fisher [15], Fisher [16] and Kasteleyn [17], at around the same time, computed the partition function for the one-periodic measure, which simply assigns the horizontal and vertical edges a different weight (see later). They reduced the calculation to the evaluation of a Pfaffian, although, in hindsight, the approach taken by Kasteleyn appears more general. It is also the one that is most commonly followed nowadays. As for us it is crucial to identify the Majorana fermions, we will here follow Kasteleyn's approach.

If we denote by A the (symmetric) weighted adjacency matrix of G, namely $A_{i,j} = w(e)$ if $v_i \overset{e}{\sim} v_j$ (the vertices v_i, v_j are connected by e),

and $A_{i,j} = 0$ otherwise, it is easy to see that the partition function can be written as the Hafnian of A,

$$Z_G = \operatorname{Haf} A = \sum_{\alpha \in \Pi_{2n}} \prod_{i=1}^{n} A_{\alpha(2i-1),\alpha(2i)} = \frac{1}{2^n\, n!} \sum_{\sigma \in S_{2n}} \prod_{i=1}^{n} A_{\sigma(2i-1),\sigma(2i)}, \tag{4.2}$$

where $2n = |V_G|$ is the size of A and Π_{2n} is the set of unordered partitions $\{(\alpha(1),\alpha(2)),(\alpha(3),\alpha(4)),\ldots,(\alpha(2n-1),\alpha(2n))\}$ of $\{1,2,\ldots,2n\}$ into pairs; the set Π_{2n} contains $(2n-1)!!$ partitions.

The main drawback of the previous formula is that the Hafnian of a generic matrix cannot be effectively computed (see for instance [102]). Kasteleyn's original idea was then to replace the Hafnian of A by the Pfaffian of a closely related and antisymmetric matrix K,

$$\begin{aligned} Z_G = \delta^{-1} \operatorname{Pf} K &= \delta^{-1} \sum_{\alpha \in \Pi_{2n}} \operatorname{sgn}\alpha \prod_{i=1}^{n} K_{\alpha(2i-1),\alpha(2i)} \\ &= \delta^{-1} \frac{1}{2^n\, n!} \sum_{\sigma \in S_{2n}} \operatorname{sgn}\sigma \prod_{i=1}^{n} K_{\sigma(2i-1),\sigma(2i)}, \end{aligned} \tag{4.3}$$

where $\operatorname{sgn}\alpha$ is the parity of α, viewed as the permutation $(1,2,\ldots,2n) \to (\alpha(1),\alpha(2),\ldots,\alpha(2n))$; δ is, at this stage, just a sign and makes sure that Z_G is positive[1].

The Pfaffian is much easier to evaluate because of its relation to the determinant, $\operatorname{Pf} K^2 = \det K$. However, in order to compensate for the signs coming from the parities and make sure that all terms in the sum contribute coherently, namely with the same sign, the matrix K should be a properly signed version of A. The existence of a matrix satisfying these contraints is highly non-trivial, but Kasteleyn managed to establish its existence when G is a planar graph [18]; a qualifying matrix is called a Kasteleyn matrix. The signs affecting the entries of K can be given by a specific orientation of the edges of G, in terms of which the entries of K read $K_{i,j} = +A_{i,j}$ if $v_i \overset{e}{\to} v_j$ and $K_{i,j} = -A_{i,j}$ if $v_i \overset{e}{\leftarrow} v_j$. Then the δ relating the partition function Z_G and the Pfaffian of K is equal to the sign of any non-zero term in the sum over the partitions α.

[1] There is in any case a global sign ambiguity: the value of Z_G does not depend on the labelling of the vertices whereas $\operatorname{Pf} K$ does. Indeed, two labellings are related by a permutation π, and so are the two Kasteleyn matrices, $K_2 = P_\pi\, K_1 P_\pi^{\mathrm{t}}$, so that $\operatorname{Pf} K_2 = (\det P_\pi) \operatorname{Pf} K_1 = \pm \operatorname{Pf} K_1$.

Once a Kasteleyn matrix K has been found, many others may be obtained. Indeed, if one multiplies by z_i the weights of all the edges adjacent to the vertex v_i, for any complex numbers $\{z_i\}_i$, then every perfect matching picks an extra global weight equal to $\prod_i z_i$, and so does the Pfaffian, implying $\delta \to \delta \times \prod_i z_i$ in order to preserve the partition function. This somewhat artificial change of weights, called a gauge transformation, amounts to form the new matrix $K_{i,j} \to z_i z_j K_{i,j}$, and although the latter may no longer be a signed weighted adjacency matrix, it is equally good to evaluate the partition function.

To connect to what we want to do in the following sections, the last step is to rewrite the Pfaffian of K as a multi-integral over anticommuting variables ψ_i attached to the vertices of G,

$$\operatorname{Pf} K = \int [\mathcal{D}\psi] \, \exp\Big\{\frac{1}{2}\sum_{i,j=1}^{|V_G|} K_{i,j}\,\psi_i\,\psi_j\Big\}, \qquad [\mathcal{D}\psi] = \mathrm{d}\psi_{2n}\ldots\mathrm{d}\psi_2\,\mathrm{d}\psi_1. \tag{4.4}$$

These variables satisfy $\psi_i^2 = \psi_i\,\psi_j + \psi_j\psi_i = 0$ for all i, j; standard integration rules for Grassmannian variables prove the above identity.

It is to be noted that the variables ψ_i have a clear interpretation on the graph. The insertion of the product $\psi_{i_1}\ldots\psi_{i_{2k}}$ in the above integral has the double effect of removing the $2k$ vertices $v_{i_1},\ldots,v_{i_{2k}}$ from the graph G (along with all incident edges) and of restricting the matrix K to the mutilated graph $G\setminus\{v_{i_1},\ldots,v_{i_{2k}}\}$. Indeed, for $I=\{i_1,i_2,\ldots,i_{2k}\}$ the set of labels, and for $i_1<i_2<\cdots<i_{2k}$, we have

$$\int [\mathcal{D}\psi]\,\psi_{i_1}\psi_{i_2}\ldots\psi_{i_{2k}}\,\exp\Big\{\frac{1}{2}\sum_{i,j=1}^{|V_G|} K_{i,j}\,\psi_i\,\psi_j\Big\} = \epsilon(I)\operatorname{Pf} K\big|_{G\setminus\{v_{i_1},\ldots,v_{i_{2k}}\}}, \tag{4.5}$$

where $\epsilon(I) = (-1)^{k+i_1+i_2+\cdots+i_{2k}}$ (we borrow the notations from [103]). By using Jacobi's identity for Pfaffians, namely (see [103]),

$$\operatorname{Pf} K\big|_{G\setminus\{v_{i_1},\ldots,v_{i_{2k}}\}} = \epsilon(I)\,(\operatorname{Pf} K)\,(\operatorname{Pf} K^{-1}\big|_{\{v_{i_1},\ldots,v_{i_{2k}}\}}), \tag{4.6}$$

the Grassmannian integral can be recasted into

$$\begin{aligned}\langle\psi_{i_1}\ldots\psi_{i_{2k}}\rangle &\equiv \frac{1}{\operatorname{Pf} K}\int [\mathcal{D}\psi]\,\psi_{i_1}\psi_{i_2}\ldots\psi_{i_{2k}}\,\exp\Big\{\frac{1}{2}\sum_{i,j} K_{i,j}\,\psi_i\,\psi_j\Big\}\\ &= \operatorname{Pf} K^{-1}\big|_{\{v_{i_1},\ldots,v_{i_{2k}}\}}.\end{aligned} \tag{4.7}$$

On account of $\langle \psi_i \, \psi_j \rangle = (K^{-1})_{i,j}$ and the definition (4.3) of the Pfaffian in terms of the partitions α, the previous identity is the Wick theorem. The two-point expectation values $\langle \psi_i \, \psi_j \rangle$ are called Wick contractions.

Importantly, one also notes that the restriction of a Kasteleyn matrix to a subgraph does not in general qualify as a Kasteleyn matrix for the latter, implying that the partition function for the subgraph is no longer proportional to the Pfaffian of the restricted Kasteleyn matrix[2]. Let us consider two complementary subgraphs of G, namely $G_1 = G|_{\{v_{i_1},\ldots,v_{i_{2k}}\}}$ and $G_2 = G \setminus \{v_{i_1}, \ldots, v_{i_{2k}}\}$; let us also denote by K_1 and K_2 the corresponding restrictions of K. Let us further assume that G_1 and G_2 have each at least one perfect matching. K being a Kasteleyn matrix for G, all non-zero terms in the sum over the permutations $\sigma \in S_{2n}$ contribute coherently, in fact each non-zero term is equal to δ times a product of edge weights $w(e)$. Among these, we consider those terms which correspond to a fixed perfect matching of G_2. They are all proportional to the non-zero terms in the sum defining the Pfaffian of K_1, which therefore also contribute coherently; it follows that K_1 is a Kasteleyn matrix for G_1. Repeating the argument with any fixed perfect matching of G_1, we obtain that K_2 is a Kasteleyn matrix for G_2. We thus obtain, under the condition that both G_1 and G_2 have at least one perfect matching,

$$Z_G = \delta^{-1} \operatorname{Pf} K, \qquad Z_{G_1} = \delta_1^{-1} \operatorname{Pf} K_1, \qquad Z_{G_2} = \delta_2^{-1} \operatorname{Pf} K_2. \tag{4.8}$$

Since the Pfaffian of K contains, as a subset of terms, the product of the Pfaffians of K_1 and K_2,

$$\operatorname{Pf} K = \epsilon(I) \, (\operatorname{Pf} K_1) \, (\operatorname{Pf} K_2) + \ldots, \tag{4.9}$$

we obtain, by comparing with $Z_G = Z_{G_1} \, Z_{G_2} + \ldots$, the identity $\delta = \epsilon(I) \, \delta_1 \, \delta_2$. In case a gauge transformed Kasteleyn matrix is used, each δ contains the product $\prod z_i$ for all vertices i in the relevant graph or subgraph.

[2] A well-known example is when two distant vertices are removed, equivalently when two monomers are introduced. In this case, the two-monomer partition function cannot be related to the Pfaffian of the restricted Kasteleyn matrix. And indeed, as we will see later in the case of a one-periodic measure on $\mathbb{Z}^2$, the insertion of two ψ fields leads to a two-point correlator that decays like r^{-1}, whereas the two-monomer correlator decays like $r^{-1/2}$. The former decays faster because massive cancellations occur in the Pfaffian.

The previous formulas provide a standard way to compute dimer probabilities and correlation functions. Consider for instance a set of k isolated[3] edges $(v_{i_1} \overset{e_1}{\sim} v_{i_2}), \dots, (v_{i_{2k-1}} \overset{e_k}{\sim} v_{i_{2k}})$. Then, the probability that these k edges belong to a random perfect matching can be computed as follows,

$$\begin{aligned}
\mathbb{P}[e_1, \dots, e_k \in M] &= w(e_1)\, w(e_2)\, \dots\, w(e_k)\, \frac{Z_{G\setminus\{v_{i_1},\dots,v_{i_{2k}}\}}}{Z_G} \\
&= \frac{\delta}{\delta_1}\, w(e_1)\, w(e_2)\, \dots\, w(e_k)\, \frac{\operatorname{Pf} K\big|_{G\setminus\{v_{i_1},\dots,v_{i_{2k}}\}}}{\operatorname{Pf} K} \\
&= \epsilon(I)\, K_{i_1,i_2}\, \dots\, K_{i_{2k-1},i_{2k}}\, \frac{\operatorname{Pf} K\big|_{G\setminus\{v_{i_1},\dots,v_{i_{2k}}\}}}{\operatorname{Pf} K} \\
&= K_{i_1,i_2}\, \dots\, K_{i_{2k-1},i_{2k}}\, \frac{1}{\operatorname{Pf} K} \int [\mathcal{D}\psi]\, \psi_{i_1} \dots \psi_{i_{2k}}\, \exp\Big\{\frac{1}{2}\sum_{i,j} K_{i,j}\, \psi_i\, \psi_j\Big\} \\
&= K_{i_1,i_2}\, \dots\, K_{i_{2k-1},i_{2k}}\, \langle \psi_{i_1}\, \psi_{i_2} \dots \psi_{i_{2k-1}}\, \psi_{i_{2k}} \rangle. \qquad (4.10)
\end{aligned}$$

Therefore, the presence of a dimer on an edge $v_i \overset{e}{\sim} v_j$ is forced by inserting $K_{i,j}\, \psi_i\, \psi_j$ in the fermionic integral.

Given a subgraph $G_1 = G\big|_{\{v_{i_1},\dots,v_{i_{2k}}\}}$ of G, one may slightly generalize to compute the probability that the restriction to G_1 of a perfect matching M of G belongs to the set $\mathcal{M}_1$ of perfect matchings of G_1. We get,

$$\begin{aligned}
\mathbb{P}[M\big|_{G_1} \in \mathcal{M}_1] = \frac{Z_{G_1}\, Z_{G_2}}{Z_G} &= \frac{\delta}{\delta_1 \delta_2}\, \frac{(\operatorname{Pf} K_1)\, (\operatorname{Pf} K_2)}{(\operatorname{Pf} K)} \\
&= (\operatorname{Pf} K_1)\, \langle \psi_{i_1}\, \psi_{i_2} \dots \psi_{i_{2k-1}}\, \psi_{i_{2k}} \rangle, \qquad (4.11)
\end{aligned}$$

where K_1 is the restriction of K to G_1, with rows and columns labelled by $i_1, i_2, \dots, i_{2k}$ (in that order).

To finish, and since we are primarily interested in the two-periodic dimer model on the plane, and its continuum limit, we specialize the above discussion to the square lattice $\mathbb{Z}^2$. The partition functions for infinite graphs clearly diverge but the large volume limit of dimer probabilities like (4.10) exists. Thus, we can consider straight away infinite volume probabilities and then compute their scaling limit.

[3] By this we mean that the $2k$ vertices $v_{i_1}, v_{i_2}, \dots, v_{i_{2k}}$ can be covered by k dimers in a unique way.

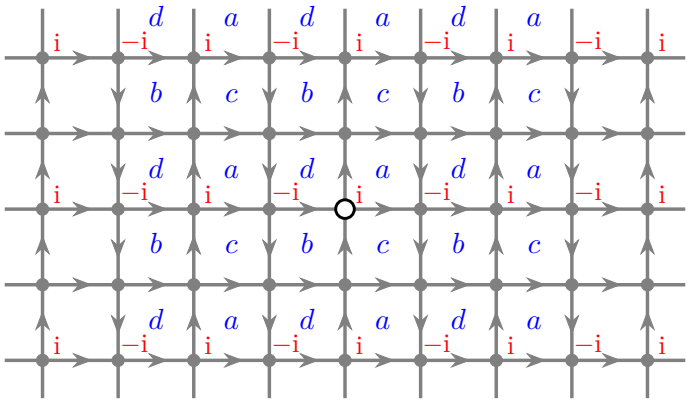

Figure 4.1: Kasteleyn orientation of the infinite graph $\mathbb{Z}^2$ and two-periodic face weights. The white circle is the origin of the coordinates. The four edges adjacent to the origin have weights ac (right), ad (up), bd (left) and bc (down). The factors $\pm\mathrm{i}$ in red are the numbers z_i used in the gauge transformation to obtain the Kasteleyn matrix (4.13).

The two-periodic edge weights we will consider are represented in Figure 4.1, as well as the Kasteleyn orientation of the infinite graph $\mathbb{Z}^2$, as originally proposed in [17]. The weights a, b, c, d, alternating two-periodically in the two directions [33] are in fact weights attached to faces, and determine the edges weights $w(e)$ as follows: each edge is adjacent to two faces and gets a weight equal to the product of the weights of these two faces. We also introduce a bias, namely an extra weight u resp. v to every horizontal resp. vertical dimer. All this yields a Kasteleyn matrix that we denote by K^{ast} to indicate that it is based on the orientation originally proposed by Kasteleyn. It is given by

$$\begin{aligned} K^{\mathrm{ast}}_{(x,y),(x+1,y)} &= \begin{cases} a\,c\,u & \text{if } x \text{ is even,} \\ b\,d\,u & \text{if } x \text{ is odd,} \end{cases} \\ K^{\mathrm{ast}}_{(x,y),(x,y+1)} &= \begin{cases} (-1)^x\,a\,d\,v & \text{if } y \text{ is even,} \\ (-1)^x\,b\,c\,v & \text{if } y \text{ is odd,} \end{cases} \end{aligned} \tag{4.12}$$

and then extended by antisymmetry.

In addition, we apply the gauge transformation corresponding to the following choice of complex numbers z_i: for $v_i = (x, y)$, we set $z_i =$

$\mathrm{i}(-1)^x$ for y even, and $z_i = 1$ for y odd; those numbers not equal to 1 are indicated in red in Figure 4.1. The new Kasteleyn matrix has non-zero entries given by $K_{i,j} = z_i z_j K^{\mathrm{ast}}_{i,j}$, namely

$$K_{(x,y),(x+1,y)} = \begin{cases} a\,c\,u & \text{if } x \text{ is even,} \\ b\,d\,u & \text{if } x \text{ is odd,} \end{cases}$$
$$K_{(x,y),(x,y+1)} = \begin{cases} \mathrm{i}\,a\,d\,v & \text{if } y \text{ is even,} \\ \mathrm{i}\,b\,c\,v & \text{if } y \text{ is odd,} \end{cases} \tag{4.13}$$

and extended by antisymmetry. If a, b, c, d are all equal to 1, the weights reduce to the bias given by u, v, and form a system of one-periodic edge weights.

We note that although we have introduced six different parameters, the correlators will only depend on the combinations $\frac{a}{b}, \frac{c}{d}$ and $\frac{u}{v}$. Indeed, one can make a further gauge transformation with factors $z_i = \frac{1}{\sqrt{bdv}}$ for all i. It has the effect of dividing all edge weights by bdv, making the new weights to be functions of $\frac{a}{b}, \frac{c}{d}$ and $\frac{u}{v}$. In what follows, this extra gauge transformation will not be included and we will use the Kasteleyn matrix (4.13).

4.2 Lattice calculations: from discrete to Majorana fermions

We will not dwell much on the way lattice calculations can be carried out, but merely point some salient features. As we saw in the previous section, the calculation of dimer correlations boil down to the evaluation of Pfaffians or determinants of finite matrices whose entries are those of the inverse Kasteleyn matrix. As we will see now, these can be related to the entries of inverse discrete Laplacians, or Green matrices. As such the involved calculations are in most cases fairly standard.

In order to invert the Kasteleyn matrix, the key observation [104] is that the square of K^{ast} is proportional to a direct sum of discrete Laplacians,

$$(K^{\mathrm{ast}})^2 = -abcd \left[\Delta^{(\mathrm{even,even})} \oplus \Delta^{(\mathrm{odd,odd})} \oplus \Delta^{(\mathrm{even,odd})} \oplus \Delta^{(\mathrm{odd,even})}\right], \tag{4.14}$$

where each copy of Δ is given by

$$\Delta_{(x,y),(x',y')} = \begin{cases} u^2\gamma_1 + v^2\gamma_2 & \text{if } x = x',\, y = y', \\ -u^2 & \text{if } x = x' \pm 2,\, y = y', \\ -v^2 & \text{if } x = x',\, y = y' \pm 2, \\ 0 & \text{otherwise,} \end{cases} \tag{4.15}$$

with

$$\gamma_1 = \frac{ac}{bd} + \frac{bd}{ac}, \qquad \gamma_2 = \frac{ad}{bc} + \frac{bc}{ad}. \tag{4.16}$$

and acts on one of the four sublattices of index 4 of $\mathbb{Z}^2$, as indicated. One sees that for generic parameters, the Laplacian Δ is anisotropic (unless $u = v$) but also massive, with a squared mass proportional to the row sums or column sums, all equal to

$$\mu^2 = u^2(\gamma_1 - 2) + v^2(\gamma_2 - 2) = u^2\Big(\sqrt{\frac{ac}{bd}} - \sqrt{\frac{bd}{ac}}\Big)^2 + v^2\Big(\sqrt{\frac{ad}{bc}} - \sqrt{\frac{bc}{ad}}\Big)^2. \tag{4.17}$$

The mass vanishes if and only if $\frac{a}{b} = \frac{c}{d} = 1$, in which case the two-periodic weighting is gauge equivalent to a simple one-periodic weighting, as noted above.

Since each copy of Δ acts on the dilated lattice $(2\mathbb{Z})^2$, its inverse can easily be obtained as

$$\Delta^{-1}_{(x,y),(x',y')} = G\Big(\frac{x - x'}{2}, \frac{y - y'}{2}\Big), \tag{4.18}$$

in terms of the inverse of the discrete Laplacian on $\mathbb{Z}^2$, namely, for $p, q \in \mathbb{Z}$,

$$G(p,q) = \frac{1}{4\pi^2} \iint_{-\pi}^{\pi} \mathrm{d}\alpha\, \mathrm{d}\beta\, \frac{\mathrm{e}^{\mathrm{i}p\alpha + \mathrm{i}q\beta}}{u^2\gamma_1 + v^2\gamma_2 - 2u^2\cos\alpha - 2v^2\cos\beta}. \tag{4.19}$$

From the relations between $(K^{\mathrm{ast}})^2$ and the Laplacian Δ, and between K and K^{ast}, one readily obtains the inverse of K,

$$\begin{aligned} K^{-1}_{(x,y),(x',y')} &= z^{-1}_{(x,y)} z^{-1}_{(x',y')} (K^{\mathrm{ast}})^{-1}_{(x,y),(x',y')} \\ &= -\frac{z^{-1}_{(x,y)} z^{-1}_{(x',y')}}{abcd} (K^{\mathrm{ast}}\,\Delta^{-1})_{(x,y),(x',y')}. \end{aligned} \tag{4.20}$$

Explicitly, it yields, for $(m,n) = (x-x', y-y')$, the following expressions depending on the parities of the coordinates,

$$K^{-1}_{(x,y),(x',y')} = \frac{1}{abcd} \times$$
$$\times \begin{cases} 0 & \text{if } x - x' = y - y' \bmod 2, \\ \mathrm{i}\, ad\, v\, G\big(\frac{m}{2}, \frac{n+1}{2}\big) - \mathrm{i}\, bc\, v\, G\big(\frac{m}{2}, \frac{n-1}{2}\big) & \text{if } (x,y,x',y') = (\mathrm{e},\mathrm{e},\mathrm{e},\mathrm{o}), \\ \mathrm{i}\, bc\, v\, G\big(\frac{m}{2}, \frac{n+1}{2}\big) - \mathrm{i}\, ad\, v\, G\big(\frac{m}{2}, \frac{n-1}{2}\big) & \text{if } (x,y,x',y') = (\mathrm{o},\mathrm{o},\mathrm{o},\mathrm{e}), \\ bd\, u\, G\big(\frac{m-1}{2}, \frac{n}{2}\big) - ac\, u\, G\big(\frac{m+1}{2}, \frac{n}{2}\big) & \text{if } (x,y,x',y') = (\mathrm{e},\mathrm{e},\mathrm{o},\mathrm{e}), \\ ac\, u\, G\big(\frac{m-1}{2}, \frac{n}{2}\big) - bd\, u\, G\big(\frac{m+1}{2}, \frac{n}{2}\big) & \text{if } (x,y,x',y') = (\mathrm{o},\mathrm{o},\mathrm{e},\mathrm{o}), \end{cases} \tag{4.21}$$

to be completed by antisymmetry when $(x,y,x',y') = (\mathrm{e},\mathrm{o},\mathrm{e},\mathrm{e}), (\mathrm{o},\mathrm{e},\mathrm{o},\mathrm{o})$, $(\mathrm{o},\mathrm{e},\mathrm{e},\mathrm{e})$ and $(\mathrm{e},\mathrm{o},\mathrm{o},\mathrm{o})$.

Various correlators of distant dimers on the lattice can be computed by using these expressions. The calculations require the value of the Green matrices for close and distant points; although fairly standard, these are collected in Appendix 4.A. The main difference between one-periodic and two-periodic weights is that in the latter case, because of a non-zero mass μ, the Green matrix entries decay exponentially with the distance, making all correlators to similarly decay exponentially. In the one-periodic case, all correlators decay algebraically and the corresponding model is critical. Thus, the ratios $\frac{a}{b}$ and $\frac{c}{d}$ are relevant parameters which drive the model away from its critical point.

We will not give more details on the calculations or the results. The correlators reported in the following sections will be computed directly in the continuum limit, but all of them have been checked to exactly reproduce the lattice results at dominant order.

For the rest of this section, we start from Eq. (4.10) expressing lattice joint probabilities in terms of correlators of a discrete fermion theory whose action is given by $S = \frac{1}{2}\sum_{i,j\in\mathbb{Z}^2} K_{i,j}\,\psi(i)\,\psi(j)$ and compute its continuum limit. A simple calculation shows that the limit gives rise to two pairs of massive Majorana fermions, which, as discussed above, become massless for one-periodic weights, thereby recovering the results of [105]. Our derivation is however completely straightforward and equally easy in the two-periodic case.

Because the entries of the Kasteleyn matrix in (4.13) depend on the parities of the coordinates of the vertices, we separate the discrete fermions into four families, namely $\psi^1(i)$, $\psi^2(i)$, $\psi^3(i)$, $\psi^4(i)$, attached respectively to the vertices of the four sublattices $\mathbb{Z}^2_{(\mathrm{e,e})}$, $\mathbb{Z}^2_{(\mathrm{e,o})}$, $\mathbb{Z}^2_{(\mathrm{o,e})}$ and $\mathbb{Z}^2_{(\mathrm{o,o})}$. The action then reads (we denote by $\mathbf{e}_1$ and $\mathbf{e}_2$ the horizontal and vertical unit vectors on the $\mathbb{Z}^2$ lattice)

$$\begin{aligned}
S = {} & \frac{1}{2}\sum_{\mathbf{m}=(\mathrm{e,e})} \psi^1(\mathbf{m})\Big[ac\,u\,\psi^3(\mathbf{m}+\mathbf{e}_1) - bd\,u\,\psi^3(\mathbf{m}-\mathbf{e}_1) \\
& \qquad + \mathrm{i}\,ad\,v\,\psi^2(\mathbf{m}+\mathbf{e}_2) - \mathrm{i}\,bc\,v\,\psi^2(\mathbf{m}-\mathbf{e}_2)\Big] \\
& + \frac{1}{2}\sum_{\mathbf{m}=(\mathrm{e,o})} \psi^2(\mathbf{m})\Big[ac\,u\,\psi^4(\mathbf{m}+\mathbf{e}_1) - bd\,u\,\psi^4(\mathbf{m}-\mathbf{e}_1) \\
& \qquad + \mathrm{i}\,bc\,v\,\psi^1(\mathbf{m}+\mathbf{e}_2) - \mathrm{i}\,ad\,v\,\psi^1(\mathbf{m}-\mathbf{e}_2)\Big] \\
& + \frac{1}{2}\sum_{\mathbf{m}=(\mathrm{o,e})} \psi^3(\mathbf{m})\Big[bd\,u\,\psi^1(\mathbf{m}+\mathbf{e}_1) - ac\,u\,\psi^1(\mathbf{m}-\mathbf{e}_1) \\
& \qquad + \mathrm{i}\,ad\,v\,\psi^4(\mathbf{m}+\mathbf{e}_2) - \mathrm{i}\,bc\,v\,\psi^4(\mathbf{m}-\mathbf{e}_2)\Big] \\
& + \frac{1}{2}\sum_{\mathbf{m}=(\mathrm{o,o})} \psi^4(\mathbf{m})\Big[bd\,u\,\psi^2(\mathbf{m}+\mathbf{e}_1) - ac\,u\,\psi^2(\mathbf{m}-\mathbf{e}_1) \\
& \qquad + \mathrm{i}\,bc\,v\,\psi^3(\mathbf{m}+\mathbf{e}_2) - \mathrm{i}\,ad\,v\,\psi^3(\mathbf{m}-\mathbf{e}_2)\Big].
\end{aligned} \tag{4.22}$$

Let us consider the first sum, which we call S_1, the analysis being similar for the other three. It makes no difference if one rescales the lattice to have a new lattice spacing ε,

$$\begin{aligned}
S_1 = {} & \frac{1}{2}\sum_{\mathbf{m}\in(2\mathbb{Z})^2} \psi^1(\varepsilon\mathbf{m})\Big[ac\,u\,\psi^3(\varepsilon\mathbf{m}+\varepsilon\,\mathbf{e}_1) - bd\,u\,\psi^3(\varepsilon\mathbf{m}-\varepsilon\,\mathbf{e}_1) \\
& \qquad + \mathrm{i}\,ad\,v\,\psi^2(\varepsilon\mathbf{m}+\varepsilon\,\mathbf{e}_2) - \mathrm{i}\,bc\,v\,\psi^2(\varepsilon\mathbf{m}-\varepsilon\,\mathbf{e}_2)\Big] \\
= {} & \frac{1}{8}\sum_{\mathbf{m}\in(2\mathbb{Z})^2} (2\varepsilon)^2\,\frac{\psi^1(\varepsilon\mathbf{m})}{\varepsilon}\Big[u\frac{ac\,\psi^3(\varepsilon\mathbf{m}+\varepsilon\,\mathbf{e}_1) - bd\,\psi^3(\varepsilon\mathbf{m}-\varepsilon\,\mathbf{e}_1)}{\varepsilon} \\
& \qquad + \mathrm{i}\,v\frac{ad\,\psi^2(\varepsilon\mathbf{m}+\varepsilon\,\mathbf{e}_2) - bc\,\psi^2(\varepsilon\mathbf{m}-\varepsilon\,\mathbf{e}_2)}{\varepsilon}\Big].
\end{aligned} \tag{4.23}$$

In the limit $\varepsilon \to 0$, $\varepsilon\mathbf{m}$ becomes a continuous variable $\mathbf{x}$, and the previous sum would converge to a Riemann integral over $\mathbb{R}^2$ provided the summand, except for the factor $(2\varepsilon)^2$ which is the volume of the discretization cell, converges to some function defined over $\mathbb{R}^2$. If ad, bc, ac, bd

are fixed numbers independent of ε, the factors ε in the denominator must be absorbed in the ψ's, thereby defining continuum fields $\lim_{\varepsilon\to 0}\frac{\psi^i(\varepsilon\mathbf{m})}{\varepsilon}$ with scaling dimension 1. However, the corresponding field theory would be trivial in the continuum limit, with correlators like $\langle\psi^1(\mathbf{x}_1)\,\psi^3(\mathbf{x}_2)\rangle \sim \delta(\mathbf{x}_1-\mathbf{x}_2)$.

This is of course related to the fact that the continuum limit $\varepsilon\mathbf{m}\to\mathbf{x}$ requires the lattice distance $\mathbf{m}$ to be large, proportional to ε^{-1}. If the lattice mass μ remains finite in the large distance limit, the exponentially decaying correlators quite simply converge to zero. Therefore, the continuum limit must be accompanied by the limit μ going to zero, implying, from (4.17), that the ratios $\frac{a}{b}$ and $\frac{c}{d}$ must converge to their critical value 1 at the appropriate rate. For the exponential decay to have a proper limit, the product $\mu\mathbf{m}$ must converge when ε goes to zero, implying that μ must go to zero like ε. We will therefore set $\mu = 2M\varepsilon$, where M will be the mass in the continuum[4].

From (4.17), the constant μ circles in the $(\frac{a}{b},\frac{c}{d})$ plane centered at the critical point $(1,1)$ can be parametrized as

$$\sqrt{\frac{ac}{bd}}-\sqrt{\frac{bd}{ac}}=\frac{\mu}{u}\,\sin\alpha,\qquad \sqrt{\frac{ad}{bc}}-\sqrt{\frac{bc}{ad}}=\frac{\mu}{v}\,\cos\alpha, \tag{4.24}$$

where the angle α specifies the direction in which the critical point is being approached in the $(\frac{a}{b},\frac{c}{d})$ plane. For small μ, it yields

$$\frac{ac}{bd}=1+\frac{\sin\alpha}{u}\,\mu+\ldots,\qquad \frac{ad}{bc}=1+\frac{\cos\alpha}{v}\,\mu+\ldots \tag{4.25}$$

Inserting these expansions in the expression for S_1 and appropriately distributing the powers of ε yields

$$\begin{aligned}S_1 = {}& \frac{ac}{4}\sum_{\mathbf{m}\in 2\mathbb{Z}^2}(2\varepsilon)^2\,\frac{\psi^1(\varepsilon\mathbf{m})}{\sqrt{\varepsilon}}\\ &\times\Bigg\{\frac{u}{2\varepsilon}\Big[\frac{\psi^3(\varepsilon\mathbf{m}+\varepsilon\,\mathbf{e}_1)}{\sqrt{\varepsilon}}-\frac{\psi^3(\varepsilon\mathbf{m}-\varepsilon\,\mathbf{e}_1)}{\sqrt{\varepsilon}}\Big]+\frac{\mu}{2\varepsilon}\,\sin\alpha\,\frac{\psi^3(\varepsilon\mathbf{m}-\varepsilon\,\mathbf{e}_1)}{\sqrt{\varepsilon}}+\ldots\\ &+\frac{\mathrm{i}\,v}{2\varepsilon}\Big[\frac{\psi^2(\varepsilon\mathbf{m}+\varepsilon\,\mathbf{e}_2)}{\sqrt{\varepsilon}}-\frac{\psi^2(\varepsilon\mathbf{m}-\varepsilon\,\mathbf{e}_2)}{\sqrt{\varepsilon}}\Big]+\frac{\mathrm{i}\,\mu}{2\varepsilon}\,\cos\alpha\,\frac{\psi^2(\varepsilon\mathbf{m}-\varepsilon\,\mathbf{e}_2)}{\sqrt{\varepsilon}}+\ldots\Bigg\}\end{aligned}$$

[4]The factor 2 is introduce to compensate the factor $\frac{1}{2}$ appearing in the arguments of the lattice Green matrix, see (4.21).

$$\to \frac{ac}{4}\int \mathrm{d}^2\mathbf{x}\,\psi^1(\mathbf{x})\Big[u\partial_x\psi^3(\mathbf{x})+M\sin\alpha\psi^3(\mathbf{x})+\mathrm{i}v\,\partial_y\psi^2(\mathbf{x})+\mathrm{i}M\cos\alpha\psi^2(\mathbf{x})\Big], \tag{4.26}$$

where the continuum fermionic fields are defined by $\psi^i(\mathbf{x}) = \lim_{\varepsilon\to 0}\frac{\psi^i(\varepsilon\mathbf{m})}{\sqrt{\varepsilon}}$, thereby giving them a scaling dimension $\frac{1}{2}$.

The other sums in the action S are handled in a similar way and yield the following continuum action,

$$S = \frac{ac}{4}\int \mathrm{d}^2\mathbf{x}\;[\vec{\psi}(\mathbf{x})]^{\mathrm{t}}\cdot\boldsymbol{\Omega}\cdot\vec{\psi}(\mathbf{x}), \tag{4.27}$$

with

$$\boldsymbol{\Omega} = \begin{pmatrix} 0 & \mathrm{i}\big(v\,\partial_y + M\cos\alpha\big) & u\,\partial_x + M\sin\alpha & 0 \\ \mathrm{i}\big(v\,\partial_y - M\cos\alpha\big) & 0 & 0 & u\,\partial_x + M\sin\alpha \\ u\,\partial_x - M\sin\alpha & 0 & 0 & \mathrm{i}\big(v\,\partial_y + M\cos\alpha\big) \\ 0 & u\,\partial_x - M\sin\alpha & \mathrm{i}\big(v\,\partial_y - M\cos\alpha\big) & 0 \end{pmatrix} \tag{4.28}$$

By a simple change of basis, the action can be recast in the standard form for two uncoupled pairs of massive free Majorana fermions, namely

$$S = 2ac\int \mathrm{d}^2\mathbf{x}\Big\{\chi^1\overline{\partial}\,\chi^1+\overline{\chi}^1\partial\,\overline{\chi}^1-\mathrm{i}M\chi^1\,\overline{\chi}^1+\chi^2\overline{\partial}\,\chi^2+\overline{\chi}^2\partial\,\overline{\chi}^2-\mathrm{i}M\chi^2\,\overline{\chi}^2\Big\}, \tag{4.29}$$

with $\partial = \frac{1}{2}(u\,\partial_x - \mathrm{i}\,v\,\partial_y)$ and $\overline{\partial} = \frac{1}{2}(u\,\partial_x + \mathrm{i}\,v\,\partial_y)$. A possible linear transformation is the following,

$$\begin{aligned}\psi(\mathbf{x}) = &\Big\{\chi^1(\mathbf{x}) + \big[(-1)^y\,\cos\alpha + \mathrm{i}(-1)^x\,\sin\alpha\big]\,\overline{\chi}^1(\mathbf{x})\Big\} \\ &+ \mathrm{i}(-1)^{x+y+1}\Big\{\chi^2(\mathbf{x}) + \big[(-1)^y\,\cos\alpha + \mathrm{i}(-1)^x\,\sin\alpha\big]\,\overline{\chi}^2(\mathbf{x})\Big\},\end{aligned} \tag{4.30}$$

where the four components ψ^i are obtained by selecting the appropriate parities for x and y (for instance, $\psi^1(\mathbf{x})$, defined on vertices $\mathbf{x} = (x, y)$ with x and y even, is recovered by setting $(-1)^x = (-1)^y = +1$, and similarly for the other three components). Although $\psi(\mathbf{x})$ is defined in the continuum, the various signs are the remnants of the parities of the lattice (integer) coordinates. Setting $\alpha = 0$ reproduces the relations found in [105] and rederived in [106] (in the one-periodic case, i.e. when $M = 0$, the previous transformation recasts the action in the standard form for any value of α, but we will choose $\alpha = 0$ for simplicity).

Surprisingly, the doubled Majorana fermionic theory does not depend on the relevant parameter α. However, the fields ψ^i, physically relevant in the dimer model, do depend on it, with the result that all correlators will depend on both M and α. We also note that the signs of the mass terms in (4.29), which, in the context of the Ising model, determine whether one considers the low or high temperature regime, are immaterial since they can be absorbed in a redefinition of the fermionic fields (f.i. $\overline{\chi}^a \to -\overline{\chi}^a$).

In the following two sections, we compute various correlators, first for one-periodic weights, then for two-periodic weights.

4.3 One-periodic weights

For one-periodic weights ($a = b = c = d = 1$), the action (4.29) reduces to

$$S = \int \mathrm{d}^2\mathbf{x} \ \Big\{\chi^1(u\,\partial_x + \mathrm{i}\,v\,\partial_y)\chi^1 + \overline{\chi}^1(u\,\partial_x - \mathrm{i}\,v\,\partial_y)\overline{\chi}^1 + \chi^2(u\,\partial_x + \mathrm{i}\,v\,\partial_y)\chi^2 + \overline{\chi}^2(u\,\partial_x - \mathrm{i}\,v\,\partial_y)\overline{\chi}^2\Big\}, \quad (4.31)$$

which describes the critical dimer model. Since the field theory is massless, the parameter α becomes meaningless, and the relation between the fields ψ^i and the $\chi^a, \overline{\chi}^a$ given in (4.30) holds for any value of α. As said above, we choose $\alpha = 0$, which yields

$$\psi(\mathbf{x}) = \chi^1(\mathbf{x}) + (-1)^y\,\overline{\chi}^1(\mathbf{x}) + \mathrm{i}(-1)^{x+y+1}\,\chi^2(\mathbf{x}) + \mathrm{i}(-1)^{x+1}\,\overline{\chi}^2(\mathbf{x}). \quad (4.32)$$

The propagators of the Majorana fermions are well known and more conveniently written in complex coordinates. With the points $\mathbf{x}_1 = (x_1, y_1)$, $\mathbf{x}_2 = (x_2, y_2)$ and $\mathbf{x}_1 - \mathbf{x}_2$ in $\mathbb{R}^2$, we associate the complex numbers $z_1 = v\,x_1 + \mathrm{i}u\,y_1$, $z_2 = v\,x_2 + \mathrm{i}u\,y_2$, and $z_{12} = z_1 - z_2$. Then, the two-point functions for each species of fermions read

$$\langle\chi(\mathbf{x}_1)\,\chi(\mathbf{x}_2)\rangle = \frac{1}{4\pi\,z_{12}}, \quad \langle\overline{\chi}(\mathbf{x}_1)\,\overline{\chi}(\mathbf{x}_2)\rangle = \frac{1}{4\pi\,\overline{z}_{12}}, \quad \langle\chi(\mathbf{x}_1)\,\overline{\chi}(\mathbf{x}_2)\rangle = 0. \quad (4.33)$$

From these, one easily computes the two-point correlator of ψ field using (4.32),

$$\langle\psi(\mathbf{x}_1)\,\psi(\mathbf{x}_2)\rangle = \langle\psi(\mathbf{x}_1-\mathbf{x}_2)\,\psi(0)\rangle = \frac{1-(-1)^{x_1+x_2+y_1+y_2}}{4\pi}\Big[\frac{1}{z_{12}}+\frac{(-1)^{y_1+y_2}}{\overline{z}_{12}}\Big], \tag{4.34}$$

and then compute dimer correlations by applying Wick's theorem. One may check that the propagator in (4.34) is indeed the scaling limit (dominant contribution) of $K^{-1}_{\mathbf{x}_1-\mathbf{x}_2,0}$, see Appendix 4.A.

4.3.1 Dimer correlations

As discussed in the previous section, forcing a horizontal dimer whose left vertex is located at $\mathbf{x}$ corresponds to insert[5] $H(\mathbf{x}) = u\,\psi(\mathbf{x})\,\psi(\mathbf{x}+\varepsilon\,\mathbf{e}_1)$, and likewise the insertion of $V(\mathbf{x}) = \mathrm{i}v\,\psi(\mathbf{x})\,\psi(\mathbf{x}+\varepsilon\,\mathbf{e}_2)$ forces a vertical dimer whose lower vertex is located at $\mathbf{x}$. They are given by

$$H(\mathbf{x}) = 2\mathrm{i}u\,(-1)^{x+y}\Big\{\chi^1(\mathbf{x})\,\chi^2(\mathbf{x}) + \overline{\chi}^1(\mathbf{x})\,\overline{\chi}^2(\mathbf{x}) + (-1)^y\big[\chi^1(\mathbf{x})\,\overline{\chi}^2(\mathbf{x}) + \overline{\chi}^1(\mathbf{x})\,\chi^2(\mathbf{x})\big]\Big\}, \tag{4.35}$$

$$V(\mathbf{x}) = -2v\,(-1)^{x+y}\Big\{\chi^1(\mathbf{x})\,\chi^2(\mathbf{x}) - \overline{\chi}^1(\mathbf{x})\,\overline{\chi}^2(\mathbf{x}) + \mathrm{i}\,(-1)^x\big[\chi^1(\mathbf{x})\,\overline{\chi}^1(\mathbf{x}) + \chi^2(\mathbf{x})\,\overline{\chi}^2(\mathbf{x})\big]\Big\}, \tag{4.36}$$

where in the right-hand side, all points in the scaling neighbourhood of $\mathbf{x}$ have been collapsed to $\mathbf{x}$. It may be worth to note that this very fact affects the properties of the continuous fields H and V compared to their discrete version. In particular, we see that $\langle H(\mathbf{x})\rangle = \langle V(\mathbf{x})\rangle = 0$ in the continuum, whereas in the discrete version, $\langle H(\mathbf{m})\rangle = \mathbb{P}(H(\mathbf{m}))$ and $\langle V(\mathbf{m})\rangle = \mathbb{P}(V(\mathbf{m}))$ are non-zero probabilities.

From the above explicit expressions for H, V, we obtain that $H(\mathbf{x} \pm \varepsilon\,\mathbf{e}_1) = -H(\mathbf{x})$ and $V(\mathbf{x} \pm \varepsilon\,\mathbf{e}_2) = -V(\mathbf{x})$ in the scaling limit. This is consistent with the fact that we must have $H(\mathbf{x}) + H(\mathbf{x} - \varepsilon\,\mathbf{e}_1) + V(\mathbf{x}) + V(\mathbf{x} - \varepsilon\,\mathbf{e}_1) = 0$, since a unique dimer is necessarily located on one of the four incoming edges around any vertex. As the Majorana fermions χ^a and $\overline{\chi}^a$ are fields of weight $(\frac{1}{2}, 0)$ and $(0, \frac{1}{2})$ in two uncoupled

[5] In the scaling limit, the point $\mathbf{x}+\varepsilon\,\mathbf{e}_1$ refers to same point as $\mathbf{x}$ but that writing reminds that the parity of the x-coordinate of $\mathbf{x}+\varepsilon\,\mathbf{e}_1$ is opposite to that of $\mathbf{x}$; this is essential to derive the expressions (4.35) and (4.36).

conformal field theories with central charge $c = \frac{1}{2}$, the two fields H, V are linear combinations of two primary fields of weights $(1,0), (0,1)$ and four different primary fields of weights $(\frac{1}{2}, \frac{1}{2})$, belonging to a conformal field theory with total central charge $c = 1$.

Let us now turn to the computation of the dimer correlations. On the lattice, if we view the dimer observables $D = H, V$ as random variables taking values 0 or 1 depending on whether or not a dimer is present, the correlations of n dimers far apart from each other are defined as

$$\begin{aligned}\langle\!\langle D(\mathbf{m}_1)\, D(\mathbf{m}_2) \dots D(\mathbf{m}_n) \rangle\!\rangle \\ = \mathbb{E}\Big\{ \big[D(\mathbf{m}_1) - \mathbb{E}(D(\mathbf{m}_1))\big]\, \big[D(\mathbf{m}_2) - \mathbb{E}(D(\mathbf{m}_2))\big] \dots \Big\},\end{aligned} \tag{4.37}$$

where $\mathbb{E}(D(\mathbf{m}_{i_1})\, D(\mathbf{m}_{i_2}) \dots) = \mathbb{P}(D(\mathbf{m}_{i_1}),\, D(\mathbf{m}_{i_2}), \dots)$. In the continuum, this becomes

$$\langle\!\langle D(\mathbf{x}_1)\, D(\mathbf{x}_2) \dots D(\mathbf{x}_n) \rangle\!\rangle = \Big\langle \big[D(\mathbf{x}_1) - \langle D(\mathbf{x}_1)\rangle\big]\, \big[D(\mathbf{x}_2) - \langle D(\mathbf{x}_2)\rangle\big] \dots \Big\rangle. \tag{4.38}$$

The right-hand side can be evaluated by using Wick's theorem, which requires to include all contractions of the fields ψ. Among these, some contractions are internal to a dimer $D(\mathbf{x})$, that is, involve a pair of fields located at the same point $\mathbf{x}$. As these contribute exactly to the expectation value $\langle D(\mathbf{x})\rangle$, the subtractions in (4.38) amount to exclude the internal contractions when applying Wick's theorem. We can then write

$$\langle\!\langle D(\mathbf{x}_1)\, D(\mathbf{x}_2) \dots D(\mathbf{x}_n) \rangle\!\rangle = \big\langle D(\mathbf{x}_1)\, D(\mathbf{x}_2) \dots D(\mathbf{x}_n) \big\rangle_0, \tag{4.39}$$

where $\langle \cdot \rangle_0$ indicates the exclusion of internal contractions.

In the present, one-periodic case, we have seen that the internal contractions vanish, implying $\langle D(\mathbf{x})\rangle = 0$, so that the dimer correlations are simply equal to the expectation value of the product of dimer fields. If an internal contraction does not vanish, it necessarily diverges, as will be the case later on in the two-periodic case. This is however an artefact of the continuum limit, which tries to evaluate at the origin a function which is only defined for large distances (take the $z_{12} \to 0$ limit in (4.33)).

To compute the correlations, we use the previous expressions for $H(\mathbf{x})$ and $V(\mathbf{x})$, and use the two-point functions of the Majorana fermions

(this is actually more convenient than using the field ψ because one immediately sees that many terms vanish). A quick calculation yields the following two-point correlations,

$$\langle\!\langle H(\mathbf{x}_1)\, H(\mathbf{x}_2)\rangle\!\rangle = u^2\, \frac{(-1)^{x_1+y_1+x_2+y_2}}{4\pi^2} \Big[\frac{1}{z_{12}} + \frac{(-1)^{y_1+y_2}}{\overline{z}_{12}}\Big]^2, \tag{4.40}$$

$$\langle\!\langle H(\mathbf{x}_1)\, V(\mathbf{x}_2)\rangle\!\rangle = uv\, \frac{(-1)^{x_1+y_1+x_2+y_2}}{\pi^2}\, \frac{x_{12}\, y_{12}}{|z_{12}|^4}, \tag{4.41}$$

$$\langle\!\langle V(\mathbf{x}_1)\, V(\mathbf{x}_2)\rangle\!\rangle = -v^2\, \frac{(-1)^{x_1+y_1+x_2+y_2}}{4\pi^2} \Big[\frac{1}{z_{12}} - \frac{(-1)^{x_1+x_2}}{\overline{z}_{12}}\Big]^2. \tag{4.42}$$

We see that the correlators in the continuum retain a strong sensitivity to the parities of the coordinates. For instance, if z_{12} is purely imaginary ($x_1 = x_2$), the correlator $\langle\!\langle HH\rangle\!\rangle$ decays like $|z_{12}|^{-2}$ if y_1, y_2 have opposite parities, and vanishes if y_1, y_2 have the same parity. In the latter case, the lattice correlator does not vanish identically but decays like $|z_{12}|^{-4}$, a rather unusual phenomenon although well known in the dimer model literature [107].

Three-point correlations can also be computed. One first readily checks that $\langle\!\langle HHH\rangle\!\rangle = \langle\!\langle VVV\rangle\!\rangle = 0$, and then a simple computation gives

$$\begin{aligned}\langle\!\langle H(\mathbf{x}_1)\, H(\mathbf{x}_2)\, V(\mathbf{x}_3)\rangle\!\rangle = &-\frac{u^2 v}{2\pi^3}\, \frac{(-1)^{x_1+x_2+y_2+y_3}}{|z_{12}\, z_{13}\, z_{23}|^2} \\ &\times \Big[\mathrm{Im}(z_{12}\, \overline{z}_{13}\, z_{23}) - (-1)^{y_1+y_2}\, \mathrm{Im}(z_{12}\, z_{13}\, \overline{z}_{23})\Big],\end{aligned} \tag{4.43}$$

$$\begin{aligned}\langle\!\langle H(\mathbf{x}_1)\, V(\mathbf{x}_2)\, V(\mathbf{x}_3)\rangle\!\rangle = &\frac{uv^2}{2\pi^3}\, \frac{(-1)^{x_1+x_2+y_2+y_3}}{|z_{12}\, z_{13}\, z_{23}|^2} \\ &\times \Big[\mathrm{Re}(z_{12}\, \overline{z}_{13}\, z_{23}) - (-1)^{x_2+x_3}\, \mathrm{Re}(\overline{z}_{12}\, z_{13}\, z_{23})\Big].\end{aligned} \tag{4.44}$$

4.3.2 Plaquette correlations

Because of their geometric interpretation of removing one vertex, the fermions are useful to compute the correlations of various dimer patterns. One simple example is the pattern consisting of having two parallel dimers, which one could call a (flippable) plaquette. Let us denote by $P(\mathbf{x})$ the event of having two dimers covering the four vertices $\mathbf{x}$, $\mathbf{x}+$

$\varepsilon\,\mathbf{e}_1$, $\mathbf{x}+\varepsilon\,\mathbf{e}_2$ and $\mathbf{x}+\varepsilon(\mathbf{e}_1+\mathbf{e}_2)$. Forcing the pattern $P(\mathbf{x})$ corresponds to the insertion of

$$P(\mathbf{x}) = (u^2+v^2)\,\psi(\mathbf{x})\,\psi(\mathbf{x}+\varepsilon\,\mathbf{e}_1)\,\psi(\mathbf{x}+\varepsilon\,\mathbf{e}_2)\,\psi(\mathbf{x}+\varepsilon(\mathbf{e}_1+\mathbf{e}_2)). \quad (4.45)$$

Following the same definition as in (4.38), the correlation of two such patterns is then given by

$$\begin{aligned}\langle\!\langle P(\mathbf{x}_1)\,P(\mathbf{x}_2)\rangle\!\rangle &= \mathbb{P}(P(\mathbf{x}_1),P(\mathbf{x}_2)) - \mathbb{P}(P(\mathbf{x}_1))\cdot\mathbb{P}(P(\mathbf{x}_2))\\ &= (u^2+v^2)^2\langle\psi(\mathbf{x}_1)\psi(\mathbf{x}_1+\varepsilon\mathbf{e}_1)\ldots\psi(\mathbf{x}_2)\psi(\mathbf{x}_2+\varepsilon\mathbf{e}_1)\ldots\rangle - \mathbb{P}(P(\mathbf{x}_1))\cdot\mathbb{P}(P(\mathbf{x}_2)).\end{aligned} \quad (4.46)$$

The explicit calculation of the average value containing the product of eight fermions can be carried out by using Wick's theorem (4.7) and the fact that each contraction is equal to an entry of the inverse Kasteleyn matrix, $\langle\psi_i\psi_j\rangle = K^{-1}_{ij}$. As before, a contraction can be internal (the two fermions are located around $\mathbf{x}_1$ or $\mathbf{x}_2$) or external (one fermion around $\mathbf{x}_1$, the other around $\mathbf{x}_2$). Unlike the previous section, the internal contractions should not be all excluded, because some of them will contribute to the correlator. Those we can exclude are the contractions within each group of four fermions, because they yield the product of the two plaquette probabilities, which is to be subtracted. However, the terms with two internal contractions (one in each plaquette) must be kept, and computed in terms of the inverse Kasteleyn matrix. So the calculation of plaquette correlations requires a hybrid calculation, relying on field theoretic two-point functions and on the discrete Kasteleyn matrix.

The internal contractions are pure numbers which can be computed from the inverse Kasteleyn matrix; the external ones depend on the distance $|\mathbf{x}_1-\mathbf{x}_2|$, and are also given by the element of the inverse Kasteleyn matrix, namely $K^{-1}_{\mathbf{x}_1,\mathbf{x}_2}$, of which the dominant contribution (proportional to $|\mathbf{x}_1-\mathbf{x}_2|^{-1}$) is given by the field theoretical propagator (4.34).

Among the $7!! = 105$ different ways to Wick contract the product of eight fermions, 9 of them involve internal contractions only. As mentioned earlier, there is no need to compute them anyway since they clearly yield the product $\mathbb{P}(P(\mathbf{x}_1))\cdot\mathbb{P}(P(\mathbf{x}_2))$. Then, there are 72 ways to Wick contract which involve two internal contractions and two external ones;

all these 72 contributions decay like $|\mathbf{x}_{12}|^{-2}$ and yield the dominant contribution to the correlator. Finally, the remaining 24 contributions involve only external contractions, and decay like $|\mathbf{x}_{12}|^{-4}$. They are consequently subdominant and can be neglected.

So we may focus on the contributions containing two internal contractions. These may concern two vertices which are diagonally aligned, namely $\langle\psi(\mathbf{x})\,\psi(\mathbf{x}+\varepsilon(\mathbf{e}_1+\mathbf{e}_2))\rangle$ or $\langle\psi(\mathbf{x}+\varepsilon\,\mathbf{e}_1)\,\psi(\mathbf{x}+\varepsilon\,\mathbf{e}_2)\rangle$. In each case, the two vertices are on the same sublattice (even or odd), so that these two contractions are equal to zero (hence 40 out the 72 contributions vanish identically). The other internal contractions involve two nearest neighbour vertices which are horizontally or vertically aligned, and are simply equal to $\mathbb{P}(H(\mathbf{x}))/u$ and $\mathbb{P}(V(\mathbf{x}))/v$ respectively. They do not depend on the location $\mathbf{x}$ and are found to be given by the following expressions,

$$\begin{aligned}\langle\psi(\mathbf{x})\,\psi(\mathbf{x}+\varepsilon\,\mathbf{e}_1)\rangle &= \frac{\mathbb{P}(H(\mathbf{x}))}{u} = \frac{1}{\pi u}\arctan\big(\frac{u}{v}\big),\\ \langle\psi(\mathbf{x})\,\psi(\mathbf{x}+\varepsilon\,\mathbf{e}_2)\rangle &= \frac{\mathbb{P}(V(\mathbf{x}))}{\mathrm{i}v} = \frac{-\mathrm{i}}{\pi v}\arctan\big(\frac{v}{u}\big),\end{aligned} \tag{4.47}$$

which follow from those of the inverse Laplacian at short distance collected in Appendix 4.A, and the use of (4.21).

The internal contractions discussed above are multiplied by two external contractions on the remaining four vertices. They come in pairs which are necessarily aligned horizontally or vertically, thereby reproducing the correlators $\langle\!\langle HH\rangle\!\rangle$, $\langle\!\langle HV\rangle\!\rangle$ or $\langle\!\langle VV\rangle\!\rangle$ computed in the previous section, resp. divided by u^2, $\mathrm{i}uv$ and $(\mathrm{i}v)^2$. Collecting all terms, we obtain

$$\begin{aligned}\langle\!\langle P(\mathbf{x}_1)\,P(\mathbf{x}_2)\rangle\!\rangle &= (u^2+v^2)^2\times\\ &\Big\{\frac{\mathbb{P}(H)^2}{u^4}\Big[\langle\!\langle H(z_1)\,H(z_2)\rangle\!\rangle + \langle\!\langle H(z_1)\,H(z_2+\mathrm{i}\varepsilon)\rangle\!\rangle\\ &\qquad + \langle\!\langle H(z_1+\mathrm{i}\varepsilon)\,H(z_2)\rangle\!\rangle + \langle\!\langle H(z_1+\mathrm{i}\varepsilon)\,H(z_2+\mathrm{i}\varepsilon)\rangle\!\rangle\Big]\\ &\quad - \frac{\mathbb{P}(H)\mathbb{P}(V)}{(\mathrm{i}uv)^2}\Big[\langle\!\langle H(z_1)\,V(z_2)\rangle\!\rangle + \langle\!\langle H(z_1)\,V(z_2+\varepsilon)\rangle\!\rangle\\ &\qquad + \langle\!\langle H(z_1+\mathrm{i}\varepsilon)\,V(z_2)\rangle\!\rangle + \langle\!\langle H(z_1+\mathrm{i}\varepsilon)\,V(z_2+\varepsilon)\rangle\!\rangle\\ &\qquad + \langle\!\langle V(z_1)\,H(z_2)\rangle\!\rangle + \langle\!\langle V(z_1)\,H(z_2+\mathrm{i}\varepsilon)\rangle\!\rangle\\ &\qquad + \langle\!\langle V(z_1+\varepsilon)\,H(z_2)\rangle\!\rangle + \langle\!\langle V(z_1+\varepsilon)\,H(z_2+\mathrm{i}\varepsilon)\rangle\!\rangle\Big]\end{aligned}$$

$$+\frac{\mathbb{P}(V)^2}{(\mathrm{i}v)^4}\Big[\langle\!\langle V(z_1)\,V(z_2)\rangle\!\rangle+\langle\!\langle V(z_1)\,V(z_2+\varepsilon)\rangle\!\rangle \\ +\langle\!\langle V(z_1+\varepsilon)\,V(z_2)\rangle\!\rangle+\langle\!\langle V(z_1+\varepsilon)\,V(z_2+\varepsilon)\rangle\!\rangle\Big]\Big\}$$

$$=2\frac{(u^2+v^2)^2}{\pi^4\,|z_{12}|^2}\left[\frac{\arctan^2(u/v)}{u^2}\,(-1)^{x_1+x_2}+\frac{\arctan^2(v/u)}{v^2}\,(-1)^{y_1+y_2}\right]. \tag{4.48}$$

Thus, a plaquette has scaling dimension equal to 1 in the scaling limit, which is expected for local patterns[6]. The same phenomenon as for dimer correlations occurs, and is even stronger here: in the uniform case, $u=v$, the correlation decay rate varies when one of the two plaquettes is moved by one spacing along the x- or y-axis, irrespective of the relative directional position of the two plaquettes.

4.4 Two-periodic weights

When considering two-periodic weights, for simplicity, we shall suppress the horizontal and vertical biases, by setting $u=v=1$, since their only effect in the continuum limit is to rescale the x- and y-coordinates. So the action is

$$S=2ac\int \mathrm{d}^2\mathbf{x}\Big\{\chi^1\overline{\partial}\,\chi^1+\overline{\chi}^1\partial\,\overline{\chi}^1-\mathrm{i}M\chi^1\,\overline{\chi}^1+\chi^2\overline{\partial}\,\chi^2+\overline{\chi}^2\partial\,\overline{\chi}^2-\mathrm{i}M\chi^2\,\overline{\chi}^2\Big\}, \tag{4.49}$$

where ∂ and $\overline{\partial}$ are now the usual holomorphic and antiholomorphic complex derivatives. From this action, we derive the two-point functions, in complex coordinates

$$\begin{pmatrix}\langle\chi(z)\,\chi(0)\rangle & \langle\chi(z)\,\overline{\chi}(0)\rangle\\ \langle\overline{\chi}(z)\,\chi(0)\rangle & \langle\overline{\chi}(z)\,\overline{\chi}(0)\rangle\end{pmatrix}=-\frac{M}{4\pi ac\,r}\begin{pmatrix}\overline{z}\,K_0'(Mr) & \mathrm{i}\,rK_0(Mr)\\ -\mathrm{i}\,r\,K_0(Mr) & z\,K_0'(Mr)\end{pmatrix}, \tag{4.50}$$

with $r=|z|$. These quantities are fully translation invariant, but the same property should not be expected for the dimer correlators. Indeed,

[6] The correlation of two local dimer patterns corresponds to the insertion of two finite groups of ψ fermions. When the two patterns are far apart, the terms containing only two external contractions, whose product is proportional to $|\mathbf{x}_{12}|^{-2}$, yield the dominant contribution, unless its coefficient vanishes, which is not generically expected.

on the lattice, the inhomogeneity of the weights break the translation invariance group down to $(2\mathbb{Z})^2$, and this will leave a trace in the continuum.

From the relations (4.30) between the ψ fields and the Majorana fields, we obtain

$$\langle\psi(z_1)\,\psi(z_2)\rangle = \frac{M}{4\pi ac}\,\frac{(-1)^{x_1+y_1+x_2+y_2}-1}{r}\Big[\big(\overline{z}_{12}+(-1)^{y_1+y_2}\,z_{12}\big)K_0'(Mr) - \mathrm{i}\Big\{\big((-1)^{y_1}-(-1)^{y_2}\big)\cos\alpha + \mathrm{i}\,\big((-1)^{x_1}-(-1)^{x_2}\big)\sin\alpha\Big\}\,rK_0(Mr)\Big]. \tag{4.51}$$

We see that the second term, proportional to K_0, breaks the translation invariance group down to $2\mathbb{Z}^2$. In the massless limit, this term vanishes and the full translation invariance is restored.

The same relation (4.30) allows us to express the dimer fields in terms of the Majorana fields (recall that, close to the critical point, the weights assigned to dimers are all proportional to ac),

$$H(z) = ac\,\psi(z)\,\psi(z+\varepsilon) = 2\mathrm{i}ac\,(-1)^x\Big\{(-1)^y\big[\chi^1\,\chi^2+\overline{\chi}^1\,\overline{\chi}^2\big] + \cos\alpha\,\big[\chi^1\,\overline{\chi}^2+\overline{\chi}^1\,\chi^2\big] - \sin\alpha\,\big[\chi^1\,\overline{\chi}^1+\chi^2\,\overline{\chi}^2\big]\Big\}, \tag{4.52}$$

$$V(z) = \mathrm{i}\,ac\,\psi(z)\,\psi(z+\mathrm{i}\varepsilon) = 2ac\,(-1)^{y+1}\Big\{(-1)^x\big[\chi^1\,\chi^2-\overline{\chi}^1\,\overline{\chi}^2\big] + \mathrm{i}\sin\alpha\,\big[\chi^1\,\overline{\chi}^2+\overline{\chi}^1\,\chi^2\big] + \mathrm{i}\cos\alpha\,\big[\chi^1\,\overline{\chi}^1+\chi^2\,\overline{\chi}^2\big]\Big\}. \tag{4.53}$$

Unlike the one-periodic case, the expectation values $\langle H(z)\rangle$ and $\langle V(z)\rangle$ are not defined because the contractions of the last two terms diverge. The prescription discussed in Section 4.3.1 however requires to leave them out.

It is now an easy task to compute the correlation of two horizontal dimers,

$$\langle\!\langle H(z_1)\,H(z_2)\rangle\!\rangle = \frac{M^2}{4\pi^2r^2}(-1)^{x_1+x_2+y_1+y_2}\Big\{-2\sin^2\alpha\,\big(1+(-1)^{y_1+y_2}\big)r^2K_0^2 + \Big[\big(\overline{z}_{12}+(-1)^{y_1+y_2}\,z_{12}\big)K_0' - \mathrm{i}\cos\alpha\,\big((-1)^{y_1}-(-1)^{y_2}\big)\,rK_0\Big]^2\Big\}. \tag{4.54}$$

Because of the second term in the squared brackets, the correlator is indeed not fully invariant, namely $\langle\!\langle H(z_1+\mathrm{i}\varepsilon)\,H(z_2+\mathrm{i}\varepsilon)\rangle\!\rangle \neq \langle\!\langle H(z_1)\,H(z_2)\rangle\!\rangle$.

One obtains similarly for one horizontal and one vertical dimer,

$$\langle\!\langle H(z_1)\,V(z_2)\rangle\!\rangle = \frac{M^2}{\pi^2 r^2}(-1)^{x_1+x_2+y_1+y_2} \times \Big[(x_1-x_2)K_0' - \sin\alpha\,(-1)^{x_2}\,rK_0\Big]\,\Big[(y_1-y_2)K_0' + \cos\alpha\,(-1)^{y_1}\,rK_0\Big], \tag{4.55}$$

and for two vertical dimers,

$$\langle\!\langle V(z_1)\,V(z_2)\rangle\!\rangle = -\frac{M^2}{4\pi^2 r^2}(-1)^{x_1+x_2+y_1+y_2}\Big\{2\cos^2\alpha\,(1+(-1)^{x_1+x_2})r^2K_0^2 + \Big[(\overline{z}_{12}-(-1)^{x_1+x_2}\,z_{12})K_0' + \sin\alpha\,((-1)^{x_1}-(-1)^{x_2})\,rK_0\Big]^2\Big\}. \tag{4.56}$$

One may check that the expression of $\langle\!\langle V(z_1)\,V(z_2)\rangle\!\rangle$ is fully consistent with that of $\langle\!\langle H(z_1)\,H(z_2)\rangle\!\rangle$ to which a rotation by $\frac{\pi}{2}$ is applied ($z_1, z_2 \to \mathrm{i}z_1, \mathrm{i}z_2$), including the dependence in α since the rotation changes the weights $a, b, c, d \to d, c, a, b$, resulting in the change $\alpha \to \alpha - \frac{\pi}{2}$.

4.5 Ghost systems

In Section 4.2, the field theory that emerged from the scaling limit was that of two pairs of uncoupled massive Majorana fermions, of scaling dimension $\frac{1}{2}$. However, as is well known, the Majorana fermions form a special case of a ghost system. We make the observation here that more general ghost systems may be obtained as well.

Looking back at the partial discrete action we called S_1, given in (4.26), we see that the Majorana field theory resulted from our choice to evenly distribute the powers of ε on the four fermions ψ^i. But instead we can write S_1 as

$$S_1 = \frac{ac}{4}\sum_{\mathbf{m}\in 2\mathbb{Z}^2}(2\varepsilon)^2\,\frac{\psi^1(\varepsilon\mathbf{m})}{\varepsilon^{1-\lambda}} \times \Big\{\frac{u}{2\varepsilon}\Big[\frac{\psi^3(\varepsilon\mathbf{m}+\varepsilon\,\mathbf{e}_1)}{\varepsilon^\lambda} - \frac{\psi^3(\varepsilon\mathbf{m}-\varepsilon\,\mathbf{e}_1)}{\varepsilon^\lambda}\Big] + \frac{\mu}{2\varepsilon}\sin\alpha\,\frac{\psi^3(\varepsilon\mathbf{m}-\varepsilon\,\mathbf{e}_1)}{\varepsilon^\lambda} + \dots + \frac{\mathrm{i}\,v}{2\varepsilon}\Big[\frac{\psi^2(\varepsilon\mathbf{m}+\varepsilon\,\mathbf{e}_2)}{\varepsilon^\lambda} - \frac{\psi^2(\varepsilon\mathbf{m}-\varepsilon\,\mathbf{e}_2)}{\varepsilon^\lambda}\Big] + \frac{\mathrm{i}\,\mu}{2\varepsilon}\cos\alpha\,\frac{\psi^2(\varepsilon\mathbf{m}-\varepsilon\,\mathbf{e}_2)}{\varepsilon^\lambda} + \dots\Big\}$$

$$\to \frac{ac}{4}\int \mathrm{d}^2\mathbf{x}\,\psi^1(\mathbf{x})\Big[u\partial_x\psi^3(\mathbf{x})+M\sin\alpha\psi^3(\mathbf{x})+\mathrm{i}v\partial_y\psi^2(\mathbf{x})+\mathrm{i}M\cos\alpha\psi^2(\mathbf{x})\Big]. \tag{4.57}$$

The scaling limit yields exactly the same continuous partial action, on the last line of (4.57), except that the continuous field $\psi^1(\mathbf{x})$ has scaling dimension $1-\lambda$ whereas $\psi^2(\mathbf{x})$ and $\psi^3(\mathbf{x})$ have both a scaling dimension equal to λ. Proceeding in the same way with the other three terms of the discrete action (4.22), we find that the already found dimensions are consistent provided $\psi^4(\mathbf{x})$ is also assigned a dimension $1-\lambda$.

The resulting continuous action is exactly the same as before, given in (4.27), except for the dimensions of the fields: ψ^1,ψ^4 have a dimension $1-\lambda$, the other two ψ^2,ψ^3 have a dimension λ. By introducing four new fields $\mathsf{b},\overline{\mathsf{b}},\mathsf{c},\overline{\mathsf{c}}$, related linearly to the ψ^i by

$$(\psi^1,\psi^4)=(\mathsf{b}-\mathrm{i}\,\overline{\mathsf{b}},\ \mathsf{b}+\mathrm{i}\,\overline{\mathsf{b}}),\qquad (\psi^2,\psi^3)=(\mathsf{c}-\mathrm{i}\,\overline{\mathsf{c}},\ \mathsf{c}+\mathrm{i}\,\overline{\mathsf{c}}), \tag{4.58}$$

the action takes the standard form of a massive ghost system [108–111],

$$S=2ac\int \mathrm{d}^2\mathbf{x}\,\Big\{\mathsf{b}\,\overline{\partial}\,\mathsf{c}+\overline{\mathsf{b}}\,\partial\,\overline{\mathsf{c}}+\frac{1}{2}M\mathrm{e}^{\mathrm{i}\alpha}\,\mathsf{b}\,\overline{\mathsf{c}}+\frac{1}{2}M\mathrm{e}^{-\mathrm{i}\alpha}\,\overline{\mathsf{b}}\,\mathsf{c}\Big\}. \tag{4.59}$$

The dimension of $\mathsf{b},\overline{\mathsf{b}}$ is $1-\lambda$, that of $\mathsf{c},\overline{\mathsf{c}}$ is λ.

If we form the vector $\vec{\gamma}=(\mathsf{b},\overline{\mathsf{b}},\mathsf{c},\overline{\mathsf{c}})$, the previous action implies the following two-point functions,

$$\langle\gamma^i(z)\gamma^j(0)\rangle=-\frac{M}{2\pi ac\,r}\begin{pmatrix} 0 & 0 & \overline{z}\,K_0'(Mr) & r\mathrm{e}^{-\mathrm{i}\alpha}K_0(Mr)\\ 0 & 0 & r\mathrm{e}^{\mathrm{i}\alpha}K_0(Mr) & z\,K_0'(Mr)\\ \overline{z}\,K_0'(Mr) & -r\mathrm{e}^{\mathrm{i}\alpha}K_0(Mr) & 0 & 0\\ -r\mathrm{e}^{-\mathrm{i}\alpha}K_0(Mr) & z\,K_0'(Mr) & 0 & 0\end{pmatrix}. \tag{4.60}$$

One may check that expressing the horizontal and vertical dimer fields in terms of γ^i, the previous two-point functions reproduce all correlators computed in the previous sections.

If the correlators of the γ^i fields are not at all affected by the value of λ, the field theories obtained by adding fields that are not local in the γ^i will be affected. In particular, in the massless (conformal) limit, the conformal structure clearly depends on λ, as does the field algebra. In our normalizations, the canonical stress-energy tensor of the ghost pair (b,c) in (4.59) with $M=0$ reads,

$$T_{\mathrm{c}}(z)=-2\pi\,\mathsf{b}(z)\,\partial\mathsf{c}(z). \tag{4.61}$$

With respect to $T_{\rm c}$, $\mathsf{b}, \overline{\mathsf{b}}$ are primary fields of conformal weight 1 whereas $\mathsf{c}, \overline{\mathsf{c}}$ are primary fields with conformal weight 0. Also, the Virasoro algebra generated by $T_{\rm c}$ has central charge $c = -2$.

In order to give the fields γ^i the conformal weight $1-\lambda$ or λ, one considers the following improved stress-energy tensor,

$$T_\lambda(z) = T_{\rm c}(z) - \lambda\partial J(z) = -2\pi\,\mathsf{b}(z)\,\partial\mathsf{c}(z) + 2\pi\,\lambda\,\partial\big(\mathsf{b}(z)\,\mathsf{c}(z)\big). \quad (4.62)$$

With respect to T_λ, $\mathsf{b}, \overline{\mathsf{b}}$ and $\mathsf{c}, \overline{\mathsf{c}}$ are now primary fields of conformal weight $1-\lambda$ and λ respectively, while the central charge changes to $c(\lambda) = -2\big[1 + 6\lambda(\lambda-1)\big]$. A similar discussion applies to the antiholomorphic part of the ghost system, based on the pair $(\overline{\mathsf{b}}, \overline{\mathsf{c}})$, with similar results.

For $\lambda = \frac{1}{2}$, the central charge is $c(\frac{1}{2}) = 1$ and all four ghost fields have identical weight $\frac{1}{2}$; in that case, the conformal structure of the ghost system is identical to that of the Majorana fermions. As a consistency check, one verifies that the canonical stress-energy tensor of the Majorana fermions, given by $T_\chi = -2\pi\,\chi^1\,\partial\,\chi^1 - 2\pi\,\chi^2\,\partial\,\chi^2$, is exactly mapped onto $T_{\lambda=\frac{1}{2}}$ by the linear transformation

$$\chi^1 = \frac{1}{2}(\mathsf{b} + \mathsf{c}), \qquad \chi^2 = \frac{\mathrm{i}}{2}(\mathsf{b} - \mathsf{c}), \quad (4.63)$$

obtained by combining (4.32) and (4.58).

Let us summarize this section. As far as dimer (or other local patterns like plaquettes) correlators are concerned, the two-periodic dimer model can be described by a massive field theory, which is a massive perturbation of a conformal ghost field theory possessing any central charge $c(\lambda) \leqslant 1$. Though the conformal structure does depend on λ, the dimer correlators do not. Thus, if one means by *dimer model* the study of the two-periodic measure on fully packed dimer configurations, equivalently of perfect matchings, then all is fine: any of the above massive theories will do, with no visible difference.

However, if one wishes to consider the effects of defects on the substrate or non-local dimer observables, the question arises as to which of the above field theories is (or are) the correct one(s) ? The question is not trivial, even in the massless limit.

The best-known example of such an observable is provided by monomers, which we have briefly mentioned earlier in Section 4.1. Monomers are vertices that must not be covered by dimers, or, equivalently, that are simply removed from the grid. In the case dimer configurations are uniformly distributed on the lattice $\mathbb{Z}^2$, the presence of monomers deeply affects the dimer configurations over large scales, as its two-point correlator[7] decays like $r^{-1/2}$. In conformal terms, one thus expects the monomer field to be a scalar field with conformal weights $(\frac{1}{8}, \frac{1}{8})$. It is known that this type of conformal field can indeed be accomodated in a conformal theory with central charge $c = 1$, either in terms of spin and disorder fields in a double copy of the Ising model [105], or in terms of a vertex operator in a free Gaussian theory [112]. It is not clear that monomers with the right conformal properties can be accomodated in conformal theories with a central charge different from 1, such as those discussed above.

4.6 Symplectic fermions

The massless ghost system with central charge $c = -2$ discussed in the previous section is somewhat close to the symplectic fermion theory. The latter is defined in terms of two fermionic scalar fields $\theta, \bar{\theta}$ with conformal weights $(0, 0)$ and the following action,

$$S_{\text{sym}} = \int \mathrm{d}^2\mathbf{x}\, \partial\theta\bar{\partial}\bar{\theta}. \tag{4.64}$$

The canonical stress-energy tensor is $T_{\text{sym}} \sim \partial\theta\partial\bar{\theta}$ and leads to a central charge $c = -2$. Unlike the ghost system, the symplectic fermion theory is a logarithmic conformal field theory, which exhibits logarithms in some of its correlation functions [110, 111, 113, 114].

If we formally identify $\mathsf{b} = \partial\theta$ and $\mathsf{c} = \bar{\theta}$, then the action (4.59) for $M = 0$ for the bc part becomes the above action S_{sym}, and the canonical holomorphic stress-energy tensor T_{c} reproduces T_{sym}. Thus, the bc system appear as a subtheory of the symplectic fermion model. Note that we might likewise attempt the identification $\bar{\mathsf{b}} = \bar{\partial}\theta$ and $\bar{\mathsf{c}} = \bar{\theta}$, but

[7] The correlation of monomers is defined as the partition functions of dimers in presence of the monomers divided by the partition function with no monomer.

this does not work as c and $\bar{\mathsf{c}}$ would then be the same field. The way out would be to relate $\bar{\mathsf{b}}, \bar{\mathsf{c}}$ to a second pair of symplectic fermions $\theta_2, \bar{\theta}_2$, namely $\bar{\mathsf{b}} = \bar{\partial}\theta_2$ and $\bar{\mathsf{c}} = \bar{\theta}_2$, in agreement with the fact that the bc and $\bar{\mathsf{b}}\bar{\mathsf{c}}$ systems are decoupled in the massless regime.

The symplectic fermions are known to describe some local (but not all) observables in the sandpile model [115–117]. Because the sandpile model is intrisincally related to spanning trees, themselves related to dimers via the Temperley correspondence [118], one suspects that symplectic fermions can be used to describe dimer correlations in the scaling limit. And indeed, using Temperley's correspondence, it was observed in [119] that horizontal and vertical dimers on the even-even sublattice are described respectively by $\frac{1}{2}\theta(\partial + \bar{\partial})\bar{\theta} = \theta\partial_x\bar{\theta}$ and $\frac{\mathrm{i}}{2}\theta(\partial - \bar{\partial})\bar{\theta} = \theta\partial_y\bar{\theta}$ if dimers are uniformly distributed (massless limit). However, it turns out that the extension to the other sublattices is not possible with a single pair of symplectic fermions. As somewhat suggested by the above argument, it becomes possible with two pairs of uncoupled symplectic fermions (central charge $c = -4$), which can as well account for the two-periodic, massive dimer model.

We thus consider the following action

$$S = \int \mathrm{d}^2\mathbf{x} \left\{ \partial\theta_1\, \bar{\partial}\bar{\theta}_1 + \frac{M^2}{4}\theta_1\bar{\theta}_1 + \partial\theta_2\, \bar{\partial}\bar{\theta}_2 + \frac{M^2}{4}\theta_2\bar{\theta}_2 \right\}. \tag{4.65}$$

The basic two-point correlators read

$$\langle \theta_a(z)\bar{\theta}_b(0)\rangle = \frac{1}{\pi}K_0(Mr)\,\delta_{a,b}, \qquad \langle \theta_a(z)\theta_b(0)\rangle = \langle \bar{\theta}_a(z)\bar{\theta}_b(0)\rangle = 0. \tag{4.66}$$

Since the dimer fields $H(z)$ and $V(z)$ have scaling dimension 1, we look for linear combinations of terms like $\theta_a\partial_x\bar{\theta}_b$, $\theta_a\partial_y\bar{\theta}_b$ and $M\theta_a\bar{\theta}_b$. A few trials yields the following combinations,

$$H_{\mathrm{e,e}}(z) = -\theta_1\,\partial_x\bar{\theta}_1 - \theta_1\,\partial_y\bar{\theta}_2 + M\sin\alpha\,\theta_1\bar{\theta}_1 - M\cos\alpha\,\theta_1\bar{\theta}_2, \tag{4.67a}$$

$$H_{\mathrm{o,o}}(z) = -\theta_2\,\partial_x\bar{\theta}_2 + \theta_2\,\partial_y\bar{\theta}_1 - M\sin\alpha\,\theta_2\bar{\theta}_2 - M\cos\alpha\,\theta_2\bar{\theta}_1, \tag{4.67b}$$

$$V_{\mathrm{e,e}}(z) = -\theta_1\,\partial_y\bar{\theta}_1 + \theta_1\,\partial_x\bar{\theta}_2 + M\cos\alpha\,\theta_1\bar{\theta}_1 + M\sin\alpha\,\theta_1\bar{\theta}_2, \tag{4.67c}$$

$$V_{\mathrm{o,o}}(z) = -\theta_2\,\partial_y\bar{\theta}_2 - \theta_2\,\partial_x\bar{\theta}_1 - M\cos\alpha\,\theta_2\bar{\theta}_2 + M\sin\alpha\,\theta_2\bar{\theta}_1. \tag{4.67d}$$

The indices of H and V stand to specify x, y even or odd. The fields for the other parities are obtained as before, namely $H_{\mathrm{o,e}} = -H_{\mathrm{e,e}}$,

$H_{\mathrm{e,o}} = -H_{\mathrm{o,o}}$, and $V_{\mathrm{o,e}} = -V_{\mathrm{o,o}}$, $V_{\mathrm{e,o}} = -V_{\mathrm{e,e}}$. The above field assignments reproduce correctly all the correlations we have computed so far, including all 64 three-point correlators and also some four-point correlators. The situation here is different from that of the earlier sections, since the fields $\theta_a, \bar{\theta}_a$ do not have (so far) any lattice interpretation. The checks we have carried out bring however enough confidence to conjecture that the above fields do reproduce all dimer correlators.

4.7 Outlook

In this chapter, we found two different field theories that reproduce the correlations of the dimer model in the scaling limit. The ghost system is obtained from the limit of the discrete action, which makes it somewhat more natural, whereas the symplectic fermions appear rather artificial in the sense that they do not have a lattice interpretation and merely reproduce the correlation functions. However, the links between the two theories seem to be deeper than what we have observed and remain to be properly understood.

Another interesting extension of this project would be to investigate higher periodicities of the lattice grid weights, for instance 2×3. In this case, the freedom around the critical point in the parameter space is larger, and one has to carefully set up the scaling/critical limit in order to obtain a non-trivial theory. One additional difficulty comes from the fact that the lattice periodicity does not match the natural four families of fermions we defined, contrary to the 2×2-periodic case, which makes the identification harder.

4.A Inverse discrete Laplacian: short-distance and long-range behaviour

We collect in this appendix the formulas which are useful to make concrete calculations of various lattice correlations. These require the values of the entries of the inverse discrete Laplacian on $\mathbb{Z}^2$, which turns out to be massive and/or anisotropic, depending on whether two-periodic

weights (a, b, c, d) and/or horizontal and vertical biases (u, v) are used, see (4.15). We start with the massless anisotropic discrete Laplacian, relevant for one-periodic weights.

4.A.1 Massless Green matrix

Keeping the notations used in the text, the inverse of the Laplacian is given by (4.19) for $\gamma_1 = \gamma_2 = 2$ and $p, q \in \mathbb{Z}$,

$$G(p,q) = \Delta^{-1}_{(x+p,y+q),(x,y)} = \frac{1}{8\pi^2} \iint_{-\pi}^{\pi} \mathrm{d}\alpha\, \mathrm{d}\beta \frac{\mathrm{e}^{\mathrm{i}p\alpha+\mathrm{i}q\beta}}{u^2+v^2-u^2\cos\alpha - v^2\cos\beta}. \tag{4.68}$$

This integral is (logarithmically) divergent with a divergence which is independent of (p, q), so that the following subtraction makes it well-defined,

$$\varphi(p,q) \equiv G(p,q) - G(0,0) = \frac{1}{8\pi^2 u^2} \iint_{-\pi}^{\pi} \mathrm{d}\alpha\, \mathrm{d}\beta\, \frac{\mathrm{e}^{\mathrm{i}p\alpha+\mathrm{i}q\beta} - 1}{1+t-\cos\alpha - t\cos\beta}, \tag{4.69}$$

with $t \equiv v^2/u^2$. The integration over α yields,

$$\varphi(p,q) = \frac{1}{2\pi u^2} \int_0^{\pi} \mathrm{d}\beta\, \frac{\left[1+t-t\cos\beta - \sqrt{(1+t-t\cos\beta)^2-1}\right]^{|p|} \cos q\beta - 1}{\sqrt{(1+t-t\cos\beta)^2-1}}. \tag{4.70}$$

In actual calculations, one needs to know the value of $G(p, q) - G(0, 0)$ for (p, q) close to the origin, or else very distant from the origin, in which case, the asymptotic value is required.

When p, q are small, the remaining integration can be carried out exactly. From the symmetries $G(\pm p, \pm q) = G(p, q)$ and the fact that $G(q, p)$ is obtained from $G(p, q)$ by exchanging u and v, one may assume $p \geqslant q \geqslant 0$. One obtains the following values for $p \leqslant 2$,

$$\begin{aligned}
\varphi(1,0) &= -\frac{1}{\pi u^2} \arctan\left(\frac{u}{v}\right), & \varphi(1,1) &= -\frac{1}{\pi uv}, \\
\varphi(2,0) &= \frac{2v}{\pi u^3} - \frac{2(u^2+v^2)}{\pi u^4} \arctan\left(\frac{u}{v}\right), & \varphi(2,2) &= -\frac{4}{3\pi uv}, \\
\varphi(2,1) &= -\frac{u^2+v^2}{\pi u^3 v} + \frac{v^2}{\pi u^4} \arctan\left(\frac{u}{v}\right).
\end{aligned} \tag{4.71}$$

In order to evaluate $\varphi(p,q)$ for large distances, one may follow the procedure used in [120] and [121] (both based on a method proposed in [122]) where the similar calculations were reported respectively for the isotropic Laplacian on $\mathbb{Z}^2$ and the isotropic Laplacian on the honeycomb lattice. We only quote the final result. To write it more conveniently, we introduce the rescaled coordinates $x = vp$ and $y = uq$, as well as the polar coordinates $x = r\cos\varphi$ and $y = r\sin\varphi$. One finds the following asymptotic expansion,

$$\varphi(p,q) = -\frac{1}{2\pi uv}\big[\log r + \gamma + \log 4 - \log\sqrt{u^2+v^2}\big] \tag{4.72}$$
$$+\frac{2(u^2-v^2)\cos 2\varphi + (u^2+v^2)\cos 4\varphi}{48\pi uv\, r^2}$$
$$+\frac{2(23u^4-10u^2v^2+23v^4)\cos 4\varphi + 64(u^4-v^4)\cos 6\varphi + 25(u^2+v^2)^2\cos 8\varphi}{1920\pi uv r^4} + \ldots$$

In particular, this expression allows to compute the large distance value of $K^{-1}_{(x,y),(0,0)}$. From (4.21), it is identically zero if $x+y$ is even, and in the two other cases, given by

$$K^{-1}_{(x,y),(0,0)} = \mathrm{i}v\Big[\varphi\big(\frac{x}{2},\frac{y-1}{2}\big) - \varphi\big(\frac{x}{2},\frac{y+1}{2}\big)\Big] = -\frac{\mathrm{i}uy}{\pi(v^2x^2+u^2y^2)} + \ldots, \tag{4.73}$$

for $(x,y) = (\mathrm{e},\mathrm{o})$, and

$$K^{-1}_{(x,y),(0,0)} = u\Big[\varphi\big(\frac{x+1}{2},\frac{y}{2}\big) - \varphi\big(\frac{x-1}{2},\frac{y}{2}\big)\Big] = \frac{vx}{\pi(v^2x^2+u^2y^2)} + \ldots, \tag{4.74}$$

for $(x,y) = (\mathrm{o},\mathrm{e})$, reproducing exactly the expression $\langle\psi(\mathbf{x})\,\psi(0)\rangle$ in (4.34).

4.A.2 Massive Green matrix

The entries of the Green matrix read (no subtraction is needed as the integral is convergent), for $p,q\in\mathbb{Z}$,

$$G(p,q) = \frac{1}{4\pi^2}\iint_{-\pi}^{\pi}\mathrm{d}\alpha\,\mathrm{d}\beta\,\frac{\mathrm{e}^{\mathrm{i}p\alpha+\mathrm{i}q\beta}}{u^2\gamma_1+v^2\gamma_2-2u^2\cos\alpha-2v^2\cos\beta},$$

$$= \frac{1}{2\pi u^2} \int_0^\pi \mathrm{d}\beta \, \frac{\left[\frac{\gamma_1+t\gamma_2}{2} - t\cos\beta - \sqrt{(\frac{\gamma_1+t\gamma_2}{2} - t\cos\beta)^2 - 1}\right]^{|p|} \cos q\beta - 1}{\sqrt{(\frac{\gamma_1+t\gamma_2}{2} - t\cos\beta)^2 - 1}}. \tag{4.75}$$

The remaining integral belongs to the class of elliptic integrals.

We focus here on the asymptotic value of $G(p,q)$ when the point (p,q) is distant from the origin, and for no horizontal nor vertical bias ($u = v = 1$). Then the dominant contribution is given by the continuum limit of $G(p,q)$, namely,

$$G(p,q) \simeq \frac{1}{4\pi^2} \iint_{-\infty}^{\infty} \mathrm{d}\alpha \, \mathrm{d}\beta \, \frac{\mathrm{e}^{\mathrm{i}p\alpha + \mathrm{i}q\beta}}{\mu^2 + \alpha^2 + \beta^2} = \frac{1}{2\pi} K_0(\mu\sqrt{p^2+q^2}), \tag{4.76}$$

with $\mu^2 = \gamma_1 + \gamma_2 - 4$. Note that when we set $\varepsilon(p,q) = (x,y)$ and $\mu = 2M\varepsilon$ as in Section 4.2, the limit $\varepsilon \to 0$ of the previous Green function is equal to $\frac{1}{2\pi} K_0(2Mr)$. However, on the lattice, the correlators involve the entries of the inverse Kasteleyn matrix, itself related to entries of the Green matrix at half-distances. In this way, the scaling limit of lattice correlators will only depend on $K_0(Mr)$ and derivatives thereof.

As in the massless case, one checks that the continuum limit of $K^{-1}_{(x,y),(x',y')}$ exactly reproduces the expression of $\langle \psi(\mathbf{x}_1)\, \psi(\mathbf{x}_2) \rangle$ in (4.51).

Conclusion

Throughout this thesis, we explored several aspects underlying the dimer model, especially on Aztec diamond domains, and reviewed its connections with other two-dimensional lattice models.

In Chapter 1, we have studied partition functions on several Aztec diamond subgraphs with biased and/or two-periodic probability measures using the octahedron recurrence. This equation provides an efficient method to obtain various statistical quantities and is intimately linked to the integrable structure of the model [33, 123]. In the situation of general weightings, the Robbins-Rumsey formula has been given a combinatorial interpretation in terms of Aztec diamond tilings. We also investigated the situation of inhomogeneous λ-determinants. The general discussion being complicated, we reduced to the case with inhonomogeneous weight on the central row only and extracted some polynomials for the first values of n. Unfortunately, no structure seemed to come out of it. Another direction was the study of biased two-periodic weighting of Aztec diamonds. The condensation algorithm has provided recurrence relations for the partition function that are connected to elliptic functions. We reviewed in the appendices the results we obtained in parallel with what was already known in the literature. The pursue of this work led to the second chapter of this thesis.

The connections between tilings of uniform Aztec diamonds and the six-vertex model are now common knowledge. In Chapter 2, we extended this relation to biased two-periodic Aztec diamonds and the elliptic SOS model at the free-fermion point. We have used the latter, and its inhomogeneous extension, to compute the one- and two-refined partition functions of the model. In the discrete setting, they were given by a

contour integral in the complex plane that can be analyzed using the steepest descent method (saddle point method) in the large n limit. The asymptotics of these coefficients was the key element to apply the tangent method and obtain a parametric form for the arctic curve. In the last section, we obtained an algebraic equation satisfied by the curve.

In Chapter 3, we extended a result originally obtained by Johansson and Nordenstam [44] in uniform Aztec diamonds to biased and then to two-periodic Aztec diamonds. The result concerns the convergence in distribution to the GUE-corners process of a specific subclass of dominos. In particular, we followed the strategy proposed by Fleming and Forrester [45] and computed the joint probability distribution for the particle process in the discrete setting. This distribution is given by a determinant whose entries satisfy a linear recurrence relation. From that, we computed the generating function of these coefficients and extracted the leading order in n of the determinant. It was enough to obtain the convergence in distribution to the GUE-corners process, under a suitable rescaling.

The dimer model with uniform measure is known to have an algebraic decay of its correlation functions, signature of its critical behaviour. We investigated, in Chapter 4, the field theoretic description of the model and their extensions with biased and two-periodic parameters. We found two theories that correctly describe the dimer correlators. The first given by Majorana fermions as a special case of a ghost system. The second is described by symplectic fermions in the non-logarithmic sector of a logarithmic conformal field theory.

Outlook

The project content of this thesis being quite heterogeneous, there are many directions in which the research may proceed.

- The approach followed in the second chapter, in order to apply the tangent method, has a good chance to extend to some generalizations of the elliptic SOS model. For instance, in the case of domain wall and a (partially) reflecting end boundary conditions [80]. One

could also ask whether these boundary conditions have an interpretation in terms of the dimer model. To our knowledge, this question has not yet been addressed.

There is also the question concerning other values of the η parameter. For general η, the situation is a bit fuzzy since the partition function of the model [68, 70] is only given in terms of a sum of determinants, and the method will most likely require major adjustments, if possible at all. However, the case $\eta = 1/3$, known for its correspondence with three-colourings, seems already more reasonable to approach and should lead to a better understanding of the general case.

- For the result obtained in Chapter 3, we believe the GUE-corners distribution to be universal in the case of Aztec diamonds (partly due to the determinantal structure); at least it should certainly apply to a large class of probability measures. A continuation of this work could be to investigate the situation of biased two-periodic weightings, or higher periodicities. In the former proposition, it would be interesting to see if an elliptic parametrization of the dimer weights (similarly to what is done in Chapter 2) could help to write the expressions in a more compact way. In the same flavour, a recent study [124] has investigated the case of the boundary statistics in the six-vertex model at $|\Delta| > 1$ (ferro and anti-ferroelectric phases). In one of the two cases, they found a convergence to GUE-corners.

- Concerning the field theories found in Chapter 4, one would like first to better understand the connections between both descriptions (Majorana and symplectic fermions). In a second step, it would be interesting to examine other off-critical probability measures, for instance the $2 \times k$-periodic weighting.

  Another quite involving project concerns the field theoretic description inside the disordered region of the Aztec diamond. An inhomogenous (in the sense of a non-trivial background metric) field theory was exhibited by Allegra *et al.* in the uniform/biased case [125]. To our knowledge, nothing is known about periodic weightings in this case. One would expect to find an inhomogeneous theory that is massless in the rough disordered region but

massive (and homogeneous?) inside the smooth disordered central region. Yet the mechanism underlying this change of behaviour in the theory is completely unknown and would be extremely interesting to investigate. If such a description exists, it is not even clear to us whether it is possible to consider both scaling and critical limits in such a way that the shape of the smooth region is preserved.

Bibliography

[1] J.-F. de Kemmeter, N. Robert and P. Ruelle, *On λ-determinants and tiling problems*, J. Phys. A: Math. Theor. **57 1** (2023) 015209.

[2] N. Robert, H. Rosengren, P. Ruelle and C. Walmsley Hagendorf, *Arctic curve in the elliptic SOS model at the free-fermion point*, in preparation.

[3] N. Robert and P. Ruelle, *GUE-corners in two-periodic Aztec diamonds*, arXiv preprint `arXiv:2509.14071 [math-ph]` (2025).

[4] N. Robert and P. Ruelle, *Two-periodic dimer models on the plane*, in preparation.

[5] S. Friedli and Y. Velenik, *Statistical mechanics of lattice systems: a concrete mathematical introduction*, Cambridge University Press, 2017.

[6] E. Ising, *Beitrag zur Theorie des Ferromagnetismus*, Z. Physik **31** (1925) 253–258.

[7] L. Onsager, *Crystal statistics. I. A two-dimensional model with an order-disorder transition*, Phys. Rev. **65 3-4** (1944) 117.

[8] R. J. Baxter, *Exactly solved models in statistical mechanics*, Elsevier, 2016.

[9] J. Lamers, *A pedagogical introduction to quantum integrability, with a view towards theoretical high-energy physics*, arXiv preprint `arXiv:1501.06805 [math-ph]` (2015).

[10] C.-N. Yang, *Some exact results for the many-body problem in one dimension with repulsive delta-function interaction*, Phys. Rev. Lett. **19 23** (1967) 1312.

[11] R. J. Baxter, *Solvable eight-vertex model on an arbitrary planar lattice*, Philos. Trans. R. Soc. A **289 1359** (1978) 315–346.

[12] T. Vicsek, A. Czirók, E. Ben-Jacob, I. Cohen and O. Shochet, *Novel type of phase transition in a system of self-driven particles*, Phys. Rev. Lett. **75 6** (1995) 1226.

[13] R. H. Fowler and G. S. Rushbrooke, *An attempt to extend the statistical theory of perfect solutions*, Trans. Faraday Soc. **33** (1937) 1272–1294.

[14] R. Kenyon, *An introduction to the dimer model*, arXiv preprint `arXiv:math/0310326 [math.CO]` (2003).

[15] H. N. Temperley and M. E. Fisher, *Dimer problem in statistical mechanics - an exact result*, Philos. Mag. **6 68** (1961) 1061–1063.

[16] M. E. Fisher, *Statistical mechanics of dimers on a plane lattice*, Phys. Rev. **124 6** (1961) 1664.

[17] P. W. Kasteleyn, *The statistics of dimers on a lattice: I. The number of dimer arrangements on a quadratic lattice*, Physica **27 12** (1961) 1209–1225.

[18] P. W. Kasteleyn, *Dimer statistics and phase transitions*, J. Math. Phys. **4 2** (1963) 287–293.

[19] N. Elkies, G. Kuperberg, M. Larsen and J. Propp, *Alternating-sign matrices and domino tilings (Part I)*, J. Algebr. Comb. **1** (1992) 111–132.

[20] N. Elkies, G. Kuperberg, M. Larsen and J. Propp, *Alternating-sign matrices and domino tilings (Part II)*, J. Algebr. Comb. **1** (1992) 219–234.

[21] W. Jockusch, J. Propp and P. Shor, *Random domino tilings and the arctic circle theorem*, arXiv preprint `arXiv:math/9801068 [math.CO]` (1998).

[22] D. M. Bressoud, *Proofs and confirmations: the story of the alternating-sign matrix conjecture*, Cambridge University Press, 1999.

[23] D. Bressoud and J. Propp, *How the alternating sign matrix conjecture was solved*, Not. Am. Math. Soc. **46 6** (1999) 637–646.

[24] V. Korepin and P. Zinn-Justin, *Thermodynamic limitof the six-vertex model with domain wall boundary conditions*, J. Phys. A: Math. Gen. **33 40** (2000) 7053.

[25] F. Colomo and A. Pronko, *The arctic circle revisited*, arXiv preprint `arXiv:0704.0362 [math-ph]` (2007).

[26] F. Colomo, V. Noferini and A. G. Pronko, *Algebraic arctic curves in the domain-wall six-vertex model*, J. Phys. A: Math. Theor. **44 19** (2011) 195201.

[27] H. Cohn, M. Larsen and J. Propp, *The shape of a typical boxed plane partition*, arXiv preprint `arXiv:math/9801059 [math.CO]` (1998).

[28] J. Baik, T. Kriecherbauer, K.-R. McLaughlin and P. D. Miller, *Uniform asymptotics for polynomials orthogonal with respect to a general class of discrete weights and universality results for associated ensembles: announcement of results*, Int. Math. Res. Not. **2003 15** (2003) 821–858.

[29] V. Gorin, *Lectures on random lozenge tilings*, Volume *193*, Cambridge University Press, 2021.

[30] M. Adler, K. Johansson and P. van Moerbeke, *Double Aztec diamonds and the tacnode process*, Adv. Math. **252** (2014) 518–571.

[31] M. Adler, S. Chhita, K. Johansson and P. Van Moerbeke, *Tacnode GUE-minor processes and double Aztec diamonds*, Probab. Theory Relat. Fields **162 1** (2015) 275–325.

[32] M. Ciucu, *Round Aztec windows, a dual of the Aztec diamond theorem and a curious symmetry of the correlation of diagonal slits*, arXiv preprint `arXiv:2508.06451 [math.CO]` (2025).

[33] P. Di Francesco and R. Soto-Garrido, *Arctic curves of the octahedron equation*, J. Phys. A: Math. Theor. **47 28** (2014) 285204.

[34] T. Berggren, *Domino tilings of the Aztec diamond with doubly periodic weightings*, Ann. Probab. **49 4** (2021) 1965–2011.

[35] T. Berggren and A. Borodin, *Geometry of the doubly periodic Aztec dimer model*, Communications of the American Mathematical Society **5 11** (2025) 475–570.

[36] S. Chhita, K. Johansson and B. Young, *Asymptotic domino statistics in the Aztec diamond*, Ann. Appl. Probab. **25 3** (2015) 1232–1278.

[37] C. A. Tracy and H. Widom, *On orthogonal and symplectic matrix ensembles*, Commun. Math. Phys. **177 3** (1996) 727–754.

[38] D. P. Robbins and H. Rumsey Jr, *Determinants and alternating sign matrices*, Adv. Math. **62 2** (1986) 169–184.

[39] A. Borodin and M. Duits, *Biased* 2×2 *periodic Aztec diamond and an elliptic curve*, Probab. Theory Relat. Fields **187 1-2** (2023) 259–315.

[40] R. Baxter, *Eight-vertex model in lattice statistics and one-dimensional anisotropic heisenberg chain. I. Some fundamental eigenvectors*, Ann. Phys. **76 1** (1973) 1–24.

[41] R. Baxter, *Eight-vertex model in lattice statistics and one-dimensional anisotropic heisenberg chain. II. Equivalence to a generalized ice-type lattice model*, Ann. Phys. **76 1** (1973) 25–47.

[42] R. Baxter, *Eight-vertex model in lattice statistics and one-dimensional anisotropic heisenberg chain. III. Eigenvectors of the transfer matrix and hamiltonian*, Ann. Phys. **76 1** (1973) 48–71.

[43] F. Colomo and A. Sportiello, *Arctic curves of the six-vertex model on generic domains: the tangent method*, J. Stat. Phys. **164 6** (2016) 1488–1523.

[44] K. Johansson and E. Nordenstam, *Eigenvalues of GUE minors*, Electron. J. Probab. **11** (2006) 1342–1371.

[45] B. J. Fleming and P. J. Forrester, *Interlaced particle systems and tilings of the Aztec diamond*, J. Stat. Phys. **142 3** (2011) 441–459.

[46] C. L. Dodgson, *Condensation of determinants, being a new and brief method for computing their arithmetical values*, Proc. R. Soc. Lond. (1866) 150–155.

[47] J. Propp, *Lambda-determinants and domino-tilings*, Adv. Appl. Math. **34 4** (2005) 871–879.

[48] P. Di Francesco, *An inhomogeneous lambda-determinant*, arXiv preprint `arXiv:1209.6619 [math.CO]` (2012).

[49] E. H. Kuo, *Applications of graphical condensation for enumerating matchings and tilings*, Theor. Comput. Sci. **319 1-3** (2004) 29–57.

[50] D. E. Speyer, *Perfect matchings and the octahedron recurrence*, J. Algebr. Comb. **25** (2007) 309–348.

[51] W. H. Mills, D. P. Robbins and H. Rumsey Jr, *Alternating sign matrices and descending plane partitions*, J. Comb. Theory, Series A **34 3** (1983) 340–359.

[52] P. Ruelle, *Double tangent method for two-periodic Aztec diamonds*, J. Stat. Mech. **2022 12** (2022) 123103.

[53] C. S. Swart, *Elliptic curves and related sequences*, PhD thesis, University of London, 2003.

[54] J. Propp, *Generalized domino-shuffling*, Theor. Comput. Sci. **303 2-3** (2003) 267–301.

[55] M. Ciucu, *Enumeration of perfect matchings in graphs with reflective symmetry*, J. Comb. Theory, Series A **77 1** (1997) 67–97.

[56] Z.-H. Sun, *Congruences concerning Legendre polynomials*, Proc. Am. Math. Soc. **139 6** (2011) 1915–1929.

[57] M. Ciucu, *A complementation theorem for perfect matchings of graphs having a cellular completion*, J. Comb. Theory, Series A **81 1** (1998) 34–68.

[58] É. Janvresse, T. de La Rue and Y. Velenik, *A note on domino shuffling*, Electron. J. Comb. (2006) R30–R30.

[59] S. Chhita and M. Duits, *On the domino shuffle and matrix refactorizations*, Commun. Math. Phys. **401 2** (2023) 1417–1467.

[60] G. Bastien and M. Rogalski, *On the algebraic difference equations* $u_{n+2}u_n = \psi(u_{n+1})$ *in* $\mathbb{R}_*^+$*, related to a family of elliptic quartics in the plane*, Adv. Differ. Equ. **2005** (2005) 1–35.

[61] A. Hone, *Sigma function solution of the initial value problem for Somos* 5 *sequences*, Trans. Am. Math. Soc. **359 10** (2007) 5019–5034.

[62] J. H. Silverman, *The arithmetic of elliptic curves*, Volume *106*, Springer, 2009.

[63] N. J. Sloane et al., *The on-line encyclopedia of integer sequences*, Published electronically at `https://oeis.org` (2018).

[64] L. Pauling, *The structure and entropy of ice and of other crystals with some randomness of atomic arrangement*, J. Am. Chem. Soc. **57 12** (1935) 2680–2684.

[65] O. Tsuchiya, *Determinant formula for the six-vertex model with reflecting end*, arXiv preprint `arXiv:solv-int/9804010` (1998).

[66] P. L. Ferrari and H. Spohn, *Domino tilings and the six-vertex model at its free-fermion point*, J. Phys. A: Math. Gen. **39 33** (2006) 10297.

[67] E. Date, M. Jimbo, A. Kuniba, T. Miwa and M. Okado, *Exactly solvable SOS models II: Proof of the star-triangle relation and combinatorial identities*, Research Institute for Mathematical Sciences, Kyoto University, 1987.

[68] H. Rosengren, *An Izergin–Korepin-type identity for the 8VSOS model, with applications to alternating sign matrices*, Adv. Appl. Math. **43 2** (2009) 137–155.

[69] H. Rosengren, *The three-colour model with domain wall boundary conditions*, Adv. Appl. Math. **46 1-4** (2011) 481–535.

[70] O. Foda, M. Wheeler and M. Zuparic, *Two elliptic height models with factorized domain wall partition functions*, J. Stat. Mech. **2008 02** (2008) P02001.

[71] A. N. Hone, *Elliptic curves and quadratic recurrence sequences*, Bull. London Math. Soc. **37 2** (2005) 161–171.

[72] N. Bogoliubov, A. Pronko and M. Zvonarev, *Boundary correlation functions of the six-vertex model*, J. Phys. A: Math. Gen. **35 27** (2002) 5525.

[73] R. Pemantle and M. C. Wilson, *Twenty combinatorial examples of asymptotics derived from multivariate generating functions*, Siam Rev. **50 2** (2008) 199–272.

[74] A. Aggarwal, *Arctic boundaries of the ice model on three-bundle domains*, Invent. Math. **220 2** (2020) 611–671.

[75] B. Debin, E. Granet and P. Ruelle, *Concavity analysis of the tangent method*, J. Stat. Mech. **2019 11** (2019) 113107.

[76] B. Debin and P. Ruelle, *Factorization in the multirefined tangent method*, J. Stat. Mech. **2021 10** (2021) 103201.

[77] A. Sportiello, *The tangent method: where do we stand?*, in *Conf. Integrability, Combinatorics and Representations*, 2019.

[78] P. Di Francesco and R. Soto-Garrido, *Arctic curves of the octahedron equation*, J. Phys. A: Math. Theor. **47 28** (2014) 285204.

[79] C. Charlier, Lozenge and domino tilings, `https://sites.google.com/view/cchar/random-tilings`, Access date: 10 october 2025.

[80] L. Hietala, *Exact results for the six-vertex model with domain wall boundary conditions and a partially reflecting end*, Lett. Math. Phys. **112 2** (2022) 41.

[81] E. T. Whittaker and G. N. Watson, *A course of modern analysis*, Cambridge University Press, fifth edition, 2021.

[82] W. P. Reinhardt and P. L. Walker, NIST Digital Library of Mathematical Functions: Chapter 20 Theta Functions, `https://dlmf.nist.gov/20`, Version 1.2.4; Release date 2025-03-15.

[83] I. Avramidi, *Lecture notes on asymptotic expansion*, University lectures (2000).

[84] V. Gorin, *Lectures on random lozenge tilings*, Volume *193*, Cambridge University Press, 2021.

[85] S. Mkrtchyan and L. Petrov, *GUE corners limit of q-distributed lozenge tilings*, Electron. J. Probab. **22** (2017) 1 – 24.

[86] S. Mkrtchyan, *Turning point processes in plane partitions with periodic weights of arbitrary period*, in *Representation Theory, Mathematical Physics, and Integrable Systems: In Honor of Nicolai Reshetikhin*, pages 497–527, Springer, 2021.

[87] S. Mkrtchyan, *Plane partitions with two-periodic weights*, Lett. Math. Phys. **104** (2014) 1053–1078.

[88] E. Dimitrov, *Six-vertex models and the GUE-corners process*, Int. Math. Res. Not. **2020 6** (2020) 1794–1881.

[89] E. Dimitrov and M. Rychnovsky, *GUE corners process in boundary-weighed six-vertex models*, in *Annales de l'Institut Henri Poincare (B) Probabilites et statistiques*, Volume *58*, pages 188–219, 2022.

[90] V. Gorin, *From alternating sign matrices to the Gaussian unitary ensemble*, Commun. Math. Phys. **332 1** (2014) 437–447.

[91] M. Duits and A. B. Kuijlaars, *The two-periodic Aztec diamond and matrix valued orthogonal polynomials*, J. Eur. Math. Soc. **23 4** (2020) 1075–1131.

[92] C. Krattenthaler, *Advanced determinant calculus*, in *The Andrews Festschrift*, pages 349–426, Springer, 2001.

[93] H. Cohn, N. Elkies and J. Propp, *Local statistics for random domino tilings of the Aztec diamond*, Duke Math. J. **85 1** (1996).

[94] K. Johansson, *Non-intersecting paths, random tilings and random matrices*, Probab. Theory Relat. Fields **123 2** (2002) 225–280.

[95] K. Johansson, *Discrete orthogonal polynomial ensembles and the Plancherel measure*, Ann. Math. (2001) 259–296.

[96] K. Johansson, *The arctic circle boundary and the Airy process*, Ann. Probab. **33 1** (2005) 1 – 30.

[97] K. Johansson, *Random matrices and determinantal processes*, in *Mathematical Statistical Physics*, Volume *83* of *Les Houches*, pages 1–56, Elsevier, 2006.

[98] A. Aggarwal and V. Gorin, *Gaussian unitary ensemble in random lozenge tilings*, Probab. Theory Relat. Fields **184 3** (2022) 1139–1166.

[99] V. Gorin and G. Panova, *Asymptotics of symmetric polynomials*, Discrete Math. & Theor. Comput. Sci. (2013).

[100] S. Chhita and K. Johansson, *Domino statistics of the two-periodic Aztec diamond*, Adv. Math. **294** (2016) 37–149.

[101] V. Beffara, S. Chhita and K. Johansson, *Local geometry of the rough-smooth interface in the two-periodic Aztec diamond*, Ann. Appl. Probab. **32 2** (2022) 974–1017.

[102] A. Björklund, B. Gupt and N. Quesada, *A faster hafnian formula for complex matrices and its benchmarking on a supercomputer*, J. Exp. Algorithm. **24** (2019) 1–17.

[103] S. Caracciolo, A. D. Sokal and A. Sportiello, *Algebraic/combinatorial proofs of Cayley-type identities for derivatives of determinants and pfaffians*, Adv. Appl. Math. **50 4** (2013) 474–594.

[104] V. B. Priezzhev and P. Ruelle, *Boundary monomers in the dimer model*, Phys. Rev. E–Stat., Nonlinear, and Soft Matter Physics **77 6** (2008) 061126.

[105] P. Fendley, R. Moessner and S. L. Sondhi, *Classical dimers on the triangular lattice*, Phys. Rev. B **66 21** (2002) 214513.

[106] N. Allegra and J.-Y. Fortin, *Grassmannian representation of the two-dimensional monomer-dimer model*, Phys. Rev. E **89 6** (2014) 062107.

[107] M. E. Fisher and J. Stephenson, *Statistical mechanics of dimers on a plane lattice. II. Dimer correlations and monomers*, Phys. Rev. **132 4** (1963) 1411.

[108] H. G. Kausch, *Curiosities at $c = -2$*, arXiv preprint `arXiv:hep-th/9510149` (1995).

[109] W. Eholzer, L. Feher and A. Honecker, *Ghost systems: a vertex algebra point of view*, Nucl. Phys. B **518 3** (1998) 669–688.

[110] H. G. Kausch, *Symplectic fermions*, Nucl. Phys. B **583 3** (2000) 513–541.

[111] M. A. Flohr, *Bits and pieces in logarithmic conformal field theory*, Int. J. Mod. Phys. A **18 25** (2003) 4497–4591.

[112] N. Allegra, *Exact solution of the 2d dimer model: Corner free energy, correlation functions and combinatorics*, Nucl. Phys. B **894** (2015) 685–732.

[113] V. Gurarie, *Logarithmic operators in conformal field theory*, Nucl. Phys. B **410 3** (1993) 535–549.

[114] M. R. Gaberdiel and H. G. Kausch, *A local logarithmic conformal field theory*, Nucl. Phys. B **538 3** (1999) 631–658.

[115] S. Mahieu and P. Ruelle, *Scaling fields in the two-dimensional Abelian sandpile model*, Phys. Rev. E **64 6** (2001) 066130.

[116] G. Piroux and P. Ruelle, *Boundary height fields in the Abelian sandpile model*, J. Phys. A: Math. Gen. **38 7** (2005) 1451.

[117] P. Ruelle, *Logarithmic conformal invariance in the Abelian sandpile model*, J. Phys. A: Math. Theor. **46 49** (2013) 494014.

[118] J. Brankov, V. Poghosyan, V. Priezzhev and P. Ruelle, *Transfer matrix for spanning trees, webs and colored forests*, J. Stat. Mech. **2014 9** (2014) P09031.

[119] P. Ruelle, *Sandpile models in the large*, Front. Phys. **9** (2021) 641966.

[120] S. Grigorev, V. Poghosyan and V. Priezzhev, *Three-leg correlations in the two-component spanning tree on the upper half-plane*, J. Stat. Mech. **2009 09** (2009) P09008.

[121] N. Azimi-Tafreshi, H. Dashti-Naserabadi, S. Moghimi-Araghi and P. Ruelle, *The Abelian sandpile model on the honeycomb lattice*, J. Stat. Mech. **2010 02** (2010) P02004.

[122] M. Jeng, G. Piroux and P. Ruelle, *Height variables in the Abelian sandpile model: scaling fields and correlations*, J. Stat. Mech. **2006 10** (2006) P10015.

[123] A. B. Goncharov and R. Kenyon, *Dimers and cluster integrable systems*, in *Ann. Sci. Éc. Norm. Supér.*, Volume *46*, pages 747–813, 2013.

[124] V. Gorin and K. Liechty, *Boundary statistics for the six-vertex model with dwbc*, Commun. Pure Appl. Math. (2025).

[125] N. Allegra, J. Dubail, J.-M. Stéphan and J. Viti, *Inhomogeneous field theory inside the arctic circle*, J. Stat. Mech. **2016 5** (2016) 053108.